An Investigation into the Immune Landscape of the Abdominal Aortic Aneurysm-Thrombus Complex and its Systemic Effects

Ismail Cassimjee

Nuffield Department of Surgical Sciences

&

Wolfson College



Thesis submitted for the Degree of Doctor of Philosophy

University of Oxford

Trinity Term 2019

This thesis is submitted to the University of Oxford, in partial fulfilment of the requirements for the degree of Doctor of Philosophy.

This thesis is entirely my own work, and except where otherwise stated, describes my own research.

An Investigation into the Immune Landscape of the Abdominal Aortic Aneurysm-Thrombus Complex and its Systemic Effects

Ismail Cassimjee

Wolfson College, University of Oxford
A thesis submitted for the degree of Doctor of Philosophy in Surgical Sciences
Trinity Term 2019

Degenerative abdominal aortic aneurysms (AAA) are characterised by aortic smooth muscle apoptosis, elastin degradation and a chronic inflammatory cell infiltrate. The inciting antigen is yet unknown. AAAs share many features with autoimmune conditions whilst overlapping several risk factors with atherosclerosis. The majority of AAAs of an operable size are lined with intraluminal thrombus (ILT), which is in constant contact with the aortic wall and flowing arterial blood. Flow mediated dilatation (FMD) is a surrogate marker for endothelial dysfunction and a predictor of future cardiovascular events. Patients with AAAs have a deteriorating FMD, which improves after surgery, thus implicating the aneurysm-thrombus complex as a potential driver of the systemic endothelial dysfunction.

The immunological contribution of ILT to the pathology is under investigated. This thesis aims to comprehensively define the immune landscape of the aortic wall and intraluminal thrombus through deep phenotyping, thus providing new insights into the mechanisms of degeneration in advanced stage aneurysms. Furthermore, it aims to explore a mechanistic link between ILT and systemic endothelial dysfunction.

Patients were prospectively recruited on to the Oxford Abdominal Aortic Aneurysm study. Peripheral blood, aortic wall and ILT specimens were collected intraoperatively and optimised for deep phenotyping with Time-of-flight mass cytometry (CyTOF). Cell sorting the aortic complex tissues provided high quality single cell suspensions for discovery analyses using different approaches.

The aortic wall was replete with T and B cells demonstrating new evidence of T and B cell crosstalk. In particular, T follicular helper cells were identified, thus providing evidence for class-switching to memory B cells in the aortic wall. The aortic and ILT lymphocytes contained the cytotoxic granule Granzyme B. This is a novel alternate mechanism of tissue destruction in late stage disease and its finding in the peripheral blood suggests a role as a potential biomarker. The myeloid cells had significant overlap in their markers of expression and the ILT also contained active monocyte derived dendritic cells, which is another novel finding. Both the T cells and myeloid cells had no dominant effector phenotype and rather represented a complex continuum aiming to achieve homeostatic balance. Finally, the ILT secretome was found to be cytotoxic to aortic endothelial cells and induced changes in gene expression consistent with endothelial dysfunction.

This thesis defines in detail the immune landscape of the aortic aneurysm-thrombus complex. It highlights the involvement of both innate and adaptive immune systems, as well as pro- and anti-inflammatory pathways involved in chronic non-resolving inflammation. The finding that ILT induces gene changes of endothelial dysfunction provides a novel mechanistic link for the changes in FMD of patients with AAA. These observations highlight potential targets for translational therapeutics.

Table of Contents

List of Figures ..... **v**

List of Tables ..... **viii**

List of Abbreviations ..... **ix**

1. INTRODUCTION ***0***

1.1 Background **1**

1.2 Risk factors **6**

1.3 The aneurysm prone infrarenal aorta **7**

1.4 Pathophysiology of AAA **8**

1.5 Cell types in the AAA wall **12**

1.6 The Intraluminal Thrombus **15**

1.7 Flow mediated dilatation and AAA **21**

1.8 Conclusion **23**

1.9 Hypothesis and Aims **23**

2. METHODS ***24***

2.1 Ethics and regulatory approval **25**

2.2 OxAAA Study design **26**

2.3 Flow mediated dilatation **28**

2.4 Specimen collection and biobanking **30**

2.4.1 Blood 30

2.4.2 Tissue 31

2.5 Specimen processing **33**

2.5.1 Aorta and intraluminal thrombus 34

2.6 Flow cytometry of the aortic complex **46**

2.6.1 General staining for flow cytometry 46

2.6.2 Fluorescence activated cell sorting 48

2.6.3 Magnetic bead selection 49

2.6.4 Biolegend® LegendsScreen™ antibody array 50

2.7 CyTOF Methods **54**

2.7.1 General CyTOF staining 54

2.7.2 Metal-Antibody conjugation and titration for CyTOF 56

2.7.3 Overview of CyTOF analysis workflow 58

2.8 Mechanistic experiments on tissue secretome **63**

2.8.1 Conditioning media with the tissue secretome 64

2.8.2 Using the protein concentration of the tissue secretome as a means of comparison 66

2.8.3 Determining the non-toxic concentration of the tissue secretome for use in gene expression studies 67
2.8.4 Determining lipopolysaccharide (LPS) levels in the ILT secretome 68
2.8.5 Heat inactivation of the ILT supernatants 70
2.8.6 Filtering the ILT supernatants 70

2.9 *In-Vitro* cell culture 71
2.9.1 Human Umbilical Vein Endothelial Cells (HUVEC) used for determining the non-toxic concentration of the tissue secretome 71
2.9.2 Aortic Endothelial Cells (AOEC) used for determining the gene expression of the tissue secretome 72
2.9.3 Human retinal pigment epithelial-1 cells (RPE-1) used for demonstration of biological activity in the tissue secretome 73

2.10 Human retinal pigment epithelial-1 cells (RPE-1) used for NF-κB nuclear translocation 74

2.11 Real-Time Quantitative Polymerase Chain Reaction (RT-qPCR) 76
2.11.1 RNA isolation 76
2.11.3 Qiagen RT^2 profiler PCR endothelial cell array 77
2.11.4 The cytokine profile of the aortic tissue supernatants 81

2.12 Statistical analysis 81

2.13 Conclusion 82

3. OPTIMISING DEEP IMMUNOPHENOTYPING INVESTIGATIVE TECHNIQUES IN ABDOMINAL AORTIC ANEURYSMS 83

3.1 Introduction 84

3.2 Principles of mass cytometry 88

3.3 Hypothesis and Aims 92

3.4 Experimental design 93

3.5 Results 93
3.5.1 Immune cell composition of the aortic complex 93
3.5.2 Further developments of the sampling and isolation technique 95
3.5.3 Enriching the CD45 fraction 97
3.5.4 Validating and optimising the flow sorted sample for CyTOF 104
3.5.5 CyTOF staining closely correlates with results from flow cytometry 109
3.5.6 The Biolegend® Legendscreen™ antibody array 111
3.5.7 CyTOF panel design 117
3.5.8 Titrating antibodies 117
3.5.9 The final panels 120

3.6 Discussion 122

3.7 Conclusion 124

4. DEEP IMMUNOPHENOTYPING THE ABDOMINAL AORTIC ANEURYSM COMPLEX. 125

4.1 Introduction 126

4.2 Hypothesis and aims 127

4.3 Methods: 129

4.3.1 Experimental design and workflow 129
4.3.2 Gating strategy for CyTOF 131

4.4 Results 133

4.4.1 Frequency of the primary immune populations in aorta, ILT and blood 133
4.4.2 Comparison of immune cell types in the aortic aneurysm complex 139
4.4.3 Lymphocyte phenotypic diversity of the aortic aneurysm complex tissues 141
4.4.4 B cell phenotypic diversity in the aortic aneurysm complex tissues 146
4.4.5 Mononuclear phagocyte phenotypic diversity in the aortic aneurysm complex tissues 148
4.4.6 NK cell subtypes 152
4.4.9 CD8 and CD4 subsets in the aortic aneurysm complex tissues 154
4.4.10 T Effector (helper) cell diversity in the aortic aneurysm complex 160
4.4.8 Granzyme B diversity in the cells of the aneurysm complex tissues 163

5. ELUCIDATING THE BIOLOGICAL ACTIVITY OF INTRALUMINAL THROMBUS IN AORTIC ANREURYSMS 178

5.1 Introduction 179

5.2 Hypothesis and Aims 179

5.3 Experimental workflow 179

5.4 Results 180

5.4.1 Establishing the biological activity of ILT supernatants 180
5.4.2 ILT supernatants also result in cytotoxicity of RPE-1 cells 181
5.4.3 Excluding bacterial contamination as a cause of cytotoxicity 184
5.4.4 Heat treatment of ILT supernatants removes cytotoxicity and biological activity 186
5.4.5 Filtering the ILT supernatants 188
5.4.6 Cytokine and proteomic profile of the tissue secretome 190
5.4.7 Identifying the 'physiological' concentration of ILT secretome supernatant 190
5.4.8 Assessing gene changes of endothelial cell dysfunction 192

5.4 Discussion 197

5.5 Conclusion 204

6. FINAL DISCUSSION 205

6.1 Original hypothesis 207
6.2 Principal findings of this research 207
6.3 Future work 209
6.4 Conclusion 211

7. APPENDICES 212

7.1 Supplementary Methods 213

7.1.1 List of Antibodies 213

7.2 Optimisation in preparation for Biolegend Legends Screen 216

7.3 Defining T cell subsets 218

7.4 Research publications arising during DPhil 220

7.5 Abstract presentations at scientific meetings 221

7.6 Acknowledgments 222

References 224

List of Figures

Figure 1.1: The intraluminal thrombus (ILT) within the sac of the AAA 4

Figure 1.2: Flow mediated dilatation measurements in a cohort of patients with abdominal aortic aneurysms (AAA) 22

Figure 2.1: An integrated study workflow, detailing the recruitment and follow up streams of the OxAAA study 27

Figure 2.2: Workflow between patient recruitment and intraoperative specimen collection 28

Figure 2.3: Flow mediated dilatation (FMD) is measured using the semi-automated UNEX-EF machine 29

Figure 2.4: Intraoperative trolley preparation 31

Figure 2.5: Intraoperative specimen retrieval 33

Figure 2.6: Intraluminal thrombus comparator groups 36

Figure 2.7: Cell yields comparing enzymatic digestion with a control in the intraluminal thrombus 37

Figure 2.8: Percoll® separates out cells and debris with differing densities 41

Figure 2.9: Lysing blood with ACK, improves the yield of granulocytes, in comparison to the density centrifugation methods 42

Figure 2.10: Flow cytometry staining on lysed blood compared to a laboratory full blood count 43

Figure 2.11: A comparison of common leucocyte markers in enzymatically digested blood to a sample with no added enzymes 44

Figure 2.12: The staining of CD66b (granulocytes), before and after a freeze thaw cycle 45

Figure 2.13: Experimental workflow for Biolegend® antibody array 51

Figure 2.14: Gating strategy for Biolegend® antibody array panel 53

Figure 2.15: The curse of dimensionality 59

Figure 2.16: Examples of various CyTOF visualisation methods 61

Figure 2.17: Workflow for conditioning media with aortic and ILT tissue 65

Figure 2.18: Plate layout for the RT^2 QC array 78

Figure 2.19: Plate layout for the RT^2 profiler array 80

Figure 3.1: Schematic of CyTOF processing and acquisition 90

Figure 3.2: Flow cytometry gating strategy for Aorta and ILT 94

Figure 3.3: The frequency of immune cell types in the aorta, ILT and PBMC..... 96

Figure 3.4: CyTOF analysis of magnetic bead enrichment..... 98

Figure 3.5: Flow cytometry analyses assessing CD45 enrichment of the ILT using Percoll®..... 100

Figure 3.6: A comparison of cells in the luminal and abluminal ILT..... 101

Figure 3.7: Analysis of cell sorted vs. non cell-sorted aortic tissue..... 103

Figure 3.8: Analysis of CD45 positive enrichment in FACS sorted ILT..... 104

Figure 3.9: CyTOF analysis of CD45 positive cell sorted aortic tissue 105

Figure 3.10: Mass cytometry (CyTOF) dot plots comparing markers of T cell expression in cell-sorted and unsorted aortic cells..... 106

Figure 3.11: Analysis comparing two clones of CD45 antibodies..... 107

Figure 3.12: Analysis of FITC-CD45 antibody after a freeze thaw cycle..... 108

Figure 3.13: Flow cytometry compared with CyTOF analysis in aortic and ILT specimens..... 110

Figure 3.14: Analysis of core lineage markers in the Biolegend® antibody array panel..... 114

Figure 3.15: Analysis of common mononuclear phagocyte markers in the Biolegend® antibody array panel..... 115

Figure 3.16: Analysis of co-stimulatory markers in the Biolegend® antibody array panel..... 116

Figure 3.17: CD15 CyTOF antibody titration..... 118

Figure 3.18: Assessment of CD57 spill-over in to +16 at higher concentrations 119

Figure 3.19: Design of the lymphocyte panel, incorporating core and specific cell identifiers..... 120

Figure 3.20: Design of the myeloid panel, incorporating core and specific cell identifiers..... 121

Figure 4.1: Experimental design and workflow for CyTOF immunophenotyping of AAA tissues.. 128

Figure 4.2: Gating strategy for identifying live CD45+ leukocytes 132

Figure 4.3: viSNE analysis of CD45+ cells isolated from ten aortic aneurysms 135

Figure 4.4: viSNE analysis of CD45+ cells isolated from eight patient's intraluminal thrombus ... 137

Figure 4.5: A combined viSNE analysis of CD45+ cells isolated from blood samples..... 138

Figure 4.6: Immune cell composition of the aortic wall, ILT and peripheral blood 140

Figure 4.7: tSNE analysis and heatmaps highlighting the lymphocyte phenotypic diversity in the aorta of AAA patients..... 142

Figure 4.8: tSNE analysis and heatmaps highlighting the lymphocyte phenotypic diversity in the intraluminal thrombus..... 144

Figure 4.9: tSNE analysis and heatmaps highlighting the lymphocyte phenotypic diversity in the peripheral blood of AAA patients..... 145

Figure 4.10: B Cell subsets in the aortic aneurysm complex 147

Figure 4.11: Myeloid cell phenotypic diversity of the Blood 149

Figure 4.12: Myeloid cell phenotypic diversity of the ILT 150

Figure 4.13: Myeloid cell phenotypic diversity of the aortic wall..... 151

Figure 4.14: NK Cell subsets in the aortic aneurysm complex..... 153

Figure 4.15: CD8 subsets in the aortic aneurysm complex..... 156

Figure 4.16: CD4 subsets in the aortic aneurysm complex..... 159

Figure 4.17: T effector cell phenotypic diversity within the aortic aneurysm complex..... 161

Figure 4.18: Granzyme B diversity in the aortic complex lymphocytes..... 164

Figure 5.1: Protein concentrations of ILT, aortic and omentum secretome supernatants..... 180

Figure 5.2: Immunofluorescence of RPE-1 cells after stimulation with tissue secretome supernatants 182

Figure 5.3: Immunofluorescence of RPE-1 cells after stimulation with ILT secretome supernatants 183

Figure 5.4: Quantification of NF-kB translocation and immunofluorescence of RPE-1 cells after stimulation with LPS in serial dilutions 185

Figure 5.5: Immunofluorescence of RPE-1 cells after stimulation with heat inactivated ILT secretome supernatants..... 187

Figure 5.6: Immunofluorescence of RPE-1 cells after stimulation with filtered (5kDa) ILT secretome supernatants 188

Figure 5.7: Cytotoxicity assay of ILT supernatants using HUVECs 191

Figure 5.8: A comparison of changes in gene expression by negative controls 194

Figure 5.9: Changes in gene expression of endothelial related genes (in AOECs when stimulated by ILT supernatants) 196

Figure 7.1: Flow cytometry analysis describing optimisation steps for the Biolegend® antibody array 217

Figure 7.2: CD8 and CD4 T cell subtype definitions 219

List of Tables

Table 1.1: Key differences between atherosclerosis and abdominal aortic aneurysm pathology... 10

Table 1.2: Cell types and architecture of the intraluminal thrombus 18

Table 2.1: Constituents of the enzymatic digestion cocktail..... 38

Table 3.1: Common immune cell phenotyping markers..... 111

Table 3.2: Positive markers on Biolegend® antibody screening array 112

Table 4.1: Characteristics of study subjects included in the results phase 130

Table 4.2: CD8 subsets in the aortic aneurysm complex..... 155

Table 4.3: CD4 subsets in the aortic aneurysm complex..... 157

Table 5.1: Cytokine profile of ILT and Aortic wall supernatants 189

Table 5.2: Quality control assessment of cDNA/RNA from AOECs stimulated with ILT supernatants 192

Table 5.3: Summary of gene changes 201

Table 7.1: List of Flow Cytometry Antibodies..... 213

Table 7.2: List of CyTOF Antibodies 214

List of Abbreviations

AAA	Abdominal aortic aneurysm
ACK	Ammonium-chloride-potassium
ACTB	Beta-actin
ADAM10	A disintegrin and metalloprotease -10
ADAM17	A disintegrin and metalloprotease -17
AOECS	Aortic endothelial cells
b-ME	b-mercaptoethanol
BBE	Brain bovine extract
BCA	Bicinchoninic acid
BD	Beckon and Dickson
BSA	Bovine serum albumin
CABG	Coronary artery bypass graft
CCR5	C-C chemokine receptor type 5
CCR6	C-C chemokine receptor 6
CD	Cluster of differentiation
COPD	Chronic obstructive pulmonary disease
CRF	Clinical record form
CRP	C reactive protein
CSB	Cell staining buffer
CSM	Cell staining media
CTL	Cytotoxic lymphocytes
CyTOF	Time-of-flight mass cytometry
DAPI	4′,6-diamidino-2-phenylindole
DC	Dendritic cell
DCIR	Dendritic cell immunoreceptor
DMEM	Dulbecco's modified Eagle's medium
DMSO	Dimethyl sulfoxide
DNA	Deoxyribonucleic acid
EDN1	Endothelin 1
EDNRA	Endothelin receptor type A
EDTA	Ethylenediaminetetraacetic acid
EGM-2	Endothelial growth media-2
ELISA	Enzyme linked immunosorbent assay
EVAR	Endovascular aneurysm repair
FACS	Fluorescence activated cell sorting
FBC	Full blood cell count
FBN	Fibrillin
FC	Flow cytometry
FCS	Foetal calf serum

FGF1	Fibroblast growth factor
FITC	Fluorescein isothiocyanate
FMD	Flow mediated dilatation
FSC	Forward scatter
G-CSF	Granulocyte-colony stimulating factor
GC	Germinal centres
GDC	Genomic deoxyribonucleic acid control
GM-CSF	Granulocyte macrophage colony stimulating factor
GPIIbIIIa	Glycoprotein IIbIIIa
GWAS	Genome wide association study
GzB	Granzyme B
H&E	Haematoxylin and eosin
HBSS	Hanks balanced salt solution
HIF-1A	Hypoxia-inducible factor 1-alpha
HLA	Human leucocyte antigen
HUVECS	Human umbilical vein endothelial cells
ICAM-1	Intracellular adhesion molecule-1
IF	Immunofluorescence
IHC	Immunohistochemistry
IL	Interleukin
ILT	Intraluminal thrombus
INF	Interferon
iNKT	Invariant natural killer T cell
iNOS	Inducible nitric oxide synthase
IRF	Interferon regulatory factor
ITGAV	Integrin alpha-V
LAL	Limulus amoebocyte lysate
LDL	Low density lipoprotein
LH	Lithium heparin
LPS	Lipopolysaccharide
MACS	Magnetic activated cell sorting
MCP	Monocyte chemoattractant protein
MMP	Matrix metalloproteinases
moDC	Monocyte derived dendritic cell
MS	Mass spectrometry
Nf-kB	Nuclear factor kappa-light-chain-enhancer of activated B cells
NGAL	Neutrophil gelatinase associated lipocalin
NK	Natural killer
NKT	Natural killer T cell
NO	Nitric Oxide
NPR1	Natriuretic peptide receptor

OCLN	Occludin
OCT	Optimal cutting temperature
OSR	Open surgical repair
PAI	Plasminogen activator inhibitor
PBMC	Peripheral blood mononuclear cells
PBS	Phosphate-buffered saline
PCI	Percutaneous coronary intervention
PCR	Polymerase chain reaction
PD-1	Programmed cell death protein-1
pDC	Plasmacytoid dendritic cell
PDGF	Platelet derived growth factor
PE	phycoerythrin
PFA	Paraformaldehyde
Prf	Perforin
PVP	Polyvinylpyrrolidone
RBC	Red blood cell
RNA	Ribonucleic acid
RPE-1	Retinal pigment epithelial-1 cells
RPMI	Roswell Park Memorial institute
RTC	Reverse transcription control
SCS	Spray coated silica
Siglec	Sialic acid binding immunoglobulin-like lectin
SMC	Smooth muscle cell
SPHK1	Sphingosine kinase 1
SSC	Side scatter
Tef	T effector cell
Tfh	T follicular helper cells
TGFB1	Transforming growth factor beta 1
Th	T helper cell
THBS1	Thrombospondin 1
TLR	Toll-like receptor
TNF	Tumour necrosis factor
Treg	T regulatory cells
Trig	Triglycerides
VALT	Vascular associated lymphoid tissue
VCAM	Vascular cell adhesion molecule
WB	Western blot

Chapter 1

INTRODUCTION

"There is no disease more conducive to clinical humility than aneurysm of the aorta."

Sir William Osler

1.1 Background

Abdominal aortic aneurysms (AAAs) are an abnormal degenerative condition, characterised by dilatation of the infra-renal aorta. They are usually asymptomatic and left untreated pose a catastrophic rupture risk. A ruptured AAA has an incident mortality of 65-85%(1, 2) and in 2014 there were 9683 aneurysm related deaths in the USA alone and an estimated 175000 aneurysm related deaths worldwide (3).

Antyllus, a Greek surgeon from the second century, is credited with the first description of surgical repair for AAA:

"Those who tie the artery, as I advise, at each extremity, but amputate the intervening dilated part, perform a dangerous operation. The violent tension of the arterial pneuma often displaces the ligatures."

Ligation of AAA was the operation of choice for the ensuing 1800 years, and a review of the literature in 1940 documented 24 cases of AAA ligation with only 5 short term survivors(4). With advances in anaesthesia and the development of surgery as a speciality, a variety of techniques were attempted in the 1950's, including homografts and wrapping to prevent growth. With the introduction of Dacron grafts by DeBakey in 1954, the current technique of endoaneurysmorrhaphy and graft replacement was described by Oscar Creech in 1966(5). Albert Einstein had a cellophane wrap of his aortic aneurysm in 1952, a few years before the contemporary repair of AAAs was popularised. He demised of a ruptured aneurysm

8 years later(6). The modern era has witnessed the development of endovascular aneurysm repair (EVAR), which confers a significant initial improvement in perioperative 30-day mortality compared to open surgical repair (OSR) but their mortalities converge at 18 months(7). In long-term follow up (15 years), OSR had a small benefit over EVAR, mainly due to late ruptures in the EVAR group and thus the trade-off from the initial mortality benefit mandates life-long surveillance(8).

The typical aorta in health measures less than 2 cm, and an aneurysm by definition is a dilation of more than 1.5 times its baseline diameter (3 cm in the aorta). The rupture risk is correlated with aneurysm diameter, and at of 5.5 cm prophylactic intervention is considered. It is at this diameter that the procedure related mortality approximates the rupture risk for an overall net survival benefit. This 5.5cm threshold for intervention is informed by two landmark randomised control trials, the UK small aneurysm trial (UKSAT) and the Aneurysm detection and management study (ADAM)(9, 10).

In men above the age of 65, the prevalence is 4% - 8%(11, 12), with 0.5% meriting intervention through size criteria (13). Contemporary data from the UK screening programme report a prevalence of 1%, and this is in part related to decreases in smoking rates(14). In the UK, the remainder (+-13000 participants) are enrolled into a national surveillance screening program and referred on for intervention once they reach the 5.5 cm threshold. Aneurysm growth is insidious at an average of 2 mm per year(15, 16) and most of the clinical research over the last two decades has focused on improving outcomes in the cohort requiring intervention. However, it is the surveillance cohort that are most likely to benefit from future basic science research through targeting the prediction of growth in those destined for intervention

or by aiming to attenuate growth pharmacologically through manipulation of the inflammatory environment.

Inflammation together with smooth muscle cell apoptosis and elastin degradation are considered to be the hallmark pathophysiological findings of AAAs(17, 18). The aortic degeneration is thought to be meted out through the inflammatory cell mediators in an exaggerated or dysfunctional immune response. Anatomically, 95% of AAAs occur in the infrarenal component of the aorta(19). The area of normal aorta below the renal arteries before the aneurysm begins is known as the ‘neck’, whilst the bulging aneurysmal component is known as the ‘sac’.

As the AAA enlarges, in most instances an intraluminal thrombus (ILT) forms within the ‘sac’. The ILT has a luminal, blood facing surface, and an abluminal surface which is adherent to the intimal aspect of the aortic wall (**Figure 1.1**). The ILT is somewhat of an enigma, and large volume non-occlusive arterial thrombus which is in continuous contact with flowing blood is a rarity. It is sometimes encountered in the left atrial appendage during atrial fibrillation or other sites of aneurysmal formation such as the visceral vessels, popliteal and intracranial vasculature. This makes the ILT a unique structure.

Not only can it directly influence the underlying aortic wall but there remains the possibility of systemic sequestration of cells from the ILT, as it acts as a nidus of inflammatory seeding, making the ILT an ideal target for peripheral biomarker discovery. Thrombus formation within blood vessels is associated with local and systemic effects(20). Locally, the clinical manifestations are erythema, pain, swelling and an increased temperature, as in the case of a superficial thrombophlebitis of a peripheral vein. Systemically there can be an associated

inflammatory syndrome as with a DVT(21). The ILT within AAAs develops after the aneurysm has formed, and the inflammatory responses to this have not been fully investigated.

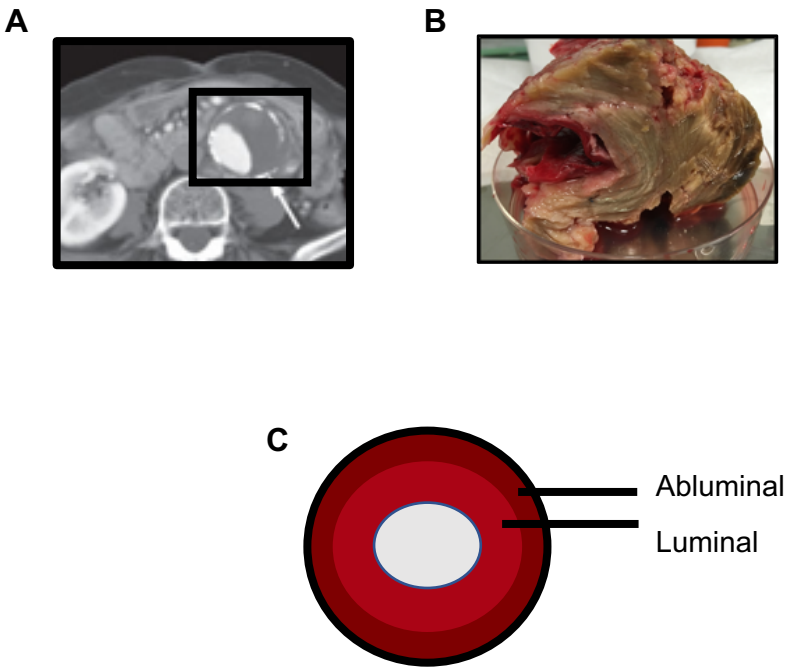


Figure 1.1: The intraluminal thrombus (ILT) within the sac of the AAA

(A) An axial slice through the abdomen of a patient with an abdominal aortic aneurysm (box). The flow lumen is bright with contrast, whilst the ILT surrounding it is non-opacified. **(B)** The ILT specimen after it was removed from the patient. Laminations are seen on its surface. **(C)** A schematic diagram highlighting the difference between the blood facing luminal surface and the wall facing abluminal surface.

The major thrust of research and management of AAAs aims to prevent rupture. Although asymptomatic AAAs are localised, their presence has systemic sequela, particularly long-term cardiovascular outcomes. Their shared atherosclerotic risk factors are a causative assumption. However, in comparison to age and risk factor matched cohorts, patients with AAA have a poorer 5-year survival, and patients with

larger aneurysms fair worse than those with smaller ones(22). This hints at the possibility of the aneurysm itself as a causative factor.

Despite the significant gains in the surgical and endovascular management of AAAs, the five year survival post elective repair has not improved significantly over a 42 year period (1969-2011) and has remained at 69% (23). Contextually, this is similar to stage 3 colon cancer(24). Even the long-term follow-up (13 years) of the initial landmark screening trial (Multicentre Aneurysm Screening Study) demonstrated significant cardiovascular and cancer related mortality which shadowed aneurysm related mortality(25). In the screened group, 41% of deaths in the patients enrolled into surveillance (<5.5cm) were due to cardiovascular causes, whilst only 2% were due to aneurysm rupture.

When examining the long-term outcomes (12 year) of the landmark UKSAT trial, the surveillance group initially had a mortality benefit presumably conferred as a result of delayed intervention. When followed out to 12 years however, both groups have a similar all-cause mortality with a trend to increased survival in the early surgery group(26). Furthermore, the data from the UKSAT trial suggested that for every 8mm increase in diameter, the relative risk of cardiovascular death increased by 1.34. The risk of cardiovascular death per year in patients with small AAA has been calculated at 3%, and this is equivalent to the risk of a 70 year old male diabetic smoker with hyperlipidaemia and hypertension(27).

Using the Framingham risk score, participants in the UK screening program were at high risk for future cardiovascular events and this risk was not addressed adequately through best practice pharmacological management and risk factor reduction strategies (28). The thickness of the ILT has also been associated with

the development of symptomatic cardiac disease as well as growth of AAAs(29) and this has not been intensively interrogated.

AAAs are a chronic inflammatory disease with potentially devastating local consequences (rupture) but are also associated with long-term systemic manifestations. The ILT is an under investigated component of the AAA complex and is in constant contact with aortic blood as well as the aneurysm wall (30). The ILT and aortic wall together form an inseparable 'aortic' complex and likely act in unison with each other. In the sections below, the risk factors for the development of AAAs, the pathophysiology and components of the inflammatory cell infiltrate, and the link of AAAs to endothelial dysfunction will be discussed.

1.2 Risk factors

The most important risk factors for developing an AAA are increased age, male gender, white race and cigarette smoking. Smoking has the strongest association, and 9.6% of current male, white smokers over the age of 55 will develop an AAA. Former smokers have a lower risk than current smokers, but not as low as those who have never smoked, with current smokers having a 6.6 times greater risk than those who have never smoked(31). Only lung cancer has a stronger association with smoking(32).

Degenerative aneurysms share common risk factors with atherosclerosis but also have intriguing differences. Hypertension is not a strong risk factor and only increases the risk by 1.44 - 1.6 fold(33) and an increased diastolic blood pressure appears to be more relevant.

Unlike atherosclerosis, the presence of diabetes appears to be protective (0.52 - 0.58 fold), through an unknown mechanism(34). The increased medial calcification found in diabetics is not enough to explain this, and other pathways are thought to be affected by diabetes (ECM volume, ECM glycation, inflammation and oxidative stress and ILT biology)(35). Several theories exist, but the most current hypothesis questions its relation to metformin therapy (36). Metformin is associated with decreased formation of AAAs(37), decreased growth of already established AAAs(38) and mechanistic mouse models demonstrate a putative link for this(37, 39). However, a randomised controlled trial on the subject is required, more especially in non-diabetic patients with AAA.

Patients with an increased LDL in the top tertile also have a 3.53 fold lifetime risk of developing an AAA but normal cut-offs increase the risk by <1.5 fold(40). Other less common risk factors are a genetic predisposition with a family history of a first degree relative increasing the risk (RR 1.9), though a specific genetic polymorphism is yet to be identified.

1.3 The aneurysm prone infrarenal aorta

The combination of altered haemodynamics, an alternate smooth muscle cell (SMC) derivation and a decreasing elastic lamella in the infrarenal aorta predispose it to aneurysm development. The embryological origin of the SMCs in the infrarenal aorta may contribute to aneurysm propensity as they are derived from the splanchnic mesoderm whereas the arch and thoracic aortic SMCs are derived from the neural crest and somite derived cells respectively(41).

There is a decrease in the elastin fibres as well as a decrease in the thickness of the wall of the aorta as it descends from the thorax into the abdominal aorta(42, 43). Additionally, the infrarenal aorta has at birth its maximum number of elastin cells (which produce elastic fibres)(44). Also, the infrarenal aorta has an increased susceptibility due to reflected pressure waves from the iliac bifurcation leading to a disturbance of the laminar flow and an alteration in the wall shear stress. When compared to the supracoeliac aorta, the infrarenal aorta has, at times, a reversal of flow during diastole and this can lead to an upregulation of factors that increase the inflammatory infiltrate and proteolytic pathways(45).

1.4 Pathophysiology of AAA

Traditionally AAAs have been classed as an aberration of atherosclerosis. However, over the last two decades this theory has been revised and they are now considered to be two separate disease states that often coincide. The generally accepted theory has evolved, and the aortic wall is thought to be degraded as a result of the inflammatory mediators produced by the cellular infiltrate, which results in the classical elastin degradation and SMC apoptosis characteristic of AAAs. Still unresolved is the precipitant of the inflammatory cell infiltrate and this may be as a result of dysregulated autoimmunity(46).

Matrix metalloproteinases (MMPs) are key mediators of extracellular matrix (ECM) degradation and the ECM degradation process in AAAs are still undefined but closely linked to MMPs. MMPs form a group of around 25 proteins consisting of elastases, collagenases, gelatinases, stromolysins and matrilysins and are released in a controlled manner from cells, acting on the ECM but also interacting

with cytokines and other MMPs. Tissue inhibitors of metalloproteinases (TIMPs) are responsible for regulating their activity. In the normal aorta, SMCs and adventitial fibroblasts are responsible for MMP production (47). MMPs (especially MMP-2 (gelatinase-A) and MMP-9 (gelatinase-B) are upregulated in aneurysmal tissue when compared to the normal controls and are thought to be released by the inflammatory cell infiltrate(48). MMP-1 (collagenase-1) and MMP-13 (collagenase-3) expression have been linked to ruptured aneurysms(49, 50). Cigarette smoke has been demonstrated to increase MMP-2 and MMP-9 expression in AAA (51, 52).

The dysregulation of MMPs/TIMPs are not enough to solely implicate them in the development of AAAs, and they are likely end result mediators of complex initiation process which brought about their activation. Indeed, doxycycline (a tetracycline antibiotic), which is an inhibitor of MMPs did not demonstrate any clinical benefit in humans(53).

AAA and atherosclerosis share many risk factors but also have several key differences. Diabetes is a major significant risk factor for the development of atherosclerosis and diabetic smokers are particularly at risk for IHD, CVD and PAD. However, as discussed, diabetes is not a risk factor for developing AAA and is somewhat protective. Other risk factors such as obesity and hypercholesterolemia are strongly associated with atherosclerosis but not as strong with AAA, whilst gender and race are strongly associated with AAA. A higher burden of atherosclerotic disease is not associated with the development of AAAs, however patients with AAA develop IHD and CVD suggesting that these are processes that run in parallel (54). AAAs are an independent risk factor for the development of coronary artery disease and conversely, patients with coronary disease are at risk for developing AAA(55). **(Table 1.1)**

Table 1.1: Key differences between atherosclerosis and abdominal aortic aneurysm pathology

Atherosclerosis	Abdominal Aortic Aneurysm
Infiltrate through intima	Adventitial Inflammation
TH1 predominately early on	TH2 response in the late stages
Diabetes is a significant risk factor	Diabetes may be protective
Stenosing with plaque burden	Dilating with wall rupture
Genetic associations with familial hypercholesterolemia	Genetic associations with soft tissue degeneration (Col3A1, FBN-1)
Affects both genders equally	Predominantly affects males

Table 1.1: TH1: T-helper cell 1, TH2 – T-helper cell 2, FBN - Fibrillin

Though AAAs overlap many risk factors with atherosclerosis, they also resemble an autoimmune disease due to their characteristic site specificity, genetic predisposition and chronic inflammatory infiltrate. Features is keeping with an autoimmune process are the predominance of CD4+ T cells which are mainly helper T cells which produce cytokines including IL-6 and TNF, together with mature B cells and plasma cells, and these are features seen in autoimmune conditions such as rheumatoid arthritis (RA) and giant cell arteritis (GCA) (56).

In health, autoreactive T cell clones are deleted by the thymus and as an additional mechanism are regulated by T regulatory cells (Treg) in the peripheral blood and tissues. These mechanisms are reported to be impaired in patients with AAA(57). Characteristic of immune cell pathologies are the involvement of both innate and adaptive immune responses, and AAAs have this. The macrophages found in the wall are thought to be the primary source of elastases such as matrix

metalloproteinases (MMPs)(48) whilst the NK cells may be cytotoxic to the smooth muscle cells.

In keeping with the autoimmune basis for AAAs, two potential candidate autoantigens have been identified, a 40kDa protein called aortic aneurysm protein-40 (AAAP-40) and an 80kDA protein found in the adventitial connective tissue(58, 59). AAAP-40 appears to be a microfibrillar protein with similarities to fibrinogen and localised to the aortic adventitia. Molecular mimicry, a process of cross-reactivity of self-antigens with pathogen encoded antigens is thought to be the mechanism underlying the T cell response of AAAs. At one stage an infectious aetiology was suspected, as some patients had positive infectious serology, including *Chlamydia pneumoniae* and several parasites. However, not all patients had an infection and it was later demonstrated that these organisms shared a variable sequence homology with epitopes of AAAP-40(60).

The autoimmune hypothesis does not account for the overwhelming influence of smoking as a risk factor the development of AAAs (several times more important than genetics and hypertension). In a mouse model, tobacco smoke lowered the threshold for developing AAA in a low dose elastase perfusion model, however there was no difference in MMP-9 levels between smoking and non-smoking mice (61). Mice exposed to tobacco smoke for 6 weeks, then a smoke-free period for 6 weeks still had a lower threshold for developing AAAs, despite stopping smoking, and this is similar to humans. This was independent of an MMP effect, and the leucocytes from the smoke exposed mice localised to the aneurysms of smoke-free mice (62). This supports the underlying inflammatory theory. The proposed theory suggests that smoking initiates an aneurysm phenotype by promoting an immune response through possible nitration of plasma and tissue proteins (AAAP-40) and

this changes the rate of proteolytic degradation thus predisposing to premature vessel wall degeneration.

In summary, features supporting the autoimmune basis for AAAs are:

1. The presence of mononuclear inflammatory cell infiltrates consisting mainly of T and B cells, macrophages and NK cells(63)
2. Mononuclear cells infiltrating the aneurysm wall show early (CD69), intermediate(CD25, CD38) and late (CD45RO, HLA Class II) activation antigens, suggesting an ongoing inflammation(64)
3. IgG antibody purified from the wall of AAA is immunoreactive with protein derived from normal aortic tissue(58)
4. AAA is associated with particular alleles such as the HLA DRB1(65)
5. Molecular mimicry may be responsible for T Cell responses in AAA(64, 66).
6. Smoking induces nitration of tissue proteins thus inducing an inflammatory reaction(62)

1.5 Cell types in the AAA wall

Macrophages are recruited early into the aneurysmal wall and macrophage cytokines play an important role in AAA progression. Macrophages exhibit plasticity with regards to their phenotypic cytokine output. They can either be M1 or M2 and can switch between the two depending on the prevailing conditions. Typically, M1 macrophages are pro-inflammatory, whereas M2 macrophages are involved in

repairing tissue. A balance between M1/M2 is thus vital in preventing a chronic inflammatory cell infiltrate which leads to persistent inflammation and aneurysm progression.

In murine models of AAA, M1 macrophages are strongly associated with aneurysm formation and elastin degradation, conversely, an M2 phenotype is protective for AAA development(67). Investigation of human aneurysm tissue has revealed an M1 phenotype, though this tissue represents an end stage of the disease. Although macrophages are a frequent cell type in murine AAA, they are not frequent in human AAA tissues procured during OSR(68). This discrepancy may represent the differing stages of the disease, where in murine disease aneurysm formation is at the initiation phase and in human disease it is characterised during the chronic progression phase. The limitation of human samples is that they are procured at an advanced stage of the disease process and to examine cells specialised techniques are required. Most human studies have focused on circulating monocytes and their link to increased elastases and ECM breakdown(69).

T-cells are the most frequent cell type in the AAA wall. As a broad categorisation, T cells can be divided up into CD4+ and CD8+ cells. CD4 cells can be further categorized into Th1, Th2, Th17 or regulatory (Treg) cells. This is dependent on drivers of cellular output as well as their cytokine expression. Th1 cells are activated by IL-12 and output INF-γ. Aneurysmal tissue displays features of Th1 upregulation with increased INF-γ in the aneurysm tissue and in the circulating blood(70-72).

Although Th2 cells are found in some specific inflammatory diseases, they are considered to be anti-inflammatory. IL-4 activity is responsible for Th2 differentiation of CD4 T cells and results are conflicting in murine and human models as to the role

of Th2 cells. This discrepancy maybe as a result of a similar cytokine profile to NK cells (Th0)(73) or from differences in the measurement of the cytokines. Th17 cells produce IL-17 and are related to several inflammatory diseases and play a key role in vascular superoxide production(74). Their role in AAA has not been fully clarified but they appear to be related to aneurysmal progression.

The frequency of CD4+CD25+FOXP3+ T Cells (Treg) is decreased in the peripheral blood of patients with AAA when compared to occlusive atherosclerotic disease or healthy donors(75). Treg cells are a unique class of T cells that serve as a counter-inflammatory mechanism. In the normal autoregulation of bodily function there is a balance between T effector cells, which promote inflammation, and Treg cells which counteract this(76). In inflammatory conditions such as rheumatoid arthritis(77), scleroderma(78), inflammatory bowel disease(79) and transplant organ rejection(80), a dysfunction of Treg cells have been implicated. Treg cells express Forkhead Box P3 (Foxp3) and are also known as $Foxp3^{+}CD4$ T Cells. They make up approximately 5% of the total CD4+ T Cells(81). The majority of Treg cells express CD25. In humans Treg's can be identified by a high expression of CD25 and an absence of IL-7Rα(82).

B cells are the second most common immune cell type, however, their phenotypic details have not as yet been fully elucidated.

In summary, aneurysms are regulated by complex processes and the degeneration is accompanied by a rich chronic inflammatory cell infiltrate. AAAs share common features with both atherosclerosis and autoimmune diseases. A deep phenotyping of the AAA wall in order to characterise this infiltrate has not been conducted in the modern era.

1.6 The Intraluminal Thrombus

The intraluminal thrombus (ILT) within the sac of AAAs is a multi-layered heterogenous blood clot that can be separated out macroscopically in to an outer 'luminal' and an inner 'abluminal' layer. The ILT is commonly viewed as an irrelevant inert bystander and is often excluded in biological studies examining the cells of the aortic wall. The mechanical properties of the ILT and its relation to predicting rupture of AAAs are well described, but less so are the biological properties of ILT. Investigators examining the biological properties of the ILT have delineated the major cell types, described the structural architecture and attempted to link the biology of ILT to further aortic wall degeneration. Thus far however, there has been no convincing mechanistic link between the two, nor has there been any suggestion that the ILT potentially sequesters active mediators resulting in systemic effects.

ILT is found in most AAAs, and in our cohort of patients (OxAAA) who had a CT scan for pre-operative planning, we found ILT in 95% of patients in at least two quadrants of the AAA sac in(83). The previous reported prevalence in AAAs above 5 cm was 75%(84). The rate of growth of the ILT and fresh bleeding in to it are related to rupture risk (85) and the ILT thickness is related to growth as well as increased cardiovascular events(29, 86).

There are currently two main theories attempting to relate the ILT to aneurysmal growth or rupture. The first proposes that the ILT contains a number of differing cell types, and these cells produce a host of inflammatory mediators (cytokines, chemokines, ECVs) which in turn release proteases that act locally on the vessel wall(87-90). The second, theory is that the ILT leads to a relative hypoxia of the

aneurysm wall and thus altered collagen formation and a more intense inflammatory response(91).

The most plausible hypotheses about the formation of ILT suggests that aneurysm growth alters the haemodynamics and lowers the shear stress of the aortic wall endothelium, leading to stasis and eddy formation in the sac which is more pronounced in diastole. The turbulence is compounded by reflected waves from the iliac artery bifurcation, and the already activated endothelium has a predilection for platelet adhesion and thrombus formation probably through an increase in endothelium nitric oxide synthase. As the thrombosis progresses the ILT enlarges presumably to a size where the haemodynamics are not as turbulent and a flow lumen with relative laminar flow is restored. Thus, the configuration and volume of the ILT is unique to each AAA, and several configurations are described: circumferential, eccentric, thin and thick. The different configurations impart differing tensile strengths and thus have variable impacts on rupture prediction(92). The luminal area is ‘stiffer’ and denser whilst the abluminal layer undergoes fibrinolysis and is less ‘stiff’(93).

To understand the biological implications of ILT, a detailed map of the cell types within it is required. In general, developing thrombi contain erythrocytes, platelets and a small number of lymphocytes, which are formed on a loose fibrin mesh. As the thrombus evolves and grows there is a loss of erythrocytes and further platelet deposition with thrombin generation. The primary fibrin network is replaced by a secondary fibrin network which is more organized, has thicker fibres and is stronger. In the ILT of AAAs, there is a continuous rejuvenation of the luminal layer with platelet and fibrin deposition, and in the abluminal layer there is ongoing fibrin degradation, which has led to what has been described as a network of canaliculi.

These canaliculi render the ILT fluid permeable with the potential to transport macromolecules and smaller cells from the luminal surface to the aortic wall(93). This fibrin rich structure with a paucity of cells and the canaliculi have been demonstrated on scanning electron microscopy(94) and are different to the acute erythrocyte rich thrombus that occurs in an acute vessel occlusion. In addition to the fibrin deposition the ILT contains collagen, which is predominately in the luminal area and has a laminar arrangement in the shoulder region of the ILT(95).

Histologically there are a greater number of cell types in the luminal layer as compared to the abluminal layer(88, 96). On electron microscopy the penetration of cells (lymphocytes, macrophages and T-cells) decreased from the luminal to the abluminal surface and there were very few cells found beyond a depth of 10mm(93). Quantification of active platelets within the thrombus using the GPIIbIIIa receptor as a marker of activity also revealed that the quantity of activated platelets decreased as the depth of thrombus increased with more fibrin deposition occurring in the luminal surface(93). **(Table 1.3)**

In addition to platelets, the predominant cell type described in the thrombus are granulocytes followed by monocytes and T-cells (89, 96). The predominance of PMNs in the luminal area is more than a 1000-fold when compared to the abluminal area(96). In contrast to the aortic wall where there is an abundance of chronic inflammatory cell types, T-cells, B-cells and mast cells have been found but are less frequent than granulocytes. There are less T-cells, B-cells and NK cells in the thrombus when compared to peripheral blood(96). The luminal area of the thrombus is rich in platelets whilst the abluminal and medial layers have fewer platelets(90), but these are active and degranulating(93). The platelets in the luminal area of the

ILT have been demonstrated to release RANTES and PAF4 which, result in immune cell recruitment to the ILT(98).

Table 1.2: Cell types and architecture of the intraluminal thrombus

Finding	Method of Investigation	Reference
Network of canaliculi, renewal of luminal layer, degradation of abluminal layer	Histology, Electron Microscopy	(93, 94)
Collagen in the luminal layer	Histology	(95)
Luminal layer has nucleated cells whilst the abluminal layer is cell poor	Histology, Electron Microscopy	(88, 93, 96)
Platelets decrease in abluminal layer but are still active	IHC, Histology, GPIIbIIIa assay	(90, 93)
Granulocytes are the most frequent cell type, then monocytes and T cells	Histology, IHC, FC	(89, 96, 97)
Distinct fibrocytic macrophage population	IHC	(95)
Less T cells than PB, but similar Treg's	FC	(96)
Higher IL-8 ILT	ELISA, WB, IHC	(98)
Increased MMP-2 and MMP-9 in luminal ILT	WB, EM, IHC	(88)
ADAM-10 and ADAM-17 in the abluminal ILT	WB, EM, IHC	(90)
Increased oxidative stress in AAA wall of thin ILT	MS, IHC, ELISA	(99)

IHC – Immunohistochemistry, GPIIbIIIa – Glycoprotein IIbIIIa, FC – Flow cytometry, ELISA – Enzyme linked immunosorbent assay, WB – Western blot, MS – Mass spectrometry

A distinct macrophage population has been described in the luminal area of the ILT using IHC. It is an activated population (HLA-DR +) but also appears to produce collagen (Coll1+ and Coll3+) and did not proliferate during cell culture, and thus has been described as an activated fibrocyte variant(95). Using flow cytometry (FC), the majority of monocytes were the classical $CD14^{+}CD16^{-}$, and this subpopulation was an activated one ($HLA\text{-}DR^{+}$, $CD11b^{+}$). The non-classical ($CD14^{-}CD16^{+}$) and the intermediate ($CD14^{+}CD16^{++}$) were decreased in the ILT when compared to the peripheral blood(96).

The proportion of T-cells is decreased in thrombus when compared to peripheral blood. There was no difference between the Treg cell numbers of the peripheral blood and thrombus and it has previously been recognized that patients with AAAs have fewer Treg cells. T-Cell chemokine receptor expression (CCR5) was also higher in the ILT and this may as a result of recruitment from platelets in the thrombus(96).

Granulocytes (neutrophils, basophils, eosinophils) are the most abundant cell type in the ILT. They are predominately in the luminal area of the ILT and this have been demonstrated on IHC and FC(96, 97). Granulocytes tend to be first responders in inflammation, and they have the ability to recruit other cell types and release proteases. In animal models of AAA, neutropenia halts the development of AAAs(100) and a neutrophil infiltrate also predominates the adventitia of the AAA wall. Neutrophil derived IL-8 (a neutrophil chemoattractant) has been found in high concentrations in the luminal ILT as well as the peripheral blood of patients with AAA(97).

The body of knowledge on the biology of the ILT has focused on linking the ongoing proteolysis in the aortic wall with the underlying ILT. Cells in the luminal layer are purported to produce mediators of proteolysis. Neutrophils have the ability to express MMPs and other elastases in their granules, and platelets have also been shown to attract MMP-2 and MMP-9(88). These are thought to be transported to the luminal layer through a network of canaliculi that are formed in the abluminal layer of the ILT as it undergoes fibrin degradation. Evidence of this proteolysis is supported by the finding that the aortic wall portion covered by ILT is thinner and the elastin more disorganised than the non-covered portion(101). Thus far however, proteolysins (MMP-2, MMP-9) have only been detected in the luminal ILT and not the abluminal ILT(88). This finding is incongruent with the hypothesis that proteases found in the thrombus result in a weakening of the aortic wall(88).

Folkesson et al investigated the role of membrane microvesicles ADAM10 (a disintegrin and protease -10) and ADAM17 (a disintegrin and protease -17). They demonstrated that ADAM10 and ADAM17 were found in the cell free abluminal area of the thrombus as well as in the aortic media(90). Hypothesising that ADAM10 and ADAM 17 migrated from the luminal to the abluminal surface, and then into the aortic media, thus adding to the degeneration of the aortic wall. A direct mechanistic link between the two was however not found.

LTB_4 is a potent neutrophil chemoattractant and mediator of inflammation. It has been associated with the formation and progression of atherosclerosis(102) and is known to stimulate the release of proteases from granulocytes. LTB_4 is upregulated in the luminal area of the ILT and its levels have been positively correlated with an increase of MMP-9/NGAL complexes in the luminal ILT. In addition, in the adventitia of the aortic wall, there is an upregulation of the BLT_1 receptor (LTB_4 is an agonist)

in the T-lymphocytes, thus suggesting a link between ILT production and inflammatory cell output in the AAA wall. However, although the suggested mechanism is that of proteases and LTB_4 diffusing through the ILT, MMP/NGAL complexes or granulocytes have not been found in the abluminal area(98).

Proteomics studies of the ILT have been performed with a view to biomarker discovery for both the detection and growth of AAAs. Several candidate proteins have been identified, but one of the key findings from these studies is that the ILT selectively sequesters proteins systemically, and these are detectable peripherally(103).

In summary, ILT forms in the majority of enlarging AAAs and it impacts biologically and mechanically on the underlying aortic wall. It's contribution to the local and systemic inflammation is not fully elucidated, though attempts have been made at identifying proteolysins within it. Underpinning the activity of the ILT are various inflammatory cells, and thus far a deep immunophenotyping of the immune cells of the ILT has not be carried out. Most publications have used histology and IHC to identify components of the cellular infiltrate. Characterising single cells through deep phenotyping would aid in the understanding of the biological effects of ILT.

1.7 Flow mediated dilatation and AAA

Flow mediated dilatation (FMD) is a widely recognised risk factor the development of atherosclerosis and future cardiovascular events. It is measured non-invasively and quantified through the response of the brachial artery to forearm compression. Since first being reported by Celermajer et al in 1992(104), it has been

demonstrated to be a reproducible tool for the surrogate physiological assessment of endothelial dysfunction.

AAAs are associated with systemic endothelial dysfunction and increased cardiovascular risk(22, 105-109). Our group demonstrated the value of FMD in predicting AAA growth(16, 110). Furthermore, we demonstrated that FMD deteriorates during AAA surveillance and improves after surgery **(Figure 1.2)**. This led to the hypothesis positing the aneurysm itself as the driver of systemic endothelial dysfunction. ILT has been linked to an increase in oxidative stress and proteolytic enzyme expression at the aortic wall facing ILT (abluminal) (99), and this has potential impacts on endothelial dysfunction and FMD. This body of work aims to explore this and thus gain mechanistic insights into these properties.

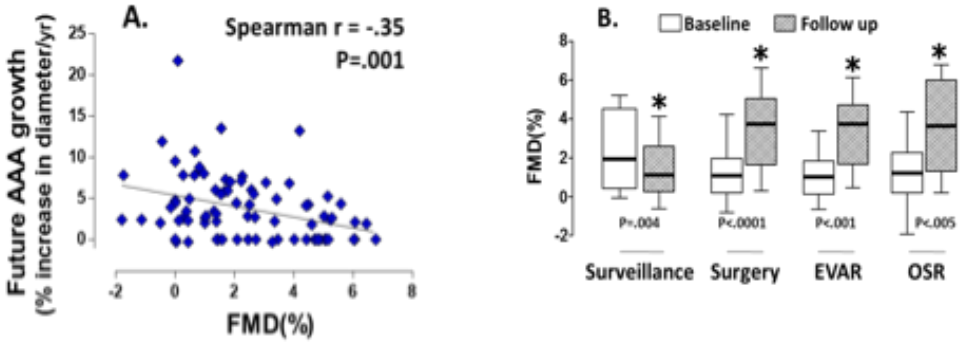


Figure 1.2: Flow mediated dilatation measurements in a cohort of patients with abdominal aortic aneurysms (AAA)

(A) In patients undergoing surveillance scans for AAAs, FMD inversely correlated with future growth. **(B)** FMD deteriorates during surveillance, and when patients are intervened on (OSR and EVAR), their FMD improves. (Figures modified with permission from Dr Regent Lee)

1.8 Conclusion

The aortic wall in AAAs are characterised by SMC apoptosis, elastin degeneration and a chronic inflammatory cell infiltrate. This chronic inflammatory cell infiltrate results in ongoing degradation of the wall and has features suggestive of autoimmunity. ILT is found in the majority of AAA sacs and the contribution of the ILT to the ongoing inflammation in the aortic wall is relatively unknown. Furthermore, FMD is deranged in patients with AAAs and improves after intervention. FMD is a predictor of cardiovascular disease development and patients with AAAs have an independently increased cardiovascular risk.

1.9 Hypothesis and Aims

In this thesis I hypothesised that AAAs (aortic wall and ILT) have a unique immune cell repertoire which underpins the characteristic pathological findings in AAAs, and that the ILT in abdominal aortic aneurysms contributes to the accelerated deterioration of systemic endothelial dysfunction.

Aims

- To standardise the sample retrieval process and optimise the aortic wall and ILT digestion (Chapter 2)
- Demonstrate the presence of immune cells in the tissues (Chapter 3)
- Explore and develop mass cytometry as a technique for deep phenotyping the tissues, anticipating the limitations of flow cytometry (Chapter 3)
- Perform a deep immunophenotyping of the aortic tissues using mass cytometry (Chapter 4)
- Explore a mechanistic link between ILT and endothelial dysfunction (Chapter5)

CHAPTER 2

METHODS

In this Chapter, a general outline of the framework of the larger Oxford abdominal aortic aneurysm study (OxAAA) study is presented, followed by a detailed discussion on the pre-analytical considerations which led to the development of the tissue preparation methods used in the final experiments. There is a particular focus and build up towards optimising the specimens for deep immunophenotyping.

2.1 Ethics and regulatory approval

The OxAAA study protocol was approved by Oxfordshire Research Ethics committee (Ethics reference: 13/SC/0250). This is a prospective, single centre longitudinal observational study of patients with AAA that has been recruiting since 2013. The study was primarily set up to investigate patients through surveillance, and then during their operative and post-operative journeys, collecting several categories of information at sequential time points, with the broad aim of biomarker discovery. This includes demographics, clinical details, growth rates, flow mediated dilatation of the brachial artery, blood and urine samples, and in those who underwent an open surgical repair (OSR), tissue specimens. Participants are also followed up post operatively, collecting similar pieces of information.

In addition, comparator tissue was procured from the Oxford transplant team and consisted of ‘healthy’ aortic tissue. This is covered under the consent for transplant and I was assisted by the transplant team and QUOD biobank personnel with this.

2.2 OxAAA Study design

There are three streams of patients in the OxAAA study **(Figure 2.1)**. Healthy volunteers (HV), stream 1 (S1) and stream 2 (S2) patients. S1 patients are recruited in the surveillance phase of AAA management, they have regular follow ups determined by their clinicians based on the diameter of their AAA at their visit. Only a few S1 patients progressed to surgery, and if it was an open surgical resection (OSR), their intraoperative specimens were collected and processed. The bulk of this research is centred around the S2 patient cohort undergoing OSR. Recruiting involved having a detailed discussion about the study and proposed uses of their tissue samples, allowing them sufficient time to go through the participant information leaflet and ending off with them initialling and signing the consent form.

After recruiting the participants **(Figure 2.2)**, a relevant history was taken as per the clinical record form (CRF), followed by peripheral venepuncture **(Figure 2.2B)**. When logistics around the timing of surgery permitted, their FMD (flow mediated dilatation) was measured **(Figure 2.2C)**. Further details of blood, FMD and specimen collection procedures are described in the following sections.

Figure 2.1: An integrated study workflow, detailing the recruitment and follow up streams of the OxAAA study

The OxAAA study has three streams of participants and recruits both patients with AAA and healthy volunteers. Stream 1 (S1) patients have a AAA that has not yet met the size threshold for an operative repair. They are recruited whilst still in surveillance, and their study appointments are scheduled to coincide with their regular NHS surveillance appointments (TPS-1 and TPS-2). Once they cross the threshold for a repair, they are seen for a pre-operative visit (TP-3) and a follow up post-operative visit (TP-5). Patients who have a AAA and already meet the criteria for an intervention are recruited in to Stream 2 (S2). They have a pre-operative visit (TP-3), post-operative visit and a six monthly follow up. At their initial study visit, participants complete a detailed clinical record form (CRF) which details their demographics, morphometrics, a relevant aneurysm related history and previous medical and surgical histories together with a detailed medication list. This is followed by peripheral venepuncture and flow mediated dilatation (FMD). At each subsequent visit patients have their CRF updated and a repeat of their FMD and bloods. (TP: time point, FMD: flow mediated dilatation) (Diagram courtesy of R.Lee, OxAAA)

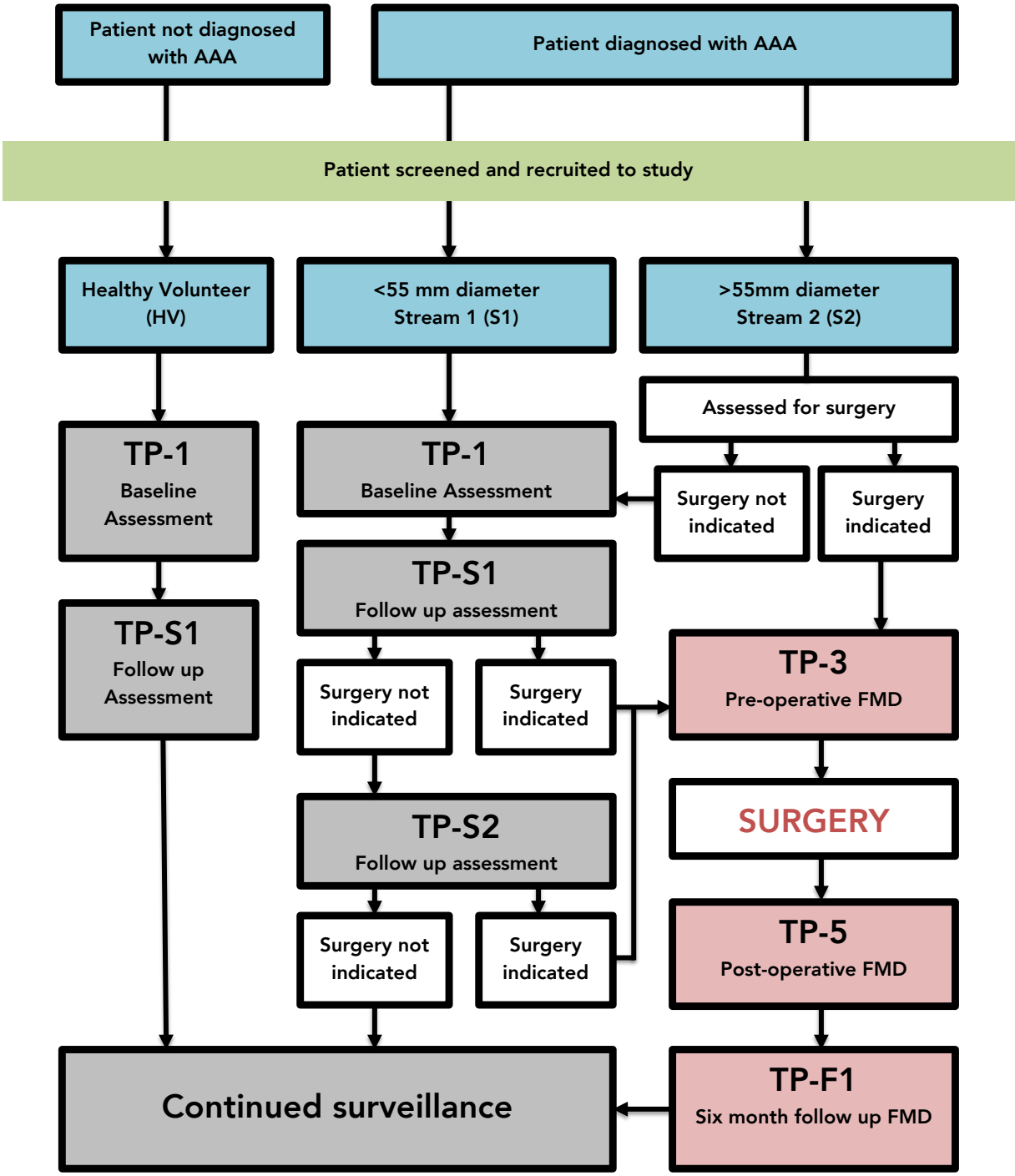


Figure 2.1: An integrated study workflow, detailing the recruitment and follow up streams of the OxAAA study (Diagram courtesy of R.Lee, OxAAA)

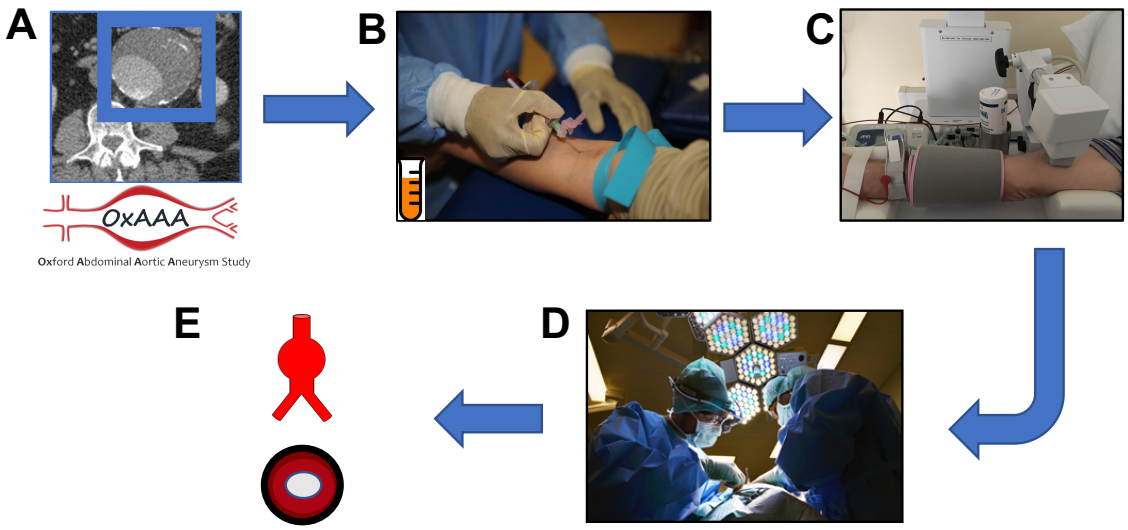


Figure 2.2: Workflow between patient recruitment and intraoperative specimen collection

After patients were discussed in the aortic multi-disciplinary team meeting, they were recruited in to the OxAAA study **(A)**. This was followed by venepuncture in the left arm and FMD measured in the right arm **(B)**. Thereafter, patients were transferred to the operating theatre for the procedure and during the operation **(D)**, several tissue samples were retrieved, most pertinent, the aortic wall and intraluminal thrombus **(E)**.

2.3 Flow mediated dilatation

The latter FMD measurements in this study were recorded using the UNEX-EF machine (UNEX). The UNEX-EF automates several of the steps required for the measurement and analysis in order to perform FMD of the brachial artery. Briefly, prior to beginning the protocol, patients confirm that they have had no caffeine or cigarettes for six hours prior to the test. Using the ultrasound probe on the UNEX **(Figure 2.3A)**, the brachial artery of the right arm is located and the machine attempts to track and find the artery in two planes **(Figure 2.3B)**. Simultaneously, the blood pressure is

measured in the left arm and the systolic measurement is used to determine the inflation pressure of the cuff during occlusion of the forearm. Once the machine tracks and locks the image, locating the intima on either side of the brachial artery in transverse section **(Figure 2.3B)**, the forearm cuff inflates to a supra-systolic pressure for 5 minutes. On deflation of the cuff, the UNEX-EF measures the intima to intima distance on transverse section for a further 90 seconds and calculates the change in brachial artery dilation. This is represented as a percentage, which is the %FMD.

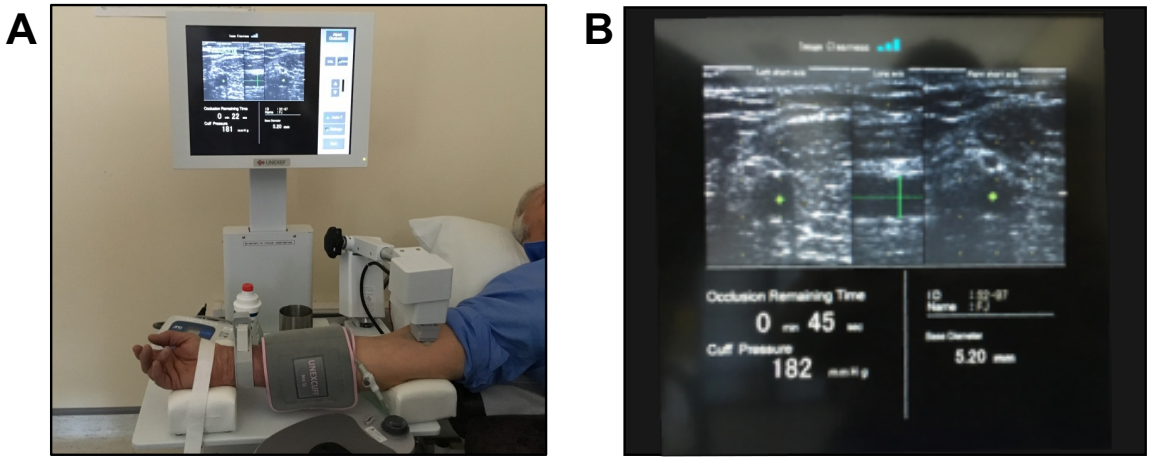


Figure 2.3: Flow mediated dilatation (FMD) is measured using the semi-automated UNEX-EF machine.

Subjects placed their right arm on the machine work surface where it was fixed in a supine position **(A)**. A blood pressure cuff was placed on the right forearm and using the ultrasound probe of the UNEX-EF, the brachial artery was located proximal to the cubital fossa. Once located, the UNEX-EF attempts to track the brachial artery lumen in two planes (right and left short axis) and measured a baseline intima to intima distance in the calculated transverse plane **(B)**. The forearm cuff was inflated to a supra-systolic pressure for 5 minutes. On deflation of the cuff, the change in brachial artery dilation was compared to the baseline. This is the %FMD.

2.4 Specimen collection and biobanking

2.4.1 Blood

Blood was collected in the left arm from the ante-cubital or cephalic vein at the elbow, using a tourniquet. This standardised collection of blood aimed to reduce variability in the subsequent FMD protocol which was performed in the right arm immediately after venepuncture. Thirty millilitres of blood were collected in vacutainers (BD) containing the following additives: Ethylenediaminetetraacetic acid (EDTA), lithium heparin and spray coated silica (SCS) with a polymer gel for serum separation.

Plasma samples were centrifuged at room temperature for 12 minutes at 1300g Thereafter, the plasma supernatants from the blood were aspirated and centrifuged again for 15 mins at 2500g. This two stage centrifugation process results in separation of platelet poor plasma as previously described by Lee et al(111). Whole blood collected in SCS tube was allowed to coagulate at room temperature for 30 minutes before centrifugation at room temperature for 15 mins at 2500g in order to separate the serum from the blood constituents. Care was taken to make sure that this blood had clotted before centrifugation, thus ensuring serum separation and not only plasma separation.

The supernatants were then aliquoted out in to sterile cryovials and frozen at -80^{o}C. Processing of the remaining blood for cytometry experiments will be discussed in more detail in the sections below.

2.4.2 Tissue

Intraoperatively, several specimens were sequentially collected as per the SOP detailed in the OxAAA protocol. These were subcutaneous fat, pre-peritoneal fat, greater omentum, an omental artery, peri-aortic and peri-lliac perivascular tissue, the intraluminal thrombus (ILT) and a strip of the aortic wall. In a designated area of theatre, a pre-prepared trolley housed all the necessary equipment and consumables required for specimen retrieval **(Figure 2.4)**.

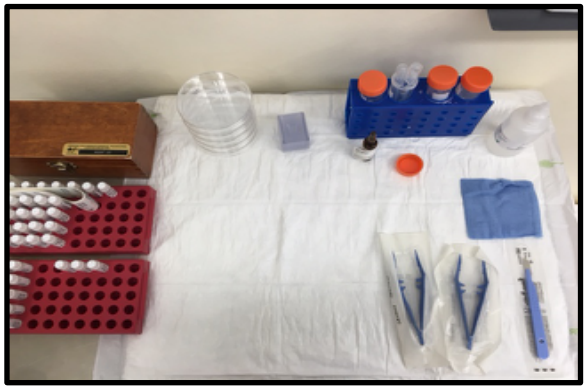


Figure 2.4: Intraoperative trolley preparation

Within the operating theatre a research trolley was set up with the aim of immediately processing the tissue samples. This contained PFA, OCT and cartridges for histology, sterile normal saline, sterile forceps and tissue culture plates together with the pre-labelled cryovials. (PFA: paraformaldehyde, OCT: optimal cutting temperature compound)

Upon entering the abdominal cavity, the surgeon removed a wedge of omentum and an omental artery (OA) was dissected from within it. Some of the omentum was stored in ice-cold RPMI 1640 + FCS 5% for the secretome experiments. The

remaining omentum and OA were biobanked and some was also kept in OCT and PFA. Prior to the aortic clamp being placed, the surgeon marked the maximal area of the aneurysm. Once the clamps were placed, a cranio-caudal incision was made through the aortic sac, and any residual blood was cleared with suction. The ILT was delivered through the aortic incision and was rinsed thoroughly with 0.9% normal saline to remove any contaminating blood **(Figure 2.5)**. This was then split up in to seven pieces, from the luminal and abluminal areas respectively, five were snap frozen and two were kept in PFA 4% and OCT. The remaining ILT was transferred to a 750ml sterile container (Medifor) and placed on ice with 1640 RPMI + 5% FCS for use with downstream experiments.

A cranio-caudal aortic anterior aneurysm wall strip from the renal arteries to the iliac bifurcation was trimmed away, spanning, approximately 15mm in width **(Figure 2.5)**. A Ligaclip® on the proximal (cranial) aspect denoted the orientation of the specimen. The aortic wall was rinsed through thoroughly with sterile 0.9% normal saline to remove any blood and debris. Any visible fat was trimmed off the adventitia and the specimen was split up in to proximal, maximal and distal areas. These were dissected in to several pieces for snap freezing, PFA and OCT as before. The remaining aortic wall was the placed in a 15ml sterile Falcon tube (Corning) with ice cold 1640 RPMI for later use. Processing of the majority of the ILT and aortic wall was carried out on ‘fresh’ tissues and will be detailed in the following sections.

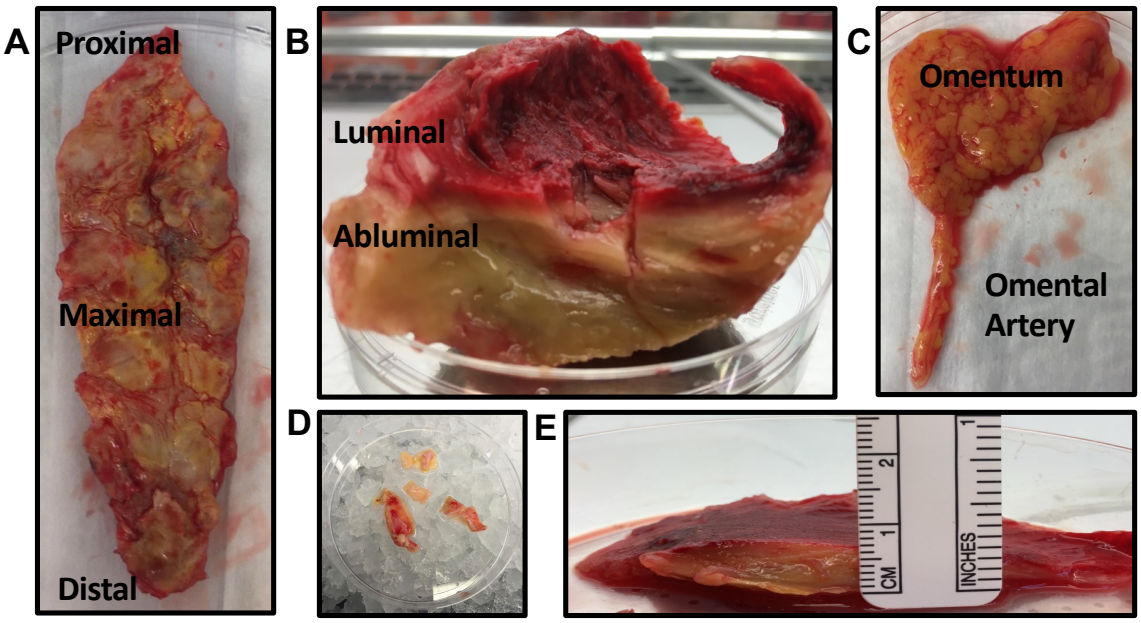


Figure 2.5: Intraoperative specimen retrieval

A strip of the anterior wall of the aortic aneurysm is excised spanning proximally from the renal arteries to the bifurcation of the aorta **(A)**. This picture is of the luminal facing surface after it was rinsed with normal saline to flush away any loose contaminating blood or thrombus. Multiple atherosclerotic plaques are visible on the surface. The strip of aortic wall is dissected in to 3mm x 3mm pieces in preparation for digestion whilst working on ice **(D)**. The intraluminal thrombus (ILT) is delivered from the aortic sac and has distinct luminal and abluminal layers. Often the ILT is a large thick structure but can also be thinner **(E)** whilst still retaining its layered structure. **(C)** Omentum is sampled from the patients, and an omental artery is dissected out and biobanked to be used as 'normal control'.

2.5 Specimen processing

Deep immunophenotyping of the 'aneurysm complex' with modern cytometry techniques posed numerous challenges and required several optimisation steps. These included, methods of digestion, enrichment of specimens and requisite validation experiments (Chapter 3). Moreover, ILT had only been interrogated using FC once before (96), and thus provided minimal guidance from the published literature.

Enzymatic digestion of complex human tissues is common, however, it is also widely recognised that these methods can alter the cellular expression of surface markers critical to cytometry based experiments(112, 113). With this in mind, and being cognisant that both the aortic wall and intraluminal thrombus required enzymatic digestion my aim was to minimise the use of enzymes whilst still retrieving a significant yield of cells that would be representative of the underlying inflammatory infiltrate. To achieve this, the aortic and ILT digestion methods were optimised using patient samples. On reviewing these results, the method of blood preparation was subsequently modified. These will be discussed below.

2.5.1 Aorta and intraluminal thrombus

After apportioning a fraction of the specimens for long term biobanking, the remainder of the 'fresh tissue' was rinsed with sterile normal saline and immediately transferred into a sterile specimen collection pot. This contained ice cold 1640 RPMI (Lonza) supplemented with L-glutamine and 5% foetal calf serum (FCS) and was then stored on ice in a cold storage box until it was transferred to a laboratory fridge (4 – 8^{o}C) immediately after specimen collection.

2.5.1.2 Tissue digestion optimisation

To prepare a single cell suspension from the aortic complex tissues, I adapted an existing protocol in our group that had been optimised on human atherosclerotic plaques(114). Cell yield and viability was compared after trialling several permutations, such as enzyme composition and concentration and cycles of digestion.

The ILT is often a large piece of tissue and has visibly distinct layers. Previous investigators that have isolated cells from the ILT used a combination of

collagenase and elastase in order to digest a smaller portion of the ILT (95, 96). There existed no standardised published protocol in the literature. Sagan et al reduced their digestion protocol from three rounds of digestion to just one with 30 minutes in a 37^{o}C water bath. They also experimented with the use of thrombolytic agents based on a previously published article that used it on coronary thrombus but found that it damaged cells with no increase in the yield of cells. We sought to answer the following methodological optimisation questions whilst refining the protocol for ILT processing:

1. Is enzymatic digestion required?
2. Is elastase required in the enzyme cocktail?
3. Is there an optimal concentration range of collagenase?
4. Does the cell yield increase as a factor of time?

Chronic intraluminal thrombus (ILT) is a unique tissue type that is not found in healthy individuals and has no appropriate positive or healthy control. In the absence of a perfect positive control, I aimed to make the two experimental comparator groups as uniform as possible. The ILT was dissected in 2-3mm squares and homogenised before splitting it up in two experimental groups that were weight matched (35g). These experiments compared viable cell yield after enzymatic and non-enzymatic digestion as well as differences in enzyme concentration, composition and time of digestion.

For instance, to determine the need for enzymatic digestion, I compared the use of enzymes vs. no enzymes in seven patients. After homogenising the ILT and weight matching the two groups to 35g, I added the enzymatic cocktail to one group and only added an equivalent volume of RPMI media (Lonza) to the other **(Figure 2.6)**.

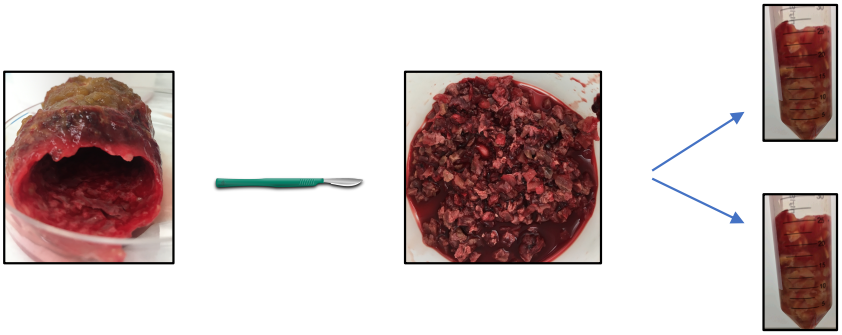


Figure 2.6: Intraluminal thrombus comparator groups

When comparing the effect of experimental conditions on ILT, it was dissected in 3mm squares, then homogenised before being split up in two comparator groups. These groups were then exposed to control and treatment conditions.

They were then placed in a 37°C water bath with an agitator for 40 minutes. Following this, the ILT was cooled in ice to stop the enzymatic processes and rinsed through a 70 µm strainer using a 2ml syringe as a plunger. After rinsing through 45ml of RPMI, the cell suspension was centrifuged at 1300 RPM (368g) for 5 minutes. The cell pellets were then resuspended in a red cell lysis buffer (BD) for five minutes and washed twice with RPMI. This was followed by counting the cells using trypan blue (Life Technologies) in an equivalent volume of the cell suspension (10 µL).

In five of the seven specimens the yield was higher in the enzymatic digested group. In total, there were 38.72 x 10^6 cells in the enzyme digested group and 17.72 * 10^6 in the non-enzyme digested group, with a mean of 5.5 vs 2.5 x 10^6 per sample, favouring the enzymatic digested group **(Figure 2.7)**. With this I concluded that enzymatic digestion was necessary to extract more cells from the ILT.

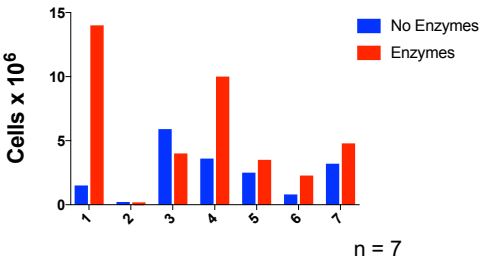


Figure 2.7: Cell yields comparing enzymatic digestion with a control in the intraluminal thrombus

After homogenising and weight matching the ILT, two groups were compared with each other. The first contained the enzymatic mixture suspended in 10mL of RPMI, and the control contained RPMI only (no enzymes). In five of the seven samples there were more cells in the treated group with a mean of 5.5 vs 2.5 x 10^6 favouring the enzymatic digested group.

Similar experiments were conducted with different enzymatic cell mixtures and digestion times. Ultimately, the optimised method of tissue digestion was as follows. The enzyme mixture was prepared beforehand. The enzymes indicated in **Table 2.1** were suspended in warm 10ml of RPMI 1640 cell culture media (Lonza) and filtered through a 40 µm sterile filter (Corning). Collagenase may contain small amounts of trypsin and so trypsin inhibitor was added to inhibit this, as trypsin is known to cleave of cell surface receptors (115). Collagenase performs optimally in the presence of calcium and hence calcium chloride was added. The DNAse was included to bind any free lying DNA that was liberated by dead cells which may lead to spurious results on cytometry staining and the Polymyxin is a prophylactic antibiotic, used to prevent contamination, especially when the cells were cultured downstream.

Table 2.1: Constituents of the enzymatic digestion cocktail

Name	Concentration	Manufacturer
Collagenase	3.9 mg/ml	Sigma-Aldrich
Elastase	3.66 mg/ml	Worthington Labs
DNAse 1	0.65 mg/ml	Sigma-Aldrich
Polymyxin B	2.5 ug/ml	Sigma-Aldrich
Trypsin Inhibitor	0.05 mg/ml	Sigma-Aldrich
Calcium Chloride	0.2 mM/ml	Sigma-Aldrich

Working in a tissue culture hood, over ice, standard aseptic precautions were adhered to. The tissues were dissected into 3 mm square cubes using a size 21 disposable scalpel (Swan-Morton) in a 100 mm tissue culture plate (Greiner), then placed in a 20 ml universal container (Sterilin®) containing the enzyme mixture. This was subsequently incubated in a pre-warmed 37°C water bath for 40 minutes with occasional shaking, removed and immediately placed in ice to stop the enzymatic reaction. The contents were then tipped in to a 70 µm strainer, draining in to a 50ml collecting falcon tube (Corning). Using cold 1640 RPMI media (Lonza), the contents were rinsed whilst being manually disaggregated with the rubber end of a 2ml syringe, topping the falcon tube (Corning) up to 50ml. The falcon tube (Corning) was then centrifuged at 1300 rpm (368g) for 5 minutes at 4°C. After removing the supernatant, 5ml of ammonium-chloride-potassium (ACK) lysis buffer (Thermofisher) was added and allowed to stand for 5 minutes in the tissue culture

hood. This was then washed twice with 40ml of RPMI (Lonza) and centrifuged for a further 5 minutes at 1300 rpm (368g). Cells were counted using a Neubauer chamber with the addition of trypan blue (Life Technologies) after resuspending the pellet in 10 ml of Roswell Park memorial institute (RPMI) 1640 media. The average of four counting blocks was recorded and the concentration calculated. The cell suspension was used for downstream experiments or frozen in 1 ml of FCS and 10% Dimethyl sulfoxide (DMSO, Sigma-Aldrich) mixture for later use.

2.5.1.3 Preparing the matching blood sample

As described earlier in the chapter, venepuncture was deliberately performed prior to anaesthesia in all of the recruited patients. The anaesthetic process may be a contributing factor to changes in blood composition. For the purposes of lymphocyte isolation, the patients' blood was collected in two 8 ml lavender top containing EDTA vacutainer® vacuum sealed sterile tubes (Becton Dickinson) using a 21g needle. Below is a description of the thought processes and methods development for the blood samples. This is followed by validation of the method, and a description of the effect of enzymes and a freeze-thaw cycle on the blood.

PMBC Isolation

The most common method of peripheral blood mononuclear cell (PBMC) isolation is through density centrifugation, and initially this was the method I used. Histopaque® (Sigma-Aldrich) is a mixture of polysucrose and sodium diatrizoate with a density of 1.077 g/ml, thus due to this property, upon centrifugation the components of blood separate out with the denser cells collecting at the bottom of the 50 ml Falcon tube (Corning) and the PBMCs forming a distinct layer in-between. After venesection, the blood was kept at room temperature and transferred to the

laboratory within 6 hours (duration of the operation). Working in a sterile tissue culture hood, I decanted the blood in to a 50 ml Falcon tube (Corning) and topped it up with HANKS balanced salt solution (HBSS, Sigma-Aldrich) to a volume of 20 ml. Thereafter, I gently layered the 20 ml of blood on to an equivalent volume of Histopaque® before centrifugation for 25 minutes at 2500 rpm without the brake in place. Applying the brake after centrifugation may lead to the mixing of the density separated layers. The distinct monolayer was then delicately aspirated, topped up with Hanks balanced salt solution (HBSS, Lonza) and washed and centrifuged at 200g for 10 minutes. Thereafter it was resuspended in 10 ml of RPMI and the cells counted with trypan blue in a Neubauer chamber.

Having optimised the protocol for the ILT and then begun staining it for FC, I noticed that the ILT contained a large proportion of granulocytes. PBMCs by definition are mononuclear, however granulocytes are polymorphonuclear and during the density centrifugation process, they are separated out. I thus changed the method to one that retrieved granulocytes as well.

Density gradient separation

Separating white from RBCs of whole blood falls in to two broad categories. The first involves density centrifugation (similar to Histopaque®) and the second lyses red blood cells (RBC). RBC lysis takes advantage of the property of RBCs to swell and burst when a hypotonic solution containing NH_4CL is added to it, and this is made more susceptible due to their biconcave shape. This lysis is selective to the RBCs and the white blood cells then remain for further analysis.

I experimented with two different types of density centrifugation methods. The first used Lympholyte-Poly® (Tebu-bio) and the second was Percoll® (Sigma-Aldrich). Lympholyte-poly contains sodium metrizoate and Dextran 500 which makes it very viscous. Similar to Histopaque® it is layered on to blood and centrifuged for 25 minutes, and the components should separate in two layers with the RBCs pelleted at the bottom of the tube. However, my results were inconsistent and on matched samples I did not retrieve as many granulocytes as I did with the ACK lysis technique. The second centrifugation technique I used was with Percoll® (Sigma-Aldrich). Percoll® consists of colloidal silica particles which are 15-30nm in diameter and coated with polyvinylpyrrolidone (PVP) which has a 23%w/w. It can be diluted to form different densities (e.g. 70%, 40%) and traps cells of similar densities between the layers after centrifugation **(Figure 2.8)**. It is also thought to be inert with respect to the cells and thus a good choice. However, again, I did not achieve consistent results.

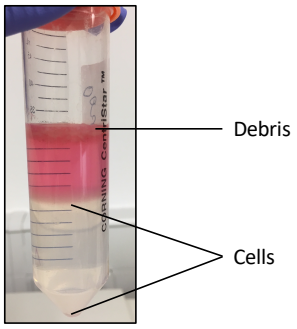


Figure 2.8: Percoll® separates out cells and debris with differing densities

Using varying concentrations of Percoll® the density can be manipulated, to form separate layers. Here it was diluted in two concentrations (70% and 40%), with RPMI containing phenol red used to dilute the 40% layer. After centrifugation, the differing densities separate out, with the dense cells pelleting at the bottom (RBCs and granulocytes), the lymphocytes and monocytes in the intermediate layer and the buoyant particulate debris on the top layer. The lymphocyte layer can then be aspirated for downstream use.

Red cell lysis

I thus explored ammonium-chloride-potassium (ACK) red cell lysis buffer (Gibco). After decanting 16ml of blood in to a 50 ml Falcon tube (Corinig), 21 ml of ACK lysis buffer was added and gently pipetted. After five minutes, the contents were centrifuged (368g at room temperature) for five minutes and the supernatant discarded. Ten millilitres of ACK lysis buffer was then added for a further five minutes and centrifuged for five minutes (368g at room temperature). This was followed by a wash with PBS and the cells were counted in a Neubauer chamber with the addition of trypan blue (Life Technologies) as a cell viability marker. With ACK lysis buffer, I achieved a more consistent and higher yield of granulocytes than with the other methods **(Figure 2.9)**. Thus, going forward, I changed my protocol from using Histopaque® and a density separation method to using ACK lysis.

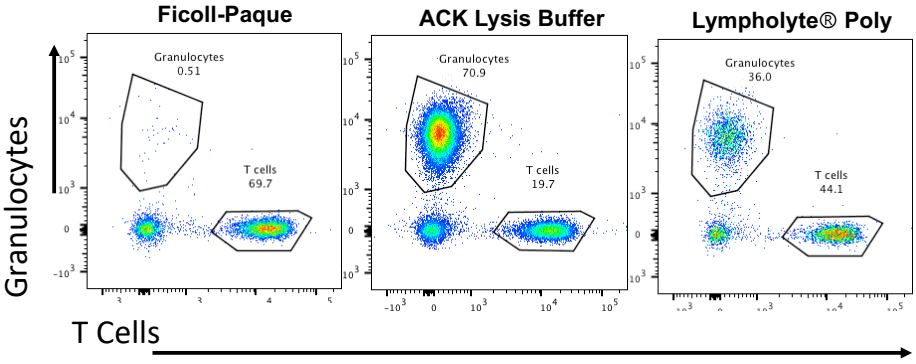


Figure 2.9: Lysing blood with ACK, improves the yield of granulocytes, in comparison to the density centrifugation methods

Peripheral blood was donated by three healthy volunteers (30 ml). This was split in to three groups containing 10 ml each, using a different method for leucocyte retrieval (Ficoll-paque, ACK lysis and Lympholyte® Poly). After retrieving the cells, they were stained for flow cytometry (CD45, CD66b, CD19, CD 11b and CD3).

ACK lysis retrieved the largest fraction of granulocytes (CD66b) as demonstrated in the flow cytometry dot plots. Ficoll-paque is a commonly used density centrifugation method for retrieving lymphocytes and as expected on the flow cytometry dot plots, there were few granulocytes (0.51%). Comparatively the ACK lysis treatment group had 70.9% granulocytes. Lympholyte® Poly did retrieve some granulocytes (36%), though not as much as the ACK lysis group. (ACK - ammonium-chloride-potassium)

I validated the ACK lysis protocol against a full blood count (FBC), as used in routine clinical tests performed by the national health laboratories. After drawing blood from three healthy volunteers, the national health laboratory performed an FBC on the specimens. I compared the percentages of the FBC and ACK lysis to each other **(Figure 2.10)**.

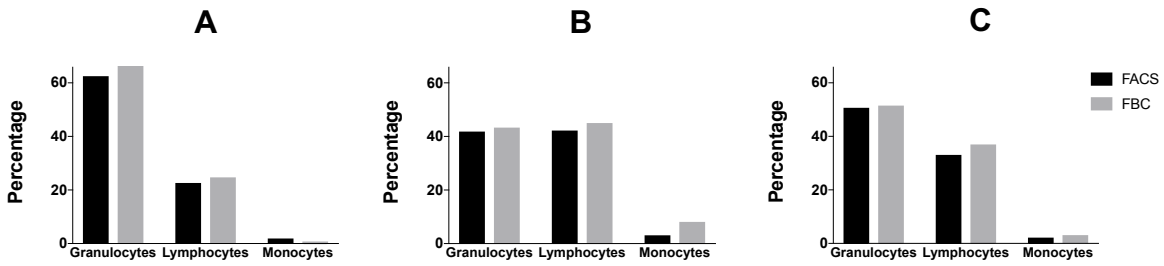


Figure 2.10: Flow cytometry staining on lysed blood compared to a laboratory full blood count

Three **(A, B, C)** healthy volunteers blood samples were separated in two groups. The first was lysed with ACK lysis buffer, and stained with flow cytometry antibodies (CD45, CD66b, CD3, CD11b, CD14). This was then compared to their paired samples using a national health laboratory full blood count (FBC). The percentage of granulocytes, lymphocytes and monocytes are similar using the different methods. (FACS = flow cytometry, FBC = full blood count)

Effect on enzymatic digestion

The ultimate aim was to compare the cell subsets of the blood to the tissues, however the tissue digest contained enzymes. I sought to determine the effect of the enzymatic digestion process on the blood sample **(Figure 2.11)**. In a matching process to the ILT digestion, 8ml of blood was decanted on to a petri dish, sham cut into small pieces, followed by the addition of the enzymatic cocktail and agitation at 37^{o}C for 40 minutes in a water bath. Thereafter, it was placed in ice to stop the

enzymatic process and rinsed through a 70µn filter with cold RPMI (Lonza). The blood was then subjected to the standard method of ACK lysis. After pelleting the cells, they were resuspended and counted using trypan blue. This was then compared to the matched healthy volunteer blood that did not undergo the digestion process, and only the standard ACK lysis step. To do this both specimens were stained with fluorophores for CD3, CD19, CD66b, CD14, CD16, CD33, HLA-DR and a Live/dead™ stain. There was no significant difference between the two groups.

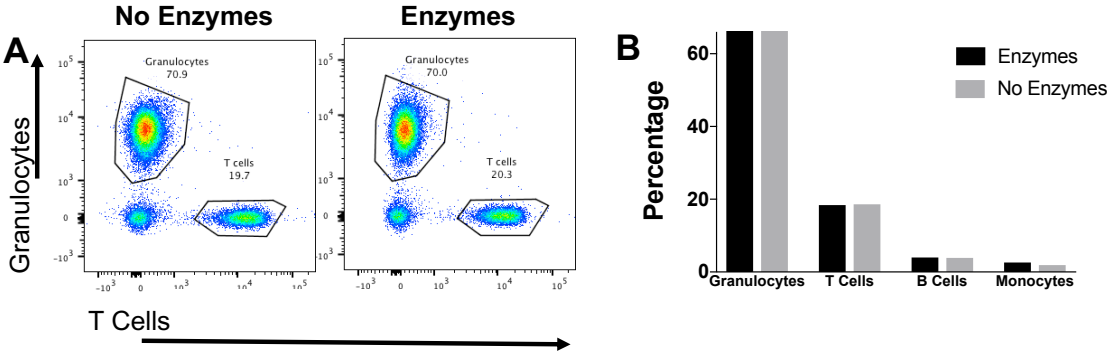


Figure 2.11: A comparison of common leucocyte markers in enzymatically digested blood to a sample with no added enzymes

Blood was provided by a healthy volunteer. After lysing the blood with ACK, the cells were separated in two groups and one was treated with enzyme protocol. The aortic wall and ILT digestion protocol was followed, including sham dissection and an incubation step at 38°C for 40 minutes. The two specimens were then stained with antibodies for flow cytometry and compared (CD45, CD66b, CD3, CD11b, CD14, CD33, CD16, HLA-DR and live/dead). **(A)** The granulocyte and T Cell populations were the same in median fluorescence intensity and **(B)** the percentages of live CD45 cell subsets (Granulocytes, T Cells, B Cells, Monocytes)

Effect of freeze-thaw cycle

Having demonstrated that the enzymes did not have a measurable effect on the surface markers of the major cell types, the next step was determining the impact of the freeze-thaw cycle on the cells. It was widely reported that neutrophils did not survive the freeze-thaw cycle due to their tendency to degranulate on thawing.

However, I observed that ILT specimens used for preliminary optimisation contained CD66b positive granulocytes on FC. To further examine this, after lysing the RBCs using the standard ACK lysis protocol outlined above, I separated the cells in two groups of 3 x 10^6 cells each and stained the first group with the following FC antibodies: CD66b, CD3, CD19, CD14, CD33, HLA-Dr, CD235a, CD41a and a Live/Dead Marker (ThermoFisher). These were analysed immediately (BD LSRII flow cytometer). The second group was frozen in freeze mixture (FCS + 10%DMSO) at -80^{o}C and resuscitated after a week. This was stained with the same antibody cocktail as the first group and also read on the BD LSRII flow cytometer. Comparing the populations that were run immediately to those exposed to a freeze thaw cycle, the CD66b granulocyte population was clearly visible and similar to the 'fresh' blood sample **(Figure 2.12)**. Thus, I resolved to freeze samples and batch process for downstream cytometry experiments.

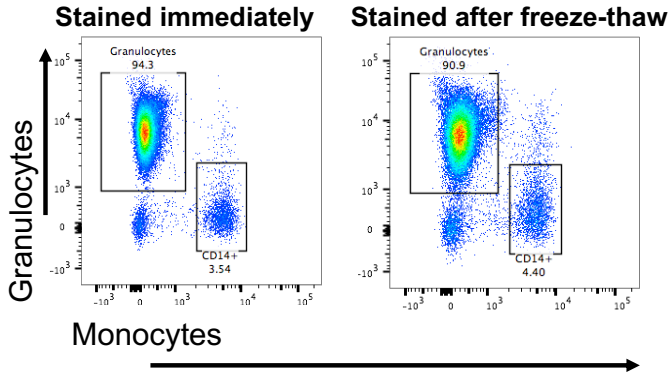


Figure 2.12: The staining of CD66b (granulocytes), before and after a freeze thaw cycle

Whole blood from a single volunteer was lysed using the ACK lysis protocol and separated in two groups. The first group was stained for flow cytometry whilst the second group was immediately frozen at -80^{o}C in 1ml of FCS + 10% DMSO. This group was then resuscitated after a week and stained with the same antibody cocktail as the first group (CD45, CD66b, CD3, CD19, CD14, CD33, HLA-DR, CD235a, CD41a and live/dead). These were read on the BD LSRII flow cytometer and the results compared. There was a slight decrease in frequency from 94% to 90.9%, but the granulocyte population was still clearly visualised.

2.6 Flow cytometry of the aortic complex

2.6.1 General staining for flow cytometry

For characterisation and optimisation of aortic tissues, multi-colour FC using a BD LSRII flow cytometer (BD) was performed on freshly isolated cells from the aortic wall, thrombus and blood (chapter 2.5). The following FC antibodies were used for the majority of the optimising experiments: CD3, CD20, CD14, HLA-DR, CD16, CD33, CD66b, Live/dead Aqua™, CD235a, CD31 (details of clones, fluorophores and vendors in supplementary methods).

The method of FC staining was as follows. Briefly, after counting cells derived from aortic tissues (chapter 2.4), they were washed with 2ml of sterile PBS (Lonza) at 300 g, and their concentration adjusted to between 1 and 3 x 10^6 cells per ml in round bottom 5ml polystyrene tubes. Thereafter, the Live/dead™ stain (Thermofisher) was added at a volume of 150 uL per tube for 10 minutes at room temperature after having been reconstituted as per the manufacturers recommendations by adding one vial of dye to the enclosed 50 uL DMSO, and this was titrated for optimal use (discussed in section 3.5.2). After washing the cells (300 g x 5 minutes) in the wash buffer (PBS +1%FBS), FC block (Miltenyi-Biotec) was added at a concentration of 5 uL per tube for 10 minutes at 4^{o}C, prior to adding the antibody cocktail. The cocktail was made up to dispense 100 uL per sample tube which was kept at 4^{o}C for 30 minutes, and then washed twice with wash buffer (300 g x 5 minutes). After this incubation, the cell pellet was fixed with a paraformaldehyde (PFA) based fixative (BD cell fix), at a concentration of 1:10, diluted in miliQ water for 10 minutes at 4^{o}C prior to washing twice and re-suspending in 200 uL of wash buffer. To protect against degradation of the fluorophores, sample

tubes were wrapped in foil and kept at 4^{o}C until it was read on the flow cytometer. A negative control, where the antibody staining cocktail was omitted, was also included for each type of tissue. Prior to running the specimens, they were filtered through a 35μm cell strainer filter which was attached to a 5 ml round bottom polystyrene tube (BD).

Simultaneously, bead compensation controls were prepared by adding one drop of negative and positive beads together with each fluorophore in separate tubes, as well as a negative compensation control containing beads only. The Live/Dead™ (ThermoFisher) required separate Arc™ compensation beads, as well as an incubation step between the addition of the positive and negative beads. In some experiments, fluorescence minus one controls' (FMO) were prepared by omitting a fluorophore in a tube whilst including the rest of the panel, thus allowing for the detection of background signal and making detection of true antibody staining more accurate.

On the BD LSRII flow cytometer, the DIVA acquisition software was used as an interface. Prior to running the first specimen, a wash cycle was performed to prevent contamination from previous user's samples (bleach, rinse and water run for 5 minutes each). Initially 10000 events were analysed, and the photo-multiplier tube (PMT) voltages of each fluorophore were adjusted and optimised. Following this compensation was performed to correct for the spill over of the fluorescence emission from one fluorophore detected in a detector designed to measure a signal from another fluorophore. This was automated by the DIVA software after setting the negative and positive peaks from the compensation controls. Thereafter each sample together with negative and FMO controls were acquired, collecting a

minimum of 100000 events per sample. The data were exported as FCS files and the FlowJo (TreeStar) analysis software was used for the analysis.

2.6.2 Fluorescence activated cell sorting

Fluorescence activated cell sorting (FACS) was used for cell enrichment and the method will be described. The initial staining steps are similar to FC but instead of an antibody cocktail, staining was limited to the Live/Dead™ and a CD45 antibody.

Briefly, after having attained the cell pellet from the aortic wall and ILT, they were washed with 2 ml of sterile PBS (Lonza) at 300 g for 5 minutes, and their concentration adjusted to between 5 x 10^6 (maximum) cells per ml in round bottom 5 ml polystyrene tubes. Thereafter, the Live/dead® aqua stain (Thermofisher) was added at a volume of 150 uL per tube for 10 minutes at room temperature after having been reconstituted as per the manufacturers recommendations by adding one vial of dye to the enclosed 50 uL DMSO. After washing the cells (300 g x 5 minutes) in the cell staining buffer (PBS +1%FBS+DNase1 1 µL/ml), FC block (Miltenyi-Biotec) was added at a concentration of 5 uL per tube for 10 minutes at 4^{o}C, prior to adding the CD45-FITC antibody. The CD45 antibody was made up by adding 5 µL in 100 uL of CSB per sample tube which was kept at 4^{o}C for 30 minutes, and then washed twice with wash buffer (300 g x 5 minutes). Prior to running the specimens, they were filtered through a 35 µm filter which was attached to a 5 ml round bottom polystyrene tube (BD). Simultaneously, four 5 ml round bottom polystyrene tubes (BD) containing 300 µL of FCS were labelled and prepared for the collection of the post-sorted cells. Tubes were kept on ice and covered with aluminium foil to minimise fluorophore degradation.

The BD FACS AriaII flow cytometer was used for enriching the cells. After initially running 10000 events, PMT voltages were set. As there is no spectral overlap between the two fluorophores being used, no compensation was required. Gates were chosen using forward scatter (FSC) and side scatter (SSC), and then gating on a live CD45 positive population. Both CD45+ and CD45- cells were collected and the aimed flow rate was 10000 events per second. After the collection, the sorted cells were run through the machine to confirm the purity of the sort. The sorted cells were then washed and counted using a haemocytometer before cryopreservation. They were cryopreserved in 1 ml of FBS + 10% DMSO and stored at -80^{o}C, before being transferred to liquid nitrogen for longer term storage.

2.6.3 Magnetic bead selection

Magnetic bead selection was attempted to enrich the aortic complex tissues. A magnetic activated cell sorting (MACS) bead selection kit (Miltenyi-Biotec) with MS columns were used for positive selection of the CD45 fraction from the isolated cells (chapter 2.5).

The principles of magnetic bead selection involve labelling the cell suspension with the CD45 magnetic beads in a MACS column which is then placed on a MACS separator with a magnetic field. The CD45 positive fraction is retained in the column and is then eluted out for downstream applications.

After retrieving and counting the cells from ILT (Chapter 2.5) they were washed (300 g x 10 minutes), resuspended in 80 µL of buffer and 20 µL of CD45 Microbeads (Miltenyi-Biotec) and then incubated at 4^{o}C for 15 minutes. This was then washed in 2 ml of buffer (300 g x 10 minutes) and resuspended in 1 ml of buffer before being placed in a pre-prepared MS MACS column. The column was then placed in the

magnetic MACS separator (Miltenyi-Biotec) and the unlabelled cell effluent collected while the magnetically labelled fraction was retained. The column with the retained CD45 labelled cells was then removed from the magnetic separator and placed in a collection tube, where it was eluted out with buffer and the plunger. This was used for downstream analysis.

2.6.4 Biolegend® LegendsScreen™ antibody array

During panel development, the LegendsScreen™ (Biolegend) was used as a screening tool to detect potential antibody targets. It is a kit, with 361 pre-titrated lyophilised antibodies to surface markers, including 10 isotype controls, on four 96-well plates. This was prepared and run on a BD Canto flow cytometer with an autosampler function for 96 well plate input.

The LegendsScreen™ (Biolegend) kit contains the four 96 well plates as well as cell staining buffer (CSB), Fixation Buffer and plate sealers.

Eight aortic wall and six ILT samples were resuscitated from LN cryopreservation and labelled with CD45 and Live/Dead™ FC antibodies (chapter 2.5.1). Two ILTs and one aortic wall were not amenable to cell sorting due to decreased viability or too much debris in the specimen. Briefly, single cell suspensions were pooled after cell sorting seven patient aortas and four patient ILT samples. This was a total of 5.9 $x10^6$ cells, thus providing a theoretical 15 $x10^3$ cells per well. This is outside the manufacturer's recommendations (3 $x10^5$ per well) but was a calculated concentration from a pre-experiment designed to test the minimum number of cells required for this (additional methods, chapter 7.2) **(Figure 2.13)**.

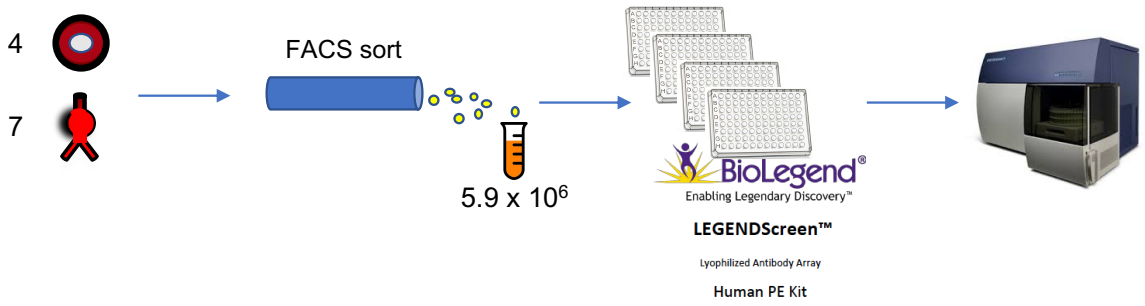


Figure 2.13: Experimental workflow for Biolegend® antibody array

The Biolegend® antibody array comprises 361 lyophilised antibodies conjugated to phycoerythrin (PE) and screens cells for surface marker expression with flow cytometry. Cells were isolated from seven aortic walls and four ILTs (chapter 2.5) and stained with CD45 and Live/Dead™ flow cytometry antibodies (chapter 2.6.1). These were cell sorted (chapter 2.6.2) and the cells were combined to form a total of 5.9 x10^6. They were dispensed in to the pre-loaded 96 well plates (15900 cells per well), incubated, fixed, washed and resuspended in 160 µL. All events were run on a BD Canto flow cytometer.

The cell sorting process for all samples took 9 hours in total, and whilst the latter cells were being sorted, the earlier ones were resuspended in 500 µL of FCS and kept at 4°C. After pooling the cells, they were washed (300 g x 5 minutes) in CSB and re-suspended in 11 ml at a density of 1.1 x10^6 cells/ml before filtering the suspension through a 35 µm filter to remove any clumps. The suspension was then kept on ice whilst the plates were being prepared.

To prepare the plates, they were removed from their aluminium pouches and centrifuged at 600 g for 10 minutes to ensure that the lyophilised cakes were firmly at the bottom of the wells. Thereafter the lyophilised antibodies were reconstituted with 25 µL of deionised miliQ water using a multichannel pipette. To this, 75 µL of the cell suspension was added to each well using the multichannel pipette (changing pipette tips after each row) and left to incubate at 4°C for 30 minutes.

After incubation, the plates were washed twice at 500 g for 10 minutes with 200 µL of CSB. To fix the cells, 100 µL of cell Fixation Buffer was added for 5 minutes and again washed twice at 500 g for 10 minutes with 200 µL of CSB. The pellets were then re-suspended with 120 µL of CSB prior to reading on the BD Canto flow cytometer. Compensations were performed for PE (channel for antibody screen), FITC (channel for CD45) and APC-CY7 (channel for live/dead stain) using beads as described in section 2.6.1

A single well was used to set the compensations and adjust the PMT voltages, and the entire volume was used for the analysis. Using the FloJo software (Treestar), the array was analysed with the following gating strategy**.** All events were analysed, and singlets were gated for (FSC-A vs. FSC-H), then only the Live-CD45 events were selected. The array was designed with an isotype control followed by the surface markers of that isotype in the 96 well plate. The isotype control was then used as a comparison to the stained markers and respective gates of positive or negative staining were set using these **(Figure 2.14)**.

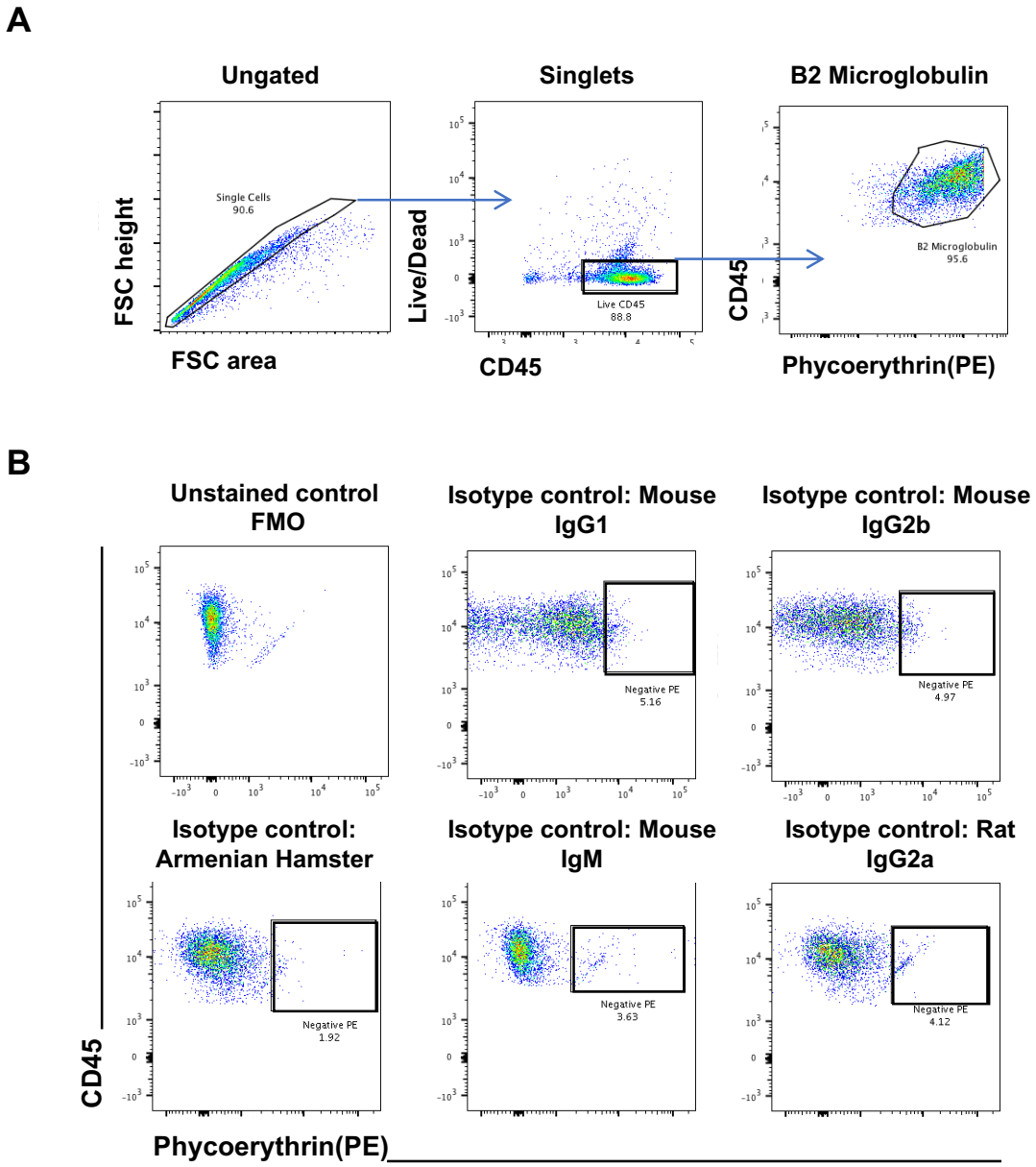


Figure 2.14: Gating strategy for Biolegend® antibody array panel

Single cells were isolated from the aortic wall and ILT of patients after enzymatic digestion (chapter 2.5), enriched for CD45+Live cells with FACS (described in 2.6.2) and pooled. In total, $5.9x10^6$ cells were dispensed in to the pre-loaded 96 well plates and run on a BD Canto flow cytometer (described in 2.6.3). Flow cytometry analysis of individual cell surface markers used the following gating strategy:
(A) Single cells were identified using FSC-Area and FSC-Height to exclude doublets and these were then gated on Live-CD45 events.
(B) For individual marker comparisons, isotype controls were used to set gates and individual antibodies were compared to their isotype matched antibodies in the PE channel. Within the design of the array, 10 isotype controls are used to define gates for their respective markers. Six of these are displayed in the figure above, clearly defining gates for positive and negative expression. (Mouse IgG1, IgG2b, IgM, Rat IgG2a, Hamster and an unstained FMO control)

2.7 CyTOF Methods

2.7.1 General CyTOF staining

For immunophenotyping the aortic complex, time-of-flight mass cytometry (CyTOF) was performed on cells isolated from the aortic wall, thrombus and blood (as described in chapter 2.5). A Helios mass cytometry system (Fluidigm) was used for this.

The process of CyTOF staining is similar to FC staining and can be broken down in to several steps. Initial staining with Intercalator 103Rh (a nucleic acid intercalator that contains natural abundance Rhodium), followed by cell surface staining, then intracellular staining with pre permeabilisation and partial fixation, and finally overnight fixation. The cells are then processed on the Helios machine (Fluidigm). Only MaxPar (Fluidigm) water and MaxPar cell staining media (CSM) are used in the preparation of cells for CyTOF as the system is sensitive to heavy metal contaminants which are commonly found in laboratory reagents.

Briefly, after counting the cells, they are washed in 2 ml of CSM (300 g x 5 min) and the supernatants are gently discarded. Cell-ID Intercalator 103Rh (Fluidigm) was diluted 500:1 using CSM and 1 ml of this solution was added to each sample, re-suspended and incubated at room temperature for 15 minutes. Intercalator 103Rh is a live cell membrane-impermeable dye and therefor only stains dead and dying cells within the sample. Thereafter, the sample was washed twice in 2 ml of CSM (300 g x 5 min) and the supernatant removed before adding 5 µl of FC block (Miltenyi-Biotec) for 10 minutes. Whilst this is incubating the antibody cocktail master mix is dispensed (generally 1 µL per pre-titrated antibody) to a total of 50 µL in CSM. The antibody cocktail is added to the cell sample to give a final staining

volume of 100 µL. This is incubated at room temperature for 30 minutes, then washed twice with 2 ml of CSM.

An eBioscience FoxP3 kit (ThermoFisher) is used for the intracellular permeabilisation and fixation steps. The fixation/permeabilisation concentrate is diluted 1:3 with the diluent (enclosed in the kit), and 1 ml is added to each tube, gently mixing through by pipetting and then incubating for 30 minutes at room temperature. This is followed by two washes (800 g x 5 minutes) in 1X Perm buffer (enclosed in kit and diluted from a 10x solution with MaxPar water) after which the intracellular antibody cocktail is added to the cells, to make a total volume of 100 µL. This is incubated for 45 minutes and washed twice in 1X Perm buffer.

Finally, samples were simultaneously fixed and stained with a second nucleic acid intercalator by addition of 1 ml of a solution comprising 1.6% PFA (Pierce) diluted in MaxPar Fix and Perm buffer (Fluidigm) and containing a 1:1000 dilution of Cell-ID Intercalator-Ir (Fluidigm). After addition to each sample, tubes are mixed and incubated overnight at 4^{o}C. This fixation step serves the purpose of ensuring the cell sample is sufficiently fixed for resuspension in water and acquisition on the Helios (no buffers containing salts can be used on the Helios) and also the Intercalator-Ir is a nucleic acid intercalator containing natural abundance iridium which allows discrimination of single nucleated cells from doublets after acquisition on the Helios.

The following day, prior to analysing the samples, they were washed (800 g x 5 minutes) in 2 ml CSM and then twice again (800 g x 5 minutes) in 2 ml MaxPar water. After counting, they were diluted with MaxPar water containing 10% EQ calibration beads (Fluidigm) to achieve a concentration of 7 x 10^5/ml.

Files were exported in *.fcs* format and normalised before being uploaded to Cytobank for further analysis.

2.7.2 Metal-Antibody conjugation and titration for CyTOF

When available, pre-conjugated and titrated antibodies were purchased from Fluidigm. In total thirteen antibodies were conjugated in-house with a MaxPar antibody labelling kit (Fluidigm). The principle of conjugating antibodies to lanthanide metals involves attaching the lanthanide metal on to a MaxPar polymer, then partially cleaving the sulphide bonds of the antibody and attaching this on to the lanthanide loaded polymer.

The kit contains several buffers (R, C, L and W buffers), together with the polymer and lanthanide solution. Loading the polymer with the lanthanide metal, and partial reduction of the antibody are performed simultaneously, so the duration of exposure of the partially reduced antibody while it is unstable is minimised. This is a critical step. In addition, care must be taken to not touch the filters of the tubes as this could render them porous, thus losing the lanthanide or antibody.

Briefly, the polymer is pre-loaded with the antibody by resuspending it in 95 µL of L-Buffer and incubating it with 5 µL of the chosen lanthanide metal for 30-40 minutes at 37^{o}C. After this, the lanthanide loaded polymer is purified by adding it to 200 µL of L-Buffer in a 3 kDa centrifugal filter unit (Millipore) and centrifuged for 25 minutes at 12000 g. This is followed by a further wash in 400 µL of C-Buffer for 30 minutes.

Whilst purifying the polymer-lanthanide, the antibody is partially reduced by adding 100 µg of the antibody to 400 µL of R-Buffer, adding it to a 50 kDa centrifugal filter tube (Millipore) and centrifuging it for 10 minutes at 12000 g. A solution of dilute 4mM TCEP (Thermofisher) is reconstituted by adding 0.5M TCEP to 992 µL of R-

Buffer and, 100µL of this solution is added to the antibody and incubated for 30 minutes at 37^{o}C. The partially reduced antibody is then purified by washing it twice in C-Buffer at 12000 g for 10 minutes.

The partially reduced antibody is then conjugated to the lanthanide loaded polymer by gently resuspending it in 60 µL of C-Buffer and transferring this to the 50 kDa filter tube containing the partially reduced antibody. The antibody-lanthanide mixture is incubated at 37^{o}C for 90 minutes. After this it is washed 4 times with 400 µL W-Buffer for 10 minutes at 12000 g. After the final wash, the conjugated antibody is resuspended using 100ul of W-Buffer and removed from the 50 kDa filter by inverting it in a new collection tube and centrifuging for 1 minute at 1000 g. The A280 absorbance is measured with a Nanodrop (Thermofisher) and antibody stabilisation buffer (Cantor) is added at a 50:50 volume. This is kept at 4^{o}C until the antibodies are titrated, where it can then be adjusted to its final concentration.

Considerations during panel design included oxidation effects as some metals oxidise at a low frequency(116). This results in ‘bleeding’ or ‘spill over’ of metals in the +1 or +16 position of the periodic table. Other considerations were abundance, metals of similar abundance were placed next to each other and in the +16 position and ‘brighter’ metals were placed in ‘dimmer’ channels and vice versa.

Antibodies that required similar cells for titration were grouped and conjugated together. Cells were labelled with CyTOF antibody lineage markers (CD45, CD3, CD4, CD19, CD14, CD11b, CD66a), to create a ‘mastermix’, then dispensed in equal proportions in to 10 tubes (CyTOF labelling described in section 2.7.1). When available, a positive control tube was created which contained the test antibodies in another metal conjugation. A negative control tube contained only the ‘mastermix’

lineage antibodies. To the titration group, the antibodies were added at a concentration of 8 µg/ml and serially diluted down to 0.0625 µg/ml (8,4,2,1,0.5,0.25,0.125, 0.0625 µg/ml). These were read on the Helios CyTOF mass cytometer and the *.fcs* files exported to Cytobank for analysis. The minimum effective concentration required to identify the cell surface marker was selected.

2.7.3 Overview of CyTOF analysis workflow

The availability of multiple markers on a cell combined with thousands of cells leads to high dimensionality of data that is challenging to interpret and visualise. It allows for several features of a cell to be studied concurrently such as identification, maturation, cell cycle and cytokine production, thus providing a phenotype and testing many hypotheses concurrently. The conventional method of 'gating' and 'subgating' each marker individually would not fully harness the power and depth of the data, whilst making analysis overwhelming when attempting to pair up markers. For example, in an eight-colour FC analysis, in order to visualise all pairs of conventional 2-dimensional plots would require 28 plots but increasing this to 37 parameters requires 666 plots ($n \times \frac{n-1}{2}$) **(Figure 2.15)**. The challenge then, is to create a two-dimensional visualisation without losing the depth of characterisation. The term used in many contexts is the 'curse of dimensionality', which refers to the exponential increase in Euclidian space volume when the number of dimensions is increased(117). Analysis tools for CyTOF data fall in to three broad categories: data visualisation methods (e.g. viSNE), stratifying algorithms which attempt to cluster in an unbiased manner (e.g. PhenoGraph) and methods that compare statistical significance (e.g. CITRUS)(118).

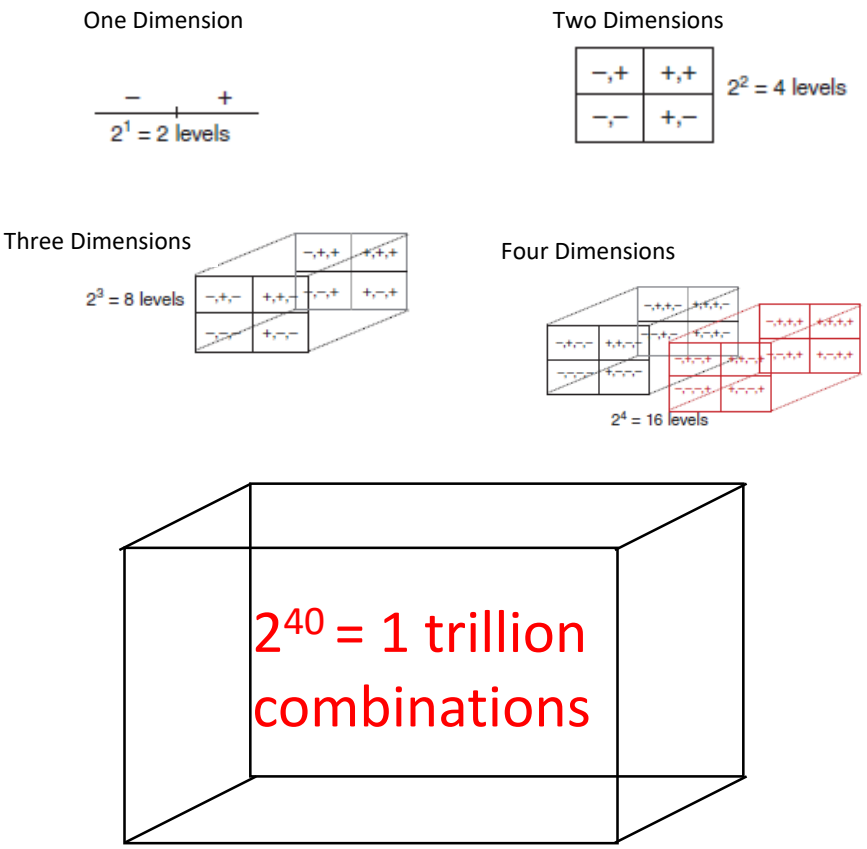


Figure 2.15: The curse of dimensionality

As the number of dimensions is increased, the potential combinations increase exponentially. Thus with 40 markers there are a theoretical 1 trillion combinations

SPADE (spanning-tree progression analysis of density normalised events) is a tool that allows visualisation of data in a tree like scaffold, with the pictorial ability to discriminate between abundant, rare and transitional phenotypes based on nodes and position in an unsupervised manner **(Figure 2.16A)**(119). It uses a density dependent sampling method to avoid down sampling rare events and then connects similar clusters with each other. The number of output nodes is predetermined, and a single cell is placed into a mutually exclusive folder. The size of a node indicates the cell number with the colour highlighting the parameter of interest.

Principal component analysis (PCA) is an older method that uses the variance within a set to make linear variables, however it assumes that the data are parametric(120). It had been adapted for use from other biological data analysis such as gene expression profiles. One of its limitations is that it relies on linear transformation that cannot capture non-linear relationships(121). PCA analysis highlights differences in populations, whereas SPADE analysis clusters around similarities. It is now a less frequently used method of visualising CyTOF data.

viSNE (visualisation of t-Distributed Stochastic Neighbour Embedding) is a more recent and commonly used strategy for visualisation of CyTOF data. viSNE is based on the t-stochastic neighbourhood embedding algorithm (*t*SNE) and allows for the 2-dimensional visualisation of this high dimensional data whilst preserving their geometry(121). The viSNE 'map' looks similar to a biaxial plot but instead of two dimensional data, it is multidimensional. In addition, the map is coloured and can be interrogated by a colour scale of individual marker expression. This again is in an unbiased manner **(Figure 2.16B)**. The difference between it and SPADE is that it does not cluster cells in to mutually exclusive groups, instead assigning each cell a coordinate in a two-dimensional space, grouping similar cells closer to each other, and iterating on this several times until a map of unsupervised clusters forms. Thus, this algorithm in its current form struggles with very large numbers of cells, with a suggested limit of 130000 per viSNE.

PhenoGraph, Citrus, Flow-Map and SCAFFOLD are other examples of data analysis techniques. PhenoGraph **(Figure 2.16C)** uses the R platform and relies on connections between the events to cluster in an unbiased manner. Results can be displayed in the *t*SNE format, similar to a viSNE map. viSNE stratifies events as continuum of phenotypes, whereas PhenoGraph stratifies events in to discrete

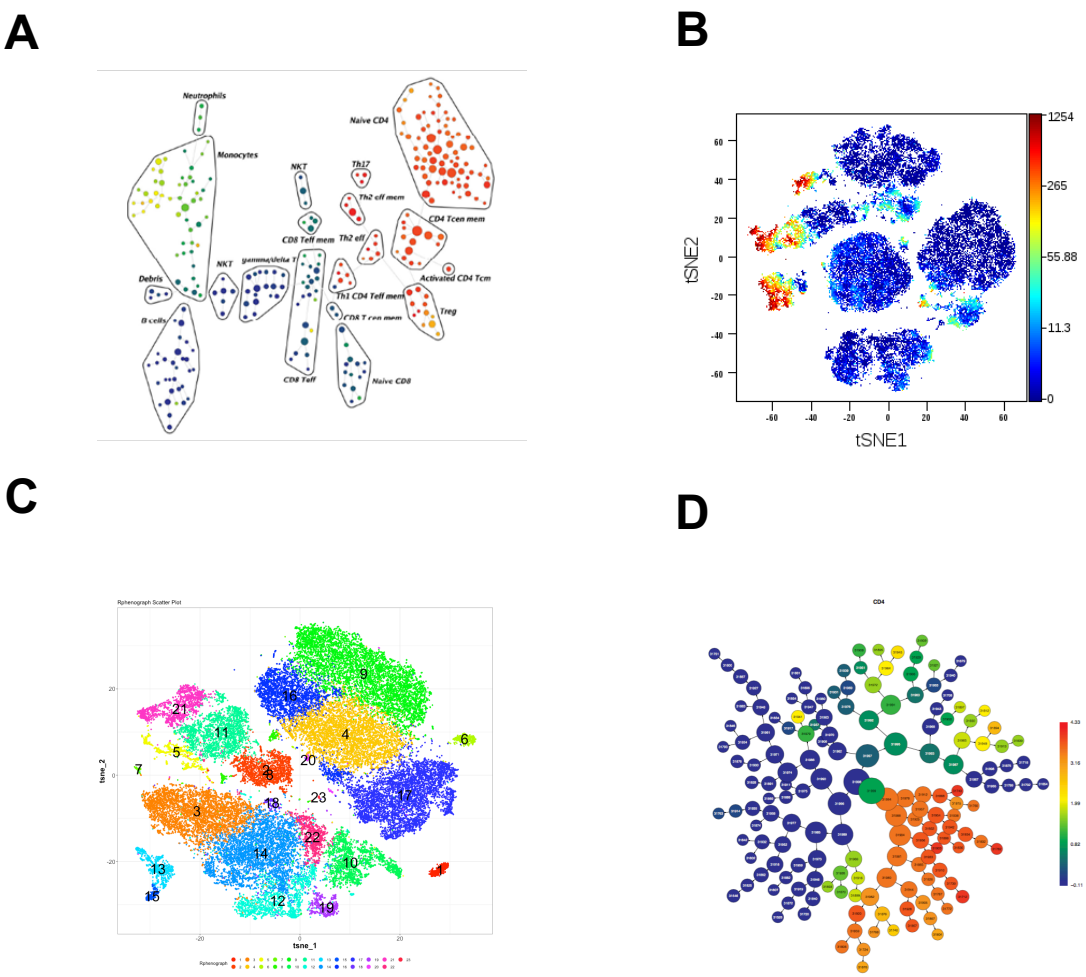


Figure 2.16: Examples of various CyTOF visualisation methods

(A) SPADE diagram of PBMCs analysed by CyTOF. Node size represents the number of cells while colour denotes levels of expression. **(B)** viSNE plot of peripheral blood labelled with markers from the myeloid panel of antibodies (Figure 3.20). Several clusters separate out in an unbiased manner denoting separate phenotypic groups. A further colour dimension highlights Granzyme B+ expression in red, which is found in three phenotypic clusters. **(C)** PhenoGraph derived *t*SNE plot of peripheral blood cells. Each number is a separate cluster as defined by the PhenoGraph algorithm. **(D)** Citrus plot of peripheral blood separated in two groups.

phenotypes(122). The Citrus (cluster, differentiation and integration) algorithm was designed to extract statistically significant differences between two experimental populations(118) **(Figure 2.16D)**. This is a growing field, and as biological questions

are increasingly left wanting by the current analysis techniques, new ones will invariably develop.

For the final analysis of the specimens, their *.fcs* files were normalised then imported in to Cytobank®. Cells were gated on CD45 events, then viSNE analysis was performed on these, clustering on the main phenotypic markers. Then, clusters of interest (from the viSNEs) were exported and further interrogated with PhenographR for a deeper profiling, which separated the phenotypic groups in several agnostic clusters. These clusters were then matched to known phenotypes and named when possible.

2.8 Mechanistic experiments on tissue secretome

A central hypothesis of this thesis was that the ILT acts in a paracrine/endocrine manner to liberate substances that result in local and systemic changes. In order to test this, a representative physiological sample of the secretome was required. When developing the methods, two of the major pre-analytical considerations taken into account were the anticipated method of downstream analysis and the appropriate inclusion of adequate controls.

One of the interests and expertise of our group is proteomics. Foetal calf serum (FCS) is regularly used as a media supplement in the tissue culture process in order to nourish cells that are out of their natural environment. However, when using a mass spectrometry method such as proteomics, FCS can make the analysis unreliable as it contains numerous proteins which potentially confound analysis of the specimen. So, when determining the methods to condition the media this was a key consideration and hence, we decided to serum starve the tissues and we conditioned them in a tissue culture incubator at 37^{o}C with 5% CO_2 in RPMI 1640 with L-Glutamine (Lonza). RPMI is widely used as a tissue culture media supplement for human lymphocytes.

The second pre-analytical consideration was the inclusion of appropriate controls for the thrombus conditioned media. From the individual patients I had collected aortic wall tissue and omentum. These could serve as biological controls but were not a direct comparator to the thrombus. The aortic tissue, in itself was of interest as the hypothesis included the ‘aortic complex’, of which the aortic wall forms a part of. As a control for this aneurysmal aortic tissue I conditioned media from the aorta of deceased transplant donors. The omentum is an entirely different type of tissue

to both the thrombus and the aortic wall but could potentially serve as unique biological “negative” control. However, the effects of the omentum were also unknown as omentum is rich in adipokines, adiponectin and leptin(123-125) which may induce downstream biological effects independently. The inclusion of omentum supernatant as a comparator/control is thus more stringent than a negative control alone. Another potential comparator/control was clot formed ex-vivo using the patient’s own blood. After careful consideration this was not utilised, as thrombus formed in the arterial system is very different to clot formed *in-vivo* by allowing blood to stand at the bench side (stasis)(126). Clot formed at the bench side develops as a result of the clotting cascade and does not rely on platelet activation, whereas clot formed in the arterial system usually forms as a result of initial platelet activation(127). In addition, the ILT of aortic aneurysms are chronic and laminated, and not acute like the bench side formed clot. Acute clot is known to cause a significant inflammatory response in diseases such as DVT(128). Even in the treatment of aneurysmal disease, the post implantation syndrome is associated with the volume of new onset acute thrombus that is laid down after EVAR(129).

2.8.1 Conditioning media with the tissue secretome

Working under sterile aseptic conditions in a tissue culture hood, six pieces of each tissue type (ILT, aortic wall, omentum, transplant aortic tissue) were dissected out in 3mm X 3mm blocks and placed in a 6-well plate (Corning, USA) and resuspended in 2ml of RPMI 1640 + 5% FCS. One well was used as a control, following the same sequential washing and media change steps with no tissue in it. The 6-well plates were then placed into the incubator at 37^{o}C with 5% CO_2.

Giving the tissue a chance to recover and equilibrate, after an hour they were removed and washed with pre-warmed PBS (Lonza) and then serum free RPMI media (Lonza) was added. After 24 hours in the incubator, the plates were removed, and the conditioned media was collected. It was then centrifuged at 3000g for 10 mins to pellet the remaining cells and cellular debris, and the secretome supernatants were then aspirated and stored at -80°C in 250µL aliquots (Cryovial) **(Figure 2.17).**

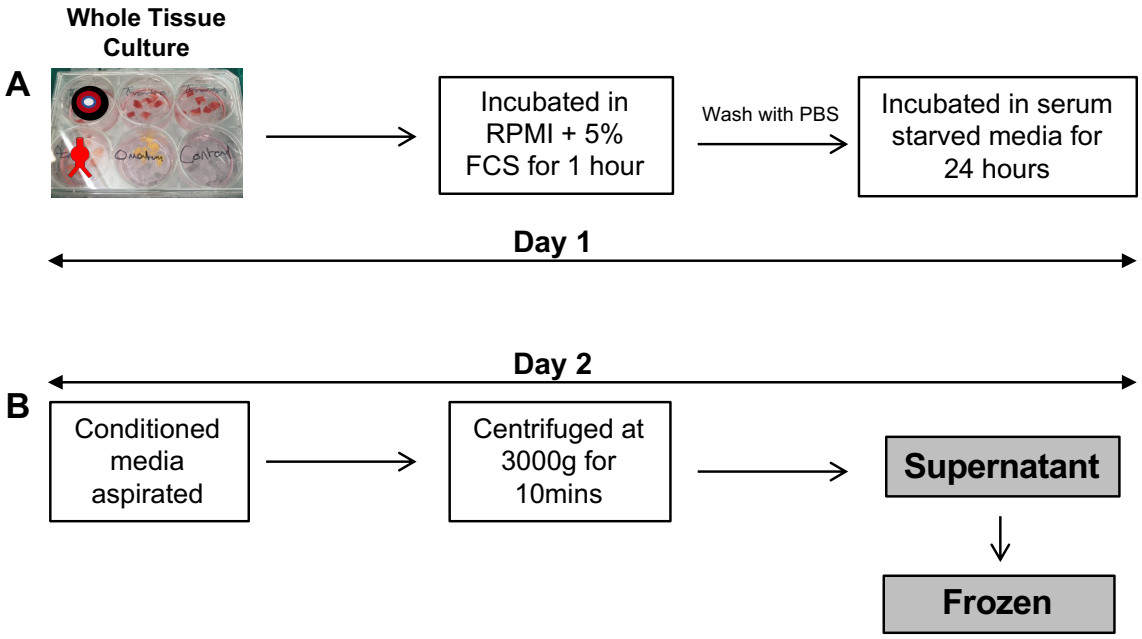


Figure 2.17: Workflow for conditioning media with aortic and ILT tissue

Aortic, ILT and omental tissue were dissected out in to 3mm pieces and placed in individual wells of a six well plate, together with RPMI 1640 supplemented with 5% FCS **(A)**. This was then equilibrated at 37°C for an hour, followed by a PBS wash and 2 ml of serum free RPMI 1640 in each well. After 24 hours in the incubator **(B)**, the conditioned media was then aspirated and centrifuged for 10 minutes at 3000 g before being removed and frozen(-80°C) in 250 uL aliquots.

2.8.2 Using the protein concentration of the tissue secretome as a means of comparison

To compare samples, their concentration was determined and normalised to their total protein concentrations. Protein concentrations can be assessed using several methods, each with advantages and disadvantages. The commonly used colorimetric methods are the Pierce BCA assay, the Bradford assay, and the Nanodrop™(Thermofisher Scientific) which measures absorbance at a fixed wavelength using a spectrophotometer. The Nanodrop™ and Bradford use the absorbance of aromatic protein residues, and therefore they act as a surrogate for total protein concentration and are dependent on these aromatic rings being present(130). The Pierce BCA assay is not dependant on known proteins and makes use of the biuret reaction, in which contact with protein chelates Cu^{2+} ions and reduces them to Cu^{1+} ions(131). The Cu^{1+} ions then react with bicinchoninic acid (BCA) to form a purple-colour that absorbs light at 562 nm. This is then compared to an albumin standard curve.

Using the Pierce BCA assay kit (Thermofisher), Compound A and Compound B are mixed together in a dilution of 100:2, and 100 uL of this is added into the test, control and standard wells of a 96 well plate. To this, 12.5 µL of the test compound and control are added in duplicates, together with a standard dilution of albumin standards. This is then placed at 37^{o}C in an incubator for 20 minutes. Thereafter, it was read on a FluorStar Optima plate reader (BMG Labtech). Values are subtracted from the control media and measured in mg/ml against the standard.

2.8.3 Determining the non-toxic concentration of the tissue secretome for use in gene expression studies

After conditioning the media with the tissue secretome and determining their protein contents, the initial experiments utilising the thrombus supernatants demonstrated widespread cytotoxicity in retinal pigment epithelial-1 cells (RPE-1) (chapter 5.4.2). The culture conditions created a concentrated supernatant which if used for downstream experiments would not be 'physiological'. To determine the sublethal yet appropriately 'physiological' concentration of the tissue supernatants, a kinetic cytotoxicity assay was used (CellTox^{TM} Green, Promega). This assay uses a proprietary cyanine dye which binds to free lying DNA liberated from cells with compromised membranes. The dyes fluorescence properties are enhanced by DNA binding when excited by a 485-500nm wavelength laser, and this fluorescence is then quantitively proportional to the number of dead cells.

For this study 3 x 10^4 cells/ml HUVECs were seeded into a 96-well plate and incubated overnight at 37°C in 5% CO_2 in endothelial cell basal media (EBM) with a BBE kit (ATCC). The 96 well plate used was black with flat bottomed wells and opaque side walls in order to prevent interference from adjacent wells. Before being stimulated with the supernatants, the wells were individually inspected to ensure confluence and the absence of bacterial contamination. Thereafter, the old media was removed from the wells with a multichannel pipette and the CellTox^{TM} Green dye was added and a single reading was captured on the analyser. This is a deviation from the protocol as one of the pitfalls of the standard method was that it did not account for any free lying DNA that already existed in the wells before

stimulation. So, to address this, I added the dye prior to stimulation to extract a baseline fluorescence reading from each well.

Thereafter, the secretome supernatants were added, having been already pre-warmed to 37^{o}C and pre-aliquoted out in 96 well plate to minimise differences in times of stimulation. The cells were then incubated at 37°C with 5% CO_2 in a FLUOstar Omega (BMG Labtech) plate reader for 24 hours, and the fluorescence measured at 485–500 nm excitation and 520–530 nm emission wavelengths. Readings were taken at five-minute intervals. Positive and negative controls were used by adding cell lysis buffer and equal volumes of cell culture medium to the cells, respectively. Two negative control culture mediums were used, the one the HUVECs were cultured in (EBM, ATCC) and the RPMI 1640 (Lonza) that the tissue supernatants were conditioned in.

The concentrations of the secretome supernatants were based on the protein concentration determined by the BCA assay. Supernatants were diluted down to concentrations ranging from 5 x 10^{-1} mg/ml down to 1 x 10^{-3} mg/ml of protein. Appropriate biological and technical replicates were used, and the assay was repeated three times.

2.8.4 Determining lipopolysaccharide (LPS) levels in the ILT secretome

Having determined the concentration of protein in the secretome supernatants and then establishing biological activity, LPS concentrations were measured in the ILT secretome to exclude contamination as a confounding source of biological activity. LPS is the major constituent of gram-negative cell membranes, and can elicit a major immune response which can ultimately lead to septic shock(132).

The test was performed with the Thermofisher LPS chromogenic assay kit (catalogue number: 88282). The principle of the assay is that bacterial endotoxin catalyses the reaction of activating proenzyme *Limulus amoebocyte lysate* (LAL), which in turn catalyses the splitting of p-Nitroaniline from the colourless chromogenic substrate and this results in a colour change. The colour change is measured on a 405 nm plate reader and this change is proportional to the sample endotoxin concentration. This is then compared to a standard curve made from a dilutions of the supplied endotoxin (*E. coli* 0111:B4). The results are quantified in endotoxin units per ml (EU/ml), where 1 EU/ml approximates 0.1 ng/ml of endotoxin. LAL is prepared from the circulating amoebocytes of the horseshoe crab *Limulus Polyphemus*.

In brief, the endotoxin is reconstituted with 1 ml of endotoxin free water and vortexed vigorously for 15 minutes. Thereafter it is diluted to make a 1 EU/ml solution, and serial dilutions from 1 EU/ml to 0.1 EU/ml (1/ 0.5/ 0.25/ 0.1 EU/ml) were made in separate 1.5 ml endotoxin free Eppendorf tubes. These concentrations are used for a standard curve. Whilst the 96 well microplate (Corning) was being temperature equilibrated (37^{o}C) in the incubator, the LAL is reconstituted by adding 1.4 ml and the chromogenic substrate was reconstituted by adding 6.5 ml of endotoxin free water (2mM).

Once the microplate is at 37^{o}C, 50 μL of the standards are added in duplicates, followed by 50 μL of each test sample in duplicates. To this, 50 μL of the LAL substrate is added, and the plate is incubated at 37^{o}C for 10 minutes. Thereafter, 100 μL of the chromogenic substrate is added to the wells of endotoxin standards and the test samples and incubated for a further 6 minutes. The reaction is then

stopped with 100 μL of 25% acetic acid and was read on the FlurostarOptima plate reader (BMG Labtech).

2.8.5 Heat inactivation of the ILT supernatants

With the aim of denaturing the protein content of the ILT secretome supernatants, they were heat inactivated.

For this, three subjects ILT secretome supernatants were aliquoted from their cryovials in to a polystyrene FACS tube (BD). Simultaneously a heat block was pre-heated to 100^{o}C and once the temperature was reached, the tubes were placed in the heat block for 10 minutes. An independent thermometer was inserted alongside to ensure that the heat block was indeed accurate. The heat inactivated supernatants were then used for downstream experiments.

2.8.6 Filtering the ILT supernatants

Suspecting that the ILT supernatants had an active protein/s in them, a filter was used with the aim of finding a size range of the active protein/s.

A 5kDa Vivaspin® filter tube (Sigma-Aldrich) with a polyethersulfone membrane was used for this. ILT supernatants (250 μL) were added to the spin columns and centrifuged at 15000 g for 30 minutes. The filtered portion was then retrieved and used for downstream experiments. To confirm that the protein content had indeed reduced in the 5kDa filtrate, a Pierce-BCA assay (methods chapter 2.8.2) was performed on the samples and compared to their matching unfiltered controls.

An attempt to retrieve the residual concentrated portion that was left on the filter was unsuccessful. Trifluoroethanol was added to the membrane and allowed to dry, then washed and the residual collected. A control sham retrieval was run alongside

this, and the control was found to be highly cytotoxic to RPE-1 cells used in downstream experiments and thus the results from the residual portion on the filter were disregarded.

2.9 *In-Vitro* cell culture

2.9.1 Human Umbilical Vein Endothelial Cells (HUVEC) used for determining the non-toxic concentration of the tissue secretome

Human Umbilical Vein Cells (HUVEC) stored in our liquid nitrogen container at passage two were resuscitated and expanded for use in the cytotoxicity optimisation experiments (Lot. 1069, 21/11/05). These cells were removed from liquid nitrogen, transported on dry ice to the tissue culture area, warmed up rapidly in a pre-heated 37^{o}C water bath, disinfected with 70% ethanol and placed in 5mL of pre-warmed endothelial cell basal media (EBM, Lonza). This media was supplemented with the Lonza Clonetics™ EGM-2 Bullet kit which contains hydrocortisone, 2% FBS, human fibroblast growth factor basic (hFGFb), human vascular endothelial growth factor (hVEGF), Analog of Human Insulin-Like growth factor-1, ascorbic acid solution, human epidermal growth factor (hEGF), gentamycin, amphotericin-B and heparin.

The cells were suspended in 35 ml of pre-warmed and supplemented EBM and then seeded into a T-150 cm^3 cell culture flask (Corning) and placed in an incubator at 37^{o}C with 5% CO_2. Prior to seeding, the cells were counted in a Neubauer chamber with trypan blue dye (Life Technologies). Cells were checked daily for signs of contamination and to monitor growth. The media was replenished every 48 hours until they had reached confluency.

Once the cells reached confluency (70 -80%), they were passaged. For this, the media was aspirated, and the flask was washed twice with PBS (Lonza). This step

removes traces of FBS, which renders the following trypsin step less effective. Then, 10 ml of pre-warmed trypsin was added, and the flask was placed in the incubator for 3-5 minutes and checked intermittently until the adherent cells had lifted of the flask. Once the majority of the cells were in suspension, 10 ml of trypsin inhibitor was added, and the suspension was transferred to a 50 ml Falcon tube (Corning). This was followed by a further two wash outs of the flask with PBS. The Falcon was then centrifuged at 200 g for 5 minutes, resuspended in 5 ml of EBM and counted. To increase cell stocks, vials were stored at a density of 2 x 10^6 cells/ml with FBS and 10% DMSO (Sigma-Aldrich) at -80^{o}C for 24 hours. Thereafter it was transferred to liquid nitrogen for long term storage. The remaining 1 x 10^6 cells were seeded in to a T-150 flask (Corning) for use in the cytotoxicity assay.

2.9.2 Aortic Endothelial Cells (AOEC) used for determining the gene expression of the tissue secretome

Primary human aortic endothelial cells (ATCC®, PCS-100-011™) were purchased from LGC STANDARDS and stored in liquid nitrogen until required. The cells are frozen at passage 2 and were guaranteed for at least 15 passages.

For studying gene changes in response to stimulation of the tissue secretome supernatants, the cells were cultured according to the manufacture's recommendations. Briefly, prior to retrieving a vial from liquid nitrogen, complete media was made up by the addition of a BBE-kit (ATCC, 100-040) to the vascular cell basal medium (ATCC, 100-030). The BBE-kit contains 0.2% Bovine brain extract (BBE), epidermal growth factor (rhEGF), L-glutamine, heparin sulphate, hydrocortisone hemisuccinate, 2% FBS, ascorbic acid and penicillin-streptomycin

with Amphotericin-B. The vial was then rapidly warmed in a 37^{o}C water bath, sterilised with 70% ethanol and the contents aliquoted out into a T-150 flask with prewarmed media. The cells were left to settle and adhere in the incubator for 48 hours prior to changing the media and were sub-cultured once they reached 70 – 80% confluency. The process of sub-culturing is the identical to that used with the HUVEC cells (section 2.9.1).

2.9.3 Human retinal pigment epithelial-1 cells (RPE-1) used for demonstration of biological activity in the tissue secretome

RPE-1 cells are used within our group (Dr N. Zanin and Miss. A. Robinson) for the demonstration of nuclear factor kappa-light-chain-enhancer of activated B cells (NF-κB) nuclear translocation downstream to activated toll-like receptors (TLR). RPE-1 cells are an immortalised cell line kindly provided by Dr C. Lamaze's group (Institut Curie, Paris). They were cultured as sub-confluent monolayers (80% confluency) in a 100 mm cell culture plate (Greiner) and maintained in Dulbecco's modified Eagle's medium (DMEM) (Sigma) supplemented with 10% FCS (v/v) (Labtech). Prior to seeding on coverslips in a six well plate for the immunofluorescence experiments, they were sub-cultured. After warming the Accutase™ (Sigma-Aldrich) at 37°C, the plates were washed with PBS (Lonza) and 1ml of Accutase™ was added to detach the cells, and then incubated for 5 minutes. The cells were then aspirated and placed in a 15ml Falcon tube (Corning) and centrifuged at 200 g for 5min at room temperature. The cell pellet was resuspended in DMEM and counted with trypan blue (Life Technologies) before being seeded at a density of (250 000 cells/ml) on a 6-well plate with 4 coverslips per well. Once confluent on the coverslips, they were used for the downstream immunofluorescence experiments.

2.10 Human retinal pigment epithelial-1 cells (RPE-1) used for NF-κB nuclear translocation

After conditioning the media with the tissue secretome supernatants, the activation status of the RPE-1 cells was examined. The RPE-1 cell line (culture methods described above), have been optimised in our laboratory with respect to NF-κB nuclear translocation downstream to several TLRs activated by their associated ligands. In my experiments, the translocation of NF-κB from the cytoplasm to the nucleus was investigated by immunofluorescence. The principles of the technique can be split up in to four parts: Preparation of the RPE-1 cells (discussed above), stimulation of the RPE-1 cells with a ligand, immunofluorescence staining for the subunit p65 of NF-κB (1:100, sc-372, Santa Cruz) with a primary antibody and a secondary antibody coupled to a specific fluorochrome (1:200, anti-Rabbit Alexa 488, Abcam), and lastly imaging and quantification of the cells.

The RPE-1 cells were seeded on to coverslips at least twenty-four hours prior to the immunofluorescence experiment. The test compound (tissue conditioned media) together with positive (TLR2 and TLR9 ligands) and negative controls (DMEM F12, RPMI) were placed in a 24 well plate containing the confluent RPE-1 cover slips. This stimulation continued for 40 minutes in the incubator at 37^{o}C with 5% CO_2. After stimulation, the reaction was halted with cold (4^{o}C) PBS, and the cells were then fixed with 4% paraformaldehyde (PFA, ThermoFisher) for 7 minutes at 4^{o}C. Ammonium chloride (NH_4CL) was subsequently added to quench the free aldehyde groups for 10 minutes, before permeabilising the cells with 0.1% Triton X-100 (Sigma) for a further 10 minutes. In order to decrease the non-specific biding of antibodies, the cells were also incubated with 0.2% bovine serum albumin (BSA, Sigma).

A square of laboratory film (Parafilm) was attached to the bench-top and marked out with grids replicating the experimental layout of the 24 well plate. The primary antibody against NF-κB at a dilution of 1:100 was then pipetted on to the grids of the laboratory film in a 30μL droplet and the coverslips, with the cells facing the droplet, were placed on it. This was incubated at room temperature for 45 minutes followed by 3 washes in PBS-0.2%BSA. Then, following the same methodology the cells were labelled with the secondary antibody, an anti-Rabbit Alexa488, at a dilution of 1:200 for 30 minutes at room temperature. The coverslips were then mounted on to a slide with 3μl of Fluoromount-G™ (Life technologies) which contain 4′,6-diamidino-2-phenylindole (DAPI) (Sigma), a DNA intercalant that allows the visualisation of the nuclei. Then the slides were left to dry overnight.

On the following day, images were captured on an Olympus BX51 microscope using the Alexa488 (green) and DAPI (blue) channels. Thereafter, further image analysis was performed on ImageJ (public domain) software which was used to merge the Alexa488 and DAPI channels in order to identify the nuclei within the cell. A minimum of 4 images were captured per sample. A proprietary plug-in software program was used to quantify the NF-κB translocation into the nucleus.

2.11 Real-Time Quantitative Polymerase Chain Reaction (RT-qPCR)

2.11.1 RNA isolation

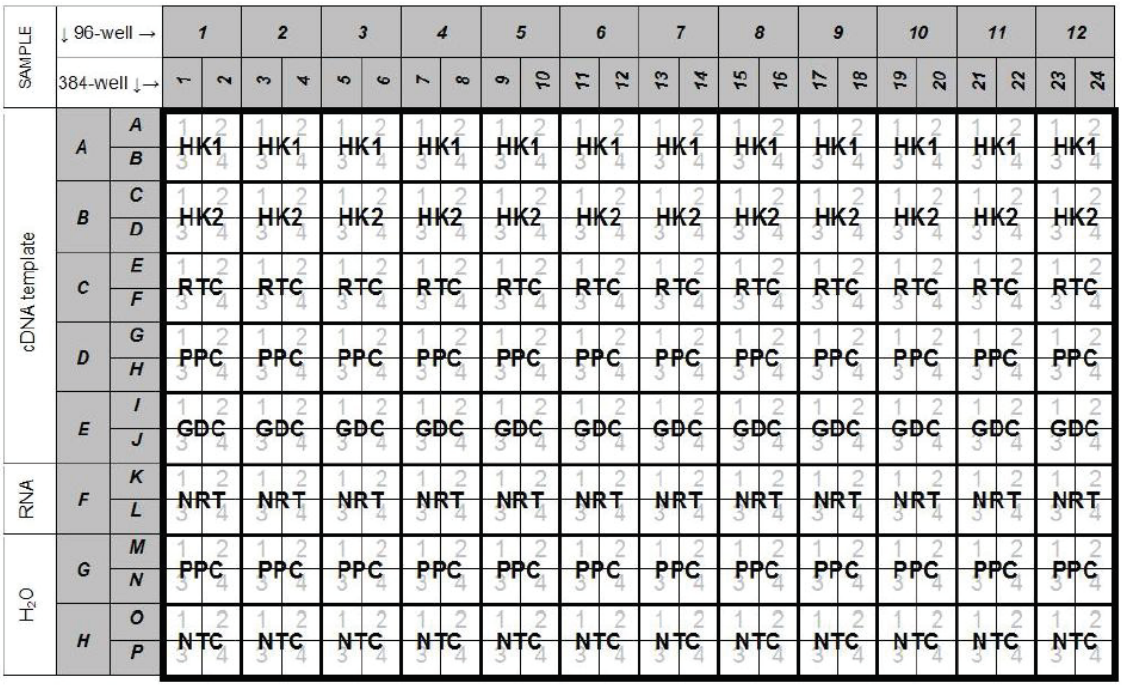
For RNA isolation, the Qiagen RNeasy mini kit (Qiagen) was used according to the manufacturer's instructions. Briefly, following cell culture (described in chapter 2.9) and cell stimulation with the tissue secretome, the culture medium was aspirated, and each well was washed once with cold PBS. Next, cells were lysed with 350 μl Buffer RLT (Qiagen) + 1% β-mercaptoethanol (β-ME). To homogenize the cells, the lysate was passed five times through a blunt 21-gauge needle fitted with an RNA-free syringe. For RNA precipitation, 350 μl of 70% ethanol was added to the lysate and passed through an RNeasy spin column placed in a 2 ml collection tube and centrifuged at 8000 g for 15 seconds. At this stage the optional on-column DNase digestion step was performed in order to eliminate genomic DNA contamination, starting off with a wash with 350 μL of RW1 buffer, then 10μl of DNase stock was added to 70 μL of RDD buffer and the 80 μL mix was added directly to the spin column membrane for 15 minutes at room temperature. The spin column was subsequently washed with 350 μL Buffer RW1(Qiagen) at 8000 g for 15 seconds. Finally, the spin column was washed with 500 μl Buffer RPE (with 70% ethanol) (Qiagen) at 8000 g for 15 seconds and washed again with 500 μl Buffer RPE at 8000 g for 2 minutes to ensure that no residual ethanol was carried over during RNA elution. The flow-through was discarded after each spin. To elute the RNA, 20 μl of RNase free water was added to the spin column and centrifuged at 8000 g for 1 minute. The eluent was collected in a RNase free tube (Qiagen) and placed on ice until quantification by ultraviolet spectroscopy at 260nm/280nm with a NanoDrop® ND-1000 Spectrophotometer (ThermoFisher) and then stored at -80° C.

2.11.2 cDNA synthesis

The RT^2 First Strand kit (Qiagen) was used for cDNA synthesis as per the manufacturer's protocol. RNA (chapter 2.11.1) was thawed out form the -80°C storage on ice, RNase free water was added to the specimens to equalise the concentration of RNA in each one (25 ng/μL). To eliminate genomic DNA, 2 μL of buffer GE was then added to 8μL of the RNA and the mix was then incubated for 5 minutes at 42°C (Bio-Rad CX100 Thermocycler) followed by cooling in ice for 1 minute. Reverse transcription was performed by adding 10 μL of the reverse transcription mix (4 μL buffer BC3, 1 μL control P2, 2 μL RE3 reverse transcription mix and 3 μL of RNase free water). This was incubated for 42°C for 15 minutes followed by 95°C for 5 minutes (halts the reaction). Finally, adding 91 μL of RNase free water brings the total to 111 μL of cDNA. The synthesised cDNA was stored at -20°C prior to use with the RT^2 q-PCR endothelial cell profiler.

2.11.3 Qiagen RT^2 profiler PCR endothelial cell array

The RT^2 profiler allows for the analysis of simultaneous gene expression in 84 related endothelial genes. Prior to using the RT^2 profiler, *Qiagen* recommends a quality control (QC) array plate (PAHS-999Z) with which to ensure reliable results from the cDNA template by excluding samples with substandard results. The QC plate is designed to test 12 samples, measuring relative expression in two housekeeping genes, a test for genomic DNA contamination, a check for reverse transcriptase efficiency which tests the First Strand kit (Qiagen) and several in-built controls **(Figure 2.18)**



Picture from Qiagen RT2 QC profiler handbook

Figure 2.18: Plate layout for the RT^2 QC array

In the 96- well format used, up to 12 samples can be tested simultaneously. **Row A** and **Row B** contain housekeeping genes ACTB and HPRT1. **Row C** tests reverse transcription, and **Row D** and **Row G** contain positive PCR controls, with water only added to **Row G,** testing for PCR inhibitors. **Row E** contains a genomic DNA control and **Row F** contains the no reverse transcription control. **Row H** contains a no template control, testing for general DNA contamination.

The procedure for the QC plate involves a polymerase chain reaction (PCR) reaction using the proprietary RT^2 SYBR Green Mastermix® (Qiagen). After thawing the cDNA samples from the -20^{o}C freezer, the first PCR component mix is made up with 6 μL of cDNA, 75 μL of SYBR Green Mastermix® and 69 μL of RNAse free water. Twenty-five microlitres of this is aliquoted out in the first 5 wells (A-E) of the QC array plate. The next well has a 25 μL of a mix containing 1 μL of 1/100 RNA with 13 μL of SYBR Green Mastermix® and 13 μL of RNAse free water. The last two rows (G-H) are the control rows and contain 25 μL of a mix of SYBR Green Mastermix® and RNAse free water. The plate was then run on a Bio-Rad CFX96

PCR analyser for 10 min at 95°C, ensuring the HotStart DNA *Taq* Polymerase is activated by this heating step. Following this, 40 cycles at 95°C for 15s and then at 65°C for 1 minute whilst capturing the fluorescence data. Data is exported from the PCR reader and analysed on an Excel template provided by Qiagen.

After successfully completing the quality control plate, the prepared cDNA was used with the RT^2 endothelial cell profiler array (Qiagen). Each well of the RT^2 endothelial cell profiler array contains a primer assay for 84 different endothelial related genes (supplementary methods) and 5 wells that contain housekeeping genes which allow for normalisation of the relative gene expression. In addition, the 96 well-plate also contains several controls, a genomic DNA control (GDC) that detects non-transcribed genomic DNA, a reverse transcription control (RTC) that tests the efficiency of the reverse transcription reaction and a positive PCR control loaded with a known artificial DNA sequence and an assay that detects it, testing the PCR chain reaction itself **(Figure 2.19).**

Similar to QC plate (above), 102µL of the remaining cDNA that was previously made up, is mixed with 1350µL RT^2 SYBR Green and 1248µL of RNase-free water. This is then gently mixed and 25µL pipetted out in to each well of the 96 well RT^2 endothelial cell profiler array using a multi-channel pipette. This is then centrifuged for a minute at 1000g to remove bubbles and is placed in an RT-PCR cycler (Bio-Rad CFX96). The analyser is programmed to run for 10 min at 95°C, ensuring the HotStart DNA *Taq* Polymerase is activated by this heating step. Following this, 40 cycles at 95°C for 15s and then at 65°C for 1 minute whilst capturing the fluorescence data. This is followed by a melting curve program.

Data was exported from the PCR reader and analysed on an Excel template provided by Qiagen which was uploaded and analysed on the online *Qiagen qPCR* analysis software. The 2-ΔΔCt formula was used to calculate fold change, and the software optimised the housekeeping genes that were present in the samples. The array has 7 in-built housekeeping genes with which to normalise data. Only genes that had a mean fold change > 1.35 in all three groups of ILT stimulated specimens were regarded as positive, and only those that had a p value of <= 0.05 were regarded as significant (paired t test calculated by the online analysis software).

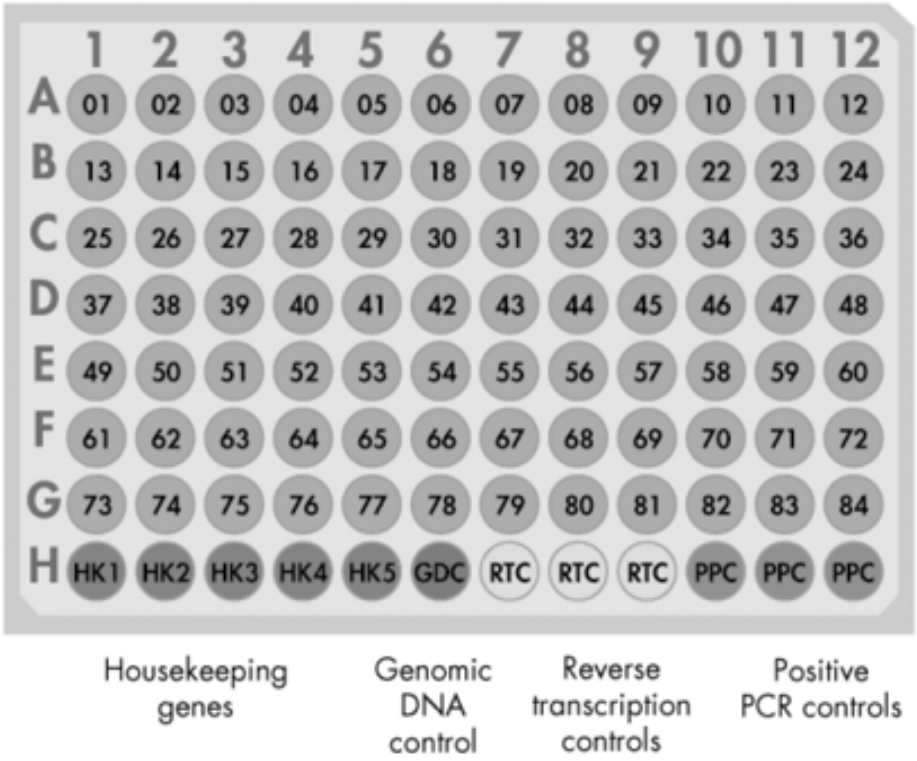


Figure 2.19: Plate layout for the RT^2 profiler array

In the 96- well format used, primers of 84 endothelial related genes occupy A1 to G84. In **Row H**, **H1 to H6** contain several housekeeping genes, **H6** contains a genomic DNA control, **H7-9** contains a reverse-transcription control and **H10-12** contain positive PCR controls.

2.11.4 The cytokine profile of the aortic tissue supernatants

This experiment was kindly performed by Dr Regent Lee. After determining the biological activity of the secretome supernatants, they were investigated with a *Human cytokine array panel* (R&D Biosystems) to determine their cytokine profile. This rapid and sensitive assay determines the relative expression of 105 cytokines simultaneously. The principle of the array relies on capture antibodies that are spotted in duplicate on a nitrocellulose membrane. The tissue supernatants are then added to a cocktail of detection antibodies and incubated. This cocktail is subsequently added to the membrane and the cytokine-capture antibody complex are fluoresced and interpreted. The *Human cytokine array panel* (R&D Biosystems) is packaged as a kit containing the nitrocellulose membranes, buffer, reagents and the cytokine detection antibody cocktail. The result was analysed using HL Image+ (Western Vision Software, Version PCM 18.0.7).

2.12 Statistical analysis

Statistical analyses were carried out using Prism software (GraphPad Software, San Diego California USA, www.graphpad.com). Values of $p<0.05$ were considered statistically significant. Results will be presented with details of their individual statistical tests.

2.13 Conclusion

This chapter presented the patient recruitment framework together with details of the informed consent process (OxAAA study). The recruitment process was finessed over the course of the study and patient interactions were documented in a structured and detailed manner, recording several clinical and anthropometric details. Attention was paid to standardisation of the methods of blood collection including the anatomical locations and timing before anaesthesia, as these could potentially confound downstream results. The methods of tissue processing and digestion were refined incrementally with specific considerations addressed. Although the aim was to analyse 10 matching patient samples in the final analysis, in excess of 55 patients were recruited and their samples processed in order to optimise these methods.

In the following chapter, the adaptation of cytometric methods for use with the aortic complex tissues will be presented and discussed.

CHAPTER 3

OPTIMISING DEEP IMMUNOPHENOTYPING INVESTIGATIVE TECHNIQUES IN ABDOMINAL AORTIC ANEURYSMS

3.1 Introduction

Abdominal aortic aneurysms are a disease characterised by disordered immunoregulatory and inflammatory mechanisms typified by elastin degradation and smooth muscle cell apoptosis. As described in the introduction (Chapter 1), the aortic walls of AAAs have a rich mononuclear inflammatory cell infiltrate and the ILT within AAAs also has an inflammatory cell infiltrate that is less well described. Thus far, several authors have characterised these, but with methods lacking the depth of resolution that is potentially achievable in the modern era.

The predominant immune cell types in the aortic wall are T cells and B cells(68, 133-135). They form part of the adaptive immune response and make up more than 90% of the cells within the immune cell infiltrate. However, T and B cells are not a homogenous group. They can be further classified into, CD4 and CD8 cells, Naïve cells, Memory cells, Effector Cells, Regulatory cells, Cytotoxic cells and several smaller subcategories and these subtypes have not been fully described in AAAs. Each has unique functional repertoire and co-exist together forming a complex interconnected network. They are identified through cell surface and intracellular markers which stain positive for antibodies. Similarly, the ILT is reported to have a large proportion of granulocytes and a distinct macrophage population(95) which form part of innate immunity.

The majority of investigators have interrogated both the aneurysm wall and ILT using histology combined with immunohistochemistry (IHC) (68, 136). IHC allows for both spatial and anatomical localisation of cells through antibody fluorescence of a protein target and is a complementary technique to cytometry-based techniques. It has the advantage of not being time sensitive as it can be used on

frozen or fixed samples lending to batch processing and comparisons of multiple samples. IHC is however limited by narrow area of visualisation leading to a potential sampling site bias which may not represent the entire sample and is also constrained by the limited number of targets that can be examined during a single experiment. Within the complexity of disease and a spectrum of activation, there can be significant overlap between cell surface markers (especially in macrophages, dendritic cells and monocytes), making identification of cells difficult without multiple makers on each cell. IHC is an invaluable method for confirming results through colocalization but is less suitable for widescale discovery experimentation.

Searching the literature (Pubmed, Medline), the last 'Immunophenotyping' of AAAs was published in 1998 and investigated with IHC(136). This confirmed that the mononuclear cell infiltrate was mainly in the adventitial layer, and in the ILT, the nucleated cells were found in the luminal layer as wells as the presence of T, B and dendritic type cells. Indeed, previous investigators have attempted to characterise the mononuclear cell infiltrate of AAAs with other techniques (such as FC), but not in the recent past. The last attempted characterisation of T and B cells were in 2003 and utilised a combination of IHC and 4-colur flow cytometry(68). This required splitting of the cells into several groups as only four markers were able to be analysed at a time, thus potentially introducing variability and overlooking unknown or uncommon cell types.

They and others have confirmed the heterogeneity in T cell subsets within the aneurysm wall, as well as described the presence of B cells within the infiltrate(68, 136, 137). These have been focused on specific subsets. AAAs are suspected to be a T cell driven disease, and more recently, the T cells in the aortic wall have

been confirmed to be clonally expanded, thus reaffirming the hypothesis of ongoing antigen presentation(138). Indeed, T Regulatory cells (Tregs) have been reported to be lower in the blood of patients with AAA, but there is limited information on their presence within the aortic wall or even the ILT(75). Most of the work on T cells has been carried out on the CD4+ population(71), and a CD8+CD27- population has been described, but its relation to cytotoxicity and aneurysmal formation has not been elucidated(139). Memory B cells are known to constitute a large component of the mononuclear cell infiltrate, again however, due to the limitations in investigative techniques, they have been studied in isolation and the cross-talk between T and B cells has also not been fully investigated. Vascular associated lymphoid tissue (VALT) has been described in the adventitia, and its role in the memory B cell switching has also not been clearly defined (140). In the ILT there is a paucity of data on the presence of T and B cells as well as their subsets, with only one study having previously investigated the ILT with FC(96).

Antigen presenting cells (macrophages, monocytes and dendritic cells) play a pivotal role in the initiation of AAAs and are the predominant cell type in mouse models of AAA formation(141). They have been associated with both pathogenic and protective roles and as described in the introduction (Chapter 1), the M1-M2 macrophage phenotype is not clearly defined in-vivo. Using laser capture microdissection, the human aortic adventitial wall has been found to have more M1 and the ILT more M2 macrophages(142) though M1 macrophages have been found in the aortic adventitia (143). This highlights the potential complexity of identification using different markers and methods. Dutertre et al characterised the aortic wall using multicolour flow cytometry and discovered several subsets including CD15-CD14+ and CD14+CD206 and four suspected dendritic cell subsets(143). There

are also various relationships with the monocyte/macrophage chemokines and interleukins in the AAA wall (IL-6, MCP-1, CCR2, CXCR3)(144), and in the peripheral blood of patients with AAA there are more CD14+CD16 monocytes suggesting a role in the disease process(145, 146).

Mouse models of AAA (predominately the Angiotensin II model) have been used to gain insights into this complex process. Regulators of G-protein signalling (RGS) target GTPase activity of chemokine receptors and RGS1 is highly expressed in human AAA, whilst RGS1 deficient mice are associated with protection from aneurysm formation(147). Developing concepts include the role of macrophages in the media and their relation to the efferocytosis pathway(141).

In human AAA wall samples however, macrophages represent between 2% and 10% of the inflammatory cell infiltrate and this is in contrast to mouse models(61, 135, 143). Macrophages as well as human macrophage elastase (HME, MMP-12) have been localised to the AAA media, but are more prominent in the media of the transition zone of normal aorta-aneurysmal aorta where the elastic fibres are still undergoing elastolysis(148). So, the paucity of macrophages in the AAA wall may represent an end stage of disease, whereas macrophages are likely to be involved in the initial aortic wall degeneration as elastolysis is thought to be the primary event in AAA formation and occurs early on in the process(149). Their role in the ILT is less clear, though they have been identified within it(95). Furthermore, the interrelation between T cells and macrophages is unknown. Dendritic cells have been described in the aortic adventitia and in close association with VALT, suggesting a role for antigen presentation to T cells(140). Phenotyping macrophages (and other APC) will provide a deeper understanding of the functional

roles of individual subtypes and may unlock insights describing the complex interplay between the inflammatory cell types.

The aortic wall and ILT of AAAs have an inflammatory cell infiltrate with features of both innate and adaptive immunity. To date, most investigators have researched a single cell lineage at a time. In part, this is due to the limitations in experimental techniques available. None has resolved the subsets to a level of detail that is attainable with modern single cell techniques such as multicolour flow cytometry or time-of-flight mass cytometry (CyTOF)

3.2 Principles of mass cytometry

Mass cytometry is a high dimensional multiparameter method of interrogating single cells(150). In essence, CyTOF is the fusion of flow cytometry and mass spectrometry. The quest for unambiguous simultaneous phenotypic and functional identification of multiple cell parameters on a single cell led to CyTOF development(150, 151). Flow cytometry is the gold standard, and it is a specialised and advanced technique which continues to develop. However, it has limitations.

Flow cytometry uses fluorophores as reporters to which antibodies are conjugated. Their fluorescent light emission is then measured by a flow cytometer containing different coloured lasers, with each cell event passing through a fluidic system. This light emission is quantified and taken as surrogate for molecular expression and is expressed in units of mean fluorescence intensity (MFI). Flow cytometry becomes technically challenging after adding more than 12 fluorophores on an antibody panel, as the fluorophores have spectral spill over in to each other which then requires the software to compensate the results with varying levels of accuracy

(150, 152). Another disadvantage of flow cytometry is the natural autofluorescence (background signal) emitted by cells in human tissues(119). This creates ambiguity in interpretation of results.

Mass spectrometry on the other hand has the ability to measure multiple masses with high accuracy. Combining the two techniques by conjugating epitope specific antibodies on to transition element heavy metal reporters of differing atomic masses (the lanthanide series of elements) takes advantage of the benefits of the two techniques whilst removing the spectral spill-over effects(150). Thus, allowing multiple heavy metal conjugated antibodies to be measured simultaneously on a single cell(152).

The technical outline of a CyTOF experiment is outlined in **Figure 3.1**. Cells labelled with antibodies coupled to heavy metal reporters are ionised as it passes through the CyTOF mass cytometer. The heavy metals reporters are distinguished by a time of flight chamber (TOF). The abundance of the heavy metal isotopes measured by the TOF is related to the abundance of the antigen expressed on the cell's surface

There are however still limitations to this technology. Due to the ionisation and atomisation of the cell suspension, the cells cannot be recovered after passing through the machine thus eliminating cell sorting capability. Flow cytometry (FC) is also a cell destructive technique. Both FC and CyTOF require high quality single cell suspensions, and these are derived from tissues requiring processing. In the processing of tissues (digestion, storage, labelling), cells surface markers can be potentially altered, thus introducing potential confounders. When compared to FC, CyTOF is not a high throughput process. Events are limited to between 300-500 events per second (and even less with tissue samples), so although it is technically

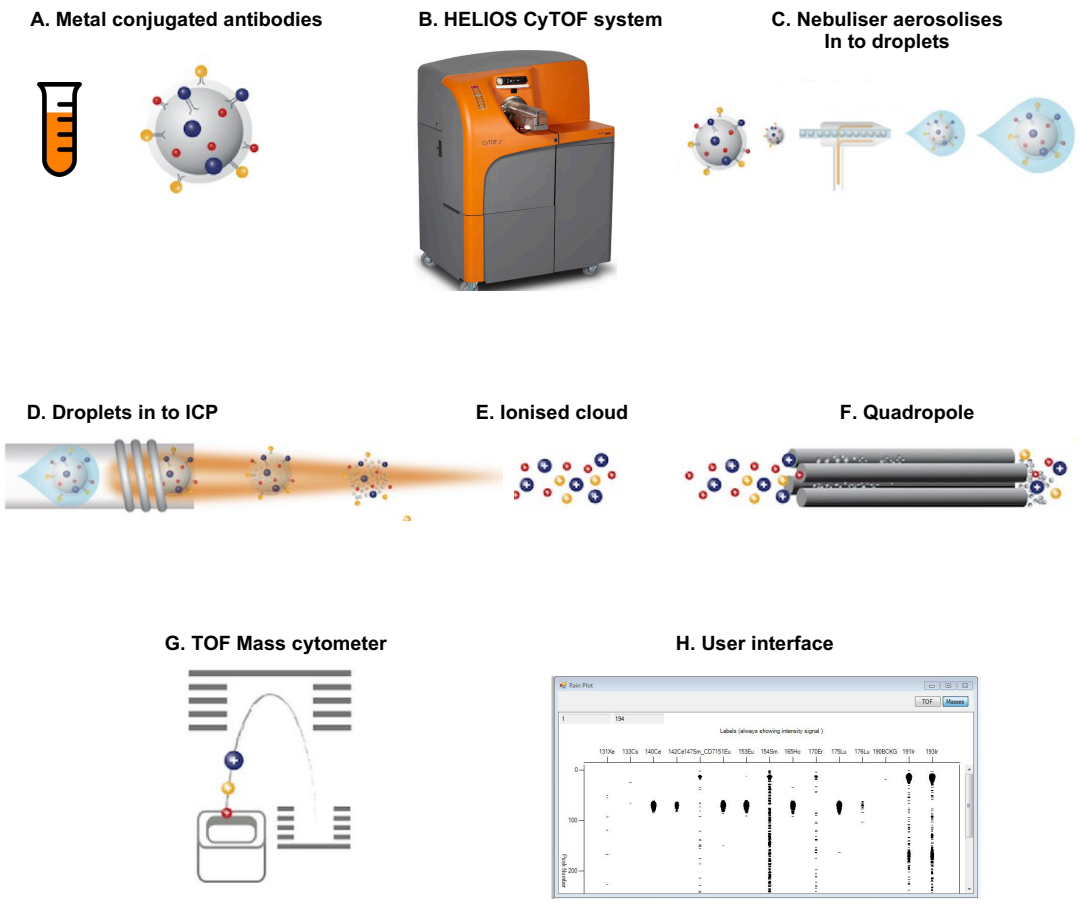


Figure 3.1: Schematic of CyTOF processing and acquisition

The cell suspension is labelled with a cocktail of metal conjugated antibodies **(A)**, which is then passed through a nebuliser that aerosolises the cell **(B)** carrying it in droplets to the mass cytometer **(C)**. Before entering the mass cytometer, the droplet is passed through a hot argon inductively coupled plasma (ICP) **(D)**, where it is ionised and the covalent bonds are broken. This becomes a charged 'cloud' **(E)**, leaving only the metal conjugated antibodies behind, before being passed through a quadrupole to discard heavy metal contaminants **(F)**. The heavy metal ions are separated by their mass-to-charge ratio in the time of flight mass spectrometer and propelled on to a detector **(G)**. This is converted in to an electrical signal where the signal is amplified by a pre-amplifier, then digitised by analogue to digital conversion. Software then plots this on to a data matrix (rain plot), where columns are different metals and a row represents a 'cloud' event **(H)**.

feasible to run millions of events, it is often not practically feasible or cost effective. This compares to tens of thousands of events run per second using flow cytometry. The sensitivity of the heavy metal reporters is good, though some of the flow cytometry fluorophores are better with a wider sensitivity range. Practically the number of metals is currently limited to around 37-40 per antibody cocktail. Although not a disadvantage per se, measuring 37 simultaneous antibodies leads to multi-dimensional data requiring tailored algorithms for decoding.

Another problem is standardisation between machines and even experiments, which has led to the use of 'normalisation' beads as an internal standard(153). The sensitivity of the machine fluctuates between runs due to changes in instrument performance and intervals between scheduled maintenance. Within a single run there is also a small gradual decrease in the sensitivity of the signal as a factor of time. Polystyrene normalisation beads embedded with isotopes of four different heavy metal elements (Ce140/142, Eu151/153, Ho165, Lu175/176), allow for the standardisation in variation between and within runs(153). This reduces technical variation thus making biological variation more reliable. The beads are spiked in to the sample at a 10% volume concentration before the run of samples. Once the *.fcs* files are generated, all files in the experiment are normalised using the normalisation tool internal to the CyTOF software package.

Another method of reducing sample to sample variation is mass-tag cell barcoding (MCB). The MCB method involves using different mass tag combinations to label individual samples with a unique mass barcode prior to combining samples into one tube for staining, processing and acquisition. MCB can increase sample throughput, reduce antibody usage and associated cost and increase data quality. There are several methods of MCB with the commonest one being the *Fluidigm commercial*

kit. This uses a unique combination of palladium-based metal barcodes added to a sample tube, then pooling of the samples and 'staining' with a single antibody cocktail thus ensuring all samples are exposed to the same antibody concentration. This is then de-barcoded using a software deconvolution algorithm. It uses a combination of six palladium isotopes (Pd102,104,105,106,108 and 110) in various combinations and allows for 20 barcodes per kit. Although there are several advantages to MCB there are also disadvantages(154). It requires an initial permeabilization step which adds time and can interfere with the expression of several surface markers. In addition, there can be loss of cells and difficulty in de-barcoding, which needs to be carefully weighed up in precious tissue samples. Another method is CD45 surface-based barcoding (thus not requiring permeabilization), but this utilises channels from the staining panel(155).

The lack of deep immunophenotyping within the AAA and ILT literature, together with the development of new techniques with which to perform this, led us to explore FC and CyTOF as potential experimental techniques.

3.3 Hypothesis and Aims

In this chapter I hypothesised that the human aneurysm complex (aortic wall, ILT, blood) is replete with immune cell diversity, and that mass cytometry techniques can be adapted and applied to explore this phenotypic heterogeneity in detail.

The aims were to systematically:

- Compare the immune cell composition of the blood, aortic wall and ILT in patients with AAA.
- Enable the deep phenotyping of the immune cell infiltrate in the aortic complex by mass cytometry (CyTOF)

3.4 Experimental design

Having developed and optimised methods for extracting single cells from the aortic complex (chapter 2.5), I first set out to investigate the cells using flow cytometry, aiming to initially establish the feasibility of cytometry in the aortic complex tissues and then to optimise the technique. Thereafter I planned to build on that knowledge through deeper phenotyping. To gain novel insights I planned to perform a multi-antibody screening panel (Biolegend Legend Screen) and subsequently designed a panel for use with CyTOF based on some of these insights. (Methods chapter 2.6 and 2.7)

3.5 Results

3.5.1 Immune cell composition of the aortic complex

Six consecutive patients' samples were processed (chapter 2.5), stained and analysed with flow cytometry (chapter 2.6). The 'CD45-Live' cells were gated on for downstream analysis after the exclusion of doublets **(Figure 3.2).** The flow cytometry panel comprised CD45, CD3, CD20, CD14, CD16, CD66b, CD33, HLA-DR, CD235a, CD41, and Live/Dead™ stains (fluorophores, clones and vendors – supplementary methods).

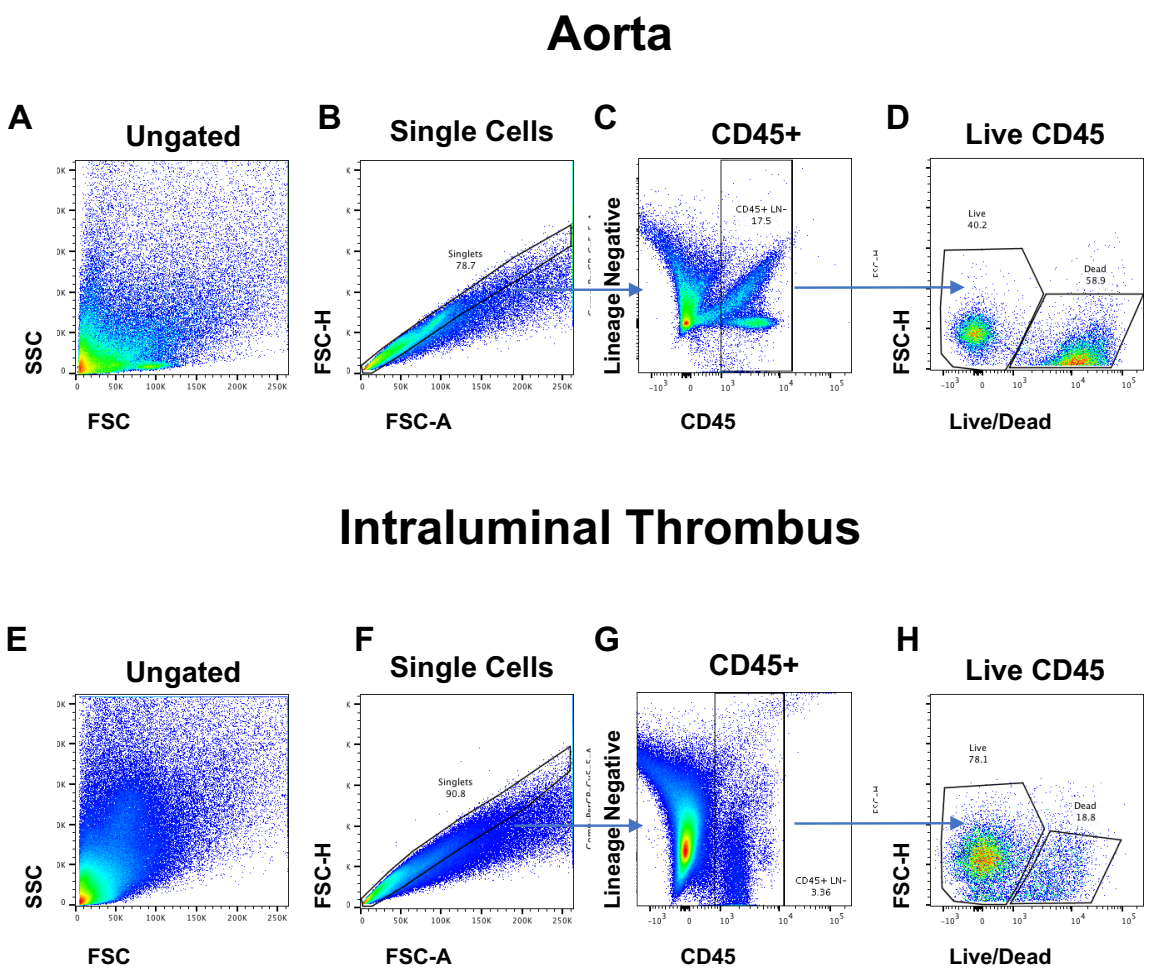


Figure 3.2: Flow cytometry gating strategy for Aorta and ILT

Single cell suspensions of aortic wall and ILT from a single participant were isolated (chapter 2.5) and stained for flow cytometry (chapter 2.6) In the first ungated colour dot plots **(A,E)** (SSC(y-axis), FSC(x-axis)), discrete cell groupings based on size and granularity are not clearly visualised. 'Doublets' are excluded through plotting FSC-height (y-axis) and FSC-area (x-axis) **(B,F)**. Thereafter, only the 'singlets' are included, and CD45 (x-axis) is plotted against a lineage negative channel containing markers for red blood cells and platelets (y-axis) **(C,G)**. The CD45 Live cells are then plotted and included for downstream analysis**(D,H)**. In both tissue types, there is a large group of CD45 negative-Lineage positive and CD45 negative-Lineage negative cells, and these also contain non-specific staining of cellular debris combined with autofluorescence.

Out of the total events recorded, 8.75 (median, IQR 7.7% – 12.4%) of the aortic wall and 4% (median, IQR 3% -14%) of the ILT cells were of hematopoietic origin as defined by CD45 positivity, compared to 50% (median, IQR 42% - 63%) in the blood. Of live CD45 events, the aorta contained mainly T cells (44.1%, SD±17.25%), which were similar to the PBMCs (56.4% SD ±14.56%) but different to the ILT (10.4%, SD ±18.29%) **(Figure 3.3A)**. The ILT however was composed mainly of CD66b positive granulocytes (67.82%, SD ±29.32%) and this was significantly different to the aorta (p=0.01) and the PBMCs (p=0.002) **(Figure 3.3B)**. The aorta contained a large population of CD20 positive B cells, whilst the ILT contained CD14 positive mononuclear phagocytes and other unidentified populations **(Figure 3.3 C,D)**. In conclusion, each segment of the aortic complex had a specific complement of immune cell subsets.

3.5.2 Further developments of the sampling and isolation technique

This first analysis, however, highlighted several challenges. These included the low yield of CD45+ cells in the tissues and the high level of autofluorescence of the cellular and acellular debris released from enzymatic tissue disruption. Thus**,** I re-evaluated both the sampling technique in our cohort and the isolation methodologies prior to staining. Firstly, the prominent granulocyte population in the ILT prompted us to re-examine our methods for blood processing and change to a method that incorporated granulocyte retrieval (chapter 2.5.1.3), as granulocytes are underrepresented in PBMC preparations that utilise density centrifugation. Secondly, the aortic and ILT tissues would require enrichment prior to downstream deeper phenotyping due to relatively low yield of CD45 cells. If multi-colour flow cytometry was pursued, then the autofluorescence would make interpretation challenging, but the low yield of CD45 cells would make CyTOF unsuitable.

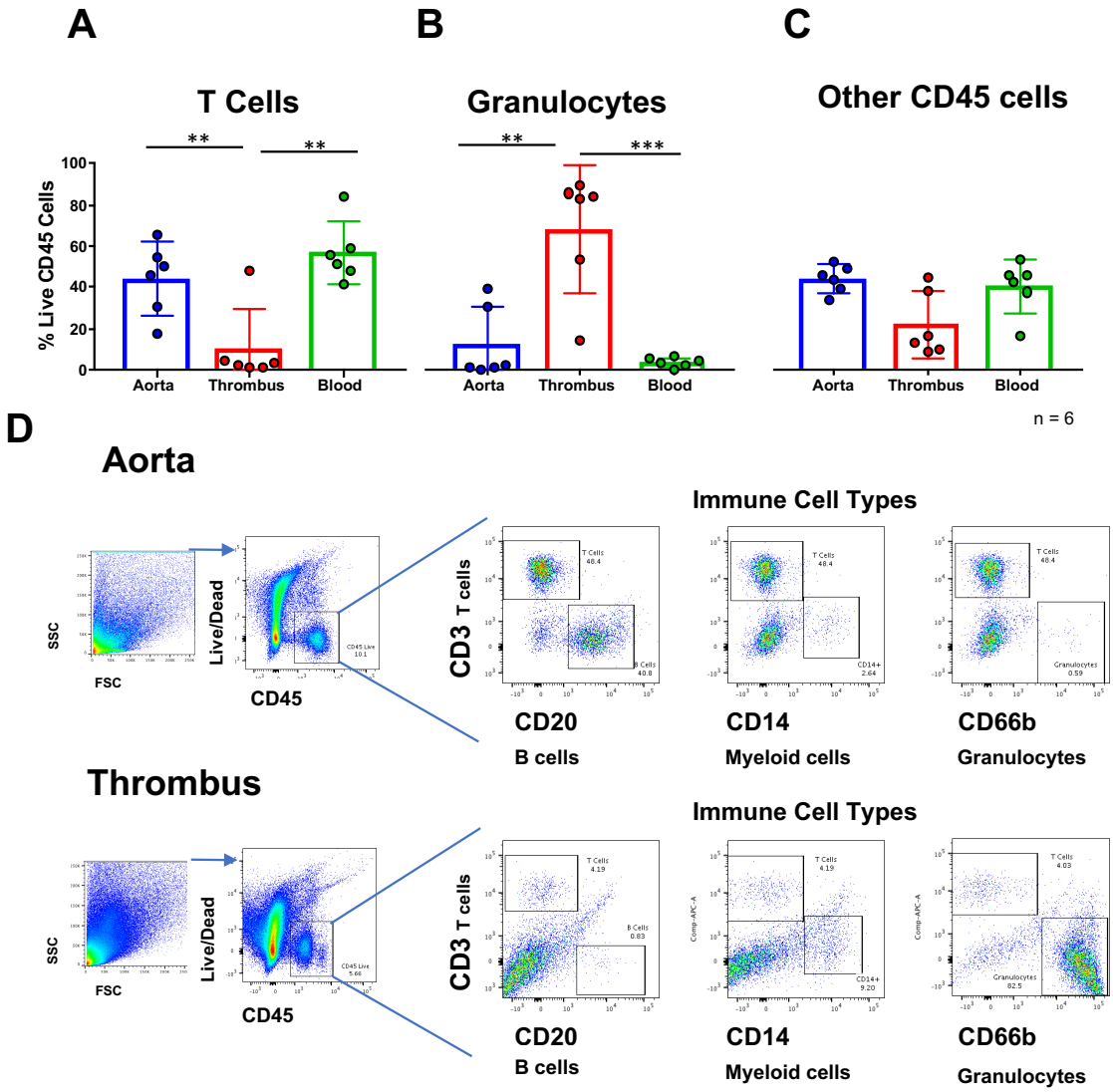


Figure 3.3: The frequency of immune cell types in the aorta, ILT and PBMC

Cells from the aortic wall, ILT and blood were isolated from six consecutive patients (chapter 2.5.1) and stained for flow cytometry (chapter 3.4.1) with an antibody cocktail.

(A) The aorta contained mainly T cells (44.1%, SD±17.25%), which was similar to the blood (56.4% SD ±14.56%) but different to the ILT (10.4%, SD ±18.29%). **(B)** The ILT however, consisted mainly of granulocytes (67.82%, SD±29.32%) and this was significantly different to the aorta (p=0.01) and the blood (p=0.002). **(C)** All three tissue types had 'other' CD45 positive immune cell types, including, CD20 positive B cells, CD14 positive mononuclear phagocytes and other unidentified populations. **(D)** Flow cytometry analysis of a patients' aorta and ILT, highlighting the distinct immune cell types found within. Additionally, the CD45% of total events is low (** = p <0.01, *** = p<0.002, students t-test) (antibody cocktail: CD45, Live/Dead, CD3, CD20, CD66a, CD14, CD16, CD235a, CD41)

3.5.3 Enriching the CD45 fraction

I compared 4 approaches to enrich the CD45 population and reduce debris in the cell preparations: 1) enrichment using magnetic beads, 2) enrichment using Percoll® density gradient centrifugation, 3) selective tissue use and 4) fluorescence activated cell sorting (FACS).

3.5.3.1 Magnetic bead enrichment was unsuccessful

Magnetic bead isolation enriches positively or negatively for cell populations and was the first technique attempted to enrich the single cell suspension. Cells were isolated from ILT (chapter 2.5) labelled with CD45 positive magnetic beads (Miltenyi-Biotec) and compared an unenriched negative control group (methods in section 2.6.3).

Macroscopically, the CD45 positive magnetic enriched group had less particulate matter than the unenriched and negatively selected groups. These were then labelled with metal tagged antibodies for CyTOF (section 3.4.2) and run on the Helios system and analysed with Cytobank. **(Figure 3.4 A,B,C)**.

The bead enriched sample did not separate out the CD45 positive cells as distinctly as the unsorted population. The enrichment in this sample increased from 15% CD45 cells to 29.8% CD45 cells, but downstream analysis revealed ‘clumping’ of cells, potentially due to the interference of cellular and acellular debris in the specimen.

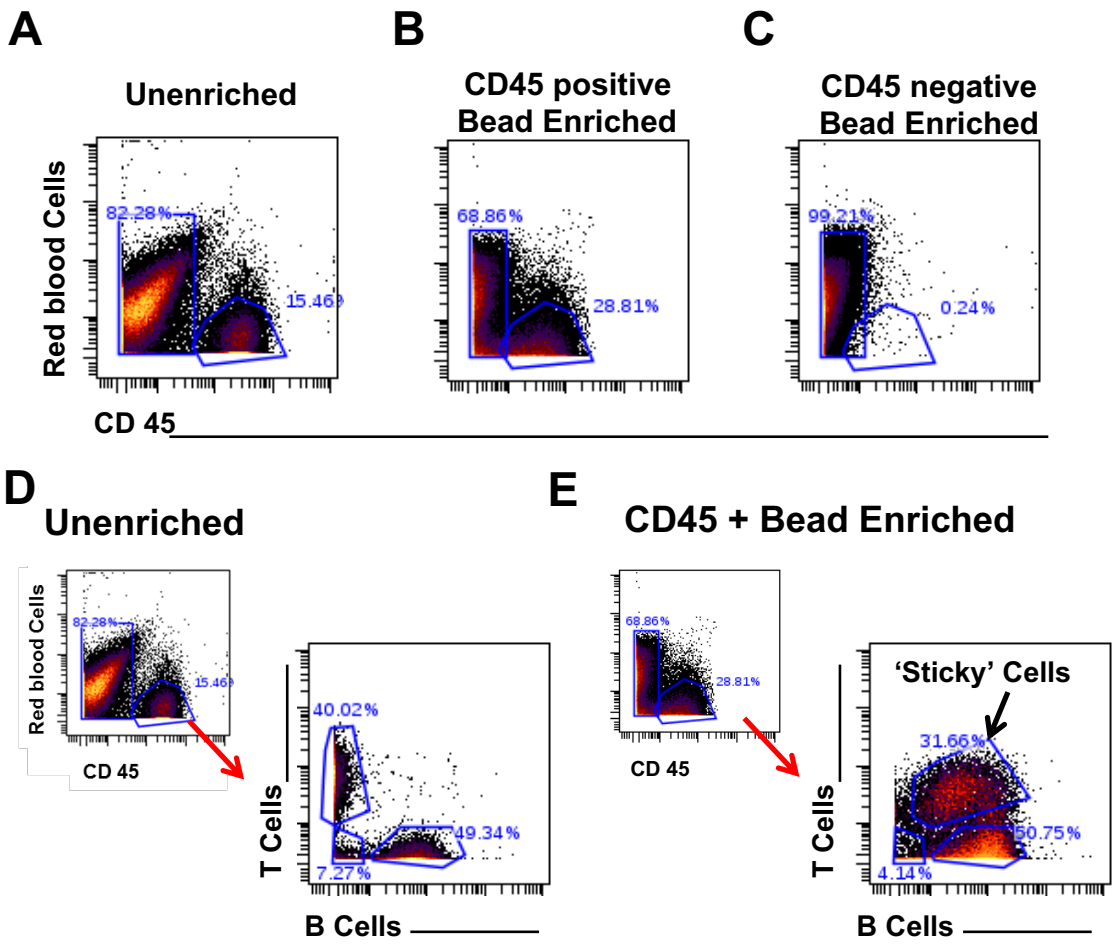


Figure 3.4: CyTOF analysis of magnetic bead enrichment

Cells were isolated from ILT and split in to two groups (chapter 2.5.1). The first group was labelled with CD45 positive magnetic beads (Miltenyi-Biotec) and passed through a MACS column (chapter 2.6.3). The positively selected fraction and the negative flow through were collected. The second group served as an unsorted control group. Both groups were then labelled with metal tagged antibodies and analysed on the Helios CyTOF system (chapter 2.7).

In the unsorted sample **(A)** there was a clear separation between the CD45 and negative population, whilst in the CD45 bead enriched group, this separation is less distinct **(B)**. The CD45 negatively selected group does not contain any CD45 positive cells **(C)**, however the purity of the sort is poor. In the bead sorted population there are only 28.81% CD45 positive cells. In addition, when comparing the sub-gated CD45 population of the unsorted group **(D)** to the CD45 positive bead sorted **(E)** group, the cells were double positive in the bead selected group. This is demonstrated by double positive staining for T and B cells, which should be clearly separated as in the unsorted group **(D)**.

3.5.3.2 Enrichment with Percoll® was unsuccessful

Having previously applied the principles of Percoll® density separation to optimising cell isolation from the blood (chapter 2.5.1.3), I attempted this technique with ILT. Cells were isolated from ILT and added to an 80/40% Percoll® gradient and compared to control groups using flow cytometry.

Compared to the unenriched group, there was minimal CD45 enrichment in the Percoll® 80/40% group (0.36 vs 0.83%) **(Figure 3.5 A,B,C)**. When a three gradient Percoll® - 80/60/40% was used, there was a ten-fold increase in enrichment (0.43 vs. 4.03%) in the 80/60/40% group. However, this was still not adequate enough for efficient CyTOF processing. Additionally, there was 'sticking' of the CD4 cells to red blood cells which would require further optimisation **(Figure 3.5 D,E,F)**.

3.5.3.3 Enrichment of cells based on anatomical location

To enrich the CD45 population and decrease the debris contaminating the specimen, I investigated using only the luminal ILT for these experiments. Other investigators (93, 95, 96), have reported a paucity of cells beyond 10mm of the luminal facing edge of ILT. To confirm these previous findings, the luminal area was separated out from the abluminal area and snap frozen in OCT. In addition, cells were independently isolated from the luminal and abluminal areas (chapter 2.5.1) and stained with antibodies for flow cytometry (chapter 3.4.1). The OCT blocks were cryosectioned in 5µm sections and stained with H&E. The photomicrographs indeed confirm a lack of nucleated cells in the abluminal area **(Figure 3.6A)**. Analysis with flow cytometry demonstrates a significant enrichment of CD45 positive cells in the luminal area when compared to the abluminal area (22% vs.1.26%) **(Figure 3.6B)**. Thus the methods were adapted to include only the luminal aspect of the ILT.

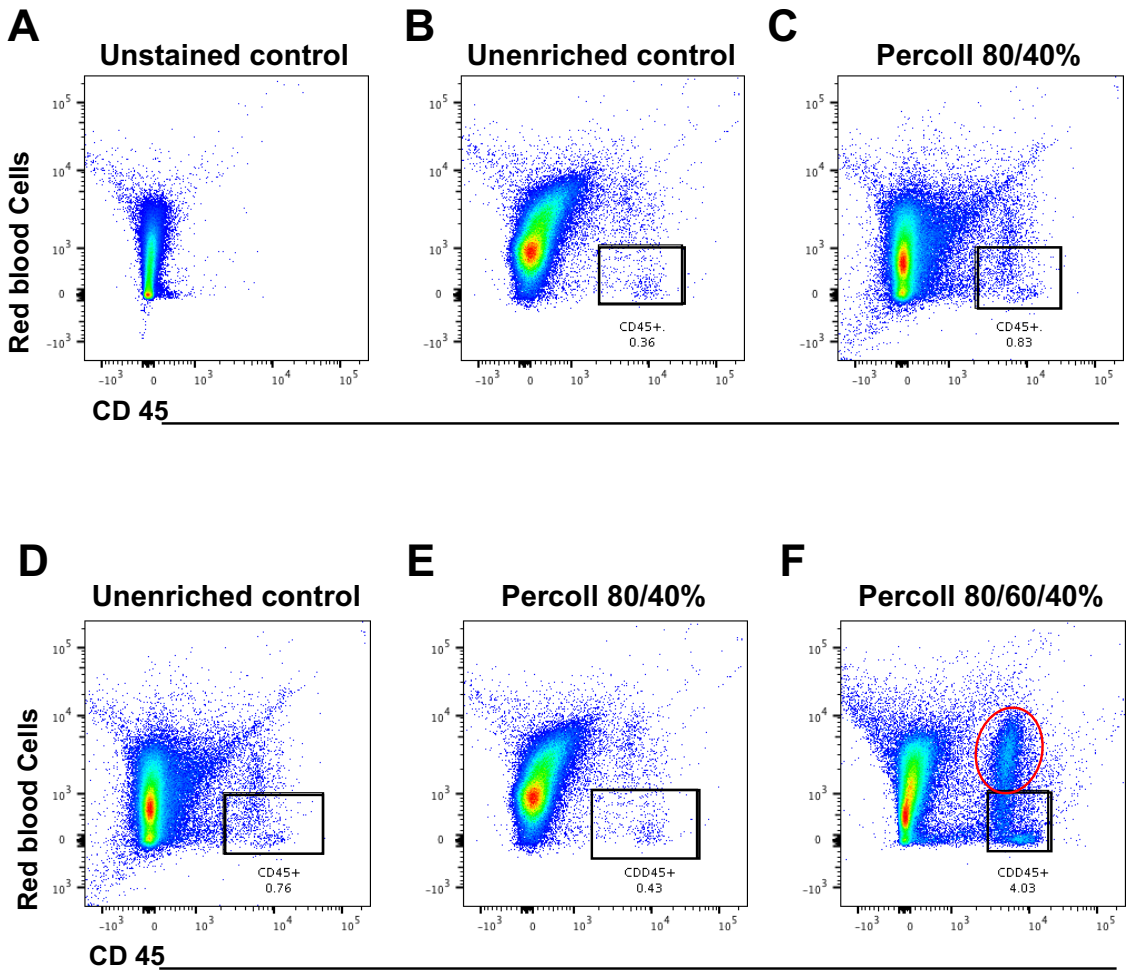


Figure 3.5: Flow cytometry analyses assessing CD45 enrichment of the ILT using Percoll®

Cells were isolated from two participants ILT (chapter 2.5.1). Percoll® is a silica based density separation product used for separating out cells of differing densities (chapter 2.5.1.3).
In the first experiment **(A,B,C)**, there was a treatment group (80/40% Percoll®) and control group (unenriched). The cellular layer was syphoned from the Percoll® and both groups were labelled for flow cytometry (chapter 2.6). Compared to the unenriched group, there was minimal enrichment in the Percoll® 80/40% group (0.36 vs 0.83%).
In the repeat experiment, **(D,E,F)** the Percoll® was prepared in three gradients (80/60/40%) and compared to Percoll® prepared in two gradients (80/40%). There was a ten-fold increase in the enrichment (0.43% to 4.03%), but the three gradient group had a population of cells that stained double positive for CD45 and CD235a (red circle).

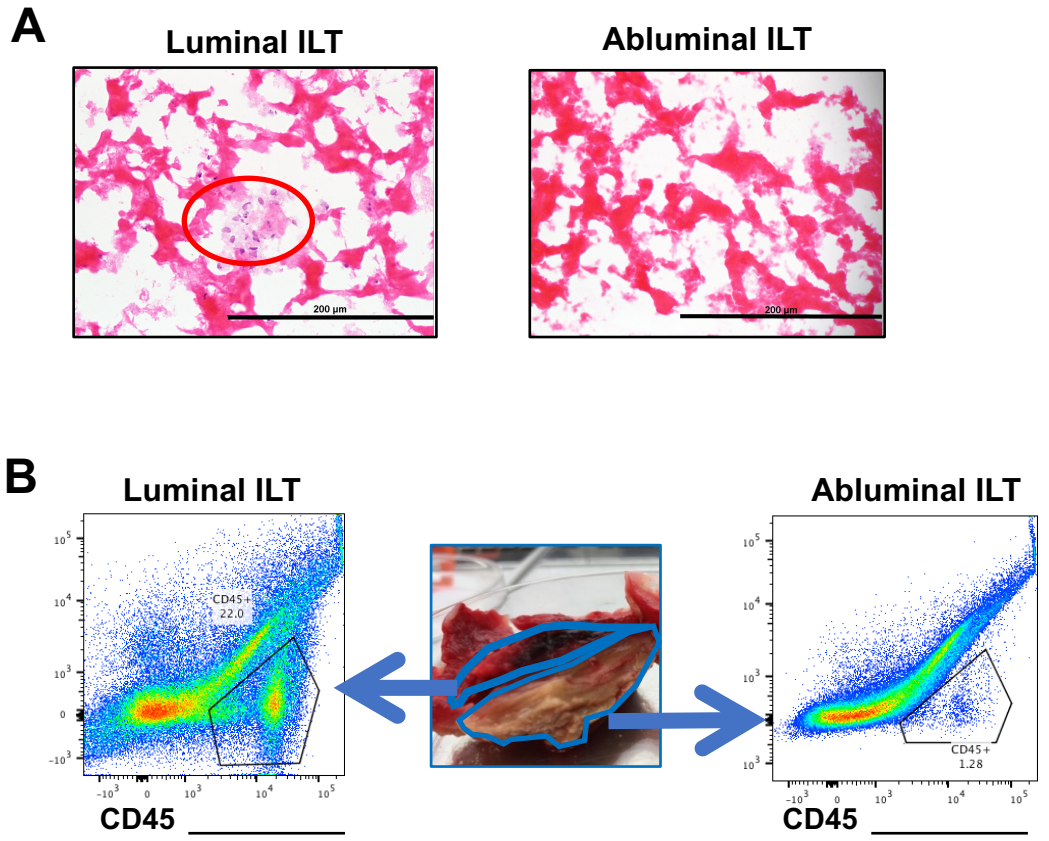


Figure 3.6: A comparison of cells in the luminal and abluminal ILT

Representative samples of the abluminal and luminal ILT were snap frozen in OCT. These were cryosectioned in 5µm sections and stained with H&E (haematoxylin and eosin). Cells were also isolated from the luminal and abluminal areas (chapter 2.5.1) and stained for flow cytometry (chapter 3.4.1).

(A) Photomicrographs show nucleated cells in the luminal area, but a paucity of cells in the abluminal area.

(B) In addition, flow cytometry analysis demonstrates an enrichment of CD45 positive cells in the luminal area as compared to the abluminal (22% vs.1.28%). (Scale bar = 200µm)

3.5.3.4 Cell sorting with FACS enriches the cell suspension

In an attempt to further enrich the ILT and aorta, fluorescence activated cell sorting (FACS) was attempted. After isolating the cells from the aorta (chapter 2.5.1) they were labelled with CD45 and Live/Dead™ flow cytometry antibodies (chapter 2.6.2).

When comparing the unsorted to the sorted CD45 positive group, the frequency of live CD45 positive events increased from 3.35% to 92%, confirming the extent and purity of the enrichment. In addition, the CD45 negatively selected group contained only 0.2% CD45 positive events, confirming the specificity of the sort **(Figure 3.7)**. This experiment demonstrated the feasibility of FACS sorting in aortic tissue but not the ILT.

The experiment was repeated using luminal ILT with similar results. Isolated ILT cells (chapter 2.5.1) were labelled with CD45 and Live/Dead™ flow cytometry antibodies (chapter 2.6.2) and were FACS sorted as described in the previous experiment. Comparing the unenriched to the enriched, discernible populations of cell groups were visible on SSC and FSC dot plots. When gated on the CD45 positive events, the enrichment demonstrates a 91.8% CD45 positive population **(Figure 3.8)**

Thus, cell sorting with FACS was a significant step towards deep phenotyping approaches.

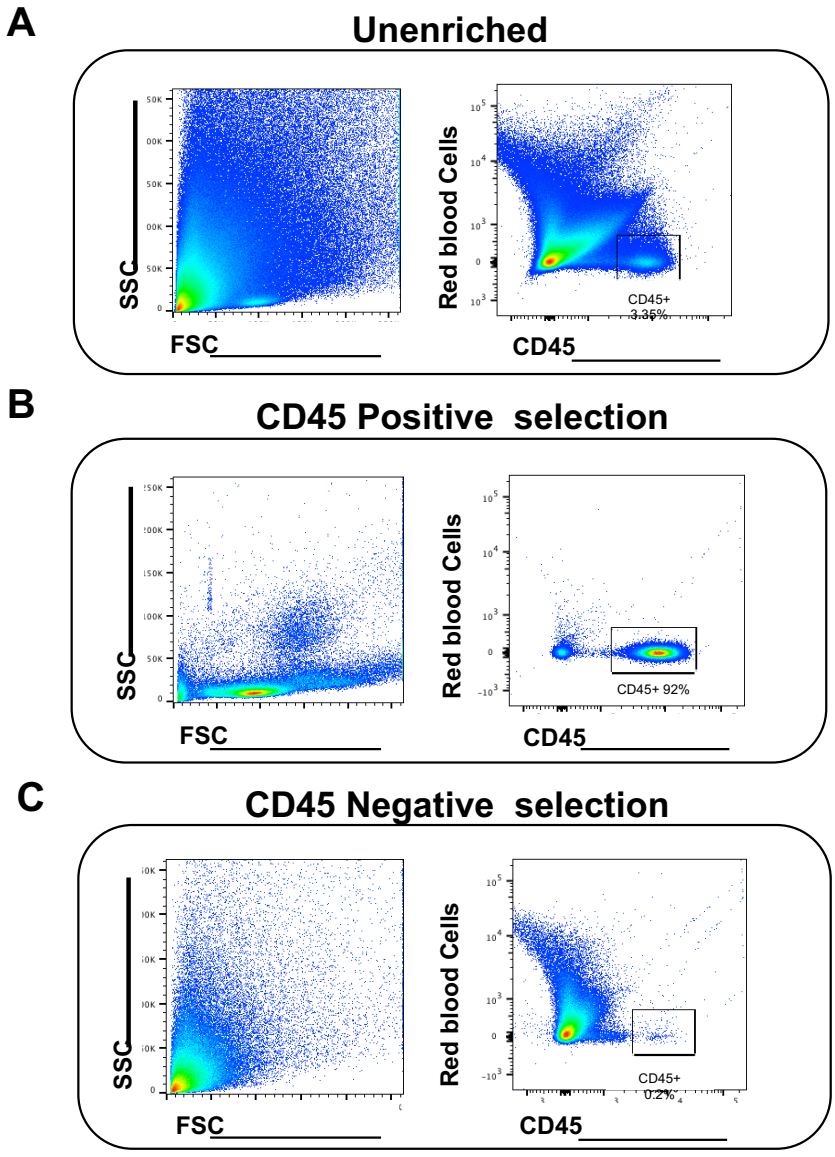


Figure 3.7: Analysis of cell sorted vs. non cell-sorted aortic tissue

Cells were isolated from aortic tissue and separated in to two groups (chapter 2.5.1). Both groups were labelled with CD45 and Live/Dead™ flow cytometry antibodies (chapter 2.6.1). The first group was then cell sorted and gated on CD45 live events (chapter 2.6.2). Both the CD45 positive selection and the negatively selected flow through were collected. The second group was analysed without pre-enrichment by cell sorting (unenriched group). Representative flow cytometry plots compare the **(A)** unenriched group to the **(B)** CD45 positively selectively group and the **(C)** CD45 negatively selected group. In the unenriched group, the frequency of live CD45 events was 3.35%, compared to 92% in the CD45 positive sorted group confirming the purity of the sort. In addition, the CD45 negatively selected group contained only 0.2% CD45 positive cells, confirming that the sort did not miss CD45 positive events

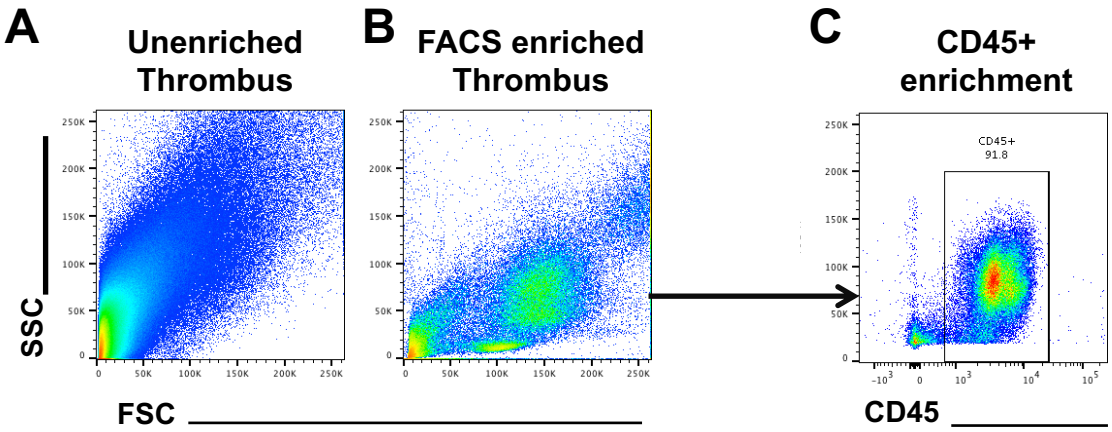


Figure 3.8: Analysis of CD45 positive enrichment in FACS sorted ILT

Cells were isolated from ILT (chapter 2.5.1) and labelled with CD45 and Live/Dead™ flow cytometry antibodies (chapter 2.6.1). These were cell sorted and enriched for CD45 live events (chapter 2.6.2).

Comparing the unenriched to the enriched samples **(A,B)**, discernible populations of cells are visible on side scatter (SSC) and forward scatter (FSC) dot plots in the enriched sample **(B)**. When gated on the CD45 positive events, the enrichment confirms a 91.8% CD45 positive population in the cell sorted sample **(C)**.

3.5.4 Validating and optimising the flow sorted sample for CyTOF

Potentially, cell surface marker expression could be altered by cell sorting, thus FACS sorted samples were compared to unsorted samples using CyTOF. After isolating the cells from the aorta (chapter 2.5.1), they were separated in to two groups (sorted and unsorted) and compared after labelling with CyTOF antibodies (methods chapter 2.7.1). The following antibodies were used: CD45, CD19, CD16, CD31, CD8, CD20, CD14, CD66, CD123, CD11c, CD15, CD3, CD45RA, CD27, CD127, TCRgd, CD28, IgM, CCR7, IgD (clones and vendors in supplementary methods).

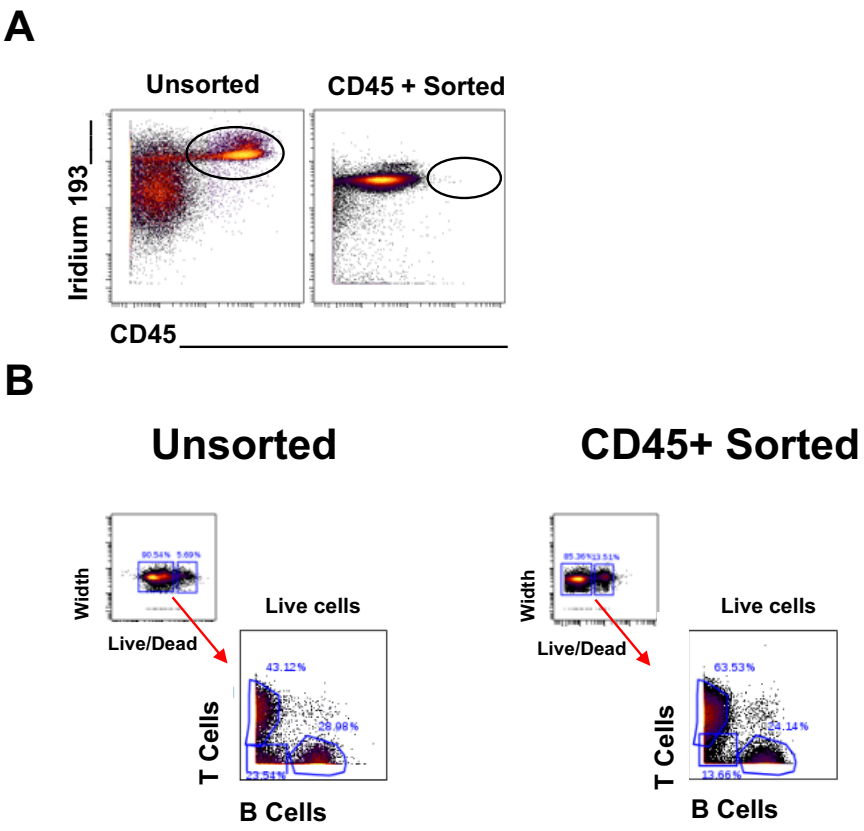


Figure 3.9: CyTOF analysis of CD45 positive cell sorted aortic tissue

Cells were isolated from aortic tissue (chapter 2.5.1) and separated in to two groups. The first group was labelled with CD45 and Live/Dead™ flow cytometry antibodies (chapter 2.6) and then cell sorted on CD45 live events (chapter 2.6.2). The second group was analysed without pre-enrichment by cell sorting (unsorted group). Both groups were labelled with metal tagged CyTOF antibodies and run on the Helios mass cytometer (chapter 2.7.1).

(A) The sorted sample appears negative for CD45 cells compared to the unsorted sample. **(B)** However, when gating on live cell events, the cell-sorted group contains T and B cells, and this is similar to the unsorted group. The difference was that the cell-sorted group had been labelled with a CD45 flow cytometry antibody prior to CD45 CyTOF antibody labelling.

Gating on 'Live' cells, revealed that both samples contained similar frequencies of T and B cells **(Figure 3.9)**. Further gating on CD3 T cells and comparing specific marker expression in the sorted and unsorted groups. The expression of CD4, CD8, CD45RA, CCR7 and CD27 with the T cell subset of both groups reveals a similar pattern of staining with CyTOF analysis. Furthermore, the frequencies of these cells are closely correlated in both groups (r=0.943, p=0.02, Spearman) **(Figure 3.10)**.

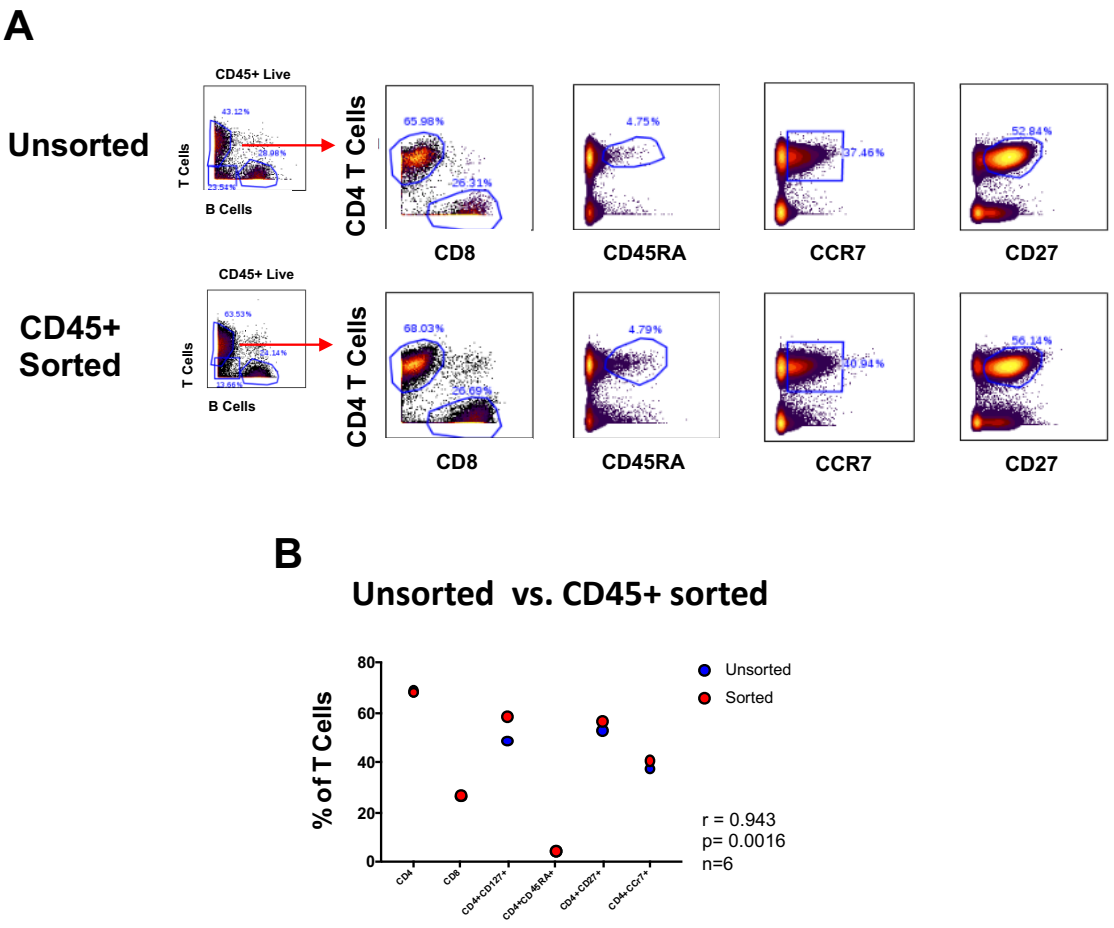


Figure 3.10: Mass cytometry (CyTOF) dot plots comparing markers of T cell expression in cell-sorted and unsorted aortic cells

Cells were isolated from aortic tissue (chapter 2.5.1) and separated in to two groups. The first group was labelled with CD45 and Live/Dead™ flow cytometry antibodies (chapter 2.6.1), then cell sorted and gated on CD45 live events (chapter 2.6.2). The second group was analysed without pre-enrichment by cell sorting (unsorted group). Both groups were labelled with metal tagged CyTOF antibodies and run on the Helios mass cytometer (chapter 2.7).

(A) These were gated on live T cell events (CD3) and compared using CyTOF analysis software on Cytobank.

(B) The expression of CD4, CD8, CD45RA, CCR7 and CD27 are closely correlated in sorted and unsorted samples. (p=0.02, r = 0.943, Spearman)

Comparing dot plot analysis of the sorted and unsorted groups, the sorted sample did not stain positive for CD45 when labelled with the CD45 CyTOF antibody. This was probably as a result of competitive binding from the flow cytometry antibody used for FACS which was of the same clone. This was confirmed by isolating cells and staining them independently and then sequentially with two different clones of CD45 antibodies (HI-30 and F-10-89-4) (**Figure 3.11).** When stained individually, the CD45 cells are clearly identified, however when the F-10-89-4 clone is added first, the HI-30 clone does not fluoresce.

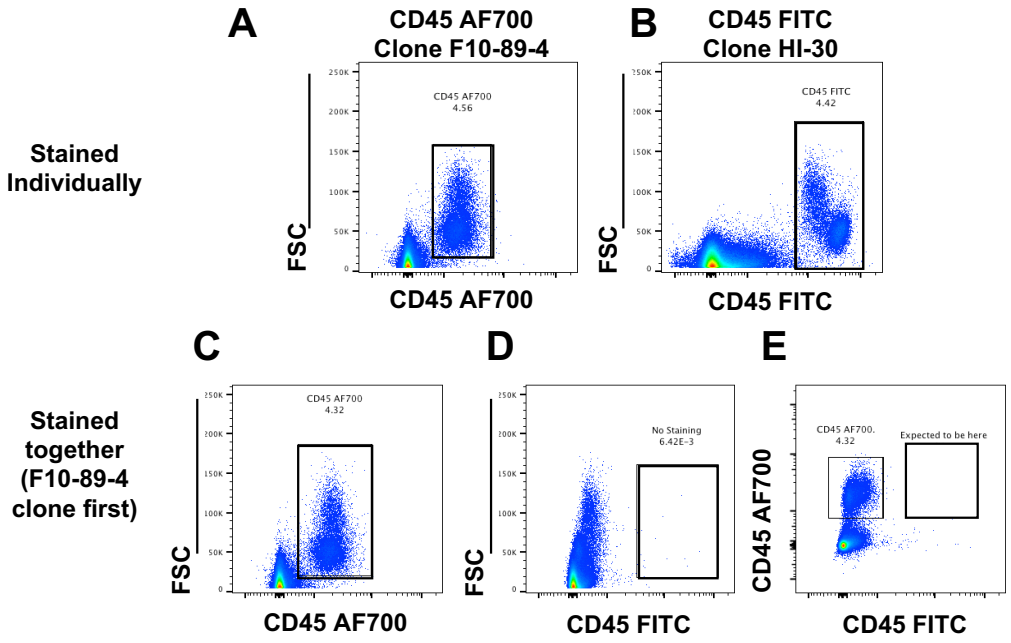


Figure 3.11: Analysis comparing two clones of CD45 antibodies

Leukocytes were isolated from the blood of a volunteer after lysis of red blood cells (described in 2.5.1.3). This was split in to three groups and labelled with with two different clones of CD45 antibodies individually and then together (chapter 2.6). Flow cytometry dot plot analysis of the blood stained individually with the CD45 clone F10-89-4 on an AF700 reporter **(A)** and clone HI-30 on a FITC reporter **(B)** demonstrate similar staining when either clone is stained individually**.** In the third sample, both clones were incubated with the cells, first the CD45 F10-89-4 clone followed by the HI-30 clone. Representative dot plots of flow cytometry analysis demonstrate staining positively with the AF700 CD45 clone (F10-89-4) on the x-axis **(C)**, but no staining with the **(D)** CD45 FITC clone (HI30). In plot **(E)**, the CD45 AF700 is on the y-axis and CD45 FITC on the x-axis, where a double positive (blue box) would be expected, but only the AF700 CD45 is positive.

A potential solution to the CD45 CyTOF antibody not binding to the cells was labelling the cells with a secondary anti-FITC antibody. Prior to testing the antibody, I sought to understand if the FITC-CD45 antibody conjugation would still be attached and report after a freeze-thaw cycle as the final samples would be cryopreserved for batch processing. Leukocytes were isolated and labelled with a FITC-CD45 flow cytometry antibody (chapter 3.4.1). This was split into two groups, and the first was cryopreserved whilst the second was analysed immediately. The first group was resuscitated after one week and analysed **(Figure 3.12)**.

The FITC antibody was still attached to the CD45 antibody after a freeze-thaw cycle. We thus used the anti-FITC labelled secondary antibody for CyTOF (Fluidigm).

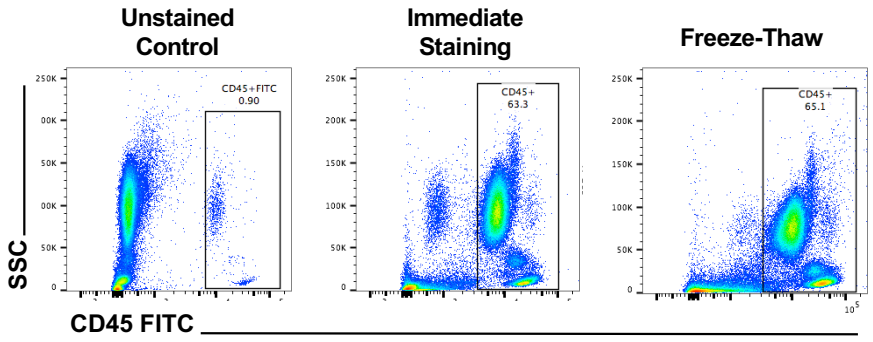


Figure 3.12: Analysis of FITC-CD45 antibody after a freeze thaw cycle

Leukocytes were isolated from the blood of a volunteer after lysis of red blood cells (described in 2.5.1.3) and labelled with a FITC-CD45 antibody (chapter 2.6). This was split into two groups, and the first was cryopreserved in FCS + 10% DMSO at -80^{o}C, whilst the second was analysed immediately on a BD LSRII flow cytometer. The first group was resuscitated after one week and then analysed. Representative flow cytometry dot plots of the first and second groups were compared with an unstained control. The FITC fluorophore was still attached to the CD45 antibody after a freeze-thaw cycle.

3.5.5 CyTOF staining closely correlates with results from flow cytometry

I sought to determine if the results from flow cytometry were comparable to CyTOF. For this, cells were isolated from matching aortic and ILT tissues (chapter 2.5). These were separated in to two groups and stained independently for FC and CyTOF.

In the aorta, live cells were 77.2% vs. 96.98% and in the ILT it was 77.8% vs. 87.35% (FC vs. CyTOF). However, the rhodium viability reporter for CyTOF required further optimisation as the separation of live and dead cells was less distinct than the FC Live/Dead antibody **(Figure 3.13 A,B)**.

CD45 Live cells and specific subsets correlated closely. In the aorta, the frequency of T cells was 48.3% vs. 49.0%, B cells 34.4% vs. 32% and granulocytes 3.6% vs 3% (FC vs. CTOF). These were similarly correlated in the ILT with, T cells 4.2% vs. 1.5%, B cells <1% in both (0.2% vs.0.8%) and granulocytes 86.5% vs. 87.7% **(Figure3.13 C,D,E,F)**. These correlation results are summarised in **(Figure 3.13 G,H)** (aorta, r = 0.987, p=0.0002, Spearman) (ILT, r = 0.943, p=0.017, Spearman).

Figure 3.13: Flow cytometry compared with CyTOF analysis in aortic and ILT specimens

Cells from matching aortic and ILT specimens were isolated from a participant (chapter 2.5). stained separately for flow cytometry (chapter 2.6) and CyTOF (chapter 2.7).

In the aorta **(A,C,E)** and ILT **(B,D,F)** the corresponding dot plots have a similar staining pattern and abundance for the markers analysed. Both the ILT and aortic markers correlate significantly with each other **(G,H)**. (Aorta r = 0.987, p=0.0002, Spearman), (ILT r = 0.943, p=0.017, Spearman)

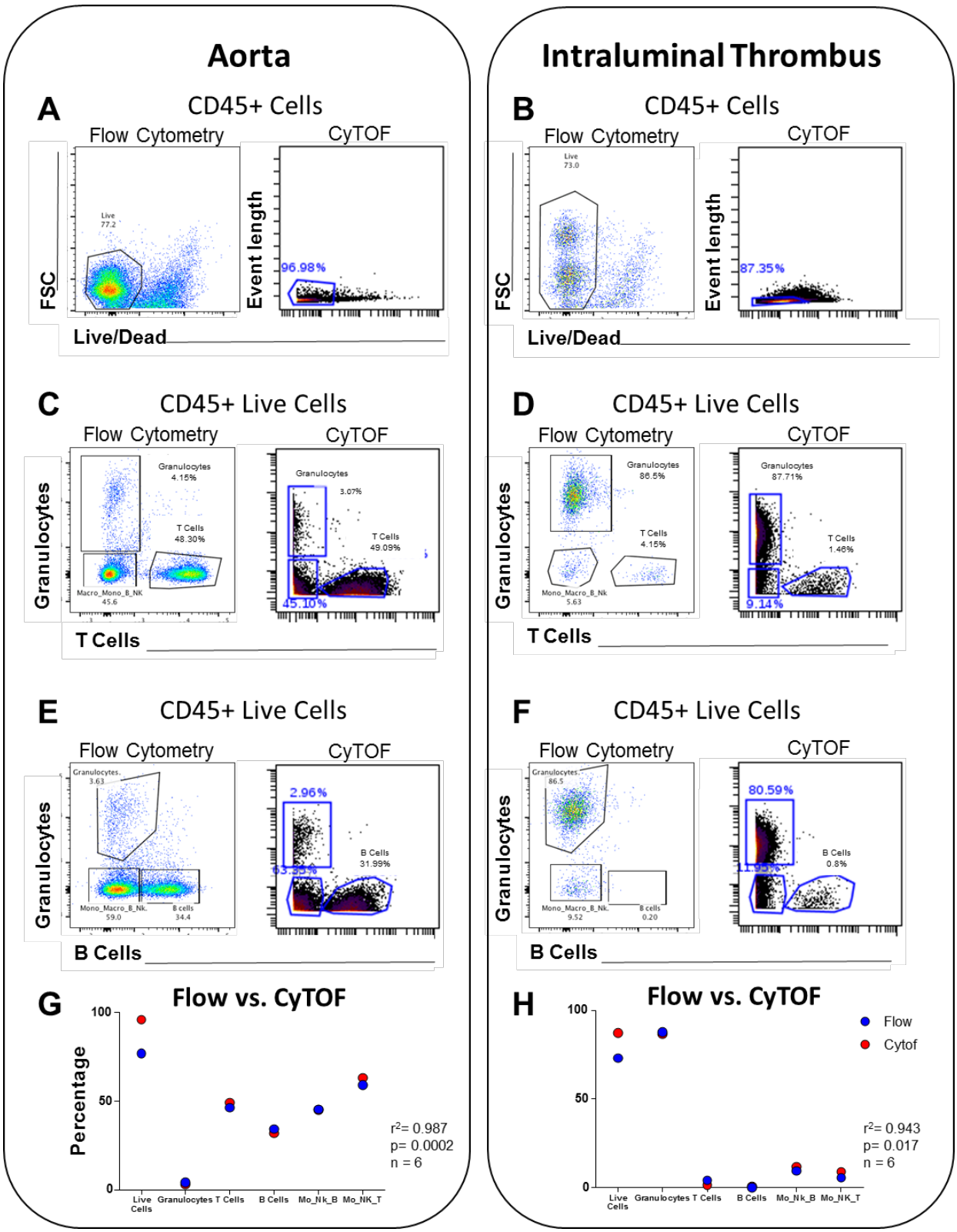


Figure 3.13: Flow cytometry compared with CyTOF analysis in aortic and ILT specimens

3.5.6 The Biolegend® Legendscreen™ antibody array

3.5.6.1 Optimisation

Having optimised and validated the aortic complex tissues for use with CyTOF, the next step was to design a panel of antibodies for immunophenotyping. The antibodies that were used in the initial flow cytometry panel formed the core antibodies on which we built upon and we examined the literature for other common markers used for deeper phenotyping (Table 3.1). The remaining antibodies in the CyTOF panel were selected through a Biolegend® Legendscreen™ screening antibody array panel (methods chapter 2.6.4).

Table 3.1: Common immune cell phenotyping markers

Lineage Markers	T Cell	B Cell	Mononuclear Phagocytes	Natural Killer cell	Granulocyte
CD3	CD4	CD20	CD33	CD56	CD15
CD19	CD8	IgD	CD14	CD16	Siglec-8
CD11b	CD127	CD27	CD16		
CD7	CD45RA	CD24	CD36		
CD66b	CCR7		CD68		
HLA-DR	CCR6		CD11c		
CD38	CXCR3				

3.5.6.2 Results of the array

Positive markers were defined through the ten in-built isotype controls in the array and gates defining positive and negative cut-offs were set using FlowJo (Treestar) (methods chapter 2.6.4, Figure 2.14). Based on these gates, data was imported in to an Excel spreadsheet where they were ranked from most frequent to least. Of the 361 markers in the array, 240 were positive (median = 25.55%, IQR 12.6% to 50.5%). **(Table 3.2)**

Table 3.2: Positive markers on Biolegend® antibody screening array

Antibody	Percentage	Antibody	Percentage	Antibody	Percentage	Antibody	Percentage
HLA-BC	97	CD11a	49,9	CD169	25,3	CD49f	12,6
CD184 (CXCR4)	95,9	CX3CR1	49,3	CD193 (CCR3)	25	CD55	12,2
CD59	94,9	CD209	49,1	CD191 (CCR1)	24,9	CD156c (ADAM10)	12,1
β2-microglobulin	94,5	CD85d (ILT4)	48,8	CD360 (IL-21r)	24,2	CXCL16	12
CD44	87,7	CD269	48,3	CD294	24	CD365 (Tim-1)	11,9
CD197 (CCR7)	87,5	CD36	47,2	CD6	24	CD255 (TWEAK)	11,8
CD47	82,2	CD14	46,8	CD35	23,9	CD73	11,8
CCR8	80,4	CD186 (CXCR6)	45,7	CD165	23,8	CD56	11,7
CD243	80,3	CD277	44,3	Ig light chain k	23,4	MSC (W7C6)	11,6
CD102 (I-CAM2)	79,3	CD51	43,9	IgGFc	23,4	CD278 (ICOS)	11,6
IgD	78,7	CD274 (PD-L1)	43,8	CD207 (Langerin)	23,4	CD258 (LIGHT)	11,5
CD24	78,1	CD217 (IL-17RA)	43,5	CD45RB	23,3	CD13	11,4
CD301	74,7	CD58	43,5	CD11c	22,3	CD81	10,7
BTLA	73,7	Ganglioside GD2	42,9	Sialyl lewis X	22	CD1b	10,5
CD43	73	CD307	42,8	CD317	21,4	CD28	10,3
CCR10	72,5	XCR1 (GPR5)	42,8	CD344 (Frizzled-4)	21,2	CD325	10,3
GPR83	71	CD183 (CXCR3)	42,5	CD276	21,1	CD220	10,1
CD199 (CCR9)	70,1	CD357(GITR)	41,9	CD29	21	CD267(TACI)	9,96
CD84	68,7	CD3	41,2	TCR g/d	20,8	EPHA2	9,89
CD48	67,9	CD323	41	CD83	20,8	CD164	9,88
CD7	66,4	CD148	40	CD97	20,8	TMEM8A	9,48
Notch 2	66	CD231 (TALLA)	39,9	CD45RA	20,5	CD218a (IL-18Rα)	9,38
CD45RO	65,8	CD181 (CXCR1)	39,3	Notch 1	20,4	CD1d	9,13
CD82	65,7	CD152 (CTLA-4)	38,7	CD261 (TRAIL-R1)	20,4	CD85j(ILT2)	9
CD88	64,2	CD57	38,2	CD300c	20	CD154	9
CD298	63,9	CD49e	37,5	CD11b	19,9	Dopamine Receptor D1	8,81
CCRL2	63,6	CD196 (CCR6)	37,4	CD120b	19,8	CD80	8,67
CD195(CCR5)	63,5	CD95	36,6	IL-15Rα	19,7	CD354 (TREM-1)	8,57
CD192 (CCR2)	63,3	CD107a (LAMP-1)	36,4	TRA-2-49	19,6	CD116	8,24
KLRG1	63,2	CD20	35,8	CD89 (FCAR)	18,9	integrin b7	7,94
MSC (W3D5)	62,9	CD79b	35,8	CD74	18,1	CD366 (Tim-2)	7,92
IL-28RA	61,8	CD115	35,7	CCX-XKR	17,5	Lymphotoxin β Receptor	7,74
Integrin b5	61,8	MSC and NPC (W4A5)	35,5	CD66b	17,3	CD93	7,71
CD230	61,2	CXCR7	34,5	CD8a	16,9	CD69	7,66
CD144	60,9	CD3030	34,3	CD170 (Siglec-5	16,8	CD92	7,57
CD284(TLR4)	60,9	CD22	34	CD304	16,5	CD180 (RP105)	7,35
CD155 (PVR)	60,6	CD254 (RANKL)	33,5	CD107b (LAMP-2)	16,3	B7-H4	7,27
CD263 (DcR1, TRAIL-R3)	59,8	CD5	33,5	CD203c (E-NPP3)	15,8	CD99	7,17
FPR3	59,4	CD31	32,5	CD252 (OX40L)	15,4	Siglec-9	7,14
CD369 (Dectin-1/CLEC7A	59,3	CD140b	32,2	CD66a/c/e	15,2	C3AR	7,03
CD52	58,7	CD371 (CLEC12A	32,1	SUSD2	15,1	TRA-1-60-R	6,95
CD124	58,5	CD194	32,1	CD100	15,1	CD334 (FGFR4)	6,93
Ig light chain λ	58,4	CD87	31,6	CD27	15	CD41	6,8
CD282(TLR2)	58,3	VEGFR3	31,5	TRA-2-54	14,8	CD213α2	6,72
CD132 (IL-2RG)	58	CD63	31,1	TRA-1-81	14,6	CD200R	6,65
TIGIT	56,6	CD210(IL-10r)	30,7	CD19	14,6	CD33	6,45
MICA/MICB	56,5	Tim-4	29,7	TLT-2	14,5	CD178 (Fas-L)	6,18
CD18	55,7	CD166	29,7	CD262 (TRAIL-R2)	14,5	NTB-A (NTBA)	6,06
LOX-1 (Clec8)	55,2	CD137L (4-1BB L)	29,2	TSLPR (TSLP-R)	14,3	CD340 (erbB2/)HER-2	6,05
CD158b (NKAT2)	54,5	CD64	29,2	CD10	14	CD227	5,9
TACSTD2	54,1	TCR a/ß	29,1	CD9	13,9	HLA-E	5,87
CD104	53,9	CD179a	29,1	HVEM (TR2)	13,8	CD94	5,86
CD50 (ICAM-3)	53,8	Podoplanin	28	MRGX2	13,8	CD290	5,81
CD26	53,3	CD130	27,3	CD8	13,8	CD158	5,79
CD71 (Transferrin Receptor1)	53,2	CD319 (CRACC	26,9	CD172a/b (SIRP/)	13,6	CD96	5,71
CD323 (JAM3)	53,1	CD85a(ILT5)	26,6	CD141	13,5	CD328 (Siglec-7)	5,6
IFN-γRβ chain	52,9	CD2	26,6	CD268 (BAFFR)	13,5	Cadherin 11	5,59
CRTAM	51,9	erbB3/HER-3	26,5	CD15	13,4	CD49a	5,59
CD45	51,7	CD129 (IL1R)	26	CD16	13,4	CD49d	5,59
CD370 (CLEC9A/DNGR1)	50,7	CD245 (p220/240)	26	CD160	12,6		

The Biolegend® antibody array has 361 lyophilised antibodies conjugated to phycoerythrin (PE) and screens cells for surface marker expression with flow cytometry. Single cells were isolated from the aortic wall and ILT of patients after enzymatic digestion (chapter 2.51), enriched for CD45+Live cells with FACS (chapter 2.6.2) and combined. In total, $5.9x10^6$ cells were dispensed in to the pre-loaded 96 well plates of the array as per manufacturers recommendations and run on a BD Canto flow cytometer (described in 2.6.4). Two-hundred and forty markers were above the five percent threshold, based on isotype controls. Names and percentages are represented in the table.

The frequency of lineage markers CD3, CD8, CD20, HLA-DR, CD14, CD11b and CD66a were within the range of expected events based on previous FC analysis of the ILT and aorta. The T cell markers, CD3 and CD8, frequencies were 39.7% and 11.9% respectively, while CD20 the B cell marker was 36.5%, CD14 was 43.9% and CD11b the myeloid marker was 20.6%, CD66A the granulocyte marker was 12.3% and HLA-DR the activation marker was 45%. Natural killer cell markers CD56 and CD57 were 3% and 5.9% respectively. HLA-BC (a pan leucocyte marker) was positive in 86.6% and was subsequently added to the CyTOF panel as a marker to distinguish cells from debris. **(Figure 3.14)**.

A few interesting antibodes were discovered through the screening array and were incorporated in to the final panels. CD172a (anti-phagocytic(156)) and CD13 (MMP release(157)) were positive from the macrophage markers. Several of the T cell chemokine receptors were positive (CCR4, CXCR3, CCR6), but an unexpected finding was that CCR5 (trafficking of leucocytes in to tissue(158)) was positive in 44% of the cells **(Figure 3.15)**. The Toll like receptors (TLR2, TLR4) were also increased, as well as the immune checkpoint inhibitor PD1 and its ligand PDL1 **(Figure 3.16)**. These have not been described in the cells of AAA before.

Although the Biolegend® Legendscreen™ antibody array required several optimisation steps and expended a significant proportion of stored cells, it was instructive and confirmed several known antibodies as well as adding novelty to the final panel design.

Figure 3.14: Analysis of core lineage markers in the Biolegend® antibody array panel

The Biolegend® antibody array uses 361 lyophilised antibodies conjugated to phycoerythrin (PE) and screens cells for surface marker expression with flow cytometry. Single cells were isolated from the aortic wall and ILT of patients after enzymatic digestion (chapter 2.51), enriched for CD45+Live cells with FACS (chapter 2.6.2) and combined. In total, $5.9x10^6$ cells were dispensed in to the pre-loaded 96 well plates of the array as per manufacturers recommendations and run on a BD Canto flow cytometer (described in 2.6.4). Events are displayed in colour dot plots gated on Live-CD45 single cells.
(A) Above are several common and core markers that were anticipated to be positive in the panel. HLA-BC is a pan leucocyte marker that was found in 86.6% of the events. The T cell markers CD3 and CD8 were positive (39.7% vs 11.9%) as well as CD20 the B cell marker (36.5%), CD14 (43.9%) and CD11b (20.6%) the myeloid marker, CD66A the granulocyte marker (12.3%) and HLA-DR (45%) the common activation marker.
(B) Above are several B cell markers that were found to be positive in the array panel. IgD is a marker of naïve B cells and CD27 is a marker of memory B and T cells. Both were positive as well as CD24, a marker of B regulatory and transitional B cells. CD43 was also positive, it is both a T and B cell marker.
(C) Neutrophil markers CD15 and Siglec-9 were positive, as well as the NK marker CD56. CD57 is often co-expressed with CD56, but was more abundant, suggesting that it was also found in other cell types.

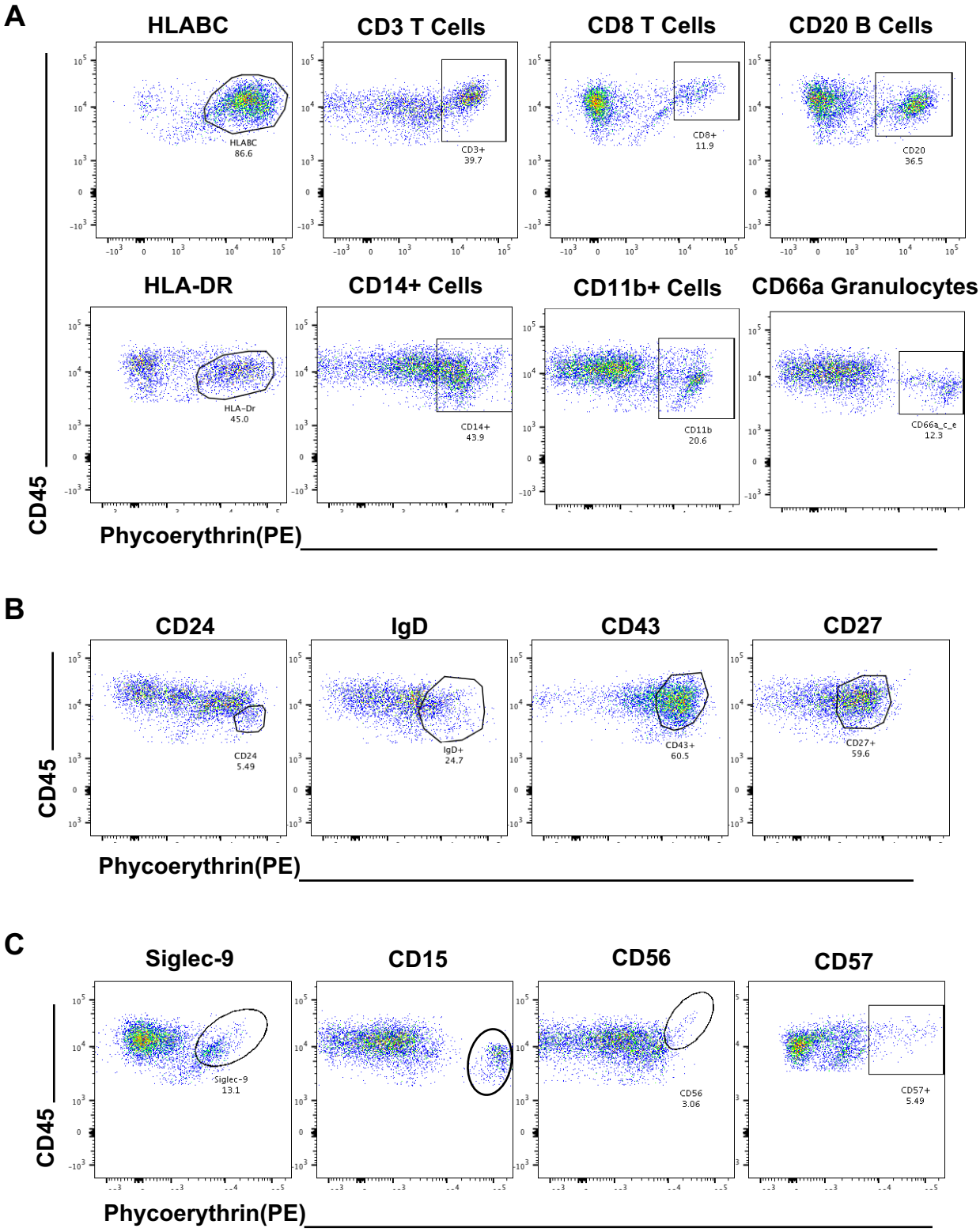


Figure 3.14 Flow cytometry analysis of core lineage markers in the Biolegend® antibody array panel

Figure 3.15: Analysis of common mononuclear phagocyte markers in the Biolegend® antibody array panel

The Biolegend® antibody array uses 361 lyophilised antibodies conjugated to phycoerythrin (PE) and screens cells for surface marker expression with flow cytometry. Single cells were isolated from the aortic wall and ILT of patients after enzymatic digestion (chapter 2.5), enriched for CD45+Live cells with FACS (chapter 2.6.2) and combined. In total, $5.9x10^6$ cells were dispensed in to the pre-loaded 96 well plates of the array as per manufacturers recommendations and run on a BD Canto flow cytometer (described in 2.6.4). Events are displayed in colour dot plots gated on Live-CD45 single cells.
(A) CD11c and CD36 which are common macrophage markers were positive, whilst several others were not clearly positive (CD86, CXCR1, CD80, CD200R). CD172a is an anti-phagocytic marker found on macrophages and dendritic cells was positive, together with CD13 which is related to the matrix metalloprotease (MMP) family and found on macrophages.
(B) CD45RA is found in naïve T cells as well as B cells and was positive in the array. CCR7 is found in both memory and naïve T cells and was also positive. CCR4, CXCR3, CCR6 and CD62 L can be used to distinguish between T helper cell subsets and were positive. An unexpected but very positive marker was CCR5, which is found in T cells and is also found on certain metastatic cancer T cell subtypes.

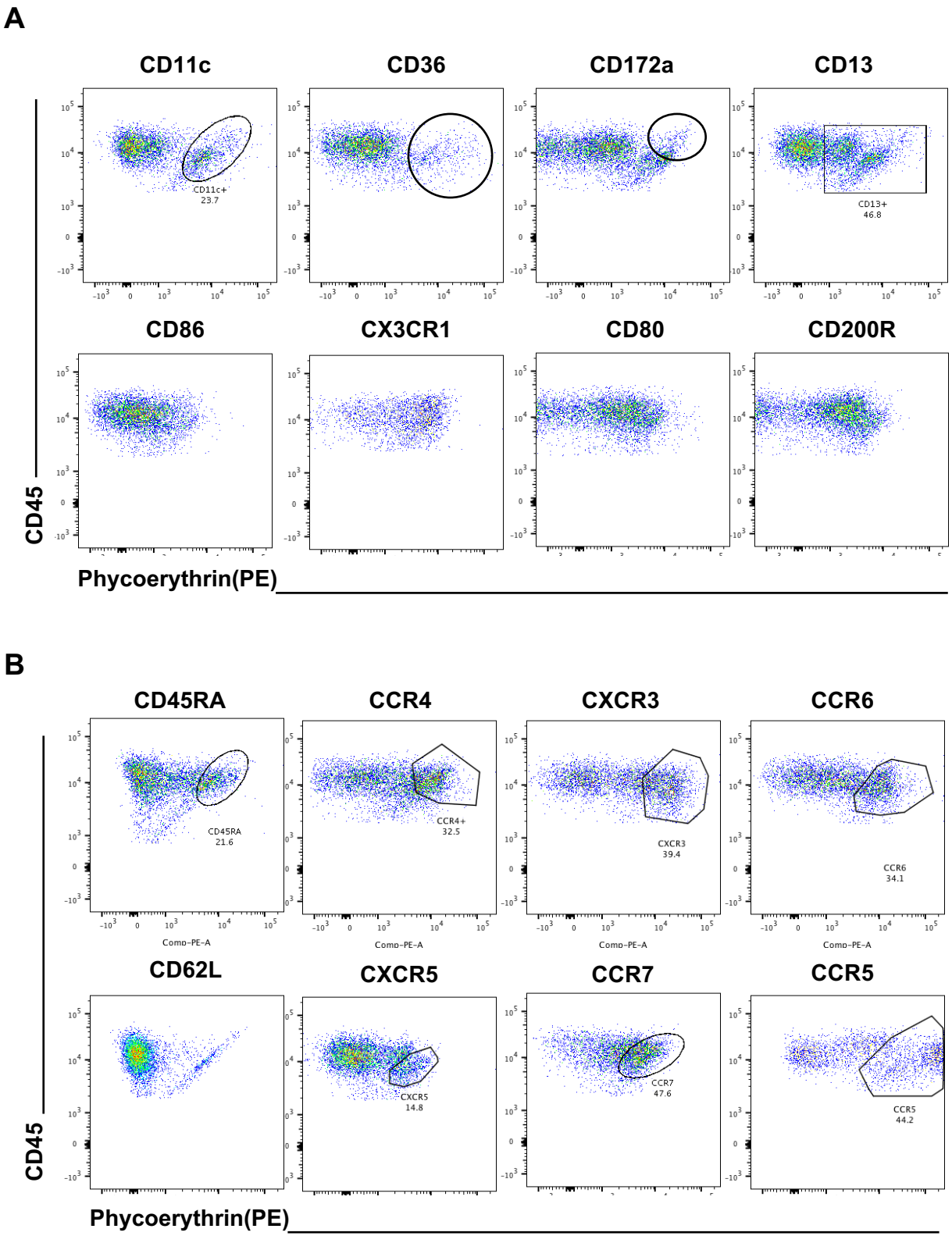


Figure 3.15 Flow cytometry analysis of common mononuclear phagocyte markers in the Biolegend® antibody array panel

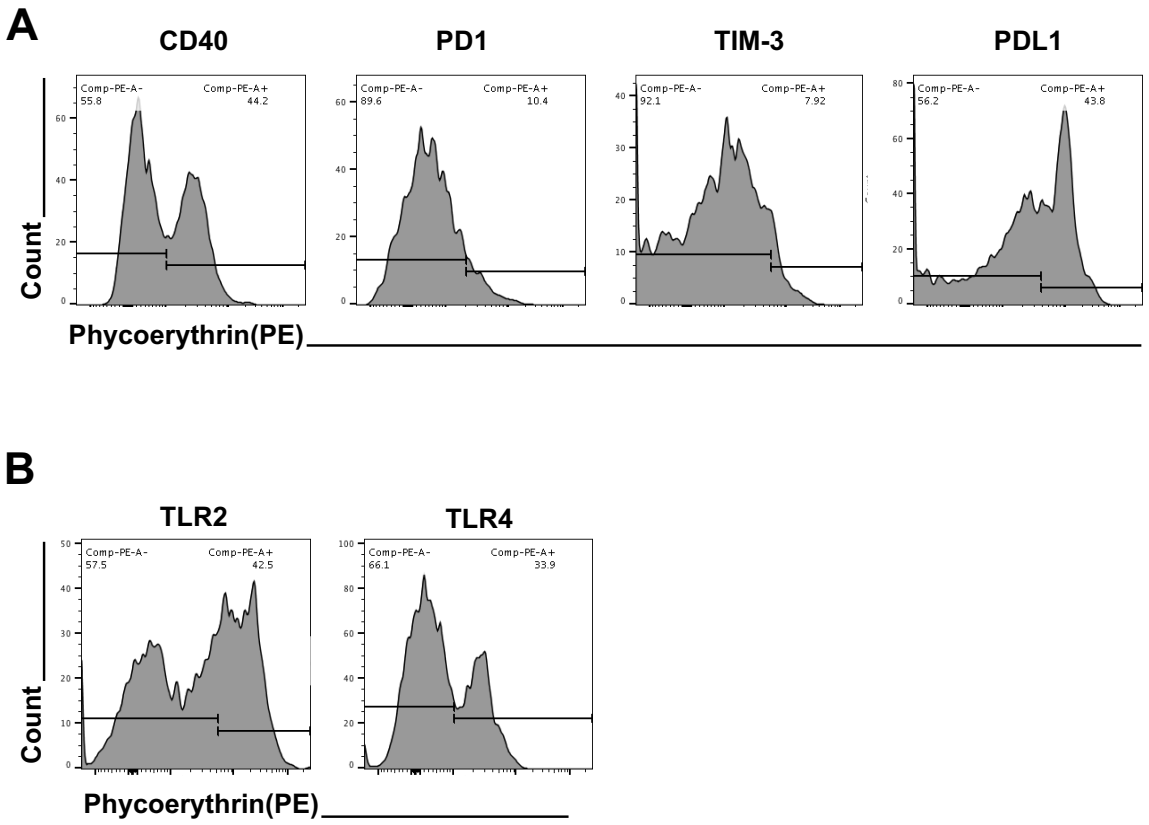


Figure 3.16: Analysis of co-stimulatory markers in the Biolegend® antibody array panel

The Biolegend® antibody array uses 361 lyophilised antibodies conjugated to phycoerythrin (PE) and screens cells for surface marker expression with flow cytometry. Single cells were isolated from the aortic wall and ILT of patients after enzymatic digestion (chapter 2.5), enriched for CD45+Live cells with FACS (chapter 2.6.2) and combined. In total, $5.9x10^6$ cells were dispensed in to the pre-loaded 96 well plates of the array as per manufacturers recommendations and run on a BD Canto flow cytometer (described in 2.6.4). Events are displayed in colour dot plots gated on Live-CD45 single cells.
Histograms of the flow cytometry data are presented. CD40, Tim-3, PD-1 and PD-L1 were all increased in the aortic complex cells **(A)**. In addition, the Toll like receptors 2 and 4 (TLR, TLR4) were positive **(B)**.

3.5.7 CyTOF panel design

Based on the preliminary findings from flow cytometry and the Biolegend® antibody array, I decided to design two separate panels, one dedicated to the lymphoid populations, the second to myeloid populations. **(Figure 3.20).**

The mononuclear phagocyte and granulocyte panel had a similar set of core lineage markers (CD45, FITC, CD19, CD14, CD66A, HLA-DR, CD3, CD16, CD7) and markers that would delineate subsets of macrophages, monocytes, dendritic cells, granulocytes, chemokines and toll like receptors (TLR) **(Figure 3.20)**.

Antibodies for these panels were purchased from Fluidigm® when available, and the remainder were conjugated to metal tags in house (methods chapter 3.4.2.2).

3.5.8 Titrating antibodies

In total thirteen antibodies were conjugated in-house and the remainder were purchased pre-conjugated and titrated from Fluidigm® (described in section 3.4.2.2). Conjugations were performed in three batches using the MaxPar® antibody conjugation kit (section 3.4.2.2) and their protein concentrations were analysed as a function of efficiency using the A280 absorbance to calculate protein content through a Nanodrop (Thermofisher) (chapter 2.7.2). Final concentrations were adjusted based on the titrated concentrations.

As an example of the titration process, the titration of CD15 antibody is presented. The CD15 antibody was conjugated to Neodymium (Nd142, chapter 3.4.2.2) and labelled (chapter 2.7) to lysed whole blood (chapter 2.5.1.3) in serial dilutions for its titrations. CD15 is a neutrophil marker.

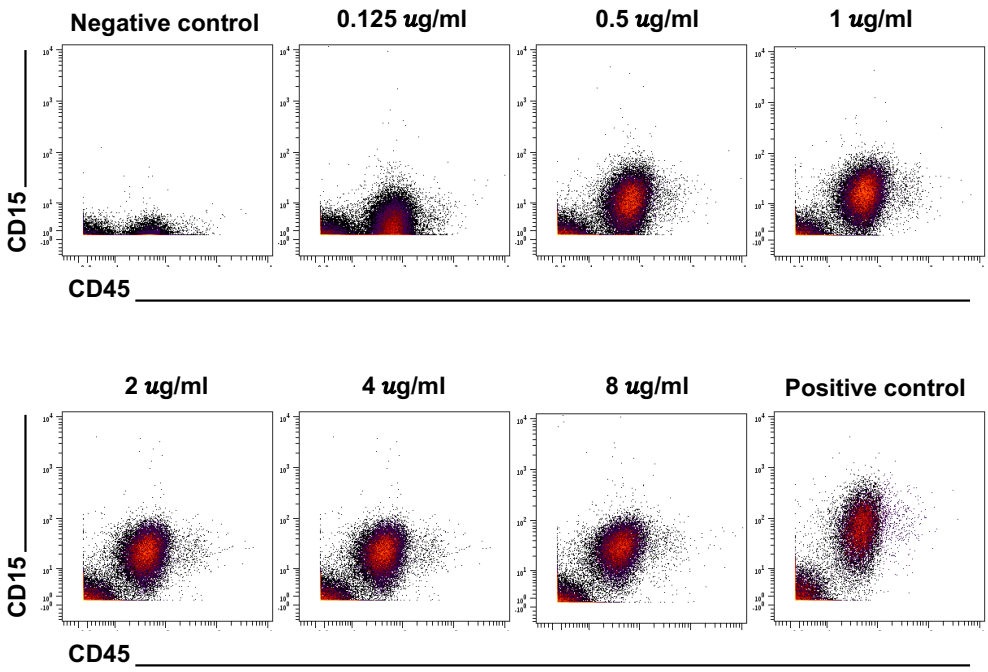


Figure 3.17: CD15 CyTOF antibody titration

The CD15 antibody was conjugated to Neodymium (Nd142, chapter 2.7.2). Leucocytes were isolated from lysed whole blood (chapter 2.5.1.3) and labelled (chapter 2.7.1) with serial dilutions of the CD15 antibody. These were analysed on the Helios mass cytometer and the *.fcs* files exported in to Cytobank.
Dot plots compared positive and negative controls to the serial dilutions (CD45 x-axis, CD15 y-axis). The reporting of the antibody improves as the concentration increases. At 2 µg/ml the antibody reports the population of CD15 positive CD45 cells with minimal improvements at higher concentrations. This concentration (2 µg/ml) was then incorporated into the panel and re-tested in combination with the entire panel and on different tissue types to assess its performance.

CyTOF analysis with dot plots compared positive and negative controls to the serial dilutions (CD45 y-axis, CD15 x-axis). At 2 µg/ml the antibody reported the population of CD15 positive CD45 cells. This was the minimum effective concentration and was then incorporated into the panel and re-tested in combination with the entire panel and on different tissue types to assess its performance **(Figure 3.17)**.

In addition to the consideration of the minimum effective concentration, metals in the were interrogated for contaminating signals. Oxidative spill over is the process

whereby metals artefactually increase the signal in adjacent metals (+1) or ones in the +16 position of the periodic table.

The CD57 antibody required re-titration. Although it reported effectively at a concentration of 0.25µg/ml, it still had significant 'spill-over' into the +16 position at this concentration. This decreased at a concentration of 0.0325µg/ml whilst still effectively reporting the antibody. Thus, CD57-Nd148 at 0.0325µg/ml was incorporated into the final panel **(Figure 3.18)**.

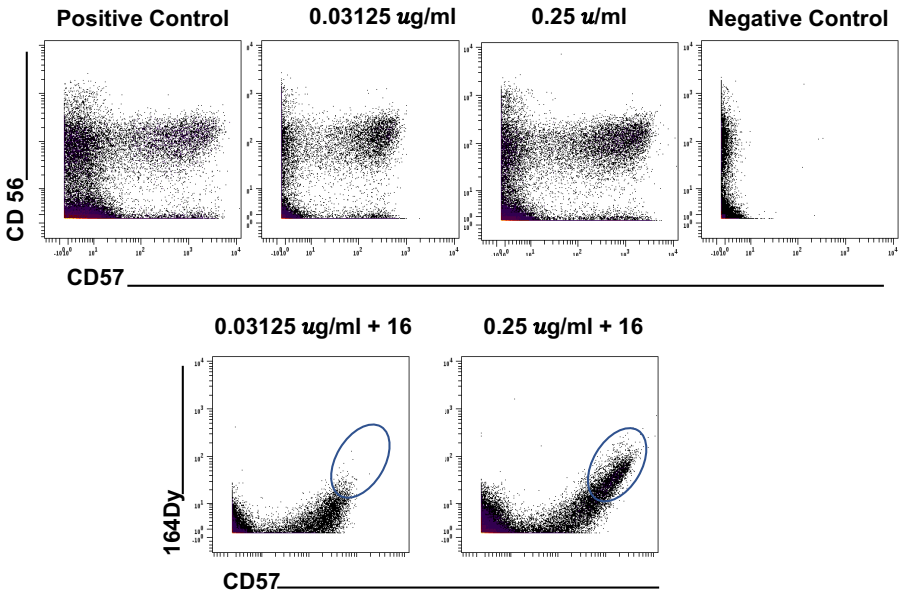
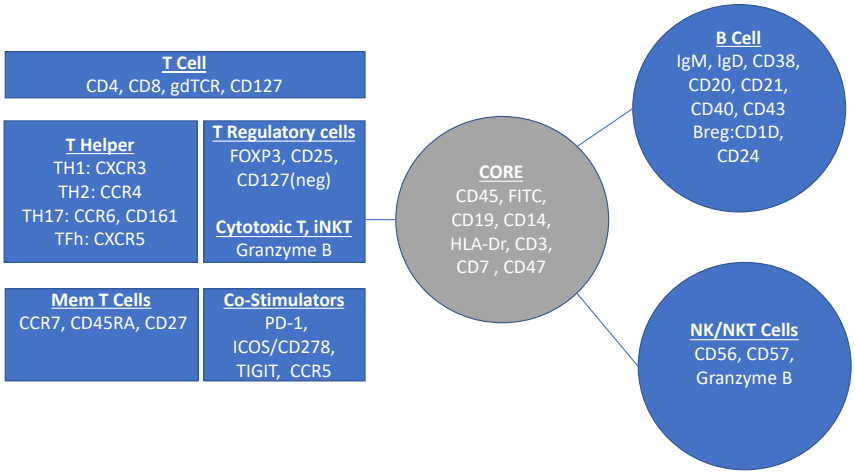


Figure 3.18: Assessment of CD57 spill-over in to +16 at higher concentrations

Initial titration of CD57 (conjugated to Nd148), had significant spill-over artefacts into the +16 position (Dy164) and required re-titration. CD57 (Nd148) was serially diluted (0.25 – 0.0039 µg/ml) and labelled to leucocytes that were isolated from cryopreserved PBMCs (chapter 2.5.1.3). These were analysed on the Helios mass cytometer and the *.fcs* files exported in to Cytobank.
(A) CD57 effectively reported at both concentrations (0.25 µg/ml and 0.0325 µg/ml),
(B) At the 0.25 µg/ml concentration it still has significant artefactual spill-over into the +16 position.
(C) This is decreased at a concentration of 0.0325µg/ml whilst still effectively reporting CD57. Thus, CD57-Nd148 at 0.0325µg/ml was incorporated into the final panel.

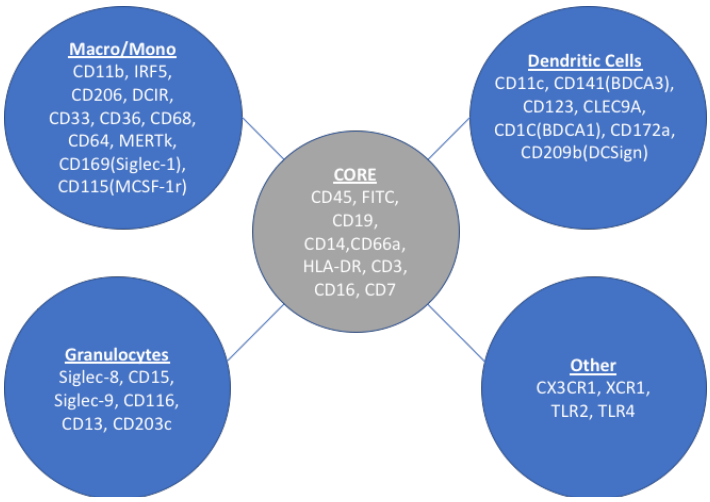
3.5.9 The final panels

Once the antibodies were titrated, the entire panel was tested on blood and then aorta and thrombus to confirm the titrated concentrations and minimise their interactions. The final myeloid panel and final lymphocyte panel is displayed in **Figure 3.19 and Figure 3.20**.



Metal		Antibody	Metal		Antibody
Pr	141	HLA-ABC	Dy	161	CD20
Nd	142	CD19	Dy	162	CD1D
Nd	143	CD127	Dy	163	CXCR3
Nd	144	FITC	Dy	164	CD161
Nd	145	CD4	Ho	165	CD40
Nd	146	IgD	Er	166	CD24
Sm	147	CD7	Er	167	CCR7
Nd	148	CD57	Er	168	CD8
Sm	149	CCR4(CD194)	Tm	169	CD25
Nd	150	CD43	Er	170	CD45RA
Eu	151	ICOS/CD278	Yb	171	Granzyme B
Sm	152	CD21	Yb	172	IgM
Eu	153	CXCR5	Yb	173	gdTCR
Sm	154	CD3	Yb	174	HLA-DR
Gd	155	CD27	Lu	175	PD-1
Gd	156	CCR5	Yb	176	CD56
Gd	158	CD38	Y	89	CD45
Tb	159	FoxP3	Bi	209	CD11b
Gd	160	TIGIT		Inhouse conjugation	

Figure 3.19: Design of the lymphocyte panel, incorporating core and specific cell identifiers



Metal		Antibody	Metal		Antibody
Pr	141	HLA-ABC	Dy	161	Clec9A/CD370
Nd	142	CD19	Dy	162	CD115
Nd	143	CD15	Dy	163	CD169(Siglec-1)
Nd	144	FITC	Dy	164	Siglec 8
Nd	145	DCIR	Ho	165	CD163
Nd	146	CD64	Er	166	CD7
Sm	147	CD13	Er	167	IRF5
Nd	148	CD16	Er	168	CD206
Sm	149	CD66a	Tm	169	CD33
Nd	150	CD1c	Er	170	CD209b(DC-Sign)
Eu	151	CD123	Yb	171	CD68
Sm	152	CD36	Yb	172	CX3CR1
Eu	153	MERTk	Yb	173	CD141/BDCA3
Sm	154	CD3	Yb	174	HLA-DR
Gd	155	Siglec 9	Lu	175	CD172a
Gd	156	PD-L1	Yb	176	TLR2
Gd	158	TLR4	Y	89	CD45
Tb	159	CD11c	Bi	209	CD11b
Gd	160	CD14		Inhouse conjugation	

Figure 3.20: Design of the myeloid panel, incorporating core and specific cell identifiers

3.6 Discussion

Herein, I optimised the methodology required for performing deep phenotyping of the aortic complex, overcoming its inherent challenges, including the low yield of hematopoietic cells and the known autofluorescence of tissues(119). This optimisation allowed the first canvassing of the main immune populations contained within the aortic complex by mass and flow cytometry.

As described in the introduction, the mononuclear cell infiltrate is the hallmark of AAAs, and adds to the tissue destruction through release of peptides such as MMPs. The aortic wall was replete with T and B cells, with a smaller contribution from other cell types. The majority of studies thus far have used histology and IHC and had described a T cell and B cell frequency similar to our findings(63, 68, 133). Some have used FC to characterise the CD4 T cells within the infiltrate(159), and building on their previously published work, Lu et al confirmed a clonally expanded T cell infiltrate, suggesting ongoing immune activation even in late-stage disease(64, 138). Furthermore, we had a low yield of CD14+ macrophages (+-2%), and this was also consistent with the human AAA literature(133). Interestingly, this is in contrast to the murine model literature, and may represent a late stage of disease as compared to the early initiation phase in mouse models(143, 147).

Sagan et al published the only other study that investigated ILT with FC. Granulocytes (70%) were the most prevalent cell type, followed by monocytes (18%) and T cells (7%), and this was similar to our findings as well others who investigated the ILT with IHC(93, 96). More recently, Rao et al described a unique macrophage phenotype within the ILT, and indeed we did have CD14+ cells which required deeper phenotyping to ascertain if it is consistent with their description(95)

CyTOF was a natural follow up step to for deep immunophenotyping. However, one of its challenges as a technology included its relatively low throughput rate and sensitivity to debris within the single cell suspension. The CD45 fraction was relatively low in these tissues and required enrichment whilst the specimens were debris laden. In the enrichment process, the proof of principle for cell sorting in complex human tissues prior to CyTOF was demonstrated. Cell sorting prior to single cell analysis had not previously been described in human vascular tissues, to the best of our knowledge. Encouragingly, during the course of this work, an investigation of murine atherosclerosis was published using a similar methodology. They had successfully cell sorted murine vascular tissues prior to RNASeq (160).

The Biolegend® Legendscreen™ array provided a novel hybrid model of marker selection over a purely pre-selected marker driven cytometry strategy. This strategy had been previously successfully implemented in a deep phenotyping investigation of renal cell carcinoma with CyTOF(161). For me, it provided several novel targets, whilst simultaneously confirming the presence of several known markers within a single experiment.

The aortic wall and the thrombus consistently demonstrated a unique complement of immune cells. Moreover, the results from flow cytometry and the first attempt by mass cytometry were overlapping, indicating that I achieved a robust approach to the analysis of these tissues.

3.7 Conclusion

The AAA wall has features of adaptive immunity, whilst the ILT has features of innate immunity. The heterogeneity of the immune cell composition within the aortic wall and the thrombus potentially has pathophysiological implications. AAA formation is an insidious process and the complex interplay between the various immune cell phenotypes requires further investigation. More especially, the ILT is in contact with the aortic wall as well as the systemic circulation and may have both local and systemic effects.

Chapter 4

DEEP IMMUNOPHENOTYPING THE ABDOMINAL AORTIC ANEURYSM COMPLEX

4.1 Introduction

Abdominal aortic aneurysms are an insidious disease that progresses slowly over years. Pharmacological treatments to attenuate growth has thus far been elusive, and have focused on broad mechanisms, such as the use of Doxycycline as an MMP inhibitor(162, 163). Deep phenotyping allows for the examination of an individual in granular detail, through collecting multiple inputs and deconvoluting these through using sophisticated algorithms which are often agnostic. Deep immune phenotyping matches a disease phenotype, and through the examination of the immune cells demonstrates the different dimensions of the disease. Breakthroughs in science often develop after we are able to describe, measure or quantify a process in a manner that was not previously achievable.

Immune cells subsets are heterogenous and this is well described (protective vs pathogenic, destructive vs reparative). However, the details of this heterogeneity have been limited by experimental constraints. Single cell technologies such as mass cytometry and RNAseq allow for the profiling of single cells at an unprecedented resolution. A better understanding of the mechanisms underlying immunologic responses will lead to better treatments for AAAs.

This chapter describes the foundational immune landscape of the aneurysm wall, ILT and peripheral blood in AAAs. Having established that the aneurysm complex does indeed have immune cells, then developed a curated panel of antibodies for its interrogation with CyTOF in the previous chapter, this chapter will provide new insights into the inflammatory cell infiltrate of the aortic wall and ILT within AAAs on a single cell level.

4.2 Hypothesis and aims

In this chapter I hypothesised that the human aortic aneurysm complex (aortic wall, intraluminal thrombus and peripheral blood) has a unique immune cell phenotype characterised by T cells, B cells, mononuclear phagocytes and granulocytes and that there is a complex interplay between the cells.

The aims were to:

- Interrogate matching patient samples with CyTOF
- Define the immune subsets within each tissue type

Figure 4.1: Experimental design and workflow for CyTOF immunophenotyping of AAA tissues

(A) Patients with abdominal aortic aneurysms (AAA) undergoing open surgical repair were recruited through the OxAAA study. Blood, aortic wall and intraluminal thrombus (ILT) were collected intraoperatively. **(B)** Single cell suspensions were isolated by enzymatic digestion of the aorta and ILT (described in 2.5.1) prior to enrichment of CD45+ cells using FACS (described in 2.6.2). Leukocytes were isolated from the blood after lysis of red blood cells (described in 2.5.1.3). Single cell samples were cryopreserved using DMSO and stored individually in liquid nitrogen for subsequent batch processing. **(C)** In total, ten matching aortas, ILT and blood (30 vials) were resuscitated from liquid nitrogen and labelled with CyTOF antibodies. The cell numbers allowed for the labelling of ten patients with the lymphocyte panel (Figure 3.19) and eight with myeloid panel (Figure 3.20) (CyTOF labelling methods in 2.7). **(D)** Samples were acquired on the Helios CyTOF mass cytometer. Data files were output in *.fcs* format and analysed using a combination of specialised techniques developed for CyTOF data, including viSNE and Phenograph analysis (discussed in chapter 2.7).

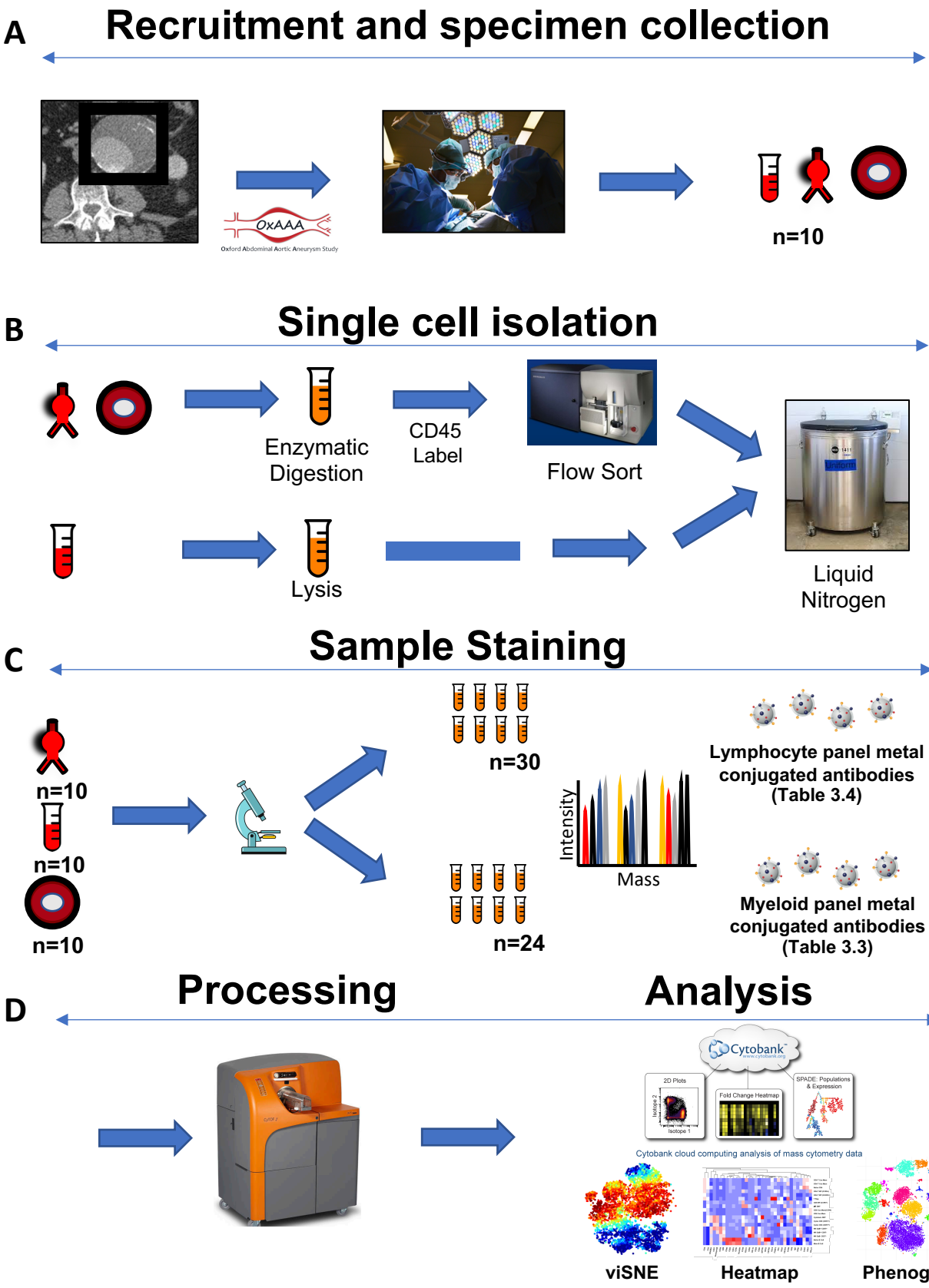


Figure 4.1 Experimental design, and workflow for CyTOF

4.3 Methods:

4.3.1 Experimental design and workflow

The recruitment process, retrieval of samples and single cell isolation have been detailed in the preceding chapters (chapter 2). Over a period of 4 months, ten consecutive patient samples were processed **(**patient characteristics in **Table 4.1**)**.** Single cell suspensions, from ten patients' aortas and ILT were isolated by enzymatic digestion (described in 2.5) prior to enrichment of CD45+ cells using FACS (described in 2.6.2). Their matching blood specimens were similarly enriched for leucocytes through red blood cell lysis (described in 2.5.2). The enriched single cell suspensions were stored in LN and batch processed. After thawing, cells were labelled with CyTOF antibodies (described in 2.7) from the curated panels (chapter 3) and acquired on the Helios CyTOF mass cytometer. The *.fcs* files were imported into Cytobank and viSNE analysis was performed on individual files (7500 iterations and perplexity of 70) after gating on CD45+ Live cells. **(Figure 4.1)**

All available aortic and ILT cells were acquired on the machine, whilst the blood samples were limited to 4 x 10^5 events per sample. Quality control samples were run between acquisitions, and the cytometer was re-calibrated daily and after any blockages to the system. Two ILT specimens were excluded due to excess heavy metal contamination (Barium) which would have damaged the detector decreasing its sensitivity and ultimately its lifespan. The files were saved in the *.fcs* format, which is the common cytometry standard. This was followed by analysis using a combination of specialised analysis tools developed for CyTOF data (discussed below) including viSNE and PhenographR analysis.

Table 4.1: Characteristics of study subjects included in the results phase

Patient Characteristics	
Number(Male)	10(8)
Age, years (SD)	71(5)
Weight(SD)	80(16)
BMI(SD)	26(4)
AAA size cm(SD)	6(0.4)
Smoking Status, n(%)	
Current	2(20)
Ex-smoker > 2months	7(70)
Pack years (SD)	38(13)
Never	2(20)
Co-Morbidities, n(%)	
COPD	0(0)
CAD	3(33)
PCI	2(20)
CABG	1(10)
Cerebrovascular disease	1(10)
Peripheral vascular disease	1(10)
Diabetes	1(10)
Hypertension	6(60)
Systolic mmHg(SD)	151(20)
Diastolic mmHg(SD)	90(15)
Hypercholesterolemia	6(60)
LDL mmol/L(SD)	2(1)
Trig mmol/L(SD)	1.5(0.8)
Creatinine µmol/L (SD)	82(19)
CRP mg/dL (SD)	6(9)
Pre-Op FMD, % (SD)	1.3(5)
Post-Op FMD, % (SD)	4.5(3)
Medications	
Statins	7(70)
Aspirin	4(40)
Thienopyridine	3(30)
Ace Inhibitor	4(40)
B Blocker	3(30)
Calcium channel blocker	1(10)

COPD – Chronic obstructive pulmonary disease, CAD- Coronary artery disease, PCI – Percutaneous coronary intervention, CABG – Coronary artery bypass graft, LDL – Low density lipoprotein, Trig – Triglycerides, CRP – C reactive protein, FMD – Flow mediated dilatation

4.3.2 Gating strategy for CyTOF

The *.fcs* files were uploaded on to Cytobank® for analysis. Individual dot plots were analysed and gated using a uniform strategy where the CD45+ leucocyte population was identified for downstream analysis. In principle, the gating sequence aimed to separate cells form debris, discriminate doublets and identify live cells.

To separate cells from debris, samples were interrogated with the Iridium intercalators (Ir191 and Ir193) on each axis. Double positivity of the Iridium intercalator (Ir191 and Ir193) indicated nucleated cells which were selected for further gating. From this gate, 'Event Length vs Ir193' was interrogated, and outlying event lengths were excluded. HLA-BC the pan leucocyte marker was then interrogated together with Ir193, and double positive leucocyte events were selected **(Figure 4.2A)**.

Three further gates were used to refine the doublet discrimination using the in-built Gaussian parameters from the Helios system which are derived from total ion current. This further discriminates cells from non-cell events. These were 'Event Length vs Centre', 'Event Length vs Width' and 'Width vs Residual' **(Figure 4.2B)**.

Then, live cells were identified using the live/dead Rhodium DNA intercalator vs Ir191. FITC as a surrogate for CD45 was plotted against HLA-ABC in order to identify the live-CD45 cells after calibration beads were removed **(Figure 4.2C)**. The cell enrichment by FACS used a FITC-CD45 flow cytometry antibody, thus the use of anti-FITC as a surrogate for CD45 (discussed in chapter 3.5.4). The peripheral blood was not labelled with CD45-FITC and thus was gated directly on the CyTOF CD45 antibody instead of FITC.

Figure 4.2: Gating strategy for identifying live CD45+ leukocytes

The gating strategy from an individual aortic aneurysm wall sample. Single cells were isolated and processed on the Helios mass cytometer after enzymatic digestion (described in 2.5.1) and CD45+ enrichment using FACS (described in 2.6.2). The enriched cells were labelled with the lymphocyte centric panel of CyTOF antibodies (chapter 2.7, Figure 3.19). The *.fcs* files were imported in to Cytobank and individual samples were interrogated with cytometry dot plots. The plots in this figure delineate the gating strategy used to identify CD45+ live events.
(A) Double positivity of the Iridium intercalator (Ir191 and Ir193) indicate nucleated cells. 'Event Length vs Ir193' excludes cell aggregates removing clumped cell debris, and the 'HLA-ABC' gate vs Ir193' selects double positive leucocytes with DNA intercalator present, thus removing non-leucocyte events. Three further gates were used to refine the doublet discrimination using the in-built Gaussian parameters from the Helios system. These are **(B)** 'Event Length vs Centre', 'Event Length vs Width' and 'Width vs Residual'. Then, **(C)**, live cells are identified using the live/dead Rhodium DNA intercalator vs Ir191. FITC as a surrogate for CD45 (discussed in chapter 3.5.4) was plotted against HLA-ABC identifying the live-CD45 leucocytes.

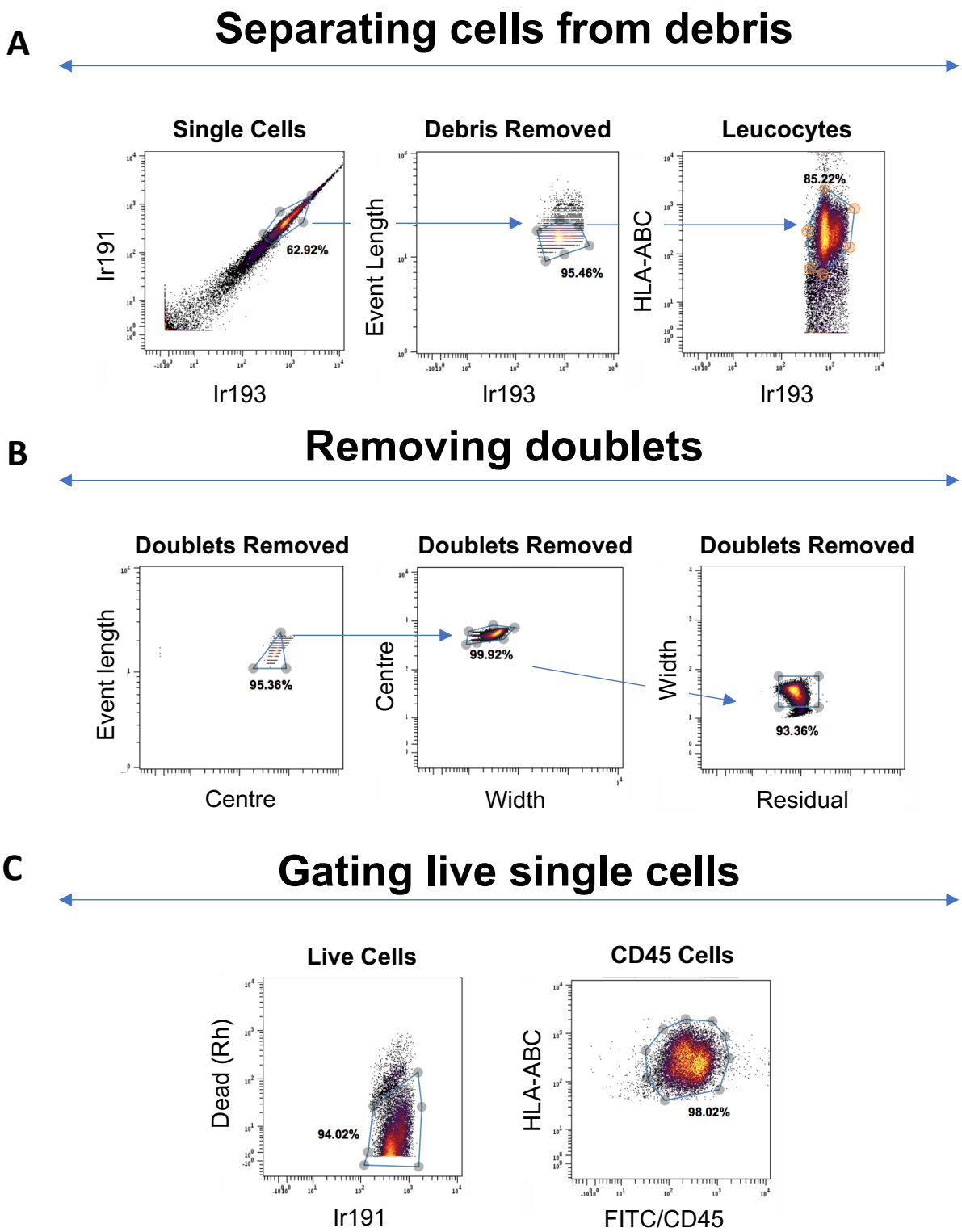


Figure 4.2 Gating strategy for identifying 'live CD45+' leukocytes

4.4 Results

4.4.1 Frequency of the primary immune populations in aorta, ILT and blood

From each individual sample, CD45 cells were gated on an analysed using viSNE, clustering on the main phenotypic markers to separate out the primary immune cell populations. The major immune cell types (T cells, B cells, Myeloid cells and NK cells) were identified across the samples using the automated unbiased viSNE clustering algorithm. The representative viSNE plots for each sample are presented in **Figures 4.3** (aortic wall samples), **4.4** (ILT samples) and **4.5** (blood samples), demonstrating the expression levels of some of the key phenotypic markers. The viSNE algorithm made a clear distinction between the major cell types, separating them out in discrete clusters. These corresponded with traditional cytometry dot-plots which commonly use two positive lineage markers for cell type identification. A summary and comparison for all the samples is presented in **Figure 4.6**. Two patients ILT (patients 1 and 10, barium contamination) and one patient's blood (Patient 10, loss of cells) did not meet the quality control requirements and were excluded from the analysis. Ten aortas, eight ILTs and nine blood samples were used in the final analysis.

The series of plots in **Figure 4.3, 4.4 and 4.5** highlights the individual tissue types and the immune cell heterogeneity in them. In the first plot of each sub figure, each cell cluster is represented by a different colour. The adjacent viSNE/s highlight the channel in which the named antibody is located. This is alongside their reciprocal individual dot plots that are used in traditional cytometry analysis. The markers are CD3, CD4, CD8, CD7, CD56, HLA-DR, CD19, CD20, CD27, IgD, CD11b, CD57 and Granzyme B. In a variation of the viSNE analysis used for the aortic wall and

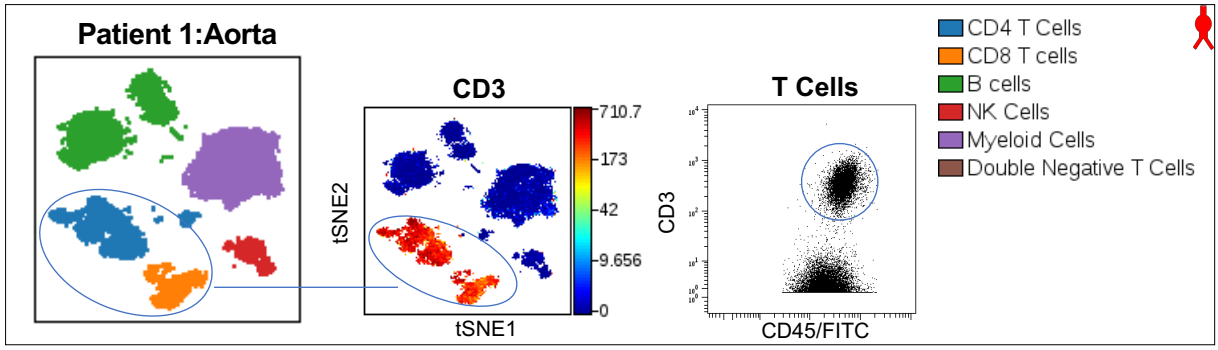
ILT, the cells in the blood from individual samples were combined and the clustering algorithm performed on 10 000 cells from each individual patient (90 000 in total). The multicoloured illustrative viSNE displays unique cell clusters in individual colours (**Figure 4.5)**. Each cluster has an associated panel displaying the highlighted lineage antibody channel as well as a traditional dot plot

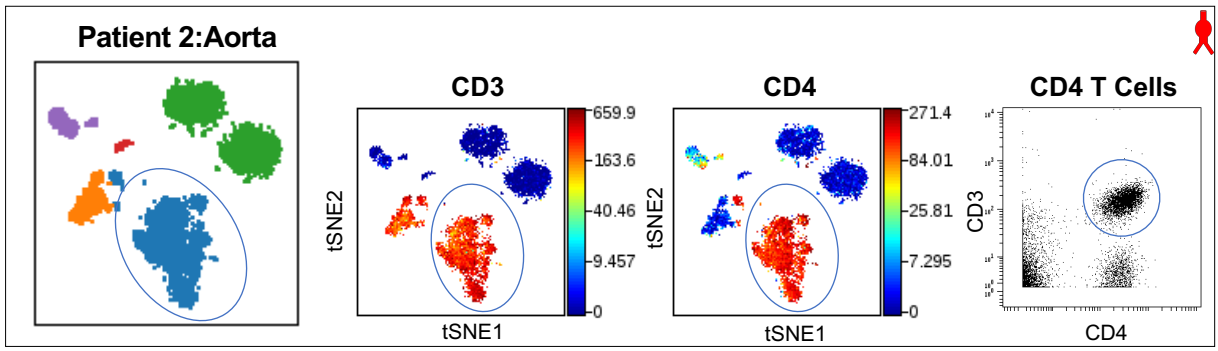
The T cells are further discriminated in to three distinct groups: CD4, CD8 or double negative T cells. NK cells cluster separately on the unbiased viSNE plots and are verified in traditional dot plots by double positivity of CD7 and CD56 whilst being CD3 negative. The myeloid cells are verified through traditional dot plots as CD11b+HLA-DR+. B-cells form a large cluster, and this is verified by traditional dot plots using CD19 and CD20 double positive staining. The memory B-cells further separate out from the larger B-cell cluster and are identified on traditional dot plots as CD19+CD27+, whilst the naïve B-cells are identified as IgD+CD19+ on dot plots. Granzyme B also features prominently in three of the clusters: CD8 T-cells, NK cells and CD4 T-cells.

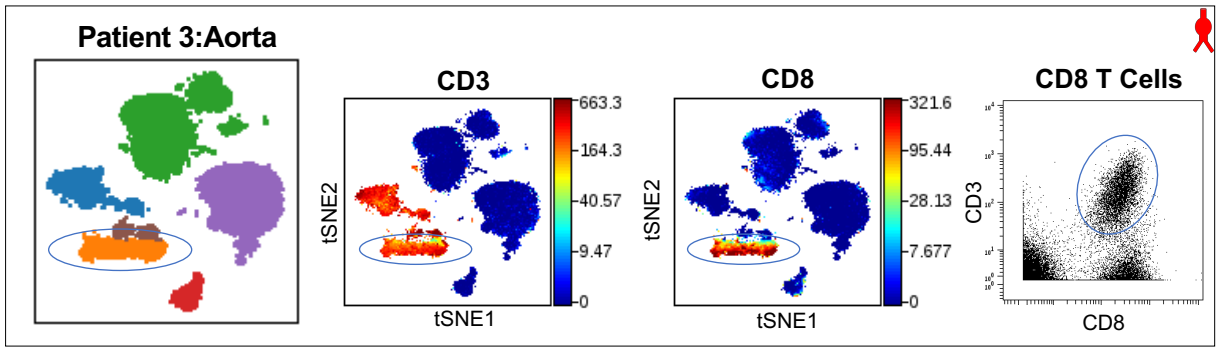
These results demonstrate the diversity and heterogeneity in the immune landscape of the aortic tissues.

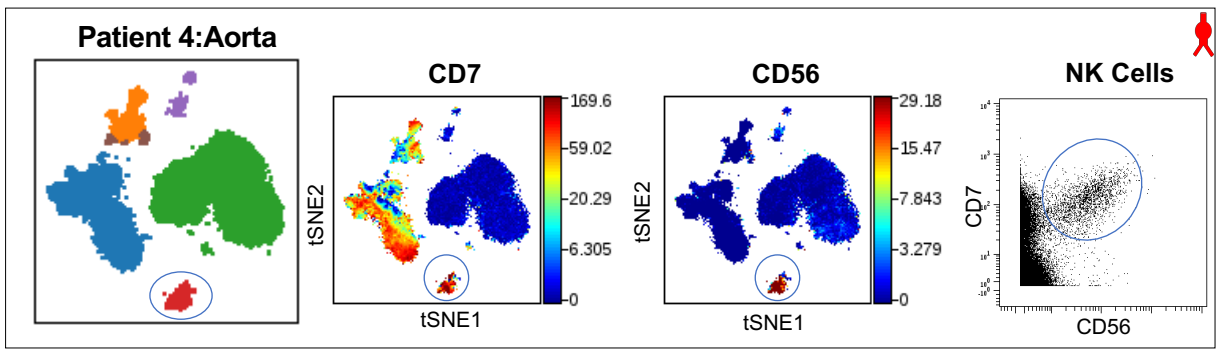
Figure 4.3: viSNE analysis of CD45+ cells isolated from ten aortic aneurysms

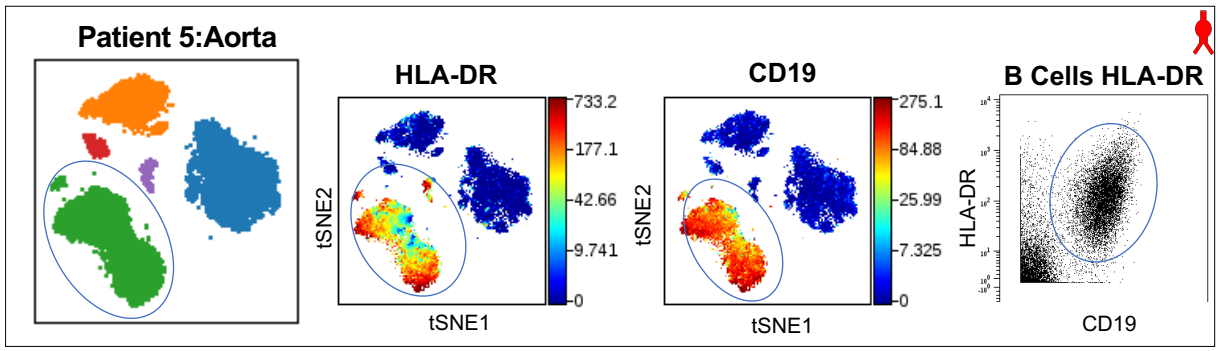
Single cell suspensions, from ten patients' aortas, were isolated by enzymatic digestion (described in 2.5.1) prior to enrichment of CD45+ cells using FACS (described in 2.6.2). The CD45+ single cell suspension was then labelled with CyTOF antibodies (CyTOF labelling methods in 2.7) from the lymphocyte centric panel (Figure 3.20) and acquired on the Helios CyTOF mass cytometer. The *.fcs* files were imported in to Cytobank and viSNE analysis was performed on individual files (7500 iterations and perplexity of 70) after gating on CD45+ Live cells (Figure 4.2).
This series of ten plots highlights common immune cell markers and their distribution and frequency using the automated viSNE clustering algorithm. Each series is an individual patient. In the first plot, each cell cluster is represented by a different colour. The adjacent viSNE/s highlight the channel in which the named antibody is located. This is alongside their reciprocal individual dot plots that are used in traditional cytometry analysis. The markers are CD3, CD4, CD8, CD7, CD56, HLA-DR, CD19, CD20, CD27, IgD, CD11b, CD57 and Granzyme B


Patient 1:Aorta
CD3
710.7
173
42
9.656
0
tSNE2
tSNE1
T Cells
CD3
CD45/FITC
CD4 T Cells
CD8 T cells
B cells
NK Cells
Myeloid Cells
Double Negative T Cells


Patient 2:Aorta
CD3
659.9
163.6
40.46
9.457
0
tSNE2
tSNE1
CD4
271.4
84.01
25.81
7.295
0
CD4 T Cells
CD3
CD4


Patient 3:Aorta
CD3
663.3
164.3
40.57
9.47
0
tSNE2
tSNE1
CD8
321.6
95.44
28.13
7.677
0
CD8 T Cells
CD3
CD8


Patient 4:Aorta
CD7
169.6
59.02
20.29
6.305
0
tSNE2
tSNE1
CD56
29.18
15.47
7.843
3.279
0
NK Cells
CD7
CD56


Patient 5:Aorta
HLA-DR
733.2
177.1
42.66
9.741
0
tSNE2
tSNE1
CD19
275.1
84.88
25.99
7.325
0
B Cells HLA-DR
HLA-DR
CD19

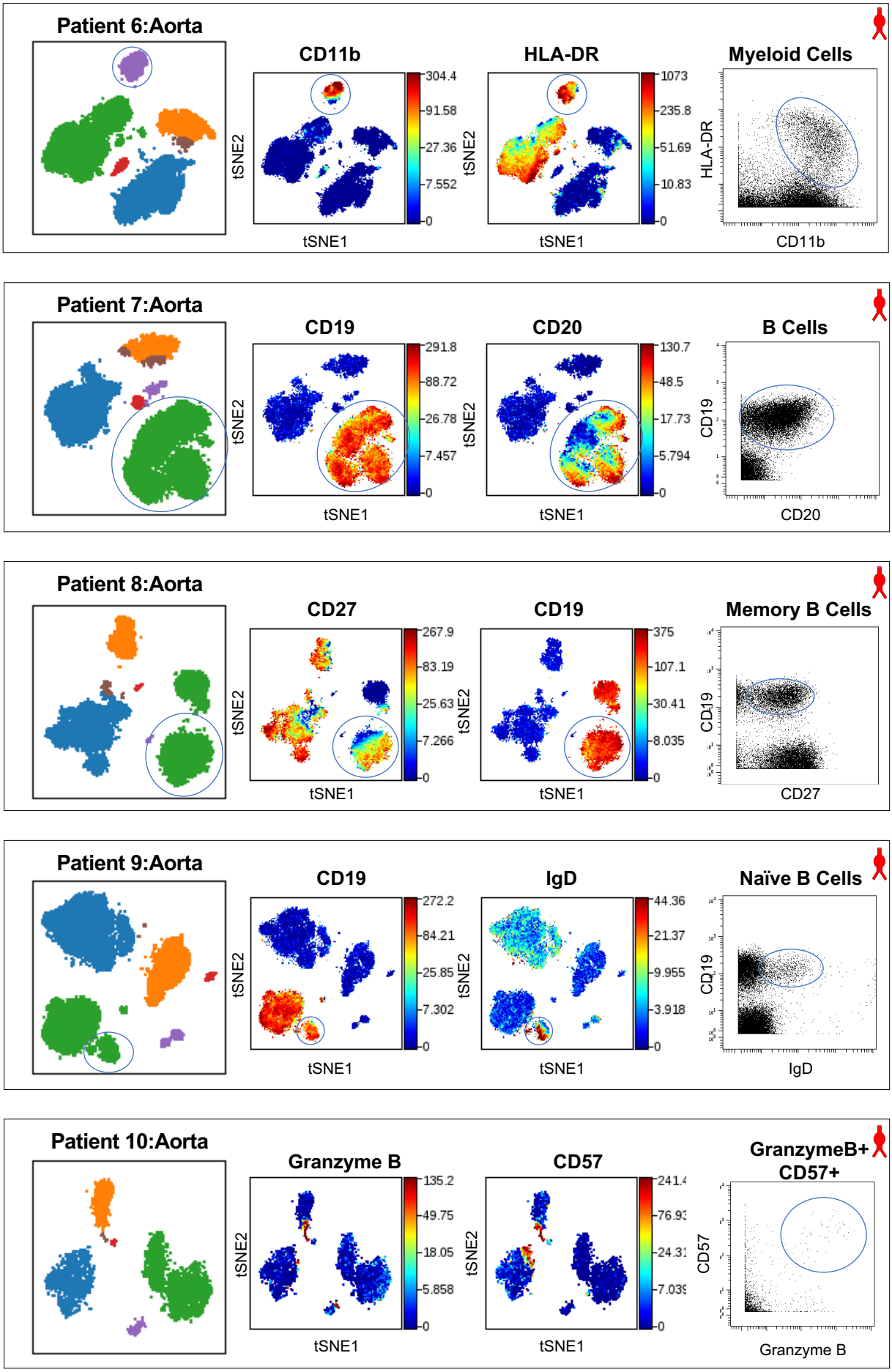
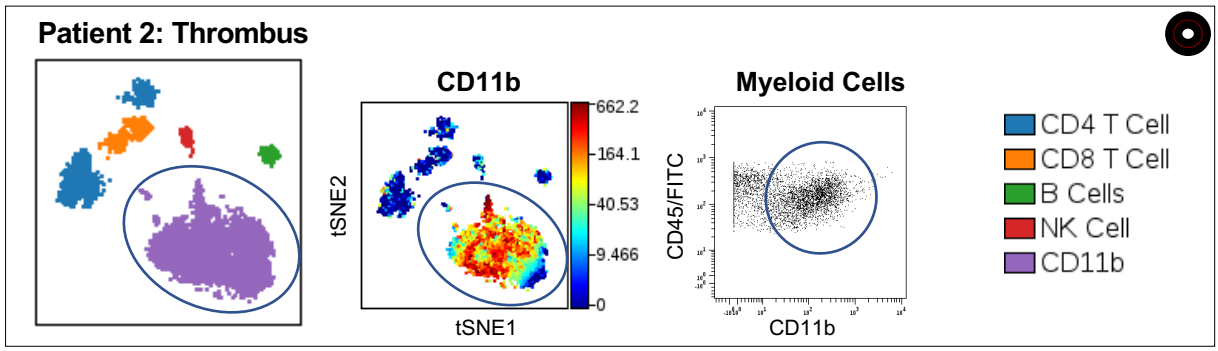
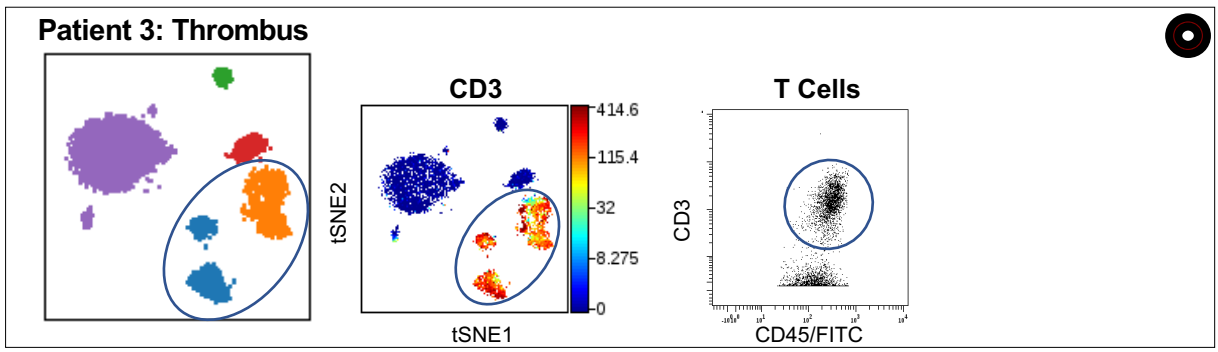
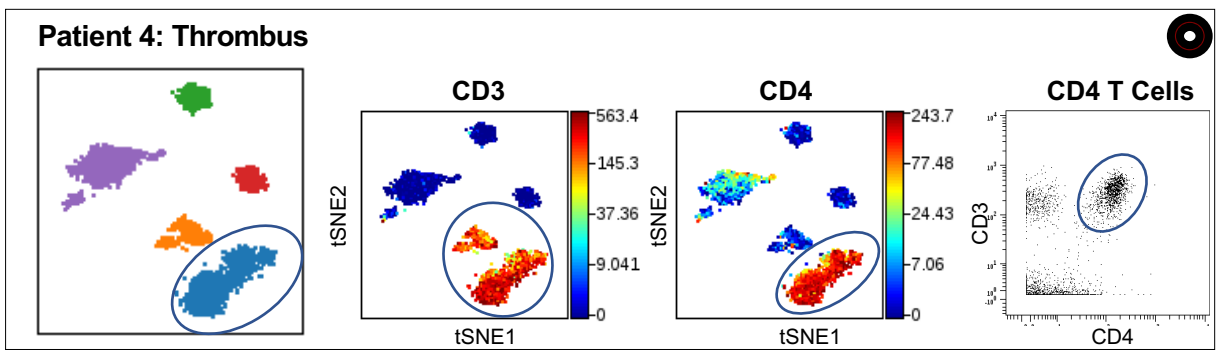
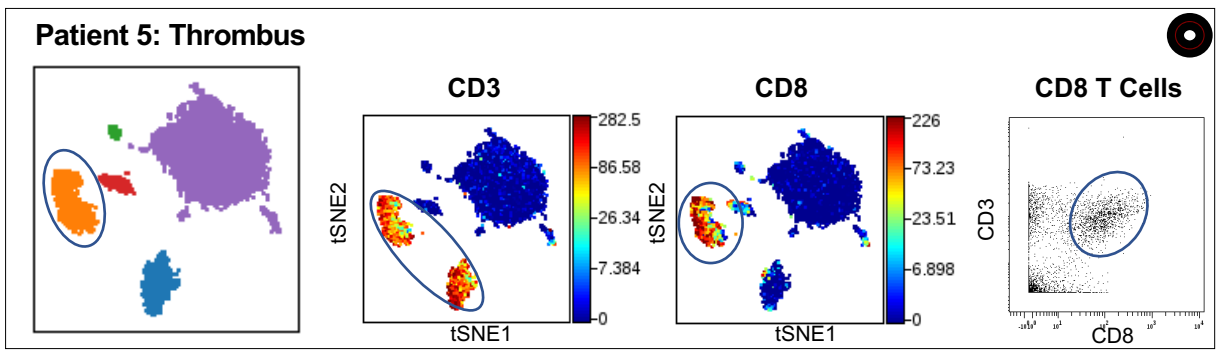


Figure 4.3 viSNE analysis of CD45+ cells isolated from ten aortic aneurysms


Patient 2: Thrombus
CD11b
662.2
164.1
40.53
9.466
0
tSNE2
tSNE1
Myeloid Cells
CD45/FITC
CD11b
CD4 T Cell
CD8 T Cell
B Cells
NK Cell
CD11b


Patient 3: Thrombus
CD3
414.6
115.4
32
8.275
0
tSNE2
tSNE1
T Cells
CD3
CD45/FITC


Patient 4: Thrombus
CD3
563.4
145.3
37.36
9.041
0
tSNE2
tSNE1
CD4
243.7
77.48
24.43
7.06
0
tSNE2
tSNE1
CD4 T Cells
CD3
CD4


Patient 5: Thrombus
CD3
282.5
86.58
26.34
7.384
0
tSNE2
tSNE1
CD8
226
73.23
23.51
6.898
0
tSNE2
tSNE1
CD8 T Cells
CD3
CD8

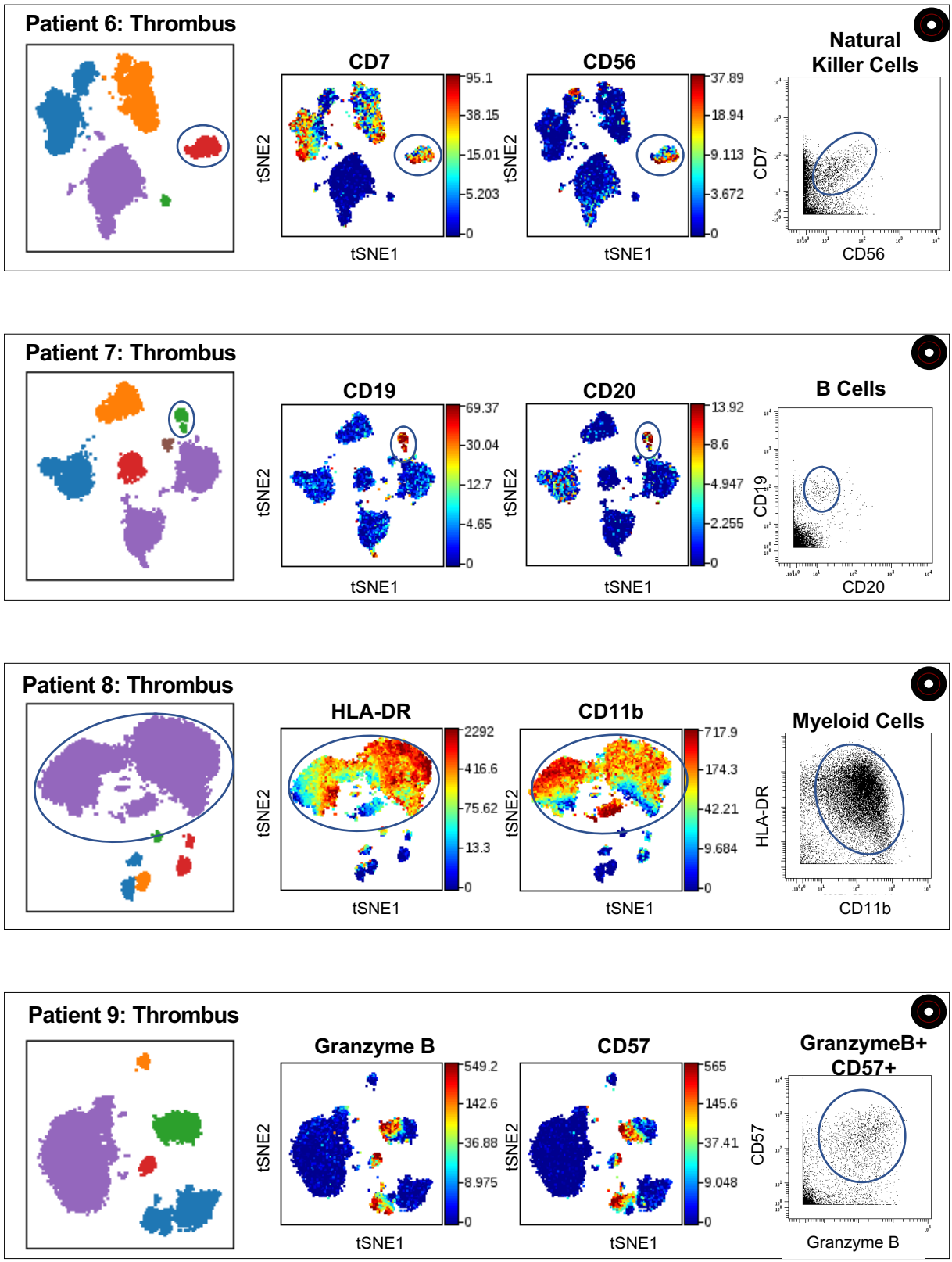


Figure 4.4 viSNE analysis of CD45+ cells isolated from eight patients aortic intraluminal thrombus

Figure 4.4: viSNE analysis of CD45+ cells isolated from eight patient's intraluminal thrombus

Single cell suspensions, from ten patients' ILTs, were isolated by enzymatic digestion (described in 2.5.1) prior to enrichment of CD45+ cells using FACS (described in 2.6.2). The CD45+ single cell suspension was then labelled with CyTOF antibodies (CyTOF labelling methods in 2.7) from the lymphocyte centric panel (Figure 3.20) and acquired on the Helios CyTOF mass cytometer. The *.fcs* files were imported in to Cytobank and viSNE analysis was performed on individual files (7500 iterations and perplexity of 70) after gating on CD45+ Live cells (Figure 4.2). Two patients (1 and 10) did not meet the quality control requirements and were excluded from the analysis.
This series of eight plots (1 from each patient) highlights common immune cell markers and their distribution and frequency using the automated viSNE clustering algorithm. Each series is an individual patient. In the first plot, each cell cluster is represented by a different colour. The following viSNE/s highlight the channel in which the named antibody is located. This is alongside their reciprocal individual dot plots that are used in traditional cytometry analysis. The markers are CD11b, CD3, CD4, CD8, CD7, CD56, HLA-DR, CD19, CD20, CD57 and Granzyme B.

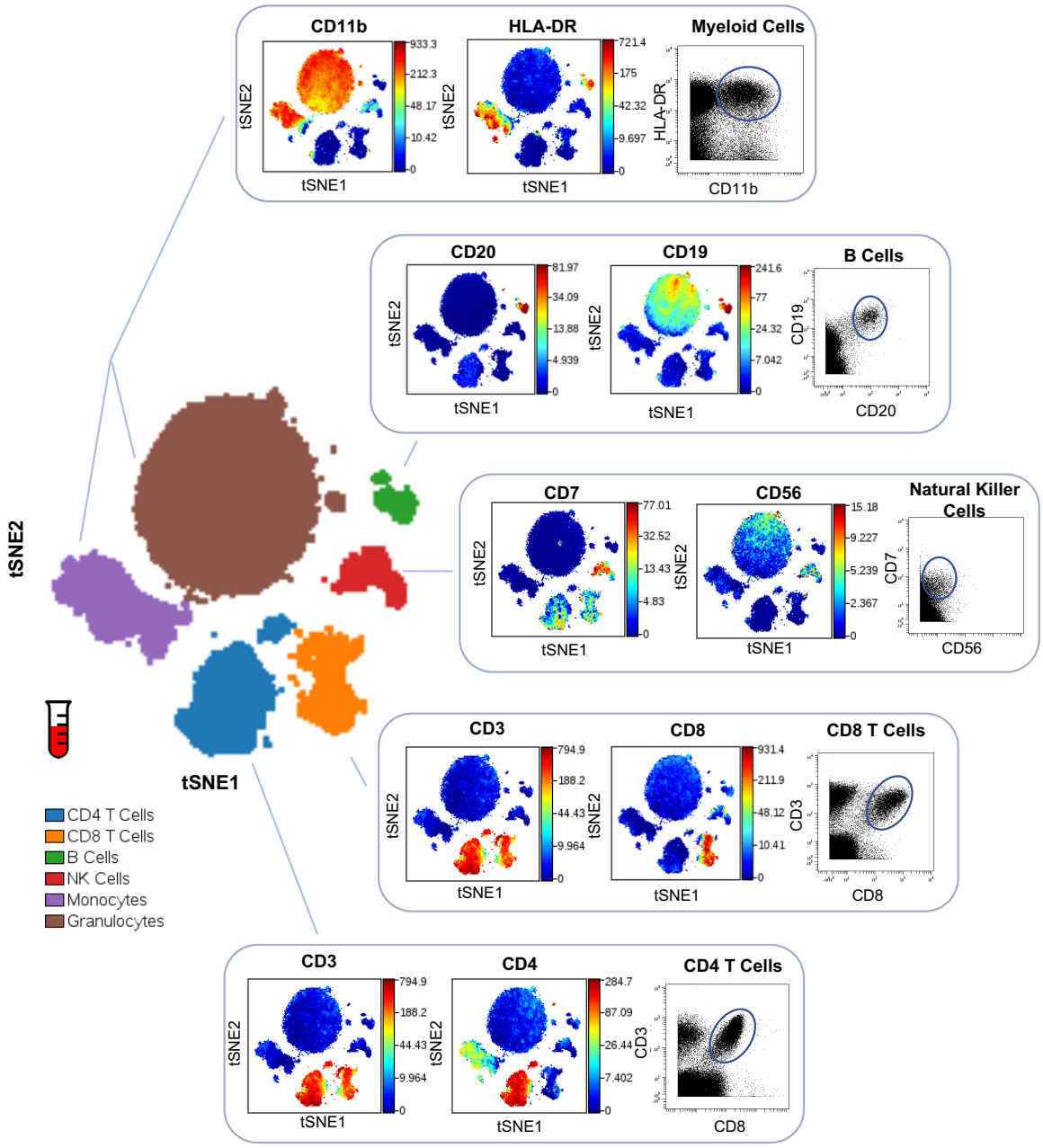


Figure 4.5: A combined viSNE analysis of CD45+ cells isolated from blood samples

Leukocytes were isolated from the blood of nine patients after lysis of red blood cells (described in 2.5.1.3). These were labelled with CyTOF antibodies (CyTOF labelling methods in 2.7) from the lymphocyte centric panel (Figure 3.20) and acquired with the Helios CyTOF mass cytometer. The *.fcs* files were imported in to Cytobank and viSNE analysis was performed by sampling 10 000 cells from each patient and analysing a combined viSNE with 90000 cells (7500 iterations and a perplexity of 70) prior to gating in CD45+ cells (Figure 4.2). The multicoloured illustrative viSNE displays unique cell clusters in individual colours. Each cluster has an associated panel displaying the highlighted lineage antibody channel as well as a traditional dot plot. The markers are CD11b, HLA-DR, CD20, CD19, CD7, CD56, CD3, CD8 and CD4.

4.4.2 Comparison of immune cell types in the aortic aneurysm complex

After describing the presence of the major immune cell types in the aortic complex tissues above, I sought to quantify and compare them with each other. The aorta, ILT and peripheral blood all contained B cells, T cells, CD11b cells and NK cells in differing frequencies **(Figure 4.6A)**.

As a percentage of CD45 cells there are more T cells in the aorta than the ILT and blood ($p < 0.0001$, 40.9% vs. 31.52% vs. 20.1%), and this is likely due to the increase in CD4 T cells in the aorta in comparison to the ILT and blood (29.31% vs. 19.01% vs. 13.53%). The CD8 fraction is also higher in the aorta than the blood, but similar to the ILT ($p<0.01$, 11.56% vs. 12.51% vs. 6.56%). In the aorta, B cells were the most frequent cell type and were significantly more frequent in the aorta than the ILT and blood ($p<0.0001$, 44.12% vs. 5.44% vs. 2.54%). The CD11b cells (myeloid cells) are more frequent in the blood and ILT than the aorta ($p<0.0001$, 73.8% vs. 54.25% vs. 9.23%), but the CD11b cells in the blood are mainly CD11b+HLA-DR- and the ILT are CD11b+HLA-DR+, which most likely represent an increase in granulocytes within the peripheral blood. Natural killer cells are more frequent in the ILT when compared to the aorta and blood ($p<0.02$, 8.3% vs. 3.3% vs. 3.56%). **(Figure 4.6B)**

Figure 4.6: Immune cell composition of the aortic wall, ILT and peripheral blood

Blood, aortic wall and ILT were collected intraoperatively (described in 2.4) from ten patients. Single cell suspensions were isolated by enzymatic digestion from the aorta and ILT (described in 2.5.1) prior to enrichment of CD45+ cells using FACS (described in 2.6.2). Leukocytes were isolated from the blood after lysis of red blood cells (described in 2.5.1.3). The *.fcs* files were imported in to Cytobank and individual viSNE's were created for each sample, clustering on the markers in the lymphocyte centric panel (Figure 3.20). Two samples from the ILT and one from the blood did not meet the quality control requirements and were excluded from the analysis.

(A) Dot plots depict the frequencies of common immune cell types (B Cells, T cells, CD11b myeloid cells and natural killer cells) in the aneurysm wall, ILT and blood alongside each other. This allows for comparison within and between the tissue types. B cells are the most frequent cell type within the aorta followed by T cells, whilst CD11b cells are more frequent in the ILT and blood.

(B) Dot plots of the frequencies of individual surface makers are compared between the tissues. As a percentage of CD45 cells there are more T cells in the aorta than the ILT and blood ($p < 0.0001$) and this is due to the increase in CD4 T Cells. B cells are also significantly more frequent in the aorta than the ILT and blood ($p<0.0001$), whilst CD11b cells (myeloid cells) are more frequent in the blood and ILT ($p<0.0001$). Natural killer cells are more frequent in the ILT when compared to the aorta ($p<0.02$). (Dot plot error bars = mean +- SD). (*$p<0.01$, **$p<0.01$, ***$p<0.001$, *$p<0.0001$, two tailed paired student t-test) (Statistics performed on matched paired samples) (aorta=8, ILT=8, blood=8)

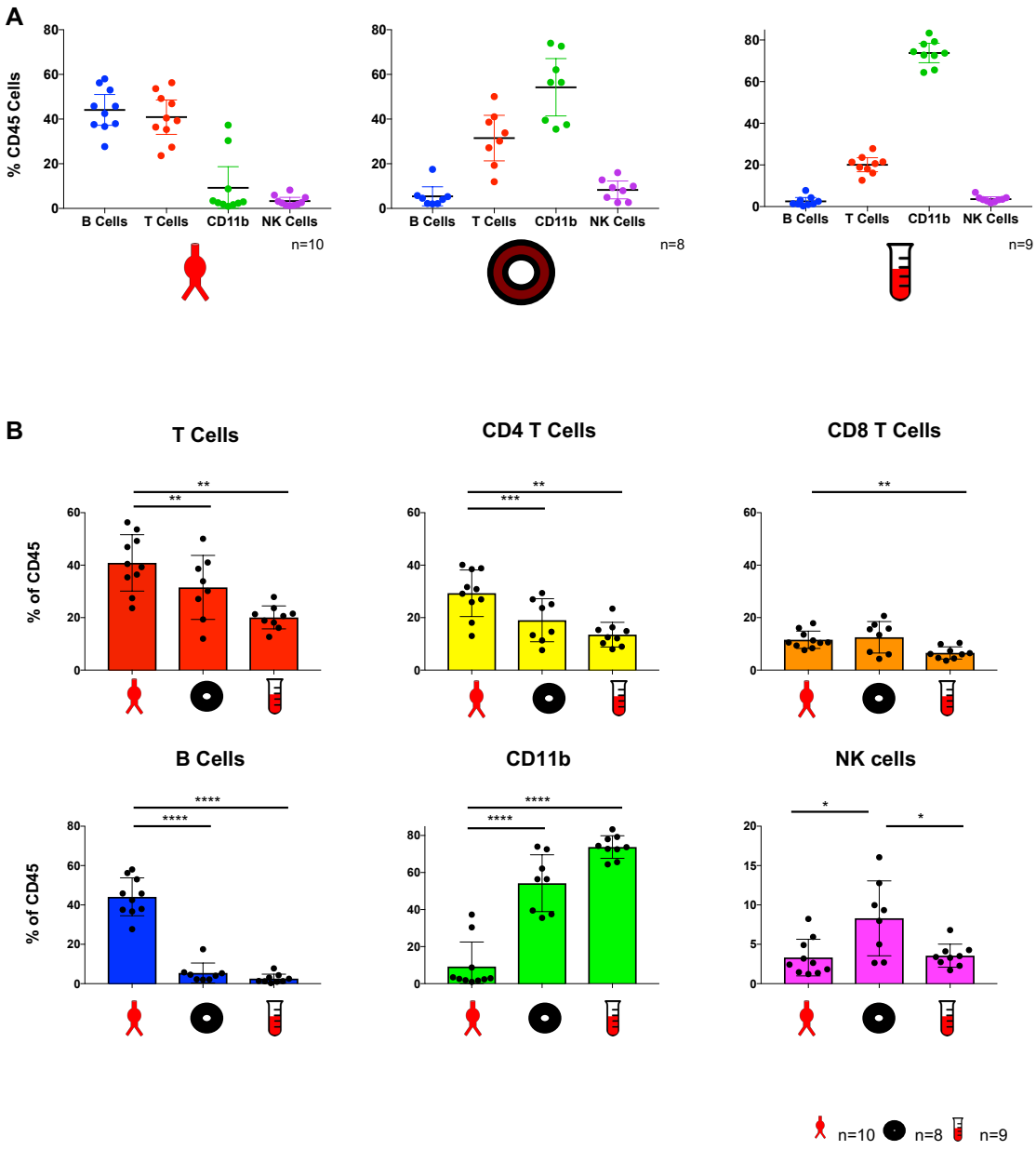


Figure 4.6: Immune cell composition of the aortic wall, ILT and peripheral blood

4.4.3 Lymphocyte phenotypic diversity of the aortic aneurysm complex tissues

Having defined the baseline frequencies of the major immune cell types within the AAA complex tissues, I next aimed to delineate the subsets within them. For this, the PhenographR Cytofkit package was used after exporting lymphocytes from Cytobank as *.fcs* files and run (k<30, perplexity of 30 and maximum iterations of 1000) (discussed in chapter 2.7.3). This program delineates clusters in an unbiased manner. Thereafter, with the aid of a heatmap, the markers were matched up with identifiers of known cell subsets.

In the aorta, a total of 26 different clusters were identified across the ten patient samples, however not all the patients had all of the subsets (median 20, IQR 18 – 23) **(Figure 4.7)**. The CD8 cells subsets included a Cytotoxic CD8 Granzyme B containing population which could be further classified on CD57 expression, a naive CD8 (CD8+CD45RA+CCR7+), CD8 central memory cells, CD8 effector cells, invariant natural killer cells (iNKT), CD8 EmRA and CD8 T follicular helper (Tfh) cells. The CD4 cells had Naïve CD4s, CD4 central memory, CD4 effector (helper) cells, T regulatory cells, Cytotoxic CD4s, CD4 iNKT cells, Tfh and the remainder were double negative T cells of which some were gamma delta (γ δ t cells). The aorta contained seven B cell clusters. Naïve B cells, two class switched memory B cell clusters split on CCR5, an IgM memory B cell cluster, plasmablasts, IGD+CD1D+ B cells and a CD127+ cluster. There were also three NK cell clusters, differentiated on granzyme B and CD56 expression. **Figure 4.7A** is a representation of a single patients PhenographR cluster map, with reciprocal heatmaps of the respective clusters and identifying cell markers **(Figure 4.7 B,C)**.

Figure 4.7: tSNE analysis and heatmaps highlighting the lymphocyte phenotypic diversity in the aorta of AAA patients

Single cell suspensions, from ten patients' aortas, were isolated by enzymatic digestion (described in 2.5.1) prior to enrichment of CD45+ cells using FACS (described in 2.6.2). The CD45+ single cell suspension was then labelled with CyTOF antibodies (CyTOF labelling methods in 2.7) from the lymphocyte centric panel (Figure 3.20) and acquired on the Helios CyTOF mass cytometer. The *.fcs* files were imported in to Cytobank and viSNE analysis was performed on individual files (7500 iterations and perplexity of 70) after gating on CD45+ Live cells (Figure 4.2). After viSNE analysis on each of the aortic samples (Figure 4.3), the T cells, B cells and NK cells (lymphocytes) were selected and exported in to the PhenographR Cytofkit analysis package (discussed in chapter 2.7.3) as a *.fcs* file (k<30, perplexity of 30 and maximum iteration s of 1000).
In this figure, a representative patient's data (Patient 1) was input in to PhenographR package, and the cells were clustered around the antibodies in the lymphocyte centric panel.
(A) In total there were 13710 cells input, and in an unbiased manner PhenographR grouped the cells in to 18 separate clusters. These clusters centered around the major immune cell types (T cells, B cells, NK cells). The sub-clusters were then matched up to known cell hierarchies and named.

(B) The PhenographR generated heatmap displays the cell clusters and their relative expression of the major immune cell types (T cells, B Cells, NK Cells).

(C) The heatmap provides a detailed expression pattern of all the sub-clusters clusters found in this sample. There were 3 NK cell clusters, differentiated on granzyme B and CD56 expression. The 6 CD4 subsets identified in this example were Naïve cells, CD4 T effector cells, CD4 T memory cells, T regulatory cells, T follicular helper cells and a cytotoxic CD4 cell containing granzyme B. There were four CD8 subsets, a cytotoxic CD8 cells subset containing granzyme B and split up on CD57 expression, a CD8 T effector memory cell cluster, CD8 iNKT cells and a CD8 T central memory cluster. Lastly, in this specimen, there were seven B cell clusters. Naïve B cells, two class switched memory B cell clusters split on CCR5, an IgM memory B cell cluster, plasmablasts, IGD+CD1D+ B cells and a CD127+ cluster.

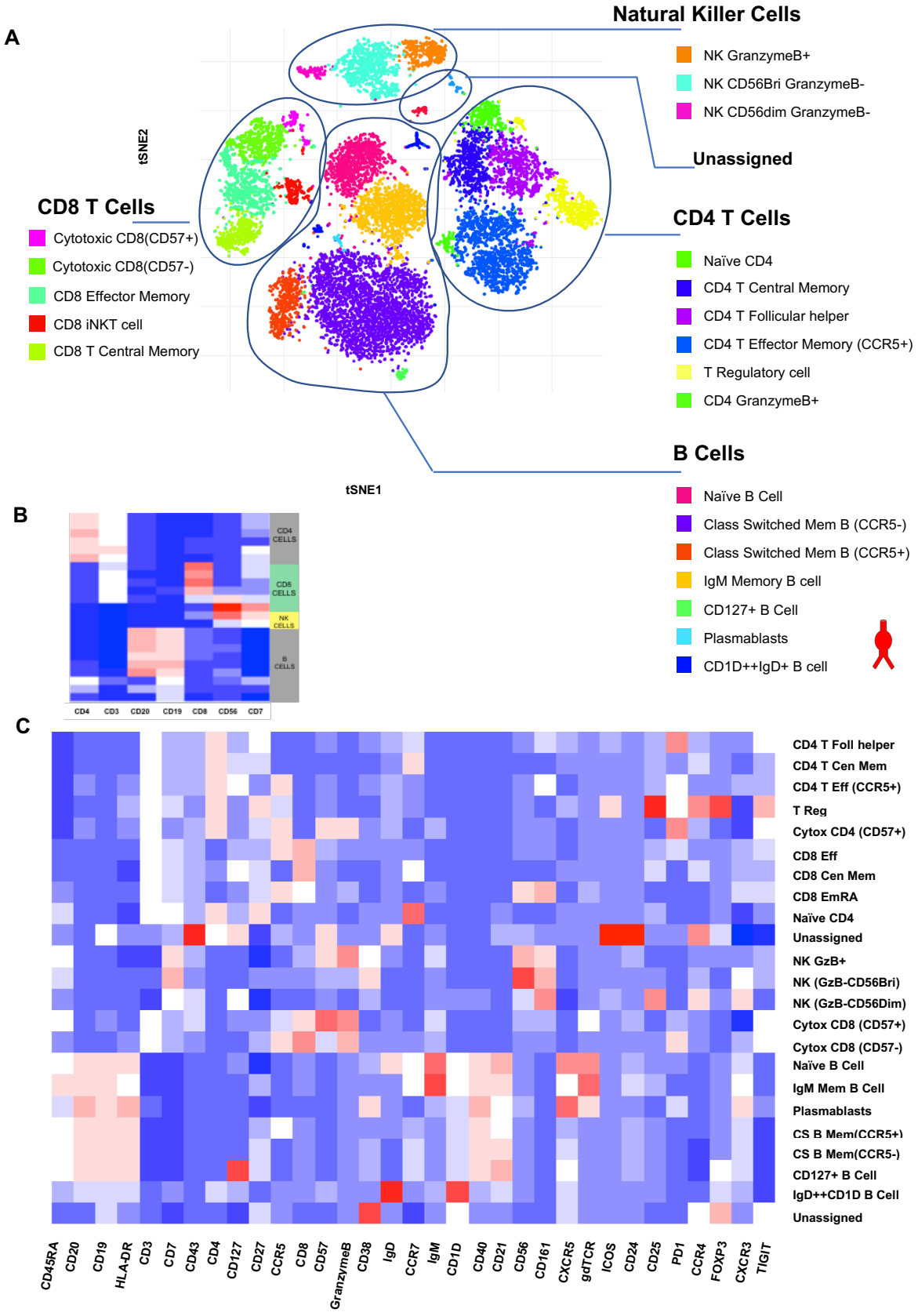


Figure 4.7: tSNE analysis and heatmaps highlighting the lymphocyte phenotypic diversity in the aorta of AAA patients

In the ILT, a total of 17 different clusters were identified across the 8 patient samples, (median 12, IQR 11 – 15) **(Figure 4.8)**. The CD8 subsets included a granzyme B positive cytotoxic CD8 and further separated on CD57+ expression as well as a naive CD8 (CD8+CD45RA+CCR7+), CD8 central memory cells, CD8 effector cells and invariant natural killer cells (iNKT). The CD4 cells had naïve CD4s, CD4 central memory, CD4 effector (helper) cells, T regulatory cells, Cytotoxic CD4s, CD4 iNKT cells and the remainder were double negative T cells, some of which were gamma delta (γ δ t cells). In comparison to the aorta, the ILT had only two B cell clusters, a naïve and a memory B-cell population. There were also three NK cell clusters, differentiated on granzyme B and CD56 expression. **Figure 4.8A** is a representation of a single patients PhenographR cluster map, and heatmaps identifying cell markers.

In the peripheral blood, a total of 21 different clusters were identified across the 9 patient samples (median 18, IQR 15 – 19) **(Figure 4.9)**. The CD8 cells subsets included a Cytotoxic CD8 Granzyme B containing subset which could be further classified on CD57 expression, a naive CD8 (CD8+CD45RA+CCR7+), CD8 central memory cells, CD8 effector cells, invariant natural killer cells (iNKT) and CD8 EmRA. The CD4 cells had naïve CD4s, CD4 central memory, CD4 effector (helper) cells, T regulatory cells, Cytotoxic CD4s, CD4 iNKT cells and the remainder were double negative T cells of which some were gamma delta (γ δ t cells). In comparison to the aorta, the peripheral blood had only 2 B cell clusters, a naïve and a memory B-cell population. There were also 3 NK cell clusters, differentiated on granzyme B and CD56 expression. **Figure 4.9A** is a representation of an individual patients PhenographR cluster map, with reciprocal heatmaps of the respective clusters and identifying cell markers **(Figure 4.9 B,C)**.

Figure 4.8: tSNE analysis and heatmaps highlighting the lymphocyte phenotypic diversity in the intraluminal thrombus

Single cell suspensions, from eight patients ILT, were isolated by enzymatic digestion (described in 2.5.1) prior to enrichment of CD45+ cells using FACS (described in 2.6.2). The CD45+ single cell suspension was then labelled with CyTOF antibodies (CyTOF labelling methods in 2.7) from the lymphocyte centric panel (Figure 3.20) and acquired on the Helios CyTOF mass cytometer. The *.fcs* files were imported in to Cytobank and viSNE analysis was performed on individual files (7500 iterations and perplexity of 70) after gating on CD45+ Live cells (Figure 4.2). After viSNE analysis on each of the aortic samples (Figure 4.4), the T cells, B cells and NK cells (lymphocytes) were selected and exported in to the PhenographR Cytofkit analysis package (discussed in chapter 2.7.3) as a *.fcs* file (k<30, perplexity of 30 and maximum iteration s of 1000).
In this figure, a representative patient's data (Patient 6) was input in to PhenographR package, and the cells were clustered around the antibodies in the lymphocyte centric panel.

(A) In total there were 11114 cells input in to PhenographR, and in an unbiased manner PhenographR grouped the cells in to 17 separate clusters. These clusters centred around the major immune cell types (T cells, B cells, NK cells). The sub-clusters were then matched up to known cell hierarchies and named.

(B) The PhenographR generated heatmap displays the cell clusters and their relative expression of the major immune cell types (T cells, B Cells, NK Cells).

(C) The heatmap provides a detailed expression pattern of all the sub-clusters clusters found in this sample. There were 2 NK cell clusters, differentiated on granzyme B expression. The 6 CD4 subsets identified in this example were Naïve cells, CD4 T effector cells (2 subtypes), CD4 T memory cells, T regulatory cells, and an iNKT CD4 cell containing granzyme B. There were four CD8 subsets, a cytotoxic CD8 cell subset containing granzyme B, two CD8 T effector cell clusters without granzyme B but split up on CD57 expression and a CD8 T central memory cluster. Lastly, in this specimen, there were two CD3+CD4-CD8- (double negative) T cell clusters split up on granzyme B expression, and only a single naïve B cell cluster.

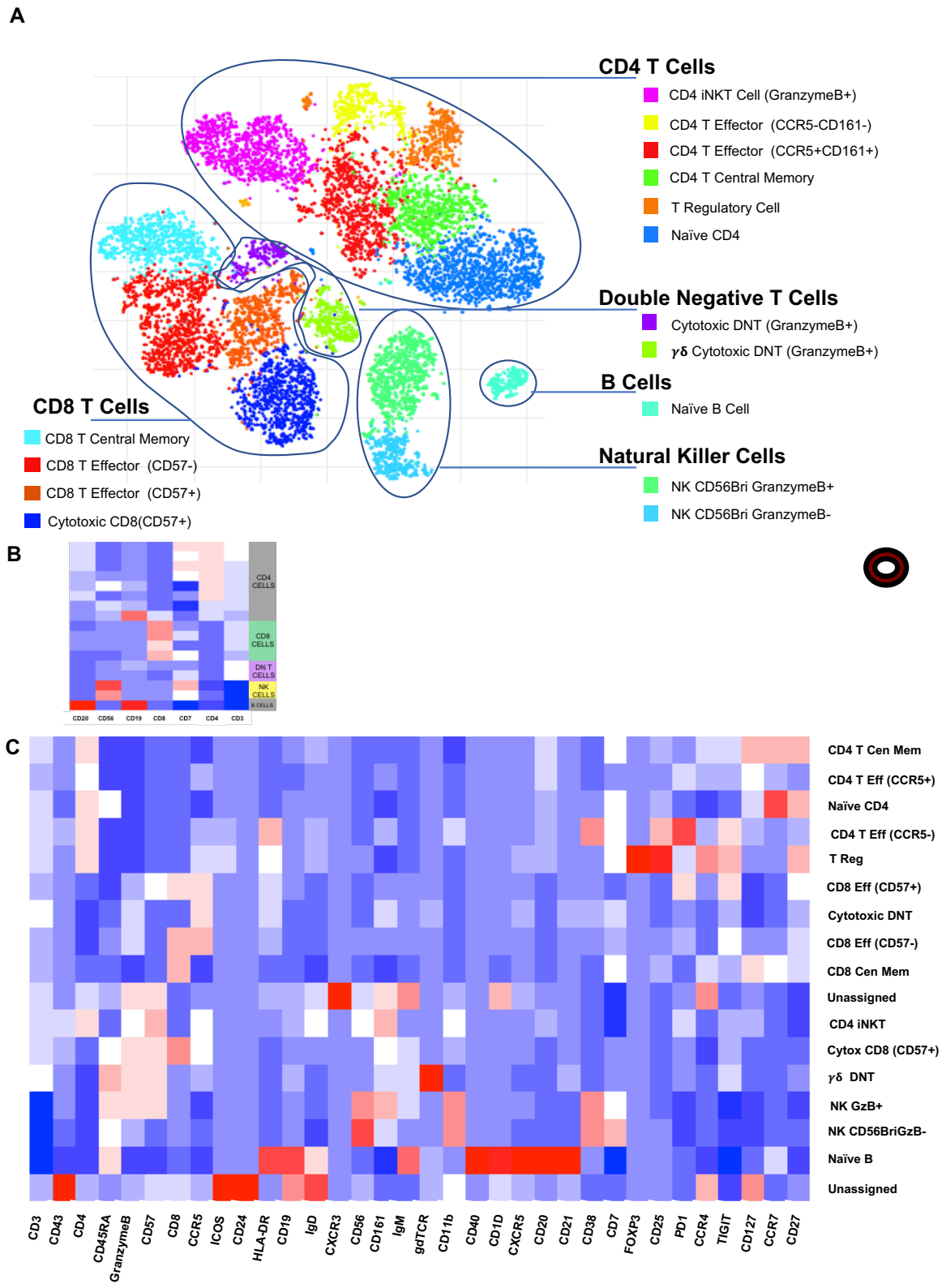


Figure 4.8: tSNE analysis and heatmaps highlighting the lymphocyte phenotypic diversity in the intraluminal thrombus

Figure 4.9: tSNE analysis and heatmaps highlighting the lymphocyte phenotypic diversity in the blood of AAA patients

Leucocytes were isolated from 9 patients' blood samples after lysis of red blood cells (described in 2.5.1.3). These were labelled with CyTOF antibodies (CyTOF labelling methods in 2.7) from the lymphocyte centric panel (Figure 3.20) and acquired on the Helios CyTOF mass cytometer. The *.fcs* files were imported in to Cytobank and viSNE analysis was performed on individual files (7500 iterations and perplexity of 70) after gating on CD45+ Live cells (figure 4.2). After viSNE analysis on each of the blood samples (Figure 4.5), the T cells, B cells and NK cells (lymphocytes) were selected and exported in to the PhenographR Cytofkit analysis package (discussed in chapter 2.7.3) (k<30, perplexity of 30 and maximum iteration s of 1000). In this figure, a representative patients' data (Patient 1) was input in to the PhenographR package, and the cells were clustered around the antibodies in the lymphocyte centric panel.

(A) In total there were 23014 cells input in to PhenographR, and in an unbiased manner Phenograph grouped the cells in to 18 separate clusters. These clusters centred around the major immune cell types (T cells, B cells, NK cells). The sub-clusters were then matched up to known cell hierarchies and named.

(B) The PhenographR generated heatmap displays the cell clusters and their relative expression of the major immune cell types (T cells, B Cells, NK Cells).

(C) The heatmap provides a detailed expression pattern of all the sub-clusters clusters found in this sample. There were 3 NK cell clusters, differentiated on granzyme B and CD57 expression. The 7 CD4 subsets identified in this example were Naïve cells, CD4 T effector cells (2 subtypes), CD4 T memory cells (2 subtypes), T regulatory cells, and cytotoxic CD4 cells containing granzyme B. There were five CD8 subsets, two cytotoxic CD8 cells subset containing granzyme B differentiated on CD57 expression, a CD8 T effector cell cluster without granzyme B and two CD8 T central memory clusters. Lastly, in this specimen, there were two CD3+CD4-CD8- (double negative) T cell clusters split up on granzyme B expression, two naïve B cell clusters and a memory B cell cluster.

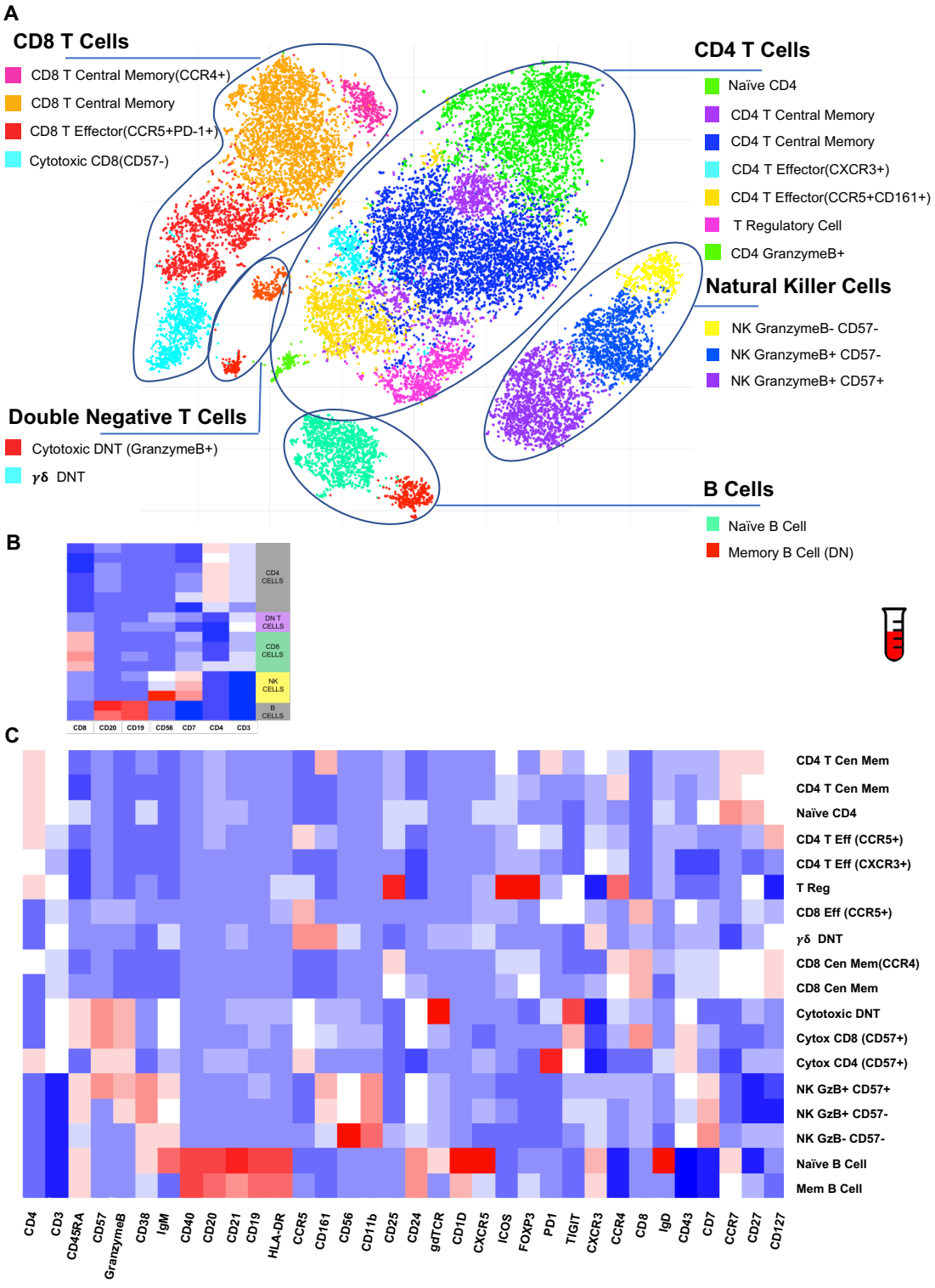


Figure 4.9: tSNE analysis and heatmaps highlighting the lymphocyte phenotypic diversity in the peripheral blood of AAA patients

4.4.4 B cell phenotypic diversity in the aortic aneurysm complex tissues

As described in section 4.4.4, B cells are the commonest cell type in the aorta (44.12%). There was an inverse ratio of memory to naïve B cells in the aorta when compared to the ILT and blood **(Figure 4.10)**. In the aorta, there are more memory B cells than naive cells ($p<0.0001$, 64.23% vs. 10.94%), whilst In the ILT (24.46% vs.75.77%) and blood (27.88 vs. 71.17%) there were predominately naïve B cells **(Figure 4.10A).** Further interrogation of the memory subset of the aorta, reveals three types (class-switched, IgM memory and double negative memory). The majority were class switched memory B cells (62.1%, CD27+IgD-IgM-) (**Figure 4.10B)**. CD1D expression was higher in the aorta and blood when compared to the ILT (61.3% vs.27.54% vs. 77.08%)**.** CD40 expression as a percentage of naïve B cells was also higher in the aorta and blood than the ILT (68.28% vs. 37.97% vs. 84.45%). The CD38hiCD40hi B cells (possible B regulatory cells) were found only in the blood and not the aorta and ILT **(Figure 4.10C)**.

Figure 4.10: B Cell subsets in the aortic aneurysm complex

Enzymatically digested and CD45 FACS sorted single cells were isolated from 10 patients Aortic wall and ILT (Chapter 2). Their matching blood samples were lysed with ACK lysis buffer (chapter 2.5.1.3) and all the specimens were labelled with CyTOF antibodies (chapter 2.7) from the lymphocyte centric panel, (Figure 3.20) then acquired on the Helios CyTOF system. The *.fcs* files were imported in to Cytobank and individual viSNEs were created for each sample, clustering on the markers in the lymphocyte centric panel. Two samples from the ILT and one from the blood did not pass the quality control and were excluded from the analysis. After running the initial viSNE plots on individual samples (Figure 4.3, 4.4, 4.5), the T cells, B cells and NK cells (lymphocytes) were selected and exported in to the PhenographR Cytofkit analysis package (discussed in chapter 3) as *.fcs* files (k<30, perplexity of 30 and maximum iterations of 1000). The frequencies of the subsets identified by Phenograph were collated and individual clusters were compared to established B cell subset nomenclature and matched.

(A) Dot plots describe the frequencies of B cell memory and naïve subsets. In the aorta there are more memory B cells than naive cells ($p<0.0001$) and other cells ($p<0.0001$). In the ILT and blood there are predominately naïve B cells.

(B) Donut charts highlighting the inverse ratio of memory to naïve B cells in the aorta when compared to the blood. Further interrogation of the memory subset of the aorta, reveals three types (class-switched, IgM memory and double negative). The majority are class switched memory B cells (CD27+IgD-IgM-).

(C) CD1D expression is higher in the aorta and blood when compared to the ILT

(D) CD40 expression is also higher in the aorta and blood than the ILT

(E) The CD38hiCD40hi B cells found only in the blood and not the aorta and ILT.

(Dot plots and bar plot error bars = mean +- SD). (*$p<0.01$, **$p<0.01$, ***$p<0.001$, ****$p<0.0001$, two tailed paired student t-test). Statistics performed on matched paired samples) (aorta=8, ILT=8, blood=8)

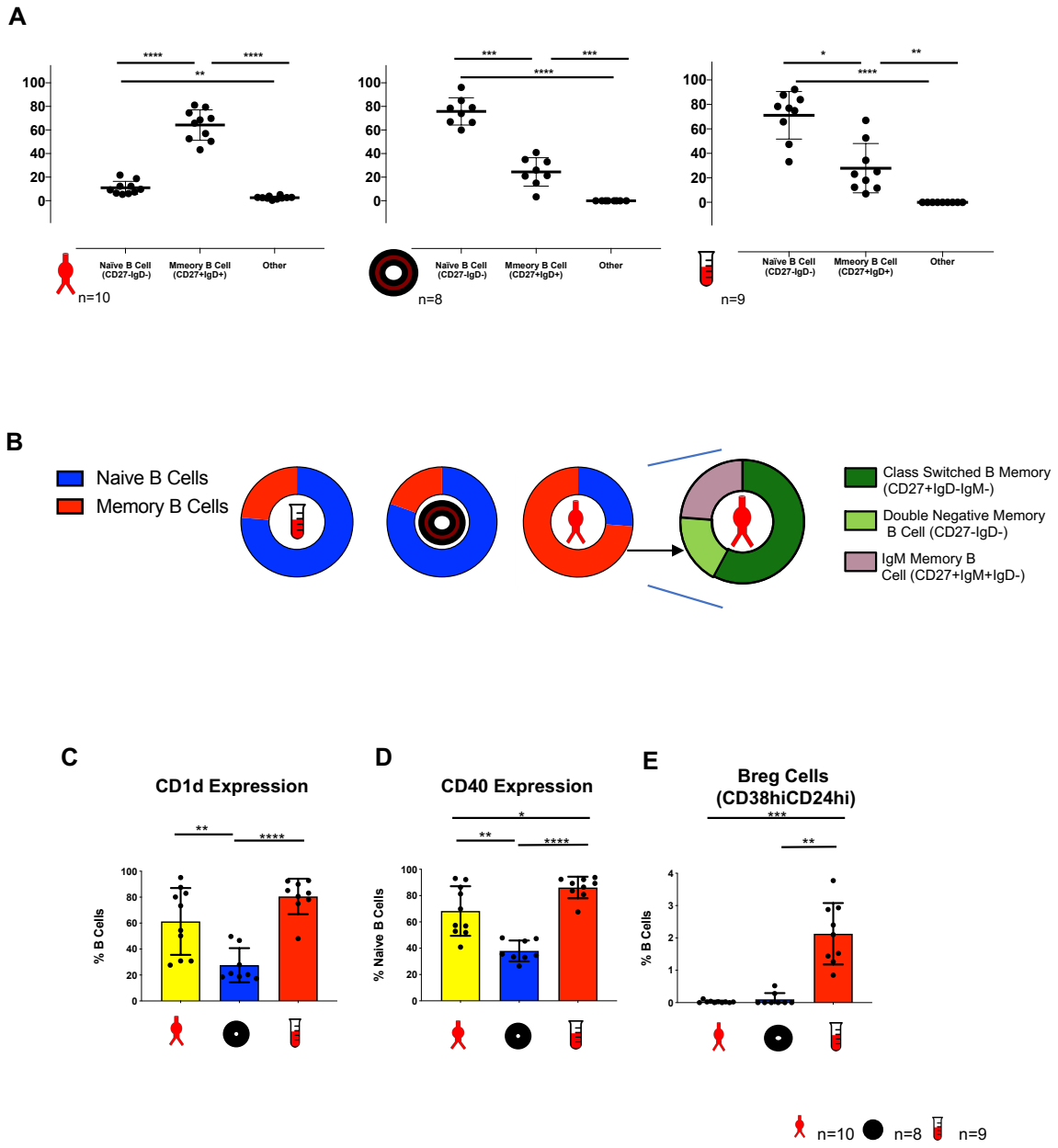


Figure 4.10: B Cell subsets in the aortic aneurysm complex

4.4.5 Mononuclear phagocyte phenotypic diversity in the aortic aneurysm complex tissues

There was significant overlap in surface marker expression within the mononuclear phagocyte cells of the aortic aneurysm complex. This resulted in the cells not separating out into discrete clusters when analysed with the automated viSNE clustering algorithm (monocytes, macrophages and dendritic cells). The markers that were expressed by the majority of the cells were CD11b, CD11c, CD68, CD64, CD36, HLA-DR and in the tissues IRF5. This is in keeping with the human DC literature, where the subsets are not as clearly defined as in the T cell compartment making differentiation based exclusively on surface marker expression challenging. The myeloid blood compartment was composed predominately of CD14+ monocytes (69.9%). There were also CD16+ monocytes (5.9%) and CD14-CD16- cells (24.9%), which were most likely DCs. Of these DCs, there were CD14-BDCA3+ (12.8%), CD1C+ DC (2.8%) and pDCs that express CD123 (2%). There was also a consistent CLEC9A++DCIR++ population, which was also found in the ILT and aorta. **Figure 4.11** is a viSNE representation of a patients' mononuclear phagocyte cell compartment (Patient 3).

The mononuclear phagocyte compartment of the ILT had 73% CD14+ positive cells of which HLA-DR split the population in to an HLA-DRint (29.3%) and HLA-DR high population, of probable macrophages. The CD14-CLEC9A++DCIR++ DC population was consistently found in all six samples (12.8%) whilst a CD14+ BDCA3+ and CD36++ (42.3%) population were thought to be monocyte derived inflammatory DCs due to their expression pattern. CD1C DCs made up 2.3% of the population and there was also a CD14loCD11cLoHLA-DR-Lo population (13%). **(Figure 4.12)**

Figure 4.11: Myeloid cell phenotypic diversity of the Blood

Leukocytes were isolated from the blood of eight patients after lysis of red blood cells (described in 2.5.1.3). These were labelled with CyTOF antibodies (methods in 2.7) from the myeloid centric panel (Figure 3.21) and acquired with the Helios CyTOF mass cytometer. In Cytobank, viSNE analysis was performed on 10 000 cells from each patient, then a combined viSNE with 90000 cells (7500 iterations and a perplexity of 70). The CD11b+CD66a- myeloid cells were selected for further viSNE analysis, clustering around the myeloid markers. A patients' data (Patient 3) is represented with an overlaid colour image centrally and clusters of highlighted viSNEs with cell markers peripherally. The myeloid compartment has a significant overlap of markers and the unbiased clustering algorithm did not separate out discrete clusters (monocytes, macrophages, dendritic cells and subtypes). Six clusters were manually identified based on the presence of one or more markers within the greater myeloid cluster.

(A) Highlights the mononuclear phagocyte markers (CD14, CD16, CD68) together with CD64 and CD36. There was a CD16+ population, and two thirds of the cells were positive for CD14, whilst the majority of the cells were positive for CD68. All except the CD16 cluster were homogenously bright for CD36 and CD64.

(B) Six potential phenotypic clusters were identified in this sample. The first was a monocyte cluster that was positive for CD14, BDCA3. HLA-DR and was bright for CD172a. The second was DCIR+CLEC9A+ but CD14- cluster that may represent a DC cluster. The third was an HLA-DR Lo monocyte cluster and the fourth a CD14Lo CD11cLo monocyte cluster. The fifth was BDCA3+CD14-, which may be a DC cluster, and the last was a CD16+CD123+BDCA3+ cluster.

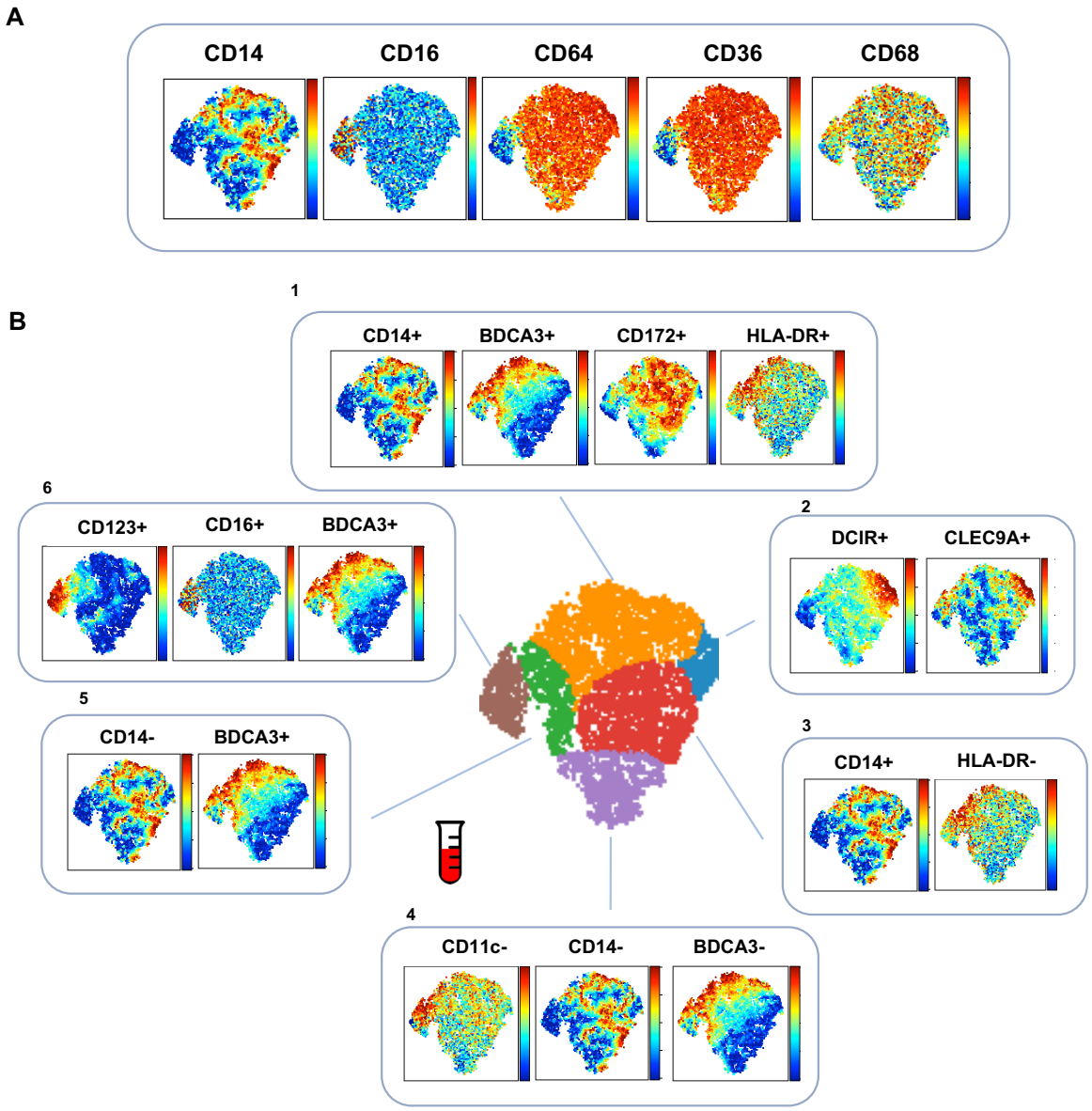


Figure 4.11: Myeloid cell phenotypic diversity of the Blood

Figure 4.12: Myeloid cell phenotypic diversity of the ILT

Single cell suspensions, from six patients' ILT, were isolated by enzymatic digestion (described in 2.5.1) prior to CD45+ enrichment using FACS (described in 2.6.2) and labelled with CyTOF antibodies (described in 2.7) from the myeloid centric panel (Figure 3.21) before acquisition on the Helios CyTOF mass cytometer. In Cytobank, viSNE analysis was performed on individual files (7500 iterations and perplexity of 70) after gating on CD11b+CD66a- (myeloid). These were selected for further viSNE analysis, clustering around the myeloid markers. A patients' data (Patient 6) is represented with an overlaid colour image centrally and clusters of highlighted viSNEs with cell markers peripherally. The myeloid compartment has a significant overlap of markers and the unbiased clustering algorithm did not separate out discrete clusters (monocytes, macrophages, dendritic cells and subtypes). Seven clusters were manually identified based on the presence of one or more markers within the greater myeloid cluster.

(A) Highlights the mononuclear phagocyte markers (CD14, CD16, CD68) together with CD64 and CD36. There was no CD16 staining, and two thirds of the cells were positive for CD14, CD68 and CD36, whilst CD64 was homogenous and bright in most cells.

(B) Seven potential phenotypic clusters were identified. The first, a CLEC9A+CD11C+CD14- cluster which is likely a DC cluster. The second is a CD14LoIRF5- CD11C- cluster, third is CD14LoCD64LoCD36Lo and HLA-DRLo cluster. The fourth cluster is a CD1C+ CD14- cluster which is likely a CD1C DC population. The fifth is a CD68briIRF5bri, CD169bri but CD14Lo cluster which is probably a CD169+ macrophage population or an activated DC cluster. Cluster 6 is suggestive of an MoDC population as it is CD14+BDCA3+ and Siglec-9 positive. The last cluster is a DCIR + one.

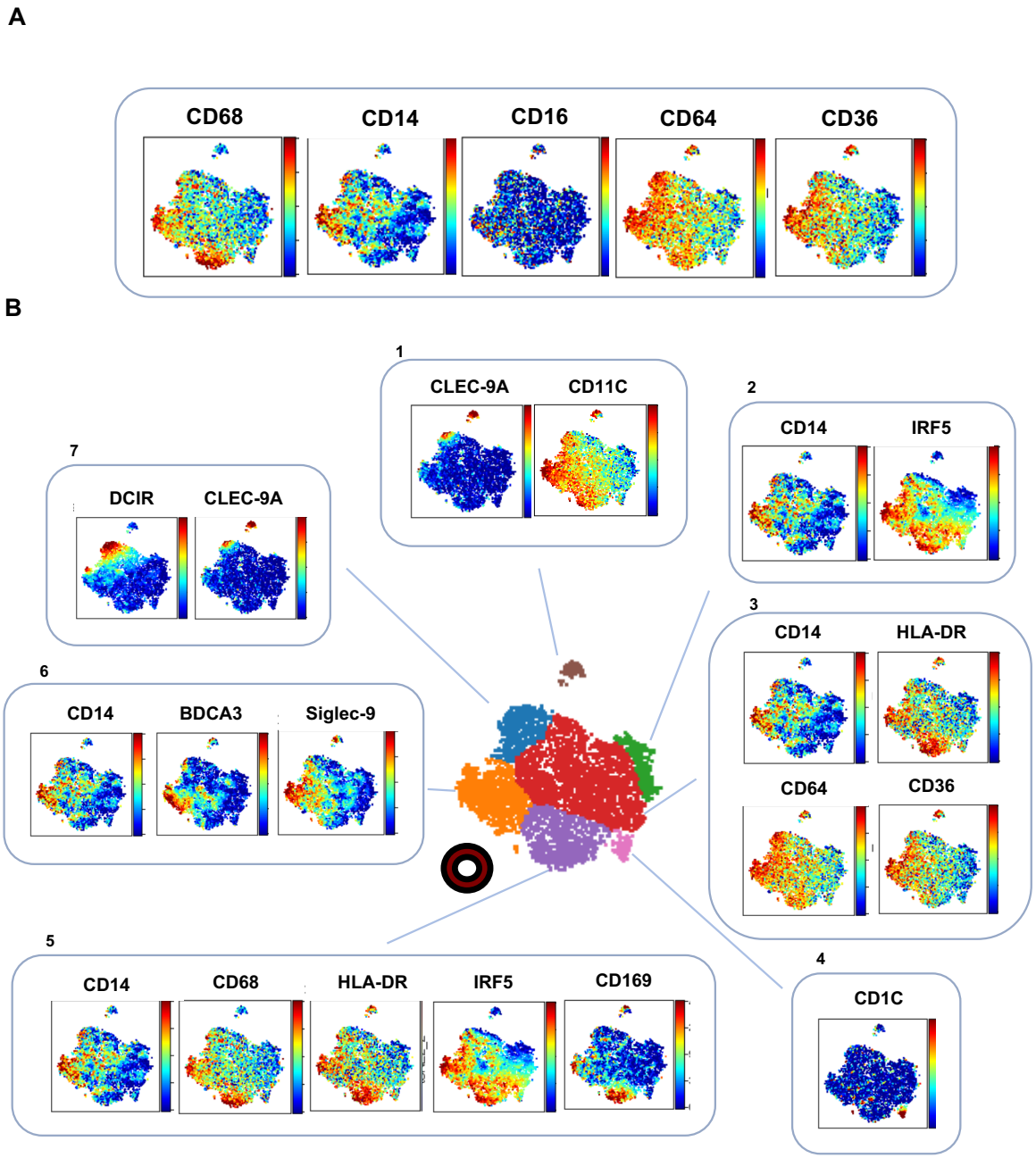


Figure 4.12: Myeloid cell phenotypic diversity of the ILT

Figure 4.13: Myeloid cell phenotypic diversity of the aortic wall

Single cell suspensions, from six patients' aortas, were isolated by enzymatic digestion (described in 2.5.1) prior to enrichment of CD45+ cells using FACS (described in 2.6.2) and labelled with CyTOF antibodies (described in 2.7) from the myeloid centric panel (Figure 3.21) before acquisition on the Helios CyTOF mass cytometer. In Cytobank, viSNE analysis was performed on individual files (7500 iterations and perplexity of 70). CD11b+CD66a- cells (myeloid) were selected for further viSNE analysis, clustering around the myeloid markers . In this figure, a patients' data (Patient 3) is represented with an overlaid colour image centrally and clusters of highlighted viSNE cell markers peripherally. The myeloid compartment has a significant overlap of markers and the unbiased clustering algorithm did not separate out discrete clusters (monocytes, macrophages, dendritic cells). Seven clusters were manually identified based on the presence of one or more markers within the greater myeloid cluster.

(A) Highlights the mononuclear phagocyte markers (CD14, CD16, CD68) together with CD64 and CD36. There was no CD16 staining, and the majority of cells were positive for CD14 and CD68, whilst CD64 and CD36 were homogenous and bright in most cells.

(B) The first cluster was CD11cLo HLA-DRLo and CD64Lo, the second was CD68int IRF5int and CD14int, whilst still being CD36+. The third was a DCIR++CLEC9A++ whilst being CD14lo and CD11cLo and may represent a DC subset. The fourth was CD11c++CD14+BDCA3++IRF5++CD169+CD68++ and CD172a+ which likely represent a M1 macrophage or MoDC. Cluster 5 is CD123+ and may represent plasmacytoid DCs+ but are also CD11c positive. Cluster 6 is likely an M2 macrophage phenotype as it is CD206+ and CD64bri and cluster seven is likely a CD1c DC (CD1c+CD14-CD36-).

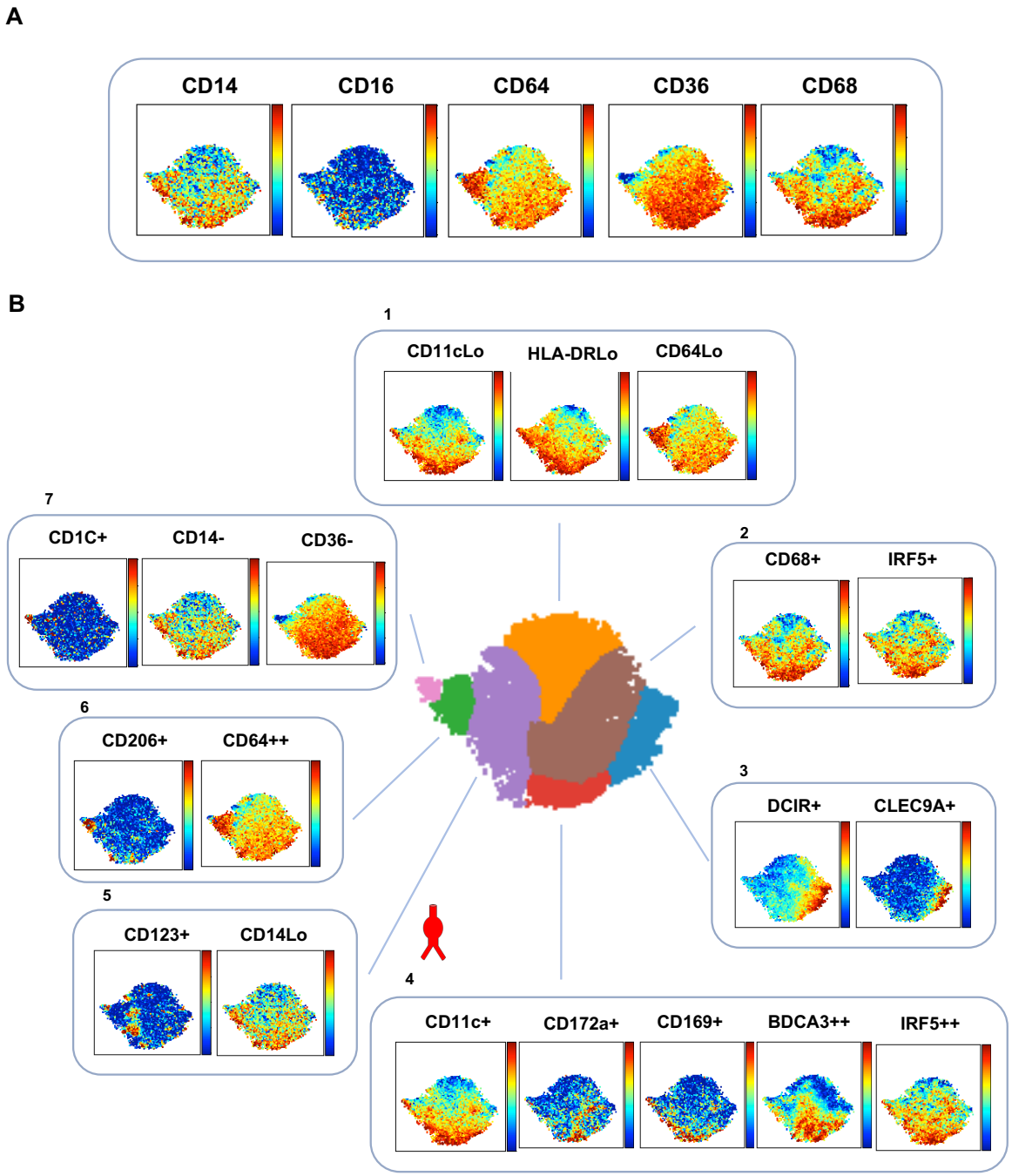


Figure 4.13: Myeloid cell phenotypic diversity of the aortic wall

The mononuclear phagocyte compartment of the aortic wall had 80% CD14 cells. There were no CD16+ cells. In addition to CD14+HLADR+ cells there was also a population of CD14+BDCA3+Siglec9+ which are likely a monocyte derived DC (moDC). A DCIR++CLEC9A++ was also identified and is also common to the ILT and peripheral blood. In contrast to the ILT and blood there was a CD68++CD169+CD14+CD172a+ population which is likely an M1 macrophage population whilst a population of CD206+ macrophages are an M2 population. CD123+ pDC's were also identified in the aortic wall as were CD1C DCs. **Figure 4.13** is a viSNE representation of a patients' mononuclear phagocyte cell ILT compartment.

4.4.6 NK cell subtypes

Natural killer (NK) cells are part of innate immunity and were the least common of the immune cell types described. As a percentage of CD45 cells in the ILT, aorta and blood they were 8.3%, 3.3% and 3.6% (section 4.4.2, Figure 4.6). The NK cells were clustered around CD56, CD16, GzB, and CD57. As a percentage of CD45 cells there were more CD16- NK cells in the ILT than the aorta and blood, although this was not statistically significant. In the blood there were more CD16+ cells (% of CD45) than the aortic wall ($p<0.01$), and more than the ILT though not statistically significant **(Figure 4.14A)**. The cytolytic granule GzB was lower in the aorta than the ILT and blood ($p<0.01$, $p<0.001$) **(Figure 4.14B)**. Of the NK cells, 54.9% were GzB positive in the aorta whilst in the ILT and blood there were 77% and 79.6%. As a proportion of total NK cells, CD56 bright NK cells were higher in the aorta than the ILT and blood (73.4% vs. 35% vs. 39%) **(Figure 4.14C)**, and CD57+ cells were more frequent in the blood and ILT than the aortic wall (60.1% vs. 60% vs. 31.2%) **(Figure 4.14D)**.

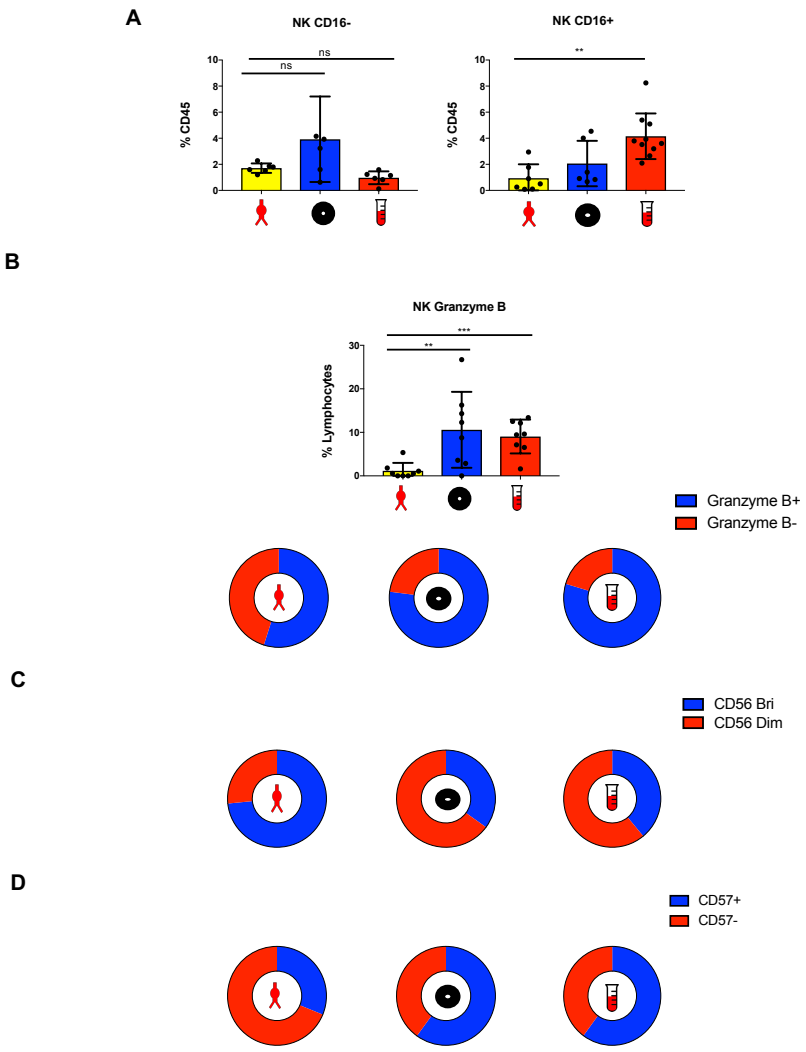


Figure 4.14: NK Cell subsets in the aortic aneurysm complex

Enzymatically digested and CD45 FACS sorted single cells were isolated from 10 patients Aortic wall and ILT (described in 2.5). The matching blood samples were lysed with ACK lysis (described in 2.5.1.3) and all the specimens were labelled with CyTOF antibodies (described in 2.7) from the lymphocyte centric panel, and six matching samples were labelled with the antibodies from the myeloid panel, (Figure 3.19, 3.20) then acquired on the Helios CyTOF system. In Cytobank individual viSNES were created for each sample (7500 iterations and perplexity of 70).
(A) The NK subsets were compared in the bar dot plots. The NK CD16+ subset as a percentage of CD45 cells was less frequently found in the aorta than the blood ($p<0.01$) and there was a non-significant difference in the CD16- NK cells across the tissue types**.** As a percentage of CD45 cells, the blood had more CD16+ NK cells than CD16- NK cells whilst the aorta and ILT had more CD16- NK cells.
(B) As a percentage of total lymphocytes, the aorta had fewer granzyme B containing NK cells than the ILT and blood ($p<0.01$, $p<0.001$), and the ratio of GranzymeB+ to GranzymeB- NK cells is visualized in the donut plots, with the aorta having a lower proportion of GranzymeB- NK cells compared to the ILT and blood. **(C)** The aorta contained a lower proportion CD56 bright NK cells as a percentage of total NK cells, than the blood and ILT as visualized on the donuts plots whilst **(D)** there was a higher proportion of CD57+ NK cells in the blood and ILT compared to the aorta.

4.4.9 CD8 and CD4 subsets in the aortic aneurysm complex tissues

Having described the phenotypic diversity of the cells, I next investigated the subsets of the immune cell types. In **Table 4.2**, the CD8 subsets of individual patient samples are highlighted. In the aortic wall all 10 samples had cytotoxic granzyme B cells and CD8 effector cells, and only 1 had naïve CD8 cells. In the ILT, all samples had cytotoxic granzyme B cells, which was similar to the blood. To facilitate easier comparison, the cells were grouped in to CD8 cytotoxic (granzyme B+), CD8 effector and 'other'.

When looking at the comparative frequencies of the CD8 subsets, in the aorta the most frequent subtype was the CD8 effector (median 63.8%, IQR 33.3% - 78.4%) followed by cytotoxic CD8 cells (median 32.99%, IQR 21.6% - 38.3%). The remainder of the cell subtypes only made up a mean of 10.5%**(Figure 4.15A).** Comparing frequencies in the ILT, the cytotoxic CD8 was the most frequent subtype (52.6%, IQR 29.8% - 73.8%). There was a non-statistically significant difference between the CD8 effector (median 22.6%, IQR 0% - 38.4%) and the remainder of the subtypes (median 30.3%, IQR 0% - 49.2%). **(Figure 4.15A).** In the peripheral blood, although not statistically significant, there were more 'other' subtypes than CD8 cytotoxic and CD8 effector **(Figure 4.15A)**.

Comparing the frequencies of the aorta, ILT and blood as a percentage of T cells, there were more CD8 effector cells in the aortic wall than the ILT ($p<0.01$) and peripheral blood ($p<0.05$). In the ILT there were more cytotoxic CD8 cytotoxic granzyme B cells compared to the aorta ($p<0.05$) and peripheral blood ($p<0.05$). **(Figure 4.15B)**

Table 4.2: CD8 subsets in the aortic aneurysm complex

CD8 Aortic T cells	CD8 Cytotoxic	CD8 Effector	CD8 Naïve	CD8 Central Memory	Other
1					
2					
3					
4					
5					
6					
7					
8					
9					
10					

CD8 ILT T cells	CD8 Cytotoxic	CD8 Effector	CD8 Naïve	CD8 Central Memory	Other
1					
2					
3					
4					
5					
6					
7					
8					

CD8 Blood T cells	CD8 Cytotoxic	CD8 Effector	CD8 Naïve	CD8 Central Memory	Other
1					
2					
3					
4					
5					
6					
7					
8					
9					

CD8 T cell subsets found in the aorta, ILT and blood. Green = present, Black = absent.

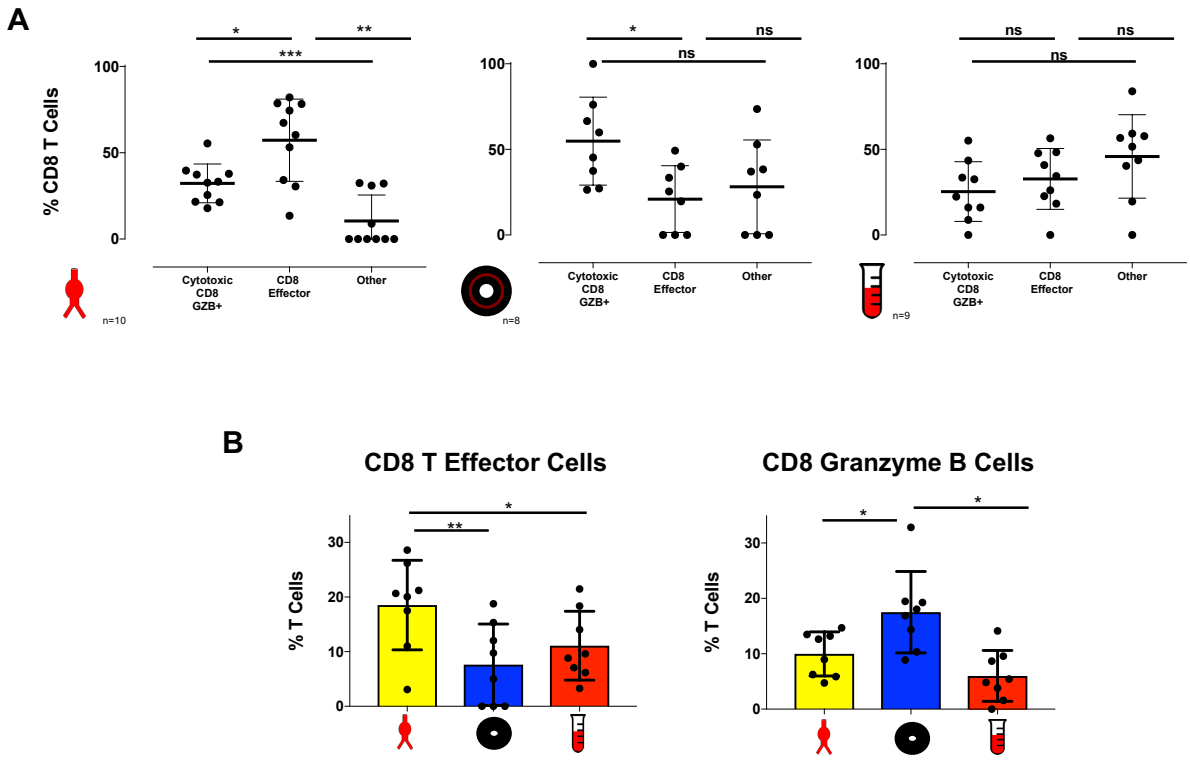


Figure 4.15: CD8 subsets in the aortic aneurysm complex

Blood, aortic wall and intraluminal thrombus (ILT) were collected intraoperatively from ten patients. Single cell suspensions were isolated by enzymatic digestion from the aorta and ILT (described in 2.5.1) prior to CD45+ cell enrichment with FACS (described in 2.6.2). Leukocytes were isolated from the blood after lysis of red blood cells (described in 2.5.1.3). In Cytobank individual viSNE's were created for each sample clustering on the markers in the lymphocyte centric panel (Figure 3.20). Two samples from the ILT and one from the blood did not meet the quality control requirements and were excluded from the analysis. After the initial viSNE plots on individual samples, the T cells, B cells and NK cells (lymphocytes) were selected and exported into the PhenographR Cytofkit analysis package (discussed in chapter 2.7.3) (k<30, perplexity of 30 and maximum iterations of 1000). The frequencies of the subsets identified by Phenograph were collated and individual clusters were compared to established CD8 subset nomenclature and matched.

(A) Dot plots describe the frequencies of Cytotoxic granzyme B cells, CD8 effector cells and the remaining subtypes found as a percentage of CD8 cells. In the aorta there are more CD8 effector cells than cytotoxic ($p<0.05$) and other cells ($p<0.001$), in the ILT there are more cytotoxic granzyme B cells compared to effector cells ($p<0.05$) whilst in the blood the frequencies were similar.

(B) Bar dot plots comparing the frequency of CD8 subsets in the aorta, ILT and blood as a percentage of T cells. The aorta has more T effector cells than the ILT ($p<0.01$) and the blood ($p<0.05$), whilst the ILT has more granzyme B containing CD8 cells than the aorta and blood ($p<0.05$). (Dot plots and bar plot error bars = mean +- SD). (*$p<0.01$, **$p<0.01$, ***$p<0.001$, ****$p<0.0001$, two tailed paired student t-test) (n=8)

Several consistent CD4 subsets were found in the aortic complex tissues. These were CD4 naïve, T regulatory cells (Treg), central memory, T follicular helper cells, cytotoxic CD4s containing granzyme B (of which some where iNKT cells) and T effector (helper) cells. Aside from cytotoxic CD4s, the aorta contained most of the other subsets. The ILT and blood samples contained most of the subsets, except there were no T follicular helper cells in either, and the ILT had fewer CD4 naïve cells **(Table 4.3)**.

Table 4.3: CD4 subsets in the aortic aneurysm complex

CD8 Aortic T cells	CD8 Cytotoxic	CD8 Effector	CD8 Naïve	CD8 Central Memory	Other
1					
2					
3					
4					
5					
6					
7					
8					
9					
10					

CD8 ILT T cells	CD8 Cytotoxic	CD8 Effector	CD8 Naïve	CD8 Central Memory	Other
1					
2					
3					
4					
5					
6					
7					
8					

CD8 Blood T cells	CD8 Cytotoxic	CD8 Effector	CD8 Naïve	CD8 Central Memory	Other
1					
2					
3					
4					
5					
6					
7					
8					
9					

CD4 T cell subsets found in the aorta, ILT and blood. Green = present, Black = absent.

In the aorta, the T effector (helper) cells were the most frequent as a % of CD4 cells (median 29.6, IQR 22.1% - 42.2%) whilst naïve, Treg and central memory where similar (mean 16.5% - 20.5%). The ILT was less consistent, with a wide range of frequencies within subsets. Although T effector cells were the most frequent, 3 of the 8 samples fell outside of the 95% confidence interval. Naïve cells (median 37.6, IQR 28.3% - 44.4%) and central memory cells (31.5%, IQR 21.5 – 45.3%) were the most frequent in the blood. **(Figure 4.16A)**

Comparing the frequencies of the aorta, ILT and blood as a percentage of total T cells, there were more naïve cells in the blood when compared to the aorta ($p<0.01$) and ILT ($p<0.001$) and the aorta had a higher frequency than the ILT ($p<0.05$). As a percentage of T cells, neither the CD4 T effectors nor the central memory cells were statistically significant from each other. Treg cells as a percentage of T cells were higher in the aorta (median 9.6, IQR 8.5% - 12.1%) and ILT (median 10.6, IQR 3.9% - 17.9%) compared to the peripheral blood (median 6.3, IQR 4.6% - 8.3%, $p<0.01$, Aorta vs. Blood). T follicular helper cells were not found in the ILT and blood, compared to the aorta (median 5.34, IQR 4.5% - 10.7%, $p<0.001$). CD4 iNKT containing granzyme B were more frequent in the ILT (median 9.9%, IQR 0% - 17.8%) when compared to the aorta ($p<0.05$) and the blood ($p<0.05$). **(Figure 4.16B)**

In summary, there was significant heterogeneity of CD4 and CD8 cells within the AAA complex, and its cytotoxic and effector cell types play an important role.

Figure 4.16: CD4 subsets in the aortic aneurysm complex

Blood, aortic wall and intraluminal thrombus (ILT) were collected intraoperatively from ten patients. Single cell suspensions were isolated by enzymatic digestion from the aorta and ILT (described in 2.5.1) prior to CD45+ cell enrichment with FACS (described in 2.6.2). Leukocytes were isolated from the blood after lysis of red blood cells (described in 2.5.1.3). In Cytobank individual viSNE's were created for each sample clustering on the markers in the lymphocyte centric panel (Figure 3.20). Two samples from the ILT and one from the blood did not meet the quality control requirements and were excluded from the analysis. After the initial viSNE plots on individual samples, the T cells, B cells and NK cells (lymphocytes) were selected and exported into the PhenographR Cytofkit analysis package (discussed in chapter 2.7.3) ($k<30$, perplexity of 30 and maximum iterations of 1000). The frequencies of the subsets identified by Phenograph were collated and individual clusters were compared to established CD4 subset nomenclature and matched.

(A) Dot plots describe the frequencies of 6 CD4 subsets as a percentage of CD4 T cells (Naïve, T regulatory, Central memory, Follicular helper, Cytotoxic granzyme B containing and Effector).

(B) Bar dot plots comparing the frequency of CD4 subsets in the aorta, ILT and blood as a percentage of T cells. There are more Naïve cells in the blood than the aorta ($p<0.01$) and ILT ($p<0.001$) and more Naïve cells in the aorta than the ILT ($p<0.05$). Effector CD4 cells and Central memory cells are found in similar frequencies across the specimen types. T regulatory cells are more frequent in the aorta than the blood ($p=0.0025$) and T follicular helper cells were only found in the aortic wall and not in the blood and ILT ($p<0.0001$). As a percentage of T cells there were more CD4 iNKT cells in the ILT than the aorta and blood ($p<0.01$). (Dot plots and bar plot error bars = mean +- SD). (*$p<0.01$, **$p<0.01$, ***$p<0.001$, ****$p<0.0001$, two tailed paired student t-test) (n=8)

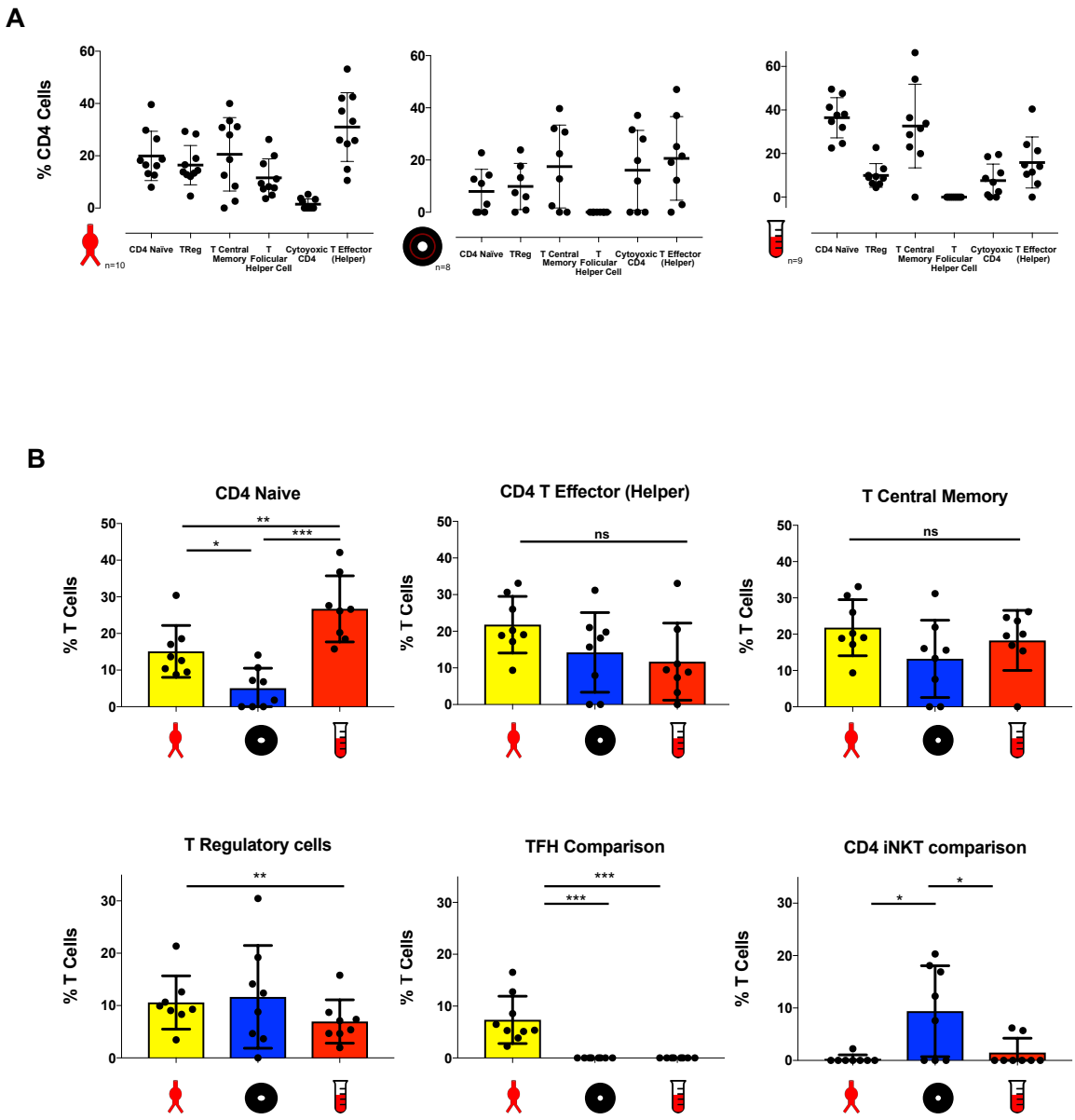


Figure 4.16: CD4 subsets in the aortic aneurysm complex

4.4.10 T Effector (helper) cell diversity in the aortic aneurysm complex

Having identified T effector cells in the CD8 and CD4 compartment, I aimed to further differentiate them based on their surface markers and cytokine output. The surface markers on the T effector cells were predominately chemokine receptors. There was diversity in both cell surface markers of the T effector cells and cytokines produced in the tissues.

From the aortic wall, ILT and peripheral blood, six groups of CD4 effector T cells were identified by PhenographR and they differed on their surface marker expression (CCR5+CD161+, CCR5+CD161-, CCR5-, CCR4+, CXCR3+, CCR5+PD1+). The aorta had 4 subtypes (CCR5+CD161+, CCR5+CD161-, CCR5-, CCR4+), the ILT (CCR5+CD161+, CCR5+CD161-, CCR5-, CCR4+ and CXCR3+) and the blood had 5 (CCR5+PD1+, CCR5+CD161-, CCR5-, CCR4+, CXCR3+). The subsets were not consistently found in all of the samples. In the aorta, CCR5+CD161- was found in 80% of samples and in the ILT it was found in 60% of subjects, but CCR5+CD161- was not found in the blood. The remaining subsets were inconsistently identified with no dominant subtype identified **(Figure 4.17A)**.

Eight groups of CD8 effector T cells were identified by PhenographR and they differed on their surface marker expression (CCR5+CD161+, CCR5+CD161-, CCR5-, CCR5-CCR4+, CXCR3+, CCR5+PD1+, CCR5-PD1+, CCR5+CCR4+). The aorta had 5 subtypes (CCR5+CD161+, CCR5+CD161-, CCR5-, CCR5-CCR4+ and CXCR3+) and ILT had 5 of these subtypes, whilst the blood had 7 subtypes. In the aorta there was no dominant subtype with an equal proportion of CCR5+ and CCR5- subtypes. In the ILT, the CCR5+CD161- subtype was found in 80% of subjects, but this subset was not found in the blood and no other dominant subtypes were found in the blood **(Figure 4.17B)**.

Figure 4.17: T cell effector phenotypic diversity within the aortic aneurysm complex

Blood, aortic wall and intraluminal thrombus (ILT) were collected intraoperatively from ten patients. Single cell suspensions were isolated by enzymatic digestion from the aorta and ILT (described in 2.5.1) prior to enrichment of CD45+ cells using FACS (described in 2.6.2). Leukocytes were isolated from the blood after lysis of red blood cells (described in 2.5.1.3). The *.fcs* files were imported in to Cytobank and individual viSNE's were created for each sample clustering on the markers in the lymphocyte centric panel (Figure 3.19). Two samples from the ILT and one from the blood did not meet the quality control requirements and were excluded from the analysis. After running the initial viSNE plots on individual samples, the T cells, B cells and NK cells (lymphocytes) were selected and exported in to the PhenographR Cytofkit analysis package (discussed in 2.7.3) ($k<30$, perplexity of 30 and maximum iterations of 1000). The frequencies of the effector cell subsets identified by Phenograph were collated and are described.
Secretome supernatants from the aorta, ILT as well as control aortas from transplant donors were analysed with a proteome profiler human cytokine array kit (R&D systems, described in chapter 2.11.4). The relative levels of selected human cytokines and chemokines were determined and are expressed as 'mean pixel densities'.

(A) Six subtype clusters of CD4 effector T cells were identified by Phenograph and they were separated based on their surface markers (CCR5+CD161+, CCR5+CD161-, CCR5-, CCR4+, CXCR3+, CCR5+PD1+). The aorta had 4 subtypes, the ILT and blood had 5.

(B) Eight subtype clusters of CD8 effector T cells were identified by Phenograph and they were separated based on their surface markers (CCR5+CD161+, CCR5+CD161-, CCR5-, CCR5-CCR4+, CXCR3+, CCR5+PD1+, CCR5-PD1+, CCR5+CCR4+). The aorta and ILT had 5 of these subtypes, whilst the blood had 7 subtypes.

(C) Bar graphs displaying the relative abundance of several aortic and ILT cytokines alongside control aortic tissue. Th1 cytokine Interferon-γ was increased in both the aorta and ILT, whilst, IL-4 a positive feedback cytokine for Th2 responses was higher in the ILT. IL-5 and IL-10 which are also Th2 cytokines were increased in both the ILT and aorta, but the other Th2 cytokine IL-13 was relatively supressed and IL-12 was similar across all three tissues. IL-17 and IL-22 which are associated with Th17 cells were also increased in the aorta and ILT when compared to the control. Pan inflammatory cytokine IL-6 was highly expressed when compared to the ILT and controls. TNF-α which can act as both a pro and anti-inflammatory cytokine was also relatively increased in the aorta and ILT when compared to the control.

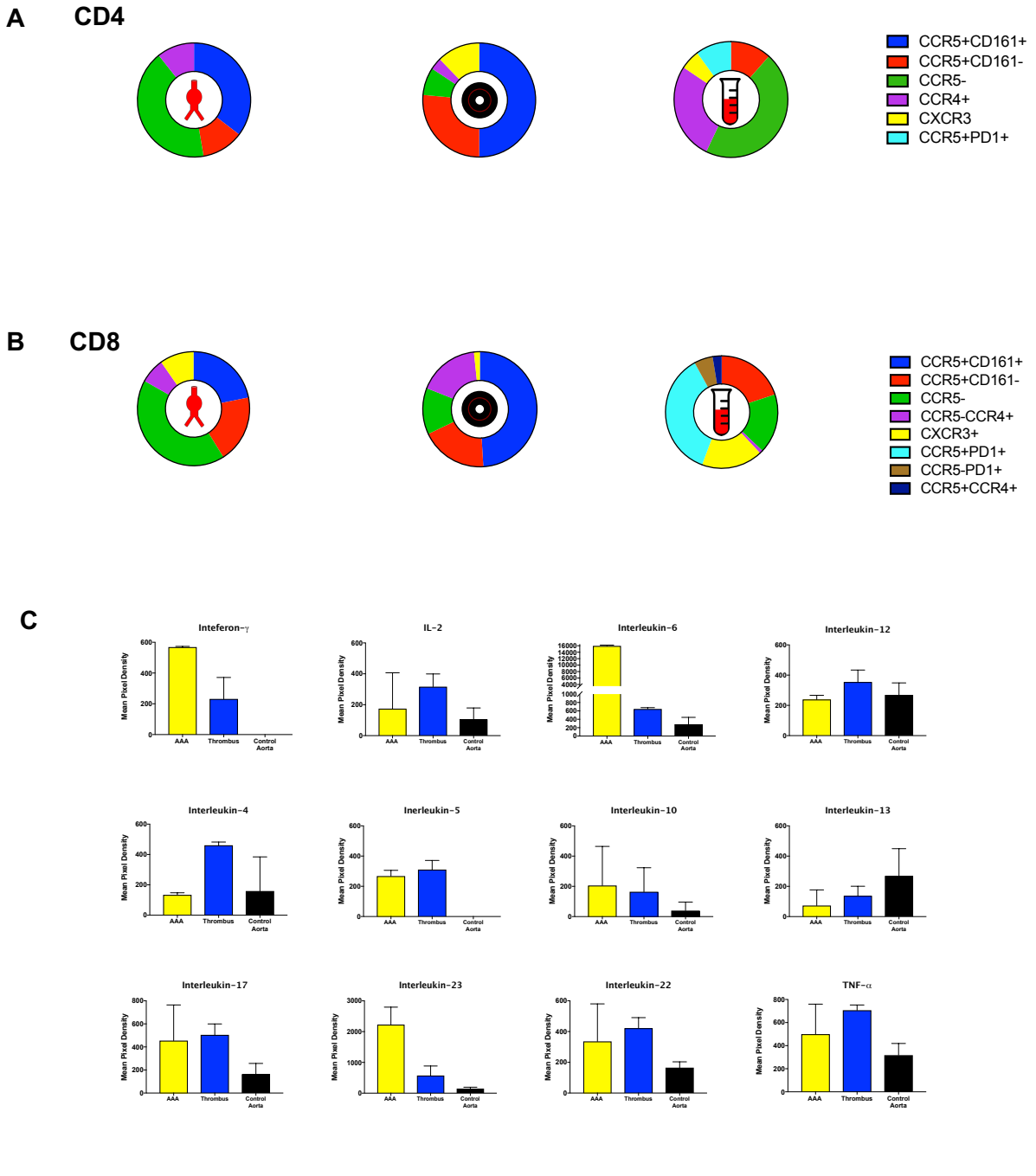


Figure 4.17: T effector cell phenotypic diversity within the aortic aneurysm complex

The significance of the different effector cell surface markers was not clear. To better understand the T helper cell responses of the aortic wall and ILT, a cytokine screen on the secretome supernatants was performed and compared to control aorta from transplant donors (methods chapter 2.11.4).

There was an upregulated cytokine response in the aortic wall and ILT compared with the control tissue but with no dominant Th response. Th1, Th2, Th17 and Th22 cytokines were increased. The Th1 cytokines, Interferon-γ (IFN-γ) and IL-2 were both increased in the aorta and ILT, and IFN-γ was higher in the aortic wall, whilst IL-2 was higher in the ILT. Together with IFN-γ and IL-2, IL-6 expression (the pan-inflammatory cytokine) was much higher in the aortic secretome when compared to the ILT and controls. However, IL-12 which stimulates IFN-γ and supresses IL-4 (Th2 cytokine) was not increased compared to the non-aneurysmal aortic tissue.

The Th2 cytokine, IL-4, was higher in the ILT together with the other Th2 cytokine, IL-5 which was increased in both, however IL-13 which is also a Th-2 cytokine was decreased in the ILT and aortic wall. The regulatory cytokine IL-10 was increased in the aortic wall and ILT. IL-12 was similar across all three tissues.

IL-17 and IL-23 which are associated with Th17 cells were also increased in the aorta and ILT when compared to the control, as well as the Th22 cytokine IL-22. TNF-α which can act as both a pro and anti-inflammatory cytokine was also relatively increased in the aorta and ILT when compared to the control **(Figure 4.17C)**. RANTES which is the natural ligand of CCR5 is relatively supressed in the aorta and ILT when compared to the control whilst MIP1-α was similarly expressed between the tissue types.

4.4.8 Granzyme B diversity in the cells of the aneurysm complex tissues

Several of the lymphocytes contained the cytolytic intracellular granule, Granzyme B (GzB). I aimed to describe the distribution of the GzB in the different cell compartments and measure cytokine outputs from cells associated with cytotoxicity.

Seven different T cell subtypes contained Granzyme B (cytotoxic CD8, CD8 iNKT, CD8 EmRA, Cytotoxic CD4, CD4 EmRA, CD4iNKT and double negative granzyme B T cells). However, the spread was heterogenous and not all of the patients had all of these cell types. **(Table 4.2, 4.3)**

In the peripheral blood cytotoxic CD8 cells were found in all but 1 patient. These were further separated by CD57 expression, 56% of patients had the CD8+GranzymeB+CD57+ subset and 33.3% had CD8+GranzymeB+CD57- cells. Cytotoxic CD4 cells were found in 66.6% of samples. PD-1 was expressed as a separate cluster of cytotoxic CD4 and CD8 cells in some patients. These PD-1 expressing clusters were not identified in the aortic wall and ILT. EmRA and iNKT (CD4 and CD8) cells were inconsistently identified in the samples **(Figure 4.18 A,B)**.

In the aorta there were also 7 different T cell subtypes containing Granzyme B (cytotoxic CD8, CD8 iNKT, CD8 EmRA, Cytotoxic CD4, CD4 EmRA, CD4iNKT and double negative granzyme B cells). Cytotoxic CD8 cells were found in 80% of the aortic wall samples, with all of them containing the CD8+GranzymeB+CD57+ subset. There were no CD8+GranzymeB+PD-1 cells and no EmRA (CD4 and CD8) in the aortic wall. Two patients had CD8 iNKT and CD4 iNKT cells respectively **(Figure 4.18 C,D)**.

Figure 4.18: Granzyme B diversity in the aortic complex lymphocytes

Blood, aortic wall and intraluminal thrombus (ILT) were collected intraoperatively from ten patients. Single cell suspensions were isolated by enzymatic digestion from the aorta and ILT (described in 2.5.1) prior to enrichment of CD45+ cells using FACS (described in 2.6.2). Leukocytes were isolated from the blood after lysis of red blood cells (described in 2.5.1.3). The *.fcs* files were imported in to Cytobank and individual viSNE's were created for each sample clustering on the markers in the lymphocyte centric panel (Figure 3.19). Two samples from the ILT and one from the blood did not meet the quality control requirements and were excluded from the analysis. After generating the initial viSNE plots on individual samples, the T cells, B cells and NK cells (lymphocytes) were selected and exported in to the PhenographR Cytofkit analysis package (discussed in 2.7.3) ($k<30$, perplexity of 30 and maximum iterations of 1000). The frequencies of the effector cell subsets identified by Phenograph were collated and are described.
Secretome supernatants from the aorta, ILT as well as control aortas from transplant donors were analysed with a proteome profiler human cytokine array kit (R&D systems, described in chapter 2.11.4). The relative levels of selected human cytokines and chemokines were determined and are expressed as 'mean pixel densities'.

viSNE analysis of the lymphocytes (T, B and NK cells) from a single patient's blood sample **(A)**, aortic wall **(C)** and ILT **(E)** are displayed. The Granzyme B plot highlights the clusters expressing Granzyme B within them. Alongside this are viSNE plots highlighting the channels expressing CD4, CD8, CD56 and CD57, thus allowing for visual colocalisation of the Granzyme B containing cell types.
(B) A donut plot displaying the diversity and relative frequencies of granzyme B containing cells within the 9 patients samples as separated out by Phenograph. Seven different T cell subtypes contained Granzyme B (cytotoxic CD8, CD8 iNKT, CD8 EmRA, Cytotoxic CD4, CD4 EmRA, CD4iNKT and double negative granzyme B cells).
(D) A donut plot displaying the diversity and relative frequencies of granzyme B containing cells within the 10 patients aortic samples as separated out by Phenograph. Seven different T cell subtypes contained Granzyme B (cytotoxic CD8, CD8 iNKT, CD8 EmRA, Cytotoxic CD4, CD4 EmRA, CD4iNKT and double negative granzyme B cells)
(F) A donut plot displaying the diversity and relative frequencies of granzyme B containing cells within the 8 patients ILT as separated out by Phenograph. Seven different T cell subtypes contained Granzyme B (cytotoxic CD8, CD8 iNKT, CD8 EmRA, Cytotoxic CD4, CD4 EmRA, CD4iNKT and double negative granzyme B cells).
(G) A bar dot plot comparing the frequencies of Granzyme B expression between the aorta, ILT and blood. The ILT has a greater frequency of Granzyme B expressing cells than the aorta and blood ($p<0.05$).
Bar graphs displaying the relative abundance of several aortic and ILT cytokines related to cytotoxic CD8 cells alongside control aortic tissue **(H,I,J,K)**.
(H,I) IL-2 and IL-15 which induce the lytic activity of Granzyme B containing cells, are both increased in the aorta and ILT when compared to the control tissue.
(J) Fas-L works as an alternate mechanism of lytic activity in cytotoxic CD8 cells and is increased in the aorta and ILT when compared to the control tissue.
(K) IL-18 is activated by Granzyme B and is increased in the ILT and aorta more than the aortic control tissue.

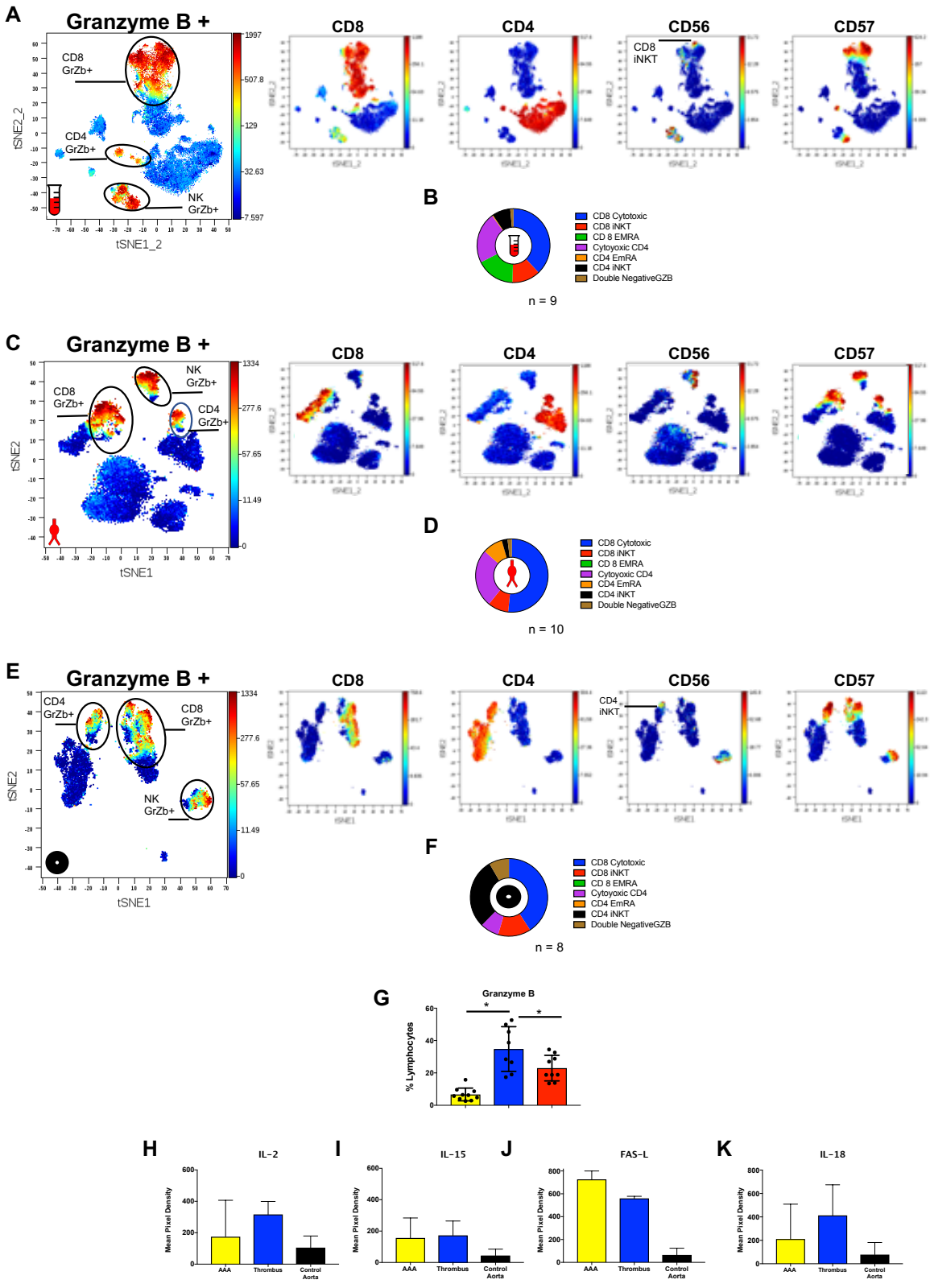


Figure 4.18: Granzyme B diversity in the aortic complex lymphocytes

Seven different T cell subtypes contained Granzyme B in the ILT (cytotoxic CD8, CD8 iNKT, CD8 EmRA, Cytotoxic CD4, CD4 EmRA, CD4iNKT and double negative granzyme B cells). Cytotoxic CD8 cells were found in all the patients and all of them contained the CD8+GranzymeB+CD57+ subset. There were no CD8+GranzymeB+PD-1 cells and no EmRA (CD4 and CD8) in the ILT. Five of the eight patients had CD4 iNKT cells **(Figure 4.18 E,F)**. When comparing the total Granzyme B containing cells in the aortic wall, ILT and peripheral blood (as a percentage of lymphocytes), the ILT had a greater frequency of Granzyme B expressing cells than the aorta and blood ($p<0.05$) **(Figure 4.18 G)**.

Having already screened the aortic wall, ILT and controls with a cytokine array (methods chapter 2.11.4), I examined the cytokines in this array related to cytotoxic CD8 cells and cytotoxicity. IL-2 and IL-15 which induce the lytic activity of Granzyme B containing cells, were both increased in the aorta and ILT when compared to the control tissue **(Figure 4.18 H,I)**. Fas-L works as an alternate mechanism of lytic activity in cytotoxic CD8 cells and is increased in the aorta and ILT when compared to the control tissue, and IL-18 is activated by Granzyme B and was increased in the ILT and aorta more than the aortic control tissue **(Figure 4.18 J,K)**.

4.5 Discussion

AAAs degenerate as a result of ongoing smooth muscle cells apoptosis and elastin degradation of the aortic wall and this is accompanied by a characteristic immune cell infiltrate. The progressive degeneration is likely facilitated by immune cells within the aortic wall. Efforts to identify the immune mechanisms involved, as well as therapeutics to inhibit growth have thus far been elusive. I therefore sought to improve the understanding of the immune landscape of the aortic wall, ILT and peripheral blood by performing mass cytometry analysis of the immune cells present in these tissues. The objective of the study was to investigate the adaptive and innate immune responses through paired analysis of the aortic wall, ILT and peripheral blood.

B Cells in the aortic complex tissues

Deep phenotyping of the immune populations of the aneurysmal wall indicated a robust engagement of the adaptive immune response, and memory B cells formed a major component of this. This work presents new evidence for T-B cell cross talk in the AAA wall.

B cells, together with T cells form part of the adaptive immune system, with B cells providing humoral immunity through the production of antibodies. Compared with the primary antibody response, the reactive humoral antibody response is typically faster, of greater magnitude and consists of antibodies of switched isotypes with higher affinity(164). Clinically, a difficult to manage variation of an AAA exists and it is commonly referred to as an ‘inflammatory’ AAA (1-5%). It is typified by a markedly thickened aneurysmal wall with dense adhesions to surrounding structures as well as perianeurysmal and retroperitoneal fibrosis(165).

Immunoglobulin G4 (IgG4) has been associated with 57% of inflammatory abdominal aortic aneurysms and is characterised by IgG4 plasma cell infiltration into the adventitia(166, 167). IgG4 is related with several sclerosing disease states (pancreatitis, biliary, retroperitoneal, salivary)(167). The contribution of B cells to the ongoing degenerative processes in AAAs are underexplored and it is often stated that AAAs are a T cell and macrophage driven disease(76, 133).

In the aortic wall, B cells were the predominant infiltrate, slightly outnumbering T cells (44.1% vs.39.9%). Strikingly, there were significant differences in the B cells of the aortic wall when compared to the ILT and peripheral blood, suggesting a significant contribution to the underlying pathology by the B cells. The aortic wall B cells were predominately memory B cells when compared to the ILT and peripheral blood (67.2% vs. 23% vs 23.7%), whilst in the ILT and peripheral blood there were mainly naïve B cells. In addition, there were other subtypes of B cells in the aortic wall, such as plasmablasts (CD38++), CD1D++IgD+ B cells and CD127+ B cells.

The memory B cells of the aortic wall were heterogeneous, containing conventional class-switched memory B cells, as well as IgM and double negative memory B cells. Class switching (Isotype switching) typically occurs in the germinal centres of secondary lymphoid organs (lymph nodes, spleen, tonsils, mucosal associated lymphoid tissue, Peyer's patches) whilst IgM memory B cells form independent of the germinal centre(168). Germinal centres (GC) represent a major site permitting crosstalk of antigen activated T, B, follicular dendritic cells and to promote T and B cell expansion(169). The intriguing question is, where does the class-switching occur? Does it occur in the spleen and the cells home to the aortic wall, or does it occur in the aorta itself? And what is the relevance?

Vascular-associated lymphoid tissue (VALT) and GC formation are described in the aortic adventitia(68, 140). Similarly, atherosclerotic vessels contain artery tertiary lymphoid organs (ALTO) which may be the same as VALT(170). Tertiary lymphoid organs arise in peripheral tissues in response to non-resolving inflammation and are capable of forming and functioning as lymph node like structures(171). T follicular helper (Tfh) cells are a distinct subset of antigen activated CD4 T cells expressing CXCR5, PD-1 and ICOS, and are essential for the formation of class switched memory B cells. They regulate the activation and function of GC B cells. Isotype switching and affinity maturation indicate that the antibody response is a T cell dependent antigen driven immune process.

Indeed, in the aortic wall we consistently found Tfh helper cells (CD4+CXCR5+ICOS+PD1+) and class-switched memory B cells. Tfh were not found in the ILT and peripheral blood. Finding Tfh cells in the aortic wall together with activated memory B cells, provides putative evidence of T-B cell cross talk. This together with the presence of plasmablasts suggests that there is ongoing class-switching at the level of the aortic adventitia (in the VALT), and therefore ongoing antigen (or auto-antigen) stimulation and production of immunoglobulins, even in these chronic and end-stage aortas.

Within the context of interrogating the CD8-Tfh axis, Clement et al, incidentally found evidence of Tfh cells in the aortic adventitia together with an increase in B cell immunoglobulins. Our findings corroborate this. The regulation of Tfh in atherosclerosis is thought to be through CD8 Treg cells(172). When we re-examined our CD8 T cells, we did not find a CD8+CD25+FoxP3+ cluster, and this may provide a clue to possible dysregulation in Tfh-GC interactions which needs further exploration.

B cells can also act as antigen presenting cells to T cells. Two further potential interactions of the T-B cells may occur in patients with AAAs. The first is the CD1d-iNKT axis. B cells can present lipid antigens to iNKT cells through cognate interaction with the CD1D receptor(173). CD1D was expressed in 79% of the peripheral blood B cells and 60% of the aortic wall B cells, which were both higher than in the ILT (23%), but there were more iNKT T cells in the ILT than the aorta and peripheral blood.

The other potential interaction of T and B cells was through the CD40-CD40L receptor, and CD40 expression was higher in aortic and peripheral blood B cells than in the ILT. The predominance of B memory cells may represent the emergence of autoreactive B cell clones, supporting the autoimmune hypothesis.

Enrichment of cytotoxic T cells

T cells were the second most frequent cell type in the aortic wall and were also more frequent in the aortic wall than the ILT and peripheral blood. The CD8 frequencies were similar across the three tissue types, but there were more CD4 cells in the aorta than the ILT and peripheral blood. T cells in the aortic wall of AAAs are well described and most authors have described a pro-inflammatory Th1 predominance. This was not our finding, and instead we found a heterogenous mix of subtypes that are likely involved in complex interactions in an effort to balance and counterbalance exaggerated responses. The peripheral blood has more CD4 Naïve cells, with the ILT having the least frequent CD4 naïve cells and this is in keeping with the hypothesis that the ILT is not an inert and passive structure. In absolute frequencies,

there was no statistically significant difference in the CD4 central memory and effector subtypes between the three tissue types.

T regulatory cells (Treg) are regulators of the T effector cell response and are a vital component of mechanisms that prevent autoreactivity. Previous reports have suggested that Tregs' were decreased in the blood of patients with AAA, and postulated that the inflammatory cell infiltrate was as a result of disordered regulation(75). At the level of the aortic wall however, and for the first time, we identified a consistent population of Treg cells (CD4+CD25+FoxP3+CD127-) in the aortic wall and ILT. Their frequency as a percentage of T lymphocytes was 9.6% in the aortic wall, in the ILT 10.6% and the blood 6.24%. This is consistent with normal values in health, ranging between 5 and 10% (174-176). So, quantitively they were not reduced, but further investigations need to examine them qualitatively. In murine AngII models of AAA, Tregs' are thought to have a protective role in aneurysm formation, and more specifically rupture(81, 177). This again highlights the potential differences between human and murine models, which may be related to different phases of the disease.

The CD8 subsets in the aorta and ILT are mainly cytotoxic CD8s and CD8 effector cells, whereas the peripheral blood had more CD8 naïve cells. We noted that the ILT had more cytotoxic CD8 granzyme B cells when compared to the aortic wall and peripheral blood, additionally CD57, the marker for terminal differentiation was expressed on the cytotoxic CD8 T cells. This will be further discussed in the section on ILT.

There were several CD4 subsets with the T effector subsets being the most common in the aortic wall and ILT. The panel of antibodies also included CXCR3, CCR4, CD161, CCR5 and PD-1. CXCR3 is a chemokine receptor expressed on Th1 cells, whereas Th2 cells favour the expression of CCR4. CD161 is preferentially expressed on Th17 cells that produce IL-17 (in CD45RA-CCR7-) and is also a marker of homing, a marker of NK cells and in CCR7+ memory T cells is found on the memory phenotype. In both the CD4 and CD8 T effector subsets, there was no dominant pattern of expression and this suggests of the plasticity of T helper cells in chronic non resolving inflammation(178).

We went on further to measure the cytokine outputs in unstimulated cells of the aortic wall and ILT, and there again was no dominant pattern of Th1/2/17 output, even though uniformly there was an increased cytokine output in the aortic wall and ILT. The Th1/Th2 axiom is one that is being challenged. Of the cytokines, IL-6 was highly expressed in the aortic wall when compared to the ILT and control aortic tissue. IL-6 has previously been implicated in the pathogenesis of AAA and was found to be secreted in to the peripheral circulation by the aneurysm(179). IL-6 is secreted by B, T, macrophages and NK cells which are all constituents of the chronic inflammatory cell infiltrate and this is further evidence that even in these 'end-stage' aortic walls, there is ongoing inflammation and destruction of the wall.

Strikingly however, CCR5 was expressed as a dominant surface marker by the T effector cells on the aortic wall and ILT, but not in the peripheral blood. CCR5 is a protein expressed mainly on Th1 CD4 T cells and its ligand is RANTES. It was initially thought of as unimportant but is now central to several pathologies including a treatment strategy for HIV-1. It plays a vital role in the inflammatory response by directing cells to sites of inflammation. A CCR5Δ32 homozygous deletion protects

from HIV-1 infection whilst people are still seemingly healthy(180). CCR5 has been implicated in various types of cancer and a CCR5 blockade has been shown to inhibit metastases in breast cancer(181) and blockades have been used successfully in patients with inflammatory bowel disease(182). However, a 2009 study investigating the role of CCR5Δ32 homozygous deletion did not find a decrease incidence, nor a slowed growth rate in AAAs(183) and this refuted an earlier study suggesting a possible link between CCR5Δ32 homozygous deletion and the development of AAA(184). Oral CCR5 inhibitors require exploration as a potential target for slowing down the degeneration of AAAs.

Finally, PD-1 (Programmed cell death protein-1), the immune checkpoint is expressed on 'exhausted' T cells, and has an ever-expanding role in cancer immunotherapy(185). We examined PD-1 expression in T effector cells, and it was not highly expressed in the aortic wall and ILT.

The immune landscape of the ILT shows an enrichment of cytotoxic lymphoid populations expressing Granzyme B

The ILT is indeed an independent structure with its own inflammatory cell signature that is distinct from the peripheral blood. In this study we examined the luminal aspect of the ILT, having initially demonstrated that the abluminal area was cell poor. The underlying premise was that the ILT is a dynamic structure that interacts with the surrounding aortic blood as opposed to a passive interaction where the blood is merely trapped within the thrombus.

Other investigators have demonstrated the renewal of the luminal ILT and the role of neutrophil elastase in this process (87, 186). It contains T cells, B cells, Myeloid and NK cells and these immune cells classes are also found in the aortic wall and peripheral blood. The absolute proportions of the cells in the ILT and peripheral blood were similar but the phenotypes within the immune cell types are different. Although the clustering algorithm was unable to differentiate discrete clusters of mononuclear phagocytes in the ILT, there were clear differences between the ILT and peripheral blood.

The ILT behaved more like the aortic tissue and did not contain any CD16+ mononuclear phagocytes and they were not IRF5 positive when compared to the blood. IRF5 expression in human macrophages is associated with the pro-inflammatory M1 phenotype(187) and was widely expressed in the aortic tissue and blood. The ILT also contained activated CD169+ and CD1C+ positive dendritic cells which is similar to the aortic wall, and this has not previously been described in the ILT. The cytokine IL-4 has multiple effects and was higher in the ILT than the control aortic tissue or aneurysm wall. It also induces monocyte to dendritic cell transformation(188), strengthening the theory of monocyte differentiation within the ILT in to inflammatory dendritic cells (MoDCs). The innate myeloid cells in the aortic wall and ILT appeared heterogenous but with significant overlap of several markers leading to differentiated capacities. Dendritic cells are mediators of T cell differentiation and both the aortic wall and ILT contain T cells, and little was previously known about the T cell phenotypes in the ILT.

Strikingly, Granzyme B (GzB), the cytolytic serine protease was found in the granules of cytotoxic T cells and NK cells. It is secreted along with the membrane disruptive protein perforin (Prf) and is utilised by cytotoxic lymphocytes (CTL) for targeted killing in both the adaptive and innate immune systems(189). GzB has been shown to be elevated in the plasma of patients with advanced atherosclerotic lesions(190), autoimmune diseases(191), viral infections and transplant graft rejection. The ILT had the highest frequency of GzB when compared to the aortic wall and peripheral blood, but all three tissues had GzB containing lymphocytes.

This is the first study that colocalises GzB to T cells and NK cells in the aortic wall, together with peripheral blood and ILT of patients with AAAs. GzB deficiency in a knockout mouse model has been shown to decrease the incidence of AAA formation as well as rupture, and GzB was found in the wall of human AAAs but not in healthy control aortas using IHC (192). In a genome wide association study of patients with AAA (GWAS), the natural killer cell mediated cytotoxicity pathways were upregulated(193). Our findings validate these previous findings and further implicate the cytotoxic lymphoid cells in the ongoing destruction of the aortic wall.

Not only is GzB cytotoxic to cells, but it also has the ability to cleave a number of extracellular matrix proteins such as fibrillin-1, vitronectin, laminin and aggrecan which are components of the aortic wall(194). Fibrillin-1 deficiency is the hallmark of Marfan's syndrome and its associated aortic aneurysm formation(195), and this effect of GzB may be an additional mechanism of aortic wall degradation. In addition, GzB acts on substrates involved in the clotting cascade such as plasmin,

plasminogen, von Willebrand Factor (VWF) and fibrinogen(196). This is a plausible explanation for its increase in the ILT.

In this study, we also found that most of the cytotoxic GzB containing T and NK cells were CD57 bright. CD57 is a marker of terminal differentiation and CD57 bright GzB+ cells have also been shown to have high levels of perforin. CD57 bright NK cells are highly cytotoxic(197). In addition, Fas-L, the cytotoxic cytokine was increased in the secretome supernatants of the ILT when compared to the aneurysm wall (chapter 5) and control aortic tissue and Fas signalling induces cytotoxic killing of GzB containing CD8 effector cells. Fas-L and CTL are known to work in concert(198). CD8 lymphocytes only express GzB after simulation and differentiation into CTL(199).

Granzyme B containing cytotoxic cells do occur in normal lymphoid tissues and are involved in immune surveillance and for rapid killing of cells infected with intracellular pathogens. GzB is present in the plasma of healthy individuals, however it is elevated in chronic inflammatory states(200). Interestingly, GzB expression was not confined to CTL and NK cells, but also included CD4+, double negative and iNKT cells. GzB expression in these cells is often associated with pro-inflammatory conditions(190). These characteristics provide additional immunological insights into cytotoxic characteristics of the cellular infiltrate in the aortic complex and add potential mechanisms to the theory of aortic wall degeneration in AAAs.

4.6 Conclusion

This chapter provided the first comprehensive map of the immune landscape in AAAs, providing novel insights into the disease process.

The ILT can no longer be thought of as an inert and passive structure. It contains activated monocyte derived dendritic cells and NK cells which form part of the innate immune system, whilst its T cell phenotypes are rich in CCR5 demonstrating features of active recruitment and are part of adaptive immunity.

For the first time, we described the presence of the cytotoxic granule, Granzyme B within the cytotoxic lymphoid cells of the aortic complex tissues. More specifically it was comparatively increased in the ILT. The aortic wall has a chronic inflammatory cell infiltrate and it is predominated by B cells, more specifically, memory B cells. We demonstrated the simultaneous presence of T follicular helper cells, which are responsible for the class-switching in memory B cells, thus suggesting that the aortic wall is the site of this class-switching and contains tertiary lymphoid structures with in. And finally, the T cell infiltrate in the aortic wall is complex, and does not fit in to the bounds of a classical Th1/Th2 axis, containing sufficient numbers of Tregs with increases in several cytokines, especially IL-6 and an increase and the expression of CCR5 in the T effector cells of the aortic wall and ILT.

This multitude of new information highlights the complexity of the pathogenesis and deviates from the standard linear model of smooth muscle cell apoptosis and elastin degeneration as a once-off initiating event, generally thought to initiated by MMP secretion. Even in these ‘end-stage’ aortas where the smooth muscle and elastin is virtually obliterated, there is ongoing destruction and disordered repair of the aortic wall. This is not isolated to aortic wall alone, as the ILT contributes significantly to

the inflammatory burden in the ‘aortic complex’. Cytotoxic lymphoid populations (CD8 T, NK, iNKT) contribute to this ongoing destruction, and are a relatively novel concept in this disease. This presents a new potential pathway for therapeutic investigation. Additionally, based on the findings of this study, the targeting the B cells or CCR5 pathways are other potential therapeutic avenues. CCR5 is particular interesting as there are commercially available CCR5 inhibitors already in use for HIV treatment.

CHAPTER 5

ELUCIDATING THE BIOLOGICAL ACTIVITY OF INTRALUMINAL THROMBUS IN AORTIC ANREURYSMS

5.1 Introduction

In this chapter, the biological activity of the ILT is examined, and evidence for linking it to systemic endothelial dysfunction is sought. Flow mediated dilation (FMD) is a well-established surrogate marker for endothelial dysfunction(104). Lee *et al* had previously demonstrated that FMD is deranged in patients with AAA and deteriorated with progression of AAA(16). Relevant to this thesis, they also demonstrated that FMD improves after an aneurysm repair (16). This provides an *in-vivo* mechanistic model of AAA driving systemic endothelial dysfunction.

5.2 Hypothesis and Aims

In this chapter, I hypothesised that the ILT in AAAs contributes to the accelerated deterioration of systemic endothelial dysfunction.

The aims were to:

- To obtain supernatants enriched with a secretome of the ILT
- To ascertain the biological activity of the ILT through an NF-kB translocation assay
- To stimulate aortic endothelial cells (AOECs) with the ILT secretome and examine gene changes associated with endothelial dysfunction.

5.3 Experimental workflow

Having established the immune landscape of the aortic tissues, and identified novel and potentially cytotoxic subsets, I set out to investigate the link between the ILT and endothelial dysfunction. FMD was measured pre and post operatively in the

study subjects. Their tissue secretome supernatants were then used to stimulate cultured cells, assessing biological activity in the tissues. Furthermore, the ILT secretome was used to stimulate aortic endothelial cells (AOECs) and the changes in gene expression of 84 endothelial cell related genes were analysed. These results will be presented. (Methods chapter 2.8)

5.4 Results

5.4.1 Establishing the biological activity of ILT supernatants

ILT, aortic wall and omental specimens were collected intraoperatively from nine study subjects. Each of the specimens was collected as described in chapter 2.4 and volume matched tissues were incubated overnight under tissue culture conditions and their respective secretome supernatants stored at -80^{o} C for later use (methods chapter 2.8).

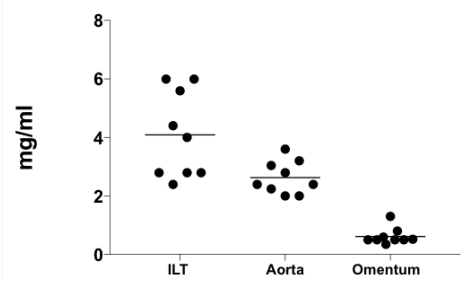


Figure 5.1: Protein concentrations of ILT, aortic and omentum secretome supernatants

ILT, aortic wall and omental specimens were collected intraoperatively from nine study subjects (methods chapter 2.4.2). Volume matched tissues were incubated overnight under tissue culture conditions and their secretome supernatants collected. Protein concentrations were measured in the supernatants using a Pierce-BCA assay. The median protein concentration in the ILT was 4mg/ml (2.8–5.8mg/ml), in the aorta 2.4mg/ml (2.1–3.1mg/ml) and the omentum 0.5mg/ml (0.5-0.7mg/ml). (n=9)

The secretome supernatants of each individual patient's protein concentration was assessed using a Pierce-BCA assay (chapter 2.8.2) **(Figure 5.1)**. The median protein concentration in the ILT was 4 mg/ml (2.8–5.8 mg/ml), in the aorta 2.4 mg/ml (2.1-3.1 mg/ml) and the omentum 0.5 mg/ml (0.5-0.7 mg/ml). This enabled extraction of the same amount of protein from each secretome sample for subsequent analysis (Values are presented as the median and interquartile range).

The secretome supernatants were then used to stimulate RPE-1 cells followed by immunofluorescence staining for the subunit p65 of NF-κB (methods chapter 2.10). The ILT secretome supernatants induced NF-κB translocation when compared to the negative control and omental secretome supernatants **(Figure 5.2)**. In addition, and unexpectedly the aortic supernatants resulted in cytotoxicity of the RPE-1 cells **(Figure 5.2).** NF-κB translocation provides direct evidence for biological activity, and cytotoxicity is implied by cell death (sparsity and non-uniform outline).

5.4.2 ILT supernatants also result in cytotoxicity of RPE-1 cells

In view of the translocation of NF-κB in RPE-1 cells by the ILT supernatant, the experiment was repeated**.** Four patients ILT secretome supernatants were used to stimulate RPE-1 cells followed by immunofluorescence staining for the subunit p65 of NF-κB (methods chapter 2.10). Prior to stimulation their protein concentrations were adjusted to 1 mg/ml based on their BCA assays (chapter 2.8.2).

The ILT of all the subjects was cytotoxic to RPE-1 cells as demonstrated by a sparsity of cells together with a non-uniform cell outline in the ILT supernatants when compared to the control (RPMI) **(Figure 5.3)**.

Figure 5.2: Immunofluorescence of RPE-1 cells after stimulation with tissue secretome supernatants

ILT, aortic wall and omental specimens were collected intraoperatively from a study subject (methods chapter 2.4.2). The tissues were incubated overnight under tissue culture conditions and their secretome supernatants collected (methods chapter 2.8). These were then used to stimulate RPE-1 cells followed by immunofluorescence staining for the subunit p65 of NF-κB (methods chapter 2.10). Images were captured using the Alexa488 (green) and DAPI (blue) channels and merged using ImageJ software. **(Negative control (RPMI 1640), Positive control (TLR2 ligand), ILT, omentum and aortic wall supernatants).**

The cells in the negative control (RPMI 1640) have a similar fluorescence in their cytoplasm and nuclei, whereas the positive control (TLR2 ligand) has prominent nuclear staining signifying that NF-kB has translocated into the nucleus. The nuclei of the thrombus stimulated RPE-1 cells fluoresce positively for NF-kB whilst the omentum stimulated cells did not and the cytoplasm and nucleus appear homogenous. Additionally, aortic supernatants resulted in cytotoxicity of the RPE-1 cells as seen by their irregular cell shapes. (Olympus BX51, X40 magnification)

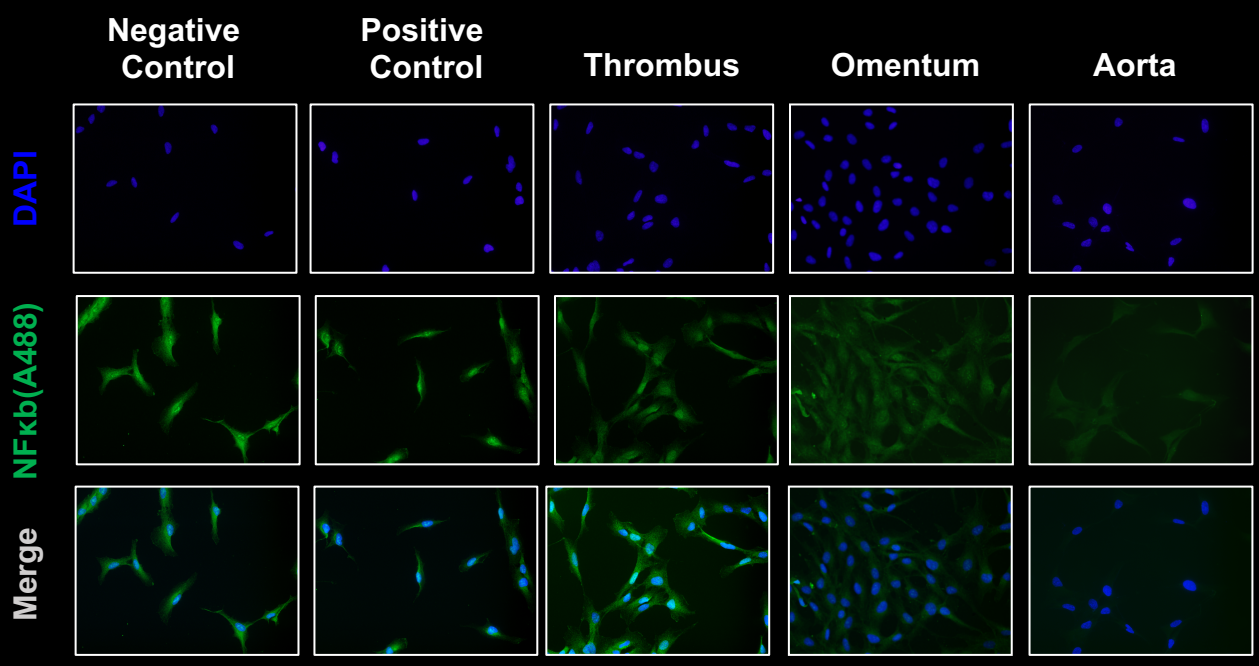


Figure 5.2: Immunofluorescence of RPE-1 cells after stimulation with tissue secretome supernatants

Figure 5.3: Immunofluorescence of RPE-1 cells after stimulation with ILT secretome supernatants

ILT specimens were collected intraoperatively from four study subjects (methods chapter 2.4.2). They were incubated overnight under tissue culture conditions and their secretome supernatants collected (methods chapter 2.8). The ILT supernatants were diluted to a protein content of 1 mg/ml. These were then used to stimulate RPE-1 cells (methods chapter 2.9.3) followed by immunofluorescence staining for the subunit p65 of NF-κB (methods chapter 2.10). Images were captured using the Alexa488 (green) and DAPI (blue) channels and merged using ImageJ software. Images from the four patients demonstrate a sparsity of cells with a non-uniform cell outline in the ILT supernatants when compared to the control (RPMI). This is indicative of cytotoxicity by the supernatants when compared to the control. (Olympus BX51 microscope, X40 magnification)

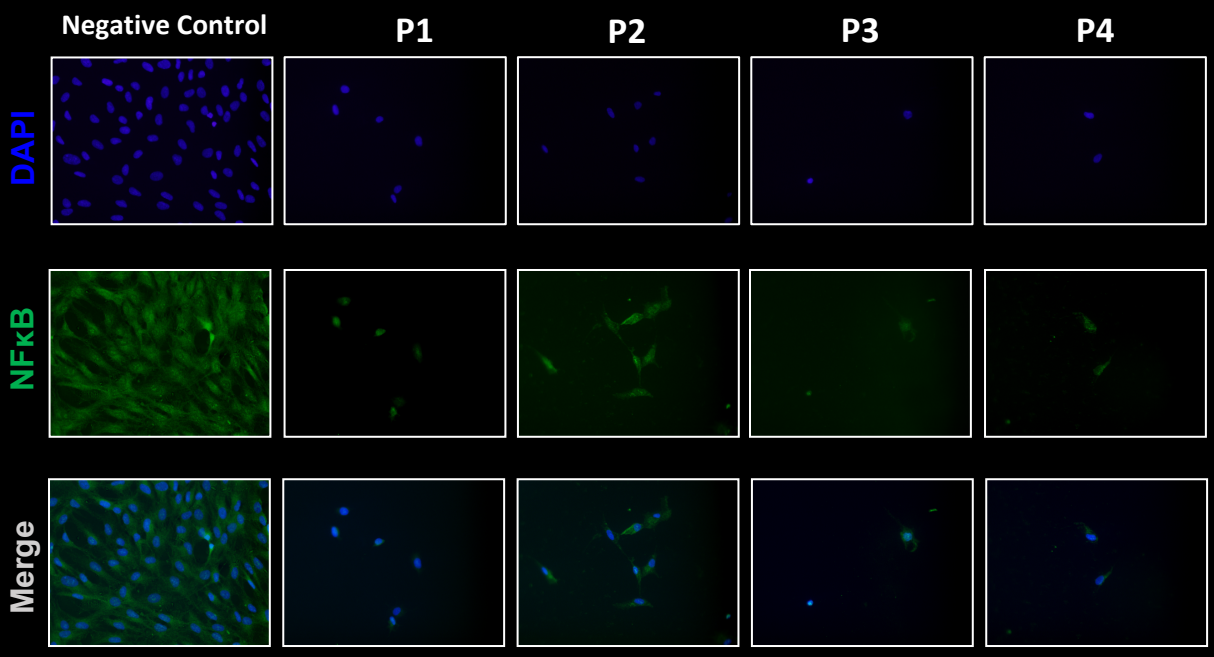


Figure 5.3: Immunofluorescence of RPE-1 cells after stimulation with ILT secretome supernatants

5.4.3 Excluding bacterial contamination as a cause of cytotoxicity

The first ILT supernatant resulted in NF-κB translocation in RPE-1 cells and the subsequent four resulted in cytotoxicity. One possibility was that during transportation and culture process, the specimens may have been contaminated by bacteria, despite best practice and prophylactic antibiotics. To exclude this, the supernatants were screened for LPS contamination (methods chapter 2.8.4) with a Thermofisher LPS chromogenic assay kit. LPS is the major constituent of gram-negative cell membranes, and can elicit a major immune response which can ultimately lead to septic shock(132).

Six subjects ILT supernatants indeed contained low levels of LPS. The results are quantified in endotoxin units per ml (EU/ml), where 1 EU/ml approximates 0.1 ng/ml of endotoxin. The median level was 0.24 EU/ml (0.18 – 0. 31 EU/mL). **(Figure 5.4A)** (Values are presented as the median and interquartile range)

Although these were low levels of endotoxin and are below recommended federal drug administration (FDA) levels for commercial intravenous preparations, I further stimulated RPE-1 cells with LPS at 0.2, 0.5 and 1 EU/ml to simulate these findings.

The stimulation with endotoxin did not result in NF-κB translocation into the nucleus and there was no difference between the negative control (RPMI 1640) and stimulation with low levels of endotoxin **(Figure 5.4B)**. This is represented through immunofluorescence in **Figure 5.4C**.

Figure 5.4: Quantification of NF-kB translocation and immunofluorescence of RPE-1 cells after stimulation with LPS in serial dilutions

ILT specimens were collected intraoperatively from six study subjects (methods chapter 2.4.2). They were incubated overnight under tissue culture conditions and their secretome supernatants collected (methods chapter 2.8). LPS levels were then measured in the supernatants (methods chapter 2.8.4). LPS was further diluted into several concentrations and these were then used to stimulate RPE-1 cells (methods chapter 2.9.3) followed by immunofluorescence staining for the subunit p65 of NF-κB (methods chapter 2.11). Images were captured using the Alexa488 (green) and DAPI (blue) channels and merged using ImageJ software and NF-κB translocation was quantified.

(A) LPS levels (EU/ml) measured in the ILT supernatants (median = 0.24EU/ml (0.09 - 0.38 EU/ml) **(B)** Quantification of the NF-κB nuclear:cytoplasm ratio across different concentrations of LPS and compared to a control (RPMI) shows no difference at these low levels of LPS stimulation (ratio <= 1 = no translocation of NF-κB). **(C)** Three concentrations of LPS stimulated RPE-1 cells demonstrate no increase in translocation of NF-κB as shown by the homogenous staining of the nucleus and cytoplasm. (Olympus BX51 microscope)

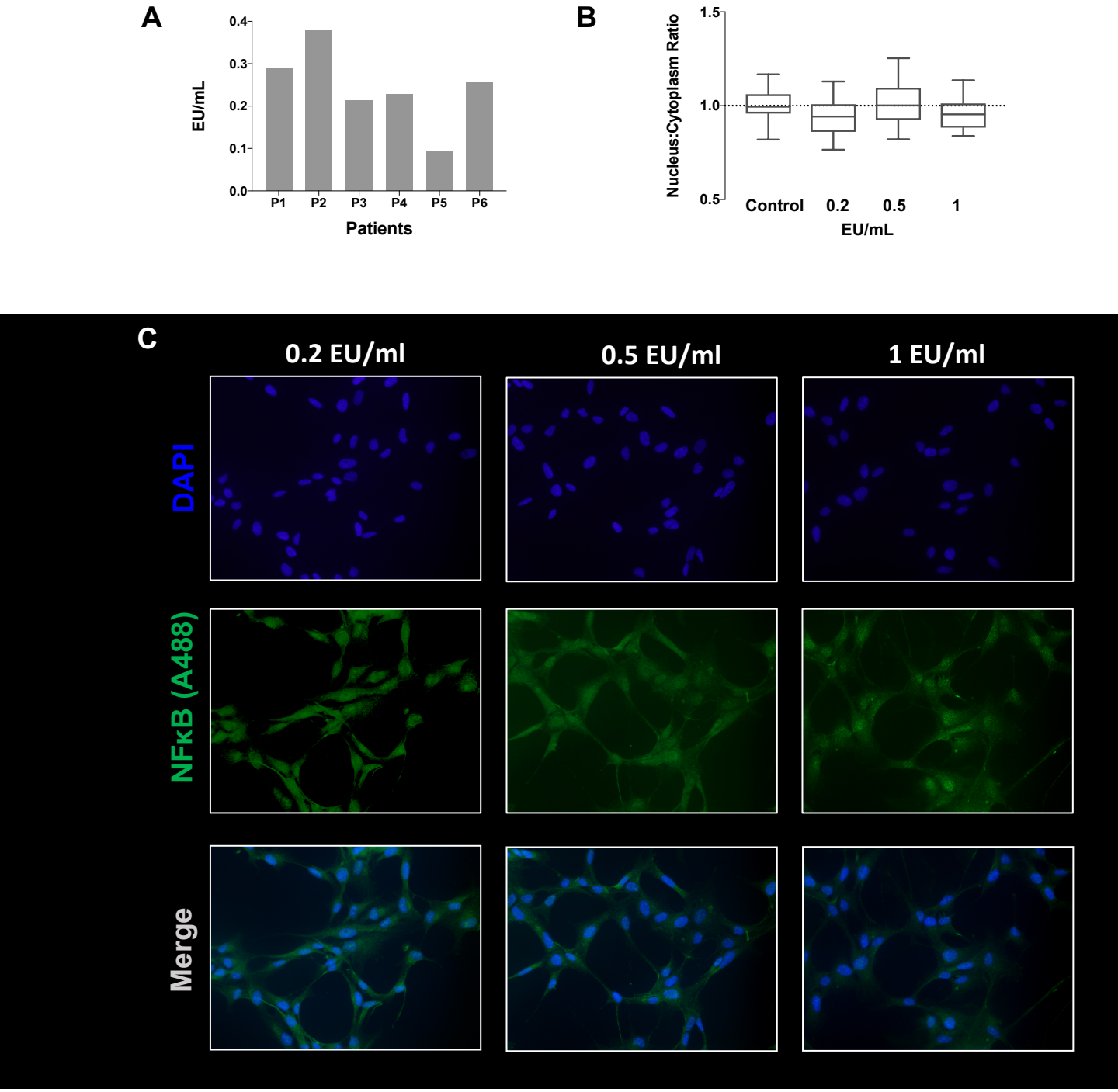


Figure 5.4: Quantification of NF-kB translocation and immunofluorescence of RPE-1 cells after stimulation with LPS in serial dilutions

5.4.4 Heat treatment of ILT supernatants removes cytotoxicity and biological activity

ILT secretome supernatants were collected intraoperatively from three study subjects, heat inactivated at 100ºC for 10 minutes (section 2.8.5), then used to stimulate RPE-1 cells followed by immunofluorescence staining for the subunit p65 of NF-κB (section 2.10). As a control, the heat inactivated supernatants were stimulated together with their matched non-heat inactivated secretome supernatants and RPMI 1640 (Lonza) used as a negative control.

The heat inactivated ILT secretome supernatant was not cytotoxic to the RPE-1 cells. The non-heat inactivated ILT supernatant was cytotoxic to the RPE-1 cells **(Figure 5.5A)**. The three heat inactivated supernatants did not result in significant NF-κB translocation into the nucleus when compared to the control group **(Figure 5.5B)**.

Figure 5.5: Immunofluorescence of RPE-1 cells after stimulation with heat inactivated ILT secretome supernatants

ILT specimens were collected intraoperatively from three study subjects (methods chapter 2.4.2). They were incubated overnight under tissue culture conditions and their secretome supernatants collected (methods chapter 2.8). The supernatants were heat inactivated (methods chapter 2.8.5). These were then used to stimulate RPE-1 cells, followed by immunofluorescence staining for the subunit p65 of NF-κB (methods chapter 2.10). Images were captured using the Alexa488 (green) and DAPI (blue) channels and merged using ImageJ software. Their NF-κB translocation into the nucleus was also quantified using proprietary software.

(A) In comparison to the negative control, the supernatant causes cytotoxicity of RPE-1 cells, and the cells appear sparse and smaller with ill-defined nuclei and cell outlines. In the heat inactivated sample there is no cytotoxicity, the cells are well formed and abundant and this appears very similar to the negative control. In addition, the heat inactivated cells do not translocate NF-κB, as the nuclei and cytoplasm are homogenous.

(B) Quantification of the NF-κB nuclear:cytoplasm ratios are presented in dot plots. The three heat inactivated supernatants were similar to the negative control and did not cause significant NF-κB translocation into the nucleus.

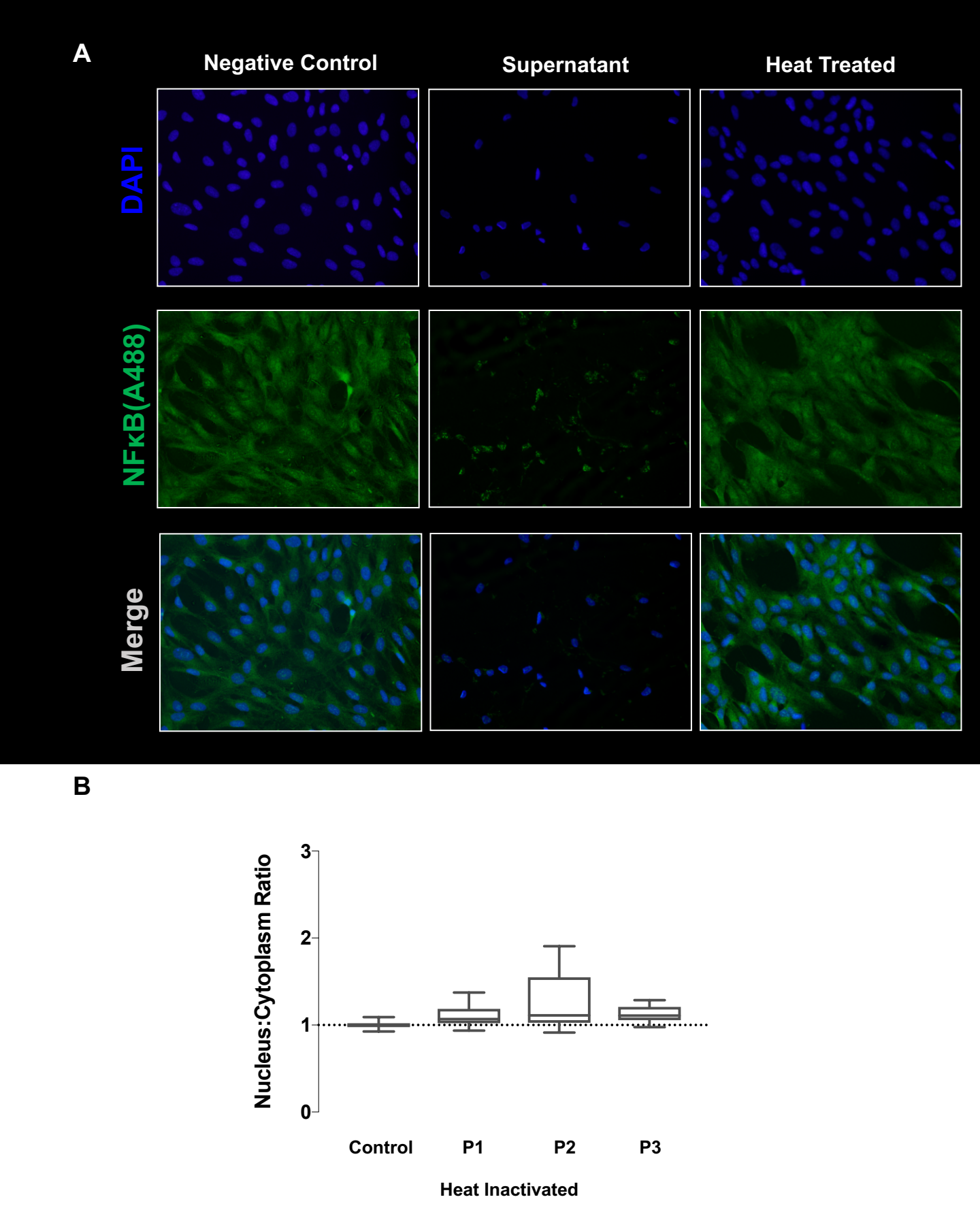


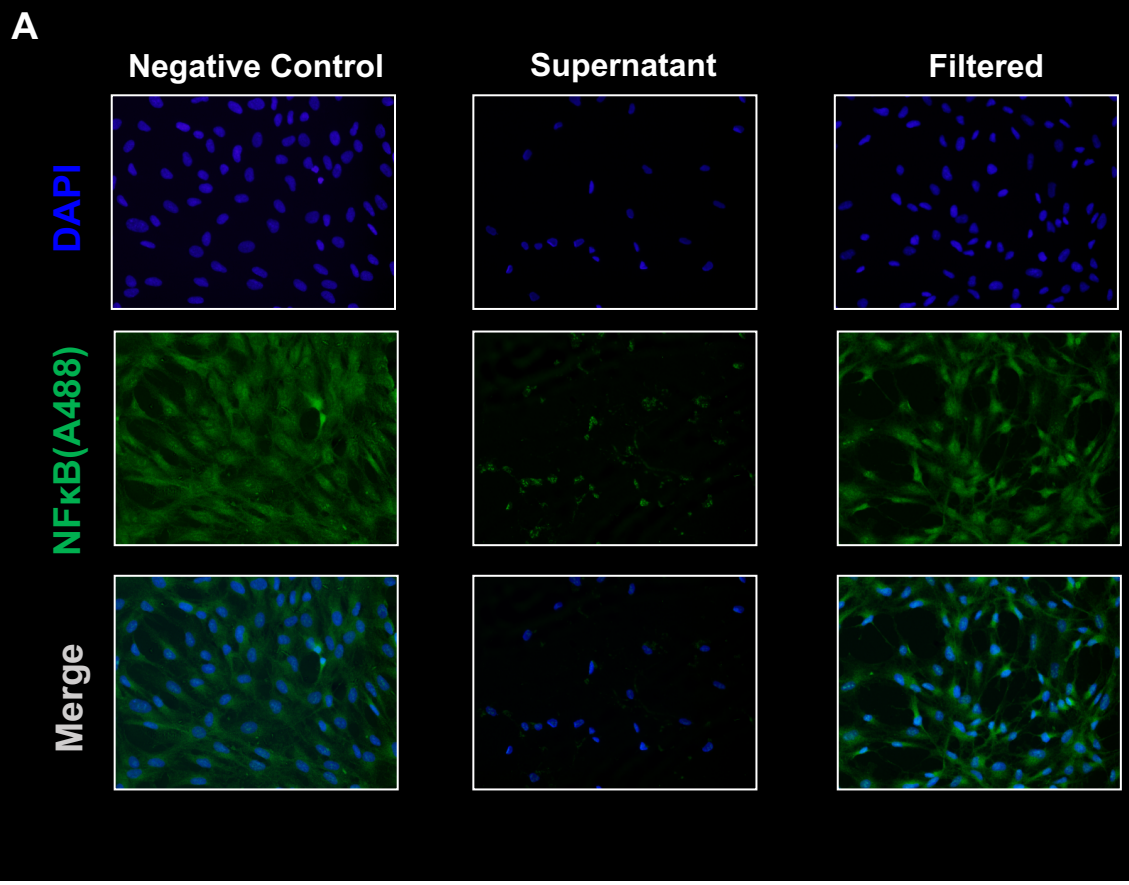
Figure 5.5: Immunofluorescence of RPE-1 cells after stimulation with heat inactivated ILT secretome supernatants

Figure 5.6: Immunofluorescence of RPE-1 cells after stimulation with filtered (5kDa) ILT secretome supernatants

ILT specimens were collected intraoperatively from three study subjects (methods chapter 2.4.2). They were incubated overnight under tissue culture conditions and their secretome supernatants collected (methods chapter 2.8). The supernatants were filtered through a 5kDa filter and the filtrates collected (methods chapter 2.8.6). These were then used to stimulate RPE-1 cells followed by immunofluorescence staining for the subunit p65 of NF-κB (methods chapter 2.10). Images were captured using the Alexa488 (green) and DAPI (blue) channels and merged using ImageJ software. Their NF-κB translocation into the nucleus was also quantified using proprietary software.

(A) In comparison to the negative control, the unfiltered supernatant causes cytotoxicity of the RPE-1 cells, and the cells appear sparse and smaller with ill-defined nuclei and cell outlines. In the filtered sample there is no cytotoxicity, the cells are well formed and abundant. In addition, the filtered cells demonstrate translocation of NF-κB, as seen by the nuclei that fluoresce when compared to cytoplasm.

(B) Quantification of the NF-κB nuclear:cytoplasm ratios are presented in dot plots. The three filtered supernatants resulted in NF-κB translocation into the nucleus when compared to the negative control.



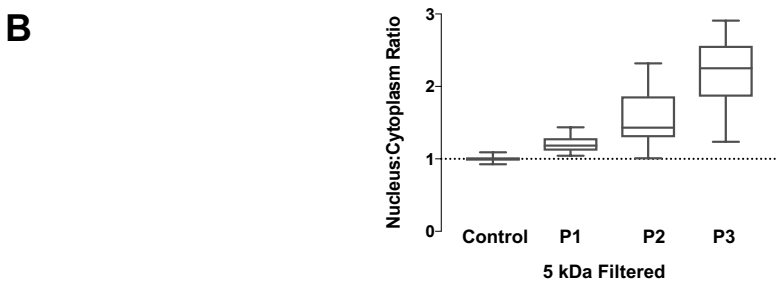


Figure 5.6: Immunofluorescence of RPE-1 cells after stimulation with filtered (5kDa) ILT secretome supernatants

5.4.5 Filtering the ILT supernatants

Having established that heat inactivates the biological activity of the supernatants, we set out to narrow the size range of the active proteins (section 2.8.6).

The 5kDa filtered supernatants were used to stimulate RPE-1 cells together with their matched non-filtered supernatants and RPMI 1640 which was used as a negative control. The 5kDa filtered supernatants resulted in in varying degrees of NF-κB translocation to the nucleus in RPE-1 cells **(Figure 5.6).**

Table 5.1: Cytokine profile of ILT and Aortic wall supernatants

Angiogenin	GDF-15	IL-1ra	Myeloperoxidase
Angiopoietin-2	GM-CSF	IL-22	Osteopontin
C-Reactive Protein	GRO-alpha	IL-23	PDGF-AA
CD14	HGF	IL-24	PDGF-AB/BB
CD31	IFN-gamma	IL-27	Pentraxin-3
CD40 ligand	IGFBP-2	IL-31	Resistin
Chitinase 3-like 1	IL-3	IL-32	SDF-1alpha
Complement C5/C5a	IL-4	IL-34	Serpin E1
Complement Factor D	IL-5	IP-10	SHBG
Cystatin C	IL-6	Leptin	TFF3
DPPIV	IL-8	LIF	TfR
EMMPRIN	IL-10	Lipocalin-2	Thrombospondin-1
ENA-78	IL-11	M-CSF	TIM-3
Endoglin	IL-15	MCP-1	TNF-alpha
Fas Ligand	IL-16	MIG	uPAR
FGF basic	IL-17A	MIP-3alpha	VCAM-1
FGF-7	IL-19	MMP-9	VEGF

Aortic and ILT supernatants were added to the cytokine detection kit and compared to 'control' transplant aortas. The relative expression of these 66 cytokines were upregulated in the *Human Cytokine array kit XL* (R&D biosystems)

5.4.6 Cytokine and proteomic profile of the tissue secretome

The ILT and aortic wall were abundant with pro and anti-inflammatory cytokines. Sixty-six cytokines were increased in the ILT and aortic wall out of a total of a hundred and five in the *R&D Human Cytokine array kit XL*. **Table 5.1** lists the cytokines that were upregulated in the and ILT supernatants when compared to the control aortic transplant tissue.

5.4.7 Identifying the 'physiological' concentration of ILT secretome supernatant

Having identified that ILT secretome supernatants are biologically active and, in particular, were cytotoxic to RPE-1 cells, I sought out to identify a 'physiological' concentration, at which toxicity is minimised. This is to determine the concentration to be used for subsequent cell culture experiments. To determine this, a kinetic cytotoxicity assay was used (section 2.8.3). The secretome supernatants were pooled in to three clinically relevant groups (n=3) with equal protein concentrations per sample. As cytotoxicity was widespread even at a normalised concentration of 1 mg/ml, the starting protein concentration for the dilutions in this experiment were 0.5 mg/ml.

There was a concentration dependent cytotoxicity on HUVECs. A fluorescence intensity of +- 10000 was chosen for the downstream experiments. At this level, when a seeded well of HUVECs was examined by microscopy, there was no cytotoxicity and thus deemed to be a 'physiological' concentration **(Figure 5.7)**.

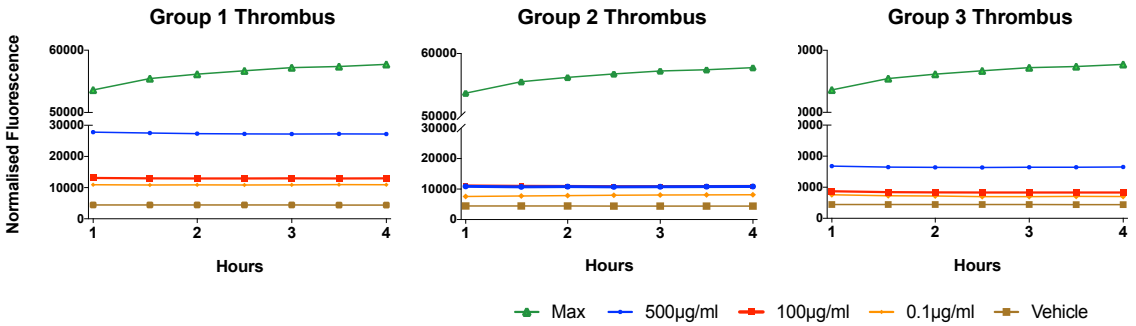


Figure 5.7: Cytotoxicity assay of ILT supernatants using HUVECs

ILT specimens were collected intraoperatively from nine study subjects (methods chapter 2.4.2). They were incubated overnight under tissue culture conditions and their secretome supernatants collected (methods chapter 2.8). The supernatants were then pooled in to three clinically matched groups. A CellTox^{TM} green cytotoxicity assay was performed using HUVEC cells, which were seeded on to a 96 well plate (methods chapter 2.9.1) and stimulated with the ILT supernatants in different concentrations followed by the addition of the green amine dye (methods chapter 2.8.3). These were read on a FLUOstar Omega plate reader (485-500 nm).

The three graphs display the fluorescence emitted over 4 hours by the different concentrations of the ILT supernatants (500, 100 and 0.1 µg/ml) compared with a positive control (Max) and a negative control (vehicle). The ILT supernatants demonstrate a concentration dependent cytotoxicity. An intermediate concentration of ILT supernatant resulting in cytotoxicity was chosen for the downstream experiments at a normalised fluorescence of approximately 10000.

5.4.8 Assessing gene changes of endothelial cell dysfunction

In this experiment, the secretome supernatants from the nine patients were pooled in to the three groups used to determine the 'physiological' concentration, prior to stimulating AOECs. Their changes in gene expression of endothelial related genes were measured and analysed by qPCR (methods 2.11). The experiment was also repeated with a different batch of AOECs.

Table 5.2: Quality control assessment of cDNA/RNA from AOECs stimulated with ILT supernatants

	Sample Name	Thrombus Group 1	Thrombus Group 2	Thrombus Group 3	Control
Row	Control Name	Ave Ct			
A	ACTB	24.22	26.01	28.31	23.83
B	HPRT1	30.91	31.72	33.81	32.09
C	RTC	23.99	23.38	24.12	24.17
D	PPC	20.65	20.63	20.48	20.66
E	GDC	35.00	35.00	35.00	35.00
F	NRT	35.00	35.00	35.00	35.00
G	PPC - H_2O	20.58	20.57	20.54	20.48
H	NTC	35.00	35.00	35.00	35.00

ACTB and **HPRT1** – Housekeeping genes, **RTC** – Reverse transcription control, **PPC** – Positive PCR control, **GDC** – Genomic DNA control, **NRT** – No reverse transcription, **NTC** – no template control

ILT specimens were collected intraoperatively from nine study subjects (methods chapter 2.4.2). They were incubated overnight under tissue culture conditions and their secretome supernatants collected (methods chapter 2.8). The supernatants were then pooled in to three clinically relevant groups. Aortic endothelial cells (AOECs) were cultured, passaged and seeded onto a 96 well plate (chapter 2.9.1), before stimulation with the ILT secretome supernatants. Following cell stimulation, RNA was isolated (chapter 2.11.1) and cDNA synthesised (chapter 2.11.2). The quality of the cDNA was assessed using a RT qPCR QC plate from *Qiagen* (chapter 2.11.3).

In this table, Row A and B are the cycle thresholds of two common housekeeping genes, expressed at different levels relative to one another. They provide information on the integrity of the RNA in the samples. They are expressed at Ct values within the accepted range and below the maximum cycle threshold of 35. They also give an indication of the expected Ct range in the subsequent qPCR experiments. Row C is a reverse transcription control providing information on the synthesis using the *First Strand Kit* and excluding the presence of reverse transcriptase inhibitors. All values are within the expected range. The PPC (Positive PCR control) tests for PCR inhibitors in the RNA samples (Row D and G), of which none are detected in the samples. Rows E and F test for DNA contamination of which there is none. The last row, No template control (NTC), tests for contamination by DNA introduced during experimental setup, of which there is no contamination.

5.4.8.1 Quality control assessment of the RT qPCR

The quality of the cDNA was assessed using a RT qPCR QC plate from *Qiagen* (section 2.11.3). All values were within the expected range. **(Table 5.2)** Row A and B are the cycle thresholds of two common housekeeping genes, expressed at different levels relative to one another. ACTB and HPRT1 were used in the QC plate **(Figure 5.8).** They provide information on the integrity and presence of RNA in the samples. They are expressed at Ct values within the accepted range and below the maximum cycle threshold of 35. They also give an indication of the expected Ct range in the subsequent qPCR experiments. Row C is a reverse transcription control providing information on the synthesis using the *First Strand Kit* and excluding the presence of reverse transcriptase inhibitors. The PPC (Positive PCR control) tests for PCR inhibitors in the RNA samples (Row D and G), of which none are detected in the samples. Rows E and F test for DNA contamination of which there is none. The last row, no template control (NTC), tests for contamination by DNA introduced during experimental setup, of which there is no contamination.

The negative controls from the two experiments (RPMI 1640 stimulation) were compared with each other on the *Qiagen* online analysis software. In **Figure 5.8B** only 8 of the 84 genes fall out of the fold change cut-off (1.35). The parallel lines represent the fold change cut-off of 1.35, alongside the central correlation line. In summary, the samples passed the quality control plate.

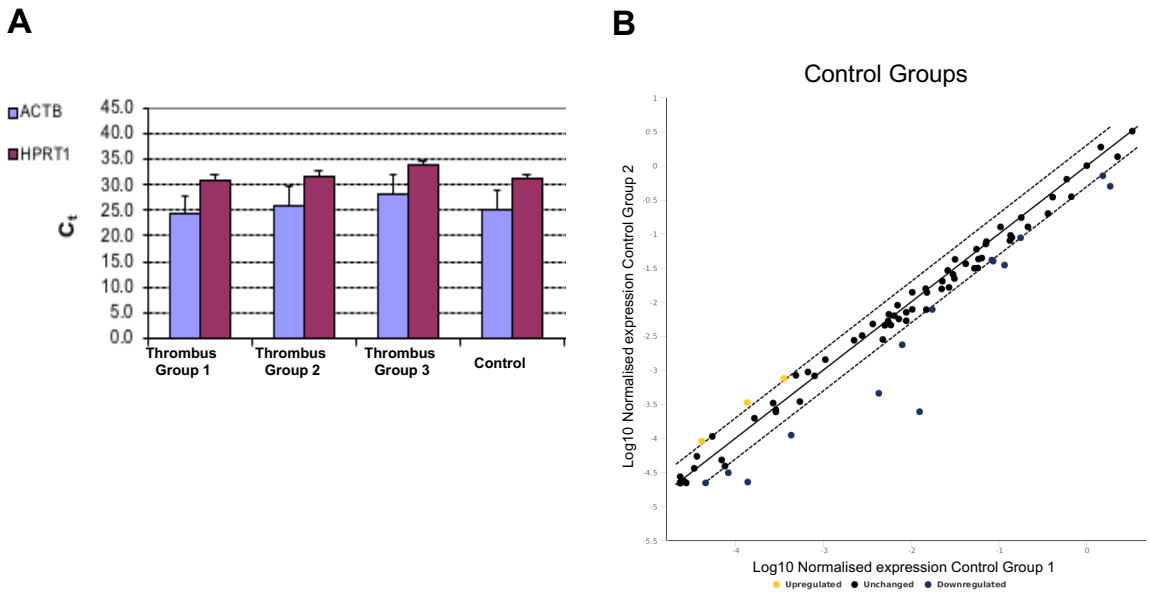


Figure 5.8: A comparison of changes in gene expression by negative controls

ILT specimens were collected intraoperatively from nine study subjects (methods chapter 2.4.2). They were incubated overnight under tissue culture conditions and their secretome supernatants collected (methods chapter 2.8). The supernatants were then pooled in to three groups. Aortic endothelial cells (AOECs) were cultured, passaged and seeded onto a 96 well plate, then stimulated with the ILT secretome supernatants. RPMI was used as a negative control. Following cell stimulation, RNA was isolated (chapter 2.11.1) and cDNA synthesised (chapter 2.11.2). The stimulation of the AOECs was repeated with a different batch of AOECs, and RNA isolatedand cDNA synthesise.

(A) The quality of the cDNA was assessed using a RT qPCR QC plate from *Qiagen* (chapter 2.13.1). The bar plots of ACTB and HPRT1 in each of the ILT stimulated AOECS demonstrate consistency of expression.

(B) The controls in the two experiments were compared to each other, in order to examine the gene changes in response to stimulation by the controls in the different batches of AOECs. The scatter plot compares the normalised expression of the 84 genes in the *Qiagen* endothelial cell array (chapter 2.13.1) in response to the RPMI stimulation. The parallel lines on either side of the correlation line represent a 1.35 fold regulation, which was the cut-off for a significant change in expression. All but 8 of the genes fall outside of this cut-off. (Bio-Rad CFX96 PCR analyser, *Qiagen* analysis software)

5.4.8.2 Changes in gene expression of endothelial cell related genes

Fourteen genes had gene expression changes associated with endothelial dysfunction **(Figure 5.9A).** Ten of these genes were upregulated and four were down regulated. The 14 genes of interest were uploaded to STRING – a protein to protein interaction algorithm (*www.string-db.org*). The diagram displays their potential interactions, with SERPINE1, TGFB1, ITGA5, ITGAW and THBS1 having multiple interactions with each other. **(Figure 5.9B)**

This provides insights to the hypothesis of ILT adding to systemic endothelial dysfunction as evidenced by a derangement in FMD.

Figure 5.9: Changes in gene expression of endothelial related genes (in AOECs when stimulated by ILT supernatants)

ILT specimens were collected intraoperatively from nine study subjects (methods chapter 2.4.2). They were incubated overnight under tissue culture conditions and their secretome supernatants collected (methods chapter 2.8). The supernatants were then pooled in to three groups. Aortic endothelial cells (AOECs) were cultured, passaged and seeded onto a 96 well plate, before stimulation with the ILT secretome supernatants. Following cell stimulation, RNA was isolated (chapter 2.11.1) and cDNA synthesised (chapter 2.11.2). The stimulation of the AOECs was also repeated with another batch of AOECs, and RNA isolated) followed by cDNA synthesis. The quality of the cDNA was assessed using a RT qPCR QC plate from *Qiagen* (chapter 2.11.3). The cDNA was analysed with an RT qPCR endothelial cell array (Qiagen*)* for changes in gene expression. The experiment was repeated and both experiments were analysed on the Qiagen qPCR platform, using $2^{-\Delta\Delta Ct}$ to calculate fold change. Only genes that had a fold change > 1.35 were regarded as positive.

In figure **(A)**14 genes had gene expression changes associated with endothelial dysfunction. Ten of these genes were upregulated and four were down regulated.

In figure **(B)** the 14 genes of interest were input in STRING – a protein to protein interaction algorithm (*www.string-db.org)*. The diagram displays their potential interactions, with SERPINE1, TGFB1, ITGA5, ITGAW and THBS1 having multiple interactions with each other.

ADAM17- a disintegrin and metalloprotease 17, ITGAV5 - Integrin alpha-V, SPHK1 - Sphingosine kinase 1, EDN1 – Endothelin 1, HIF1A - Hypoxia-inducible factor 1-alpha, FGF1 – Fibroblast growth factor 1, THBS1 – Thrombospondin 1, TGFB1 - Transforming growth factor beta 1, NPR1 - Natriuretic peptide receptor, OCLN – Occludin, EDNRA - Endothelin receptor type A, IL3 – Interleukin 3

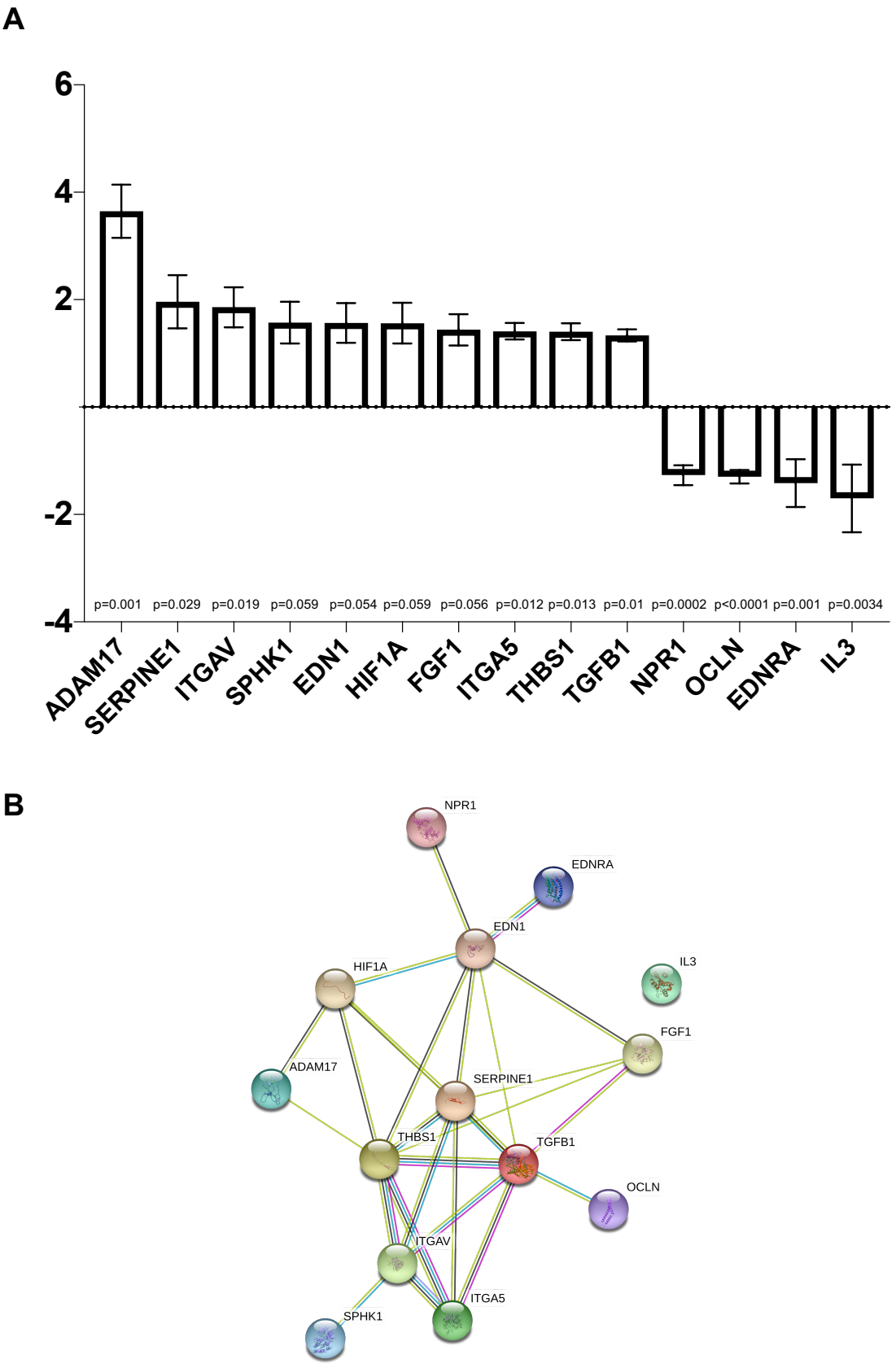


Figure 5.9: Changes in gene expression of endothelial related genes (in AOECs when stimulated by ILT supernatants)

5.4 Discussion

In this chapter, I explored the novel hypothesis that ILT contributes to the systemic endothelial dysfunction in patients with AAA. The hypothesised mechanism of action is through endocrine and/or paracrine means and as this hypothesis was discovery in nature, the aims of this chapter were broad. They were to culture the secretome, assess for biological activity and if found, further assess if this biological activity resulted in endothelial dysfunction.

FMD improves after aneurysm surgery(16) and although our patient cohort was small, this observation persisted in 6 of our 7 study subjects. FMD is a surrogate marker of endothelial dysfunction and is measured non-invasively. In assessing the FMD of patients in this study, care was taken to avoid common stimulants which may impact on the FMD e.g. smoking and caffeine.

The method of conditioning the tissue secretome was carefully considered, specifically the inclusion of appropriate controls and the use of serum (FCS). FCS contaminates supernatants with small proteins and makes it challenging for use with proteomics techniques. However, FCS is required to nourish cells and provide an environment that is conducive to growth. To ameliorate this, the supernatants were first equilibrated in warmed RPMI media supplemented with 5% FCS for an hour in the incubator, followed by 24 hours with serum free RPMI. To be able to compare the specimens with each other, the total protein content was measured in the secretome supernatants and the ILT supernatants consistently had a higher protein content than the aorta or omentum.

NF-kB is an important transcription factor found in all mammalian cells and is a key regulator of inflammation and oxidative stress. It is triggered by a variety of stimuli, including inflammatory, mechanical and lipid mediators, and has an important role to play in the regulation of endothelial dysfunction through the induction of gene expression(201-204). Endothelial dependent vasodilatation has also been found to be associated with increased nuclear translocation of NF-kB in vascular endothelial cells of older adults(203).

This provided a potential mechanism for the observed changes in FMD of patients with AAA. Indeed, linking NF-kB translocation into the nucleus and abdominal aortic aneurysms in humans was a novel idea. The expertise in the immunofluorescence of NF-kB existed in our lab and it was a natural progression to investigate its role with respect to the ILT supernatants and thus broadly demonstrate biological activity. The initial experiment did indeed demonstrate translocation of NF-kB into the nucleus of RPE-1 cells. When the experiment was repeated in a more selective manner, normalising and diluting the protein content of the four ILT supernatants to 1 mg/ml, the supernatants were cytotoxic and resulted in death of the RPE-1 cells. This was an unexpected finding, and before continuing with further experiments, I investigated the supernatants for LPS contamination. LPS, derived from gram negative bacteria, is a potent inflammatory mediator and stimulator of NF-kB, in addition to its cytotoxicity of cells(205, 206). The sensitive assay did detect very low levels of endotoxin contamination, however at these levels, neither cytotoxicity nor NF-kB translocation was found in RPE-1cells.

Having excluded LPS contamination as a source of the biological activity, I next sought to attenuate this effect by heat inactivating the ILT supernatants. Heat inactivation would theoretically denature proteins within the ILT supernatants thus rendering them ineffective. Indeed, when compared to the non-heat treated supernatants, there was a decrease in cytotoxicity, and when compared to the control there was no increase in NF-kB translocation in to the nucleus. Alongside this process, I screened the ILT and aortic secretome supernatants with a cytokine array, comparing them to 'healthy' aortic tissue from transplant donors. The aortic and ILT supernatants were rich in cytokine activity, and this was in keeping with the decrease in biological activity after heat inactivation. Simultaneously to this, our group performed proteomic analysis on the tissue from the aortic wall and ILT. There were approximately 2000 proteins in the ILT and 700 in the aortic wall.

With a view to narrow the range I filtered out the 5kDa fraction of the ILT supernatants and stimulated RPE-1 cells, unexpectedly I found that even the 5kDa fraction of the supernatants translocated NF-kB. With this knowledge together with the cytokine data, I reasoned that the secretome was in fact a complex milieu of pro and anti-inflammatory mediators working in concert. So, instead of narrowing a single source of biological activity, I then sought to determine if the supernatant in unison resulted in changes consistent with endothelial dysfunction.

Determining a 'physiological' concentration with which to use the ILT conditioned media was investigated. In our in-vitro experiments the ILT secretome supernatants were uniformly cytotoxic, however this was a concentrated lab conditioned sample, and was unlikely to be the scenario in the human body. To determine this 'physiological concentration' a kinetic cytotoxicity assay (CellTox^{TM} Green, Promega) was used to determine the sublethal cytotoxic concentration and this was

optimised on HUVECs. Their concentrations were normalised to total protein content which were used in dilutions for the cytotoxicity experiments. This demonstrated a concentration dependent cytotoxicity.

AOECs were then stimulated with the ILT secretome supernatants at the pre-determined sublethal 'physiological' concentration and the changes in gene expression of a focused qPCR endothelial cell biology array were measured. Fourteen genes had at least a 1.35-fold change in their gene expression. This was consistent over the three groups of supernatants ($p<=0.05$). These were ADAM17, SERPINE1, ITGAV, SPHK1, EDN1, HIF1A, FGF1, THBS1, TGFB1, NPR1, OCLN, EDNRA, ITGA5 and IL3. They broadly cluster around genes responsible for angiogenesis, vasoconstriction and vasodilatation (EDN1, EDNRA and NPR1), inflammatory responses, apoptosis (EDN1, HIF1A, OCLN, IL3, SPHK1), cell adhesion molecules (ADAM17, SERPINE1, THBS1, ITGA5, ITGAW and TGFB1), coagulation and platelet activation. **Table 5.3**

Several of the more interesting genes will be discussed below.

Table 5.3: Summary of gene changes

Name	Functional Group	Effect on Endothelial Cell
ADAM17	Cell Adhesion, Inflammatory Regulation	Cleaves cell surface proteins, induced by apoptosis(207)
SERPINE-1	Controlled degradation of thrombus, ECM degradation(208)	Apoptosis of endothelial cell pathway(209)
ITGAV	Cell surface and adhesion	Fibronectin receptor dysfunction, apoptosis(210)
SPHK1	Vasoconstriction, apoptosis	Cell growth, survival and differentiation(211)
EDN1	Vasoconstriction	Inflammatory response, platelet activation(212)
HIF-1A	Hypoxia	Angiogenic factors in endothelial cell(213)
FGF1	Cell survival, Mitogenic activity(214)	Endothelial cell sprouting(215)
THBS1	Cell to cell matrix interactions, platelet aggregation(216)	Endothelial cell apoptosis(217)
TGFB1	Vasoconstriction, angiogenesis, ECM degradation	Endothelial cell apoptosis and activation (218, 219)
NPR1	Blood pressure regulation(220)	Downregulated
OCLN	Cell adhesion	Endothelial permeability(221)
EDNRA	Blood pressure regulation(222)	Hypertension
IL3	Cell growth, differentiation	Apoptosis(223)

ILT supernatants were used to stimulate AOECs, and their changes in gene expression were measure with a qPCR endothelial cell array (Qiagen). Genes that changed expression greater than 1.35 fold are presented.

ADAM17- a disintegrin and metalloprotease 17, ITGAV5 - Integrin alpha-V, SPHK1 - Sphingosine kinase 1, EDN1 – Endothelin 1, HIF1A - Hypoxia-inducible factor 1-alpha, FGF1 – Fibroblast growth factor 1, THBS1 – Thrombospondin 1, TGFB1 - Transforming growth factor beta 1, NPR1 - Natriuretic peptide receptor, OCLN – Occludin, EDNRA - Endothelin receptor type A, IL3 – Interleukin 3

ADAM17 (A disintegrin and metalloproteinase 17), is a membrane bound enzyme that cleaves cell surface proteins such as cytokines, cytokine receptors and ligands, and commonly referred to as a sheddase and was the most upregulated gene. It is involved in the regulation of inflammatory processes, is also induced by apoptosis (207) and is closely related to TNF-α and IL-6 activity. ADAM17 knockout mice are embryologically lethal(224). Its production of soluble functional ectodomains can serve to initiate or inhibit autocrine or paracrine signalling which is in keeping with the hypothesis of ILT acting as an endocrine/paracrine structure. ADAM17 has previously been detected in the ILT of AAAs within microvesicles(90) and is purported to have effects in the arterial wall.

SERPINE1(gene for plasminogen activator inhibitor -1 (PAI-1)) is responsible for the controlled degradation of thrombus(208) and involved in the formation of endothelial microparticles(225). It has also been linked with increases in the apoptotic cell pathway of endothelial cells which is in keeping with our findings(209). In addition to its antifibrinolytic properties, it is involved in extracellular matrix remodelling by decreasing MMP activation. It is also upregulated in several fibrotic diseases such as cardiac fibrosis after myocardial infarction(226) and pulmonary fibrosis after bleomycin(227). In addition, inhibiting PAI-1 decreases the formation of murine carotid atherosclerosis(228).

EDN1 gene encodes a preproprotein (Endothelin-1) which is a potent vasoconstrictor. It is implicated in causing a variety of additional biological effects, including free radical formation, mitogenic and proliferative effects, inflammatory responses and platelet activation(212). This again is in keeping with the hypothesis of ILT resulting in a deranged FMD. Overexpression of endothelin-1 in $Apoe^{-/-}$ high fat diet (HFD) mouse models triggered the formation of AAA(229) and endothelin-1 levels have also been found to be higher in patients with AAA, and patients with large aneurysms had higher levels of endothelin-1(230). EDNRA (Endothelial receptor type A), is the gene that encodes for the receptor of Endothelin-1 and was down regulated by the ILT supernatants. Endothelin 1 binds to EDNRA to produce lasting hypertension.

HIF1-A encodes hypoxia inducible factor-1 and is a transcriptional factor regulator of the adaptive responses to hypoxia, and activates the transcription of over 40 genes(213). HIF-1 is critical for the production of angiogenic growth factors such as VEGF in endothelial cells. It also prevents aortic dilatation by the suppression of TGF-B signalling(231) and promotes atherosclerosis formation by upregulating microRNA-19-a(232). Expression of HIF1-A is upregulated in AAA tissue(233), is pivotal in the development of AAAs probably through the upregulation of MMP-2 and MMMP-9(234). It is also increased at the ruptured edge of an AAA(234).

THBS1 (Thrombospondin 1) is a protein encoding gene involved in cell to cell matrix interactions, platelet aggregation, angiogenesis promoter and inhibitor, and tumorigenesis(216). It also induces endothelial cell apoptosis(217). Thrombin

induces the expression of THBS1 in endothelial cells as well as increasing THBS1 protein concentration in the extracellular matrix(235). Thrombin is increased in the ILT of AAA and THBS1 is in ILT (103), as well being a contributor to the development of AAA in mouse models(236).

5.5 Conclusion

In the preceding chapters, the immune cell landscape of the aortic aneurysm tissues was defined, and initially the relationship of FMD to AAAs was highlighted. The ILT was suspected to be contribute to this as FMD improved after surgery, and the ILT also contained multiple inflammatory mediators within it. Recognising this, this chapter provides a mechanistic link for the ILT resulting in endothelial dysfunction and thus the observed changes in FMD.

The changes in gene expression are consistent with the hypothesis and results from the preliminary experiments of this study. ADAM17 and SERPINE1 regulate activity through paracrine/endocrine signalling, and together with ITGA5, THBS1, TGF-ß1 and IL3 are involved in apoptotic cell pathways, which are consistent with the findings of cytotoxicity caused by the supernatants. SPHK1, END1, FGF, TGF-ß1, NPR1 and ENDRA are regulators of vasomotor tone which are consistent with the findings of a deranged FMD in patients with AAA. SERPINE1, ITGA5, THBS1, THGFB and OCLN are regulators of matrix remodelling which is a hallmark of aneurysmal disease.

Chapter 6

FINAL DISCUSSION

The key structural findings of abdominal aortic aneurysms are elastolysis and destruction of the extracellular matrix, together with apoptotic loss of the medial aortic smooth muscle cell components(17, 18). Typically, this presents as a focal infra-renal aortic dilation which grows insidiously (2mm/yr)(15, 16) and can lead to a catastrophic rupture if left untreated. The wall degradation is accompanied by a characteristic chronic inflammatory cell infiltrate which is presumably the source of the mediators resulting in the destruction of the aortic wall components with time. Elegant basic science models have delineated the mechanisms around the initial formation of AAAs and have highlighted the importance of macrophages and T cells in the initiation phase. MMPs are the most commonly ascribed mediators of elastolysis and smooth muscle cells apoptosis. Surgery is an effective treatment modality but has an associated mortality than needs to be weighed up against rupture risk. Pharmacological treatment to slow or halt the disease would be ideal, but this is still elusive.

It has been more than 25 years since the recognition of AAAs as a divergent pathophysiological process from atherosclerosis, even though they share many common risk factors. The immune basis for AAAs hypothesises that an antigen-initiated event leads to disordered immunoregulatory mechanisms, sharing several features with autoimmune diseases such as site specificity, inciting agents, sex predilection and chronic inflammation(56). Furthermore, ILT develops in the majority of AAAs through the progression phase of AAAs, and the ILT has an inflammatory component of its own that may further exacerbate the degradation of the wall. Basic science models have thus far not been able to study the influence of the ILT on the developing AAA. Additionally, patients with AAAs have systemic manifestations of their disease, with an increased cardiovascular mortality together

with an improvement of FMD after surgery(16). The mechanism underlying the decreased mortality is unknown. The ILT is in direct continuous contact with flowing blood, and these systemic manifestations may be as a result of the aneurysm itself.

A deeper understanding of the underlying immune mechanisms of the aneurysm wall and ILT would potentially unlock further avenues of exploration and ultimately result in new therapeutic targets.

6.1 Original hypothesis

The central hypotheses of this thesis were that AAAs have an inflammatory cell infiltrate which contributes to the destruction of the aortic wall, and that the ILT adds independently to this. The AAA wall and ILT work in unison as a composite site of immune activation. To achieve this, I performed deep immunophenotyping of these tissues. I further hypothesised that the ILT adds to the deterioration of systemic endothelial dysfunction seen in patients with AAA by acting in an endocrine/paracrine manner. To achieve this, I examined the effect of the ILT secretome on endothelial cells.

6.2 Principal findings of this research

This thesis provides compelling new evidence implicating cytotoxic granzyme B (GZB) containing lymphoid cells within the chronic cellular infiltrate of the aortic wall and ILT in patients with AAA (chapter 4.4.8, Figure 4.18). This is an alternative mechanism to the traditionally held view implicating secretion of MMPs by macrophages and T cells, leading to aortic wall degeneration. Furthermore, the GZB containing cells were also found in the peripheral blood of patients with AAA (Figure

4.15: CD8 subsets in the aortic aneurysm complex), possibly as a result of seeding from the ILT which is in continuous direct contact with flowing aortic blood. Additionally, the ILT induced gene changes in endothelial cells consistent with endothelial dysfunction. This supports the hypothesis of the ILT adding to the deterioration of systemic endothelial dysfunction found in these patients (chapter 5.4.8.2).

The chronic inflammatory cell infiltrate was a consistent finding in all the study subjects (Figure 4.6). Our findings, as well as other human AAA studies, demonstrate that AAAs are primarily a T/B cell disease, which is in contrast to the basic science animal model literature which demonstrates a clear role for macrophages and monocytes in the pathophysiology(141). This would suggest that there is an initiation phase (innate immunity) followed by an insidious progression phase that is characterised by the cells of the adaptive immune system. Interestingly, the macrophages in murine studies are thought to produce MMPs which are central to the pathogenesis of early aneurysm formation.

Other key findings are summarised below:

1. The aortic wall contains class-switched memory B cells, and the finding of Tfh in the aortic wall suggests that this is occurring in tertiary lymphoid organs within the aortic wall, which is a relatively unique finding. This may have therapeutic implications(Figure 4.10).
2. The T cells display phenotypic diversity and the cell surface marker expression of the T effector cells was heterogenous. CCR5 however featured prominently and was found in both the aortic wall and ILT (chapter 4.4.4, Figure 4.17).

3. T regulatory cells were not quantitively reduced in the AAA tissues. Tregs in the peripheral blood of patients with AAA been previously reported as being decreased (chapter 4.4.9, Figure 4.16).
4. One of the most significant methodological breakthroughs of this research was the isolation of a high quality CD45 positive single cell suspension. This was achieved for the first time in the AAA wall and ILT using FACS. This has broader applicability as the cell suspension can also be utilised with other single cell technologies such as RNAseq and proteomics (chapter 2.6.2).

6.3 Future work

The finding of GZB in the aortic wall, ILT as well as the peripheral blood, suggests a role for GZB as potential biomarker of AAAs. This could be in the form of a diagnostic biomarker, but more likely to be a marker of growth, rupture or increased endothelial dysfunction. Certainly, one of the criticisms of this work is the lack of comparison of the peripheral blood to an age and risk factor matched healthy volunteer group. This would be required to ascertain its relevance as a diagnostic biomarker.

This work has the potential for several translational strategies. Thus far pharmacological agents have primarily attempted to target a single pathway, but our findings demonstrate the complexity of the cellular infiltrate with multiple potential avenues for tissue damage. Memory B cells form a large component of the inflammatory cell infiltrate and have a potential to produce autoimmune antibodies. Thus far, there has not been an attempt at utilising a monoclonal antibody that would target an entire lineage such as B cells (e.g. CD20- rituximab), with a view to disrupt

target an entire lineage such as B cells (e.g. CD20- rituximab), with a view to disrupt the cellular infiltrate and induce quiescence. With modern drug delivery techniques, this could be directed locally at the aortic wall.

Another potential strategy could be the targeting of the T-B cross talk through influencing Tfh cells, either directly or through its CD8 regulatory cells(172), and this mechanism has been successfully studied in a mouse model of atherosclerosis. Furthermore, the inhibition of IL1-ß through Canakinumab has been shown to decrease major adverse cardiovascular events in patients with an increased CRP and risk factors for IHD(237, 238) and the concept of targeting inflammation could be adapted to the inflammatory mediators of AAA. IL1-ß has been demonstrated to decrease aortic aneurysm formation in murine models(239). The receptor with the most potential however is CCR5. CCR5 was prominent in the T cell subsets, and CCR5 blockade as used in the HIV antiretroviral therapy (Maraviroc) has the potential to be adapted.

The finding of changes in gene expression of endothelial cells by the ILT secretome supernatants is alluring. Some of the associated genes were clustered around vasoconstriction (EDN1, EDNRA, NPR1) which is in keeping with the concept of FMD, with disordered vasodilation in response to forearm ischaemia. Proteinase inhibitor 9 (PI-9) is a human intracellular serpin found in cytotoxic lymphocytes and endothelial cells. It is an inhibitor of Granzyme B and protects against apoptosis by endogenous or released Granzyme B. PI-9 expression may be reduced in the presence of elevated oxidative stress as occurs in atherosclerosis and transplantation(240) and this may be a plausible explanation for the increased cytotoxicity and requires further exploration. If indeed, the ILT results in increased

systemic endothelial dysfunction, this may have implications with indications for operative repair beyond rupture prevention.

6.4 Conclusion

The aortic wall is replete with a complex heterogenous chronic inflammatory cell infiltrate. The ILT is not a bystander in the disease process and also contains activated immune cells. Furthermore, the ILT resulted in gene changes consistent with systemic endothelial dysfunction in an in-vitro model using aortic endothelial cells. These findings persuade us to take a step back and re-examine AAAs as more than a localised pathology, but as a systemic one.

Chapter 7

APPENDICES

7.1 Supplementary Methods

7.1.1 List of Antibodies

Table 7.1: List of Flow Cytometry Antibodies

Antibody	Fluorophore	Clone	Vendor
CD14	BV605	M5E2	Biolegend
CD15	APC	SSEA-1	Biolegend
CD16	FITC	3G8	Biolegend
CD16	BV421	3G8	Biolegend
CD163	BV421	RM3/1	Biolegend
CD20	PercyPCY5.5	2H7	Biolegend
CD20	BV711	2H7	Biolegend
CD235a	PercyPCY5.5	HIR2	BD Biosciences
CD3	APC	UCHT1	BD Biosciences
CD33	PECY7	WM53	Biolegend
CD4	PercyPCY5.5	SK3	Biolegend
CD41	PercyPCY5.5	HIP8	BD Biosciences
CD45	AF700	HI-30	Biolegend
CD45	FITC	HI-30	Biolegend
CD45	BV605	F-10-894	Biolegend
CD66b	PE	G10F5	BD Biosciences
CD8	APC	SK1	Biolegend
HLA-DR	Pacific Blue	L243	Biolegend
Live/Dead	Amcyan	Aqua	ThermoFisher
Live/Dead	Near Red	Aqua	ThermoFisher

Table 7.2: List of CyTOF Antibodies

Antibody	Metal Conjugate	Clone	Vendor
CCR4(CD194)	Sm149	L291H4	Fluidigm
CCR5	Gd156	NP-6G4	Fluidigm
CCR6	Pr141	11A9	Fluidigm
CCR7	Er167	G043H&	Fluidigm
CD115	Dy162	9-4D2-1E4	In-house
CD11b	Bi209	ICRF44	Fluidigm
CD11c	Tb159	Bu15	Fluidigm
CD123	Eu151	6H6	Fluidigm
CD127	Nd143	A019D5	Fluidigm
CD13	Sm147	WM-15	Fluidigm
CD14	Gd160	RMO52	Fluidigm
CD141/BDCA3	Yb173	1A4	Fluidigm
CD15	Er170	W6D3	In-house
CD16	Nd148	3G8	Fluidigm
CD161	Dy164	HP-3G10	Fluidigm
CD163	Ho165	S15046E	In-house
CD169(Siglec-1)	Dy163	7-239	In-house
CD172a	Lu175	SE585	Fluidigm
CD19	Nd142	HB19	Fluidigm
CD1D	Dy162	51.1	Fluidigm
CD20	Dy161	2H7	In-house
CD203c	Gd156	NP4D6	In-house
CD206	Er168	15-.2	Fluidigm
CD209b(DC-Sign)	Nd143	9E9A8	In-house
CD21	Sm152	BL13	Fluidigm
CD24	Er166	ML5	Fluidigm
CD25	Tm169	2A3	Fluidigm
CD27	Gd155	L128	Fluidigm
CD3	Sm154	UCHT1	Fluidigm
CD33	Tm169	WM53	Fluidigm
CD36	Sm152	5-271	Fluidigm
CD38	Gd158	HIT-2	In-house
CD4	Nd145	RPA-T4	Fluidigm
CD40	Ho165	5C3	Fluidigm
CD43	Nd150	84-3C1	Fluidigm

List of CyTOF Antibodies (Cont)

Antibody	Metal Conjugate	Clone	Vendor
CD43	Nd150	84-3C1	Fluidigm
CD45	Y89	HI-30	Fluidigm
CD45RA	Er170	H100	Fluidigm
CD47	Bi209	CC2C6	Fluidigm
CD49d	Pr141	9F10	Fluidigm
CD56	Yb176	HCD-56	Fluidigm
CD57	Nd148	HNK-1	In-house
CD64	Nd146	10.1	Fluidigm
CD66a/c/e	Sm149	ASL-32	Fluidigm
CD68	Yb171	Y1/82A	Fluidigm
CD7	Sm147	CD7-6B7	Fluidigm
CD7	Er166	M-T701	Fluidigm
CD8a	Er168	SK1	Fluidigm
Clec9A/CD370	Dy161	8F9	Fluidigm
CX3CR1	Yb172	2A9-1	Fluidigm
CXCR3	Dy163	G025-H7	Fluidigm
CXCR5	Eu153	RF8B2	Fluidigm
DCIR	Nd145	9,00E+08	In-house
FITC	Nd144	FIIT-22	Fluidigm
FoxP3	Tb159	259D/67	Fluidigm
gdTCR	Yb173	B1	In-house
Granzyme B	Yb171	GB11	Fluidigm
HLA-A,B,C	Pr141	W632	Fluidigm
HLA-DR	Yb174	YE2/36	Fluidigm
ICOS/CD278	Eu151	C398.4	Fluidigm
IgD	Nd146	IA6-2	Fluidigm
IgM	Yb172	MHM-88	Fluidigm
IRF5	Er167	Polyclonal	In-house
MERTk	Eu153	590H11G1E3	In-house
PD-1	Lu175	EH12.2H7	Fluidigm
Siglec 8	Dy164	7C9	Fluidigm
Siglec 9	Gd155	K8	Fluidigm
TIGIT	Gd160	A15153G	In-house
TLR2	Yb176	TL2.1	Fluidigm
TLR4	Gd158	HTA-125	Fluidigm

7.2 Optimisation in preparation for Biolegend Legends Screen

The manufactures guidelines of the Biolegend screening array recommended a minimum of 3 x 10^5 cells per well (Total = 1 x 10^8). This was not achievable. Preliminary experiments sought to understand:

1. Would unsorted specimens be suitable or was cell sorting necessary?
2. Was the experiment achievable with only 3 x 10^4 cells per well?
3. Would pooling of ILT and Aorta provide meaningful results?

To address the first aim, previously isolated and cryopreserved ILT and aortic cells were resuscitated (chapter 2.5) and stained with a range of antibodies that fluoresce in the PE channel. As with earlier experiments, the aortic and ILT samples autofluoresced thus obscuring clearly identifiable cell populations. **(Figure 7.1 A,B)**.

Cell sorting with FACS was thus performed (chapter 2.6.2), and only 30 000 events per well were captured in order to simulate the potential experimental array. Additionally, pooled samples were compared to individual samples, with a view to pool samples and increase absolute cell numbers.

Briefly, cells were isolated from the aorta and ILT (chapter 2.5), stained with CD45 and Live/Dead™ and then cell sorted (chapter 2.6.2). 3 x 10^4 aortic wall and ILT cells were dispensed into 6 wells and a combined in another 3 wells, with two unstained control wells (total = 11 wells of a 96 well plate). To each of the aorta, ILT and mixed wells, either HLA-DR, CD66b and DCIR were added, incubated, washed and fixed. This was resuspended in a volume of 100µL and 10 000 events were recorded on a BD Canto flow cytometer from the 96 well plate thus simulating the array experimental conditions. Cell sorting and pooling was an effective strategy **(Figure 7.1 C, D).**

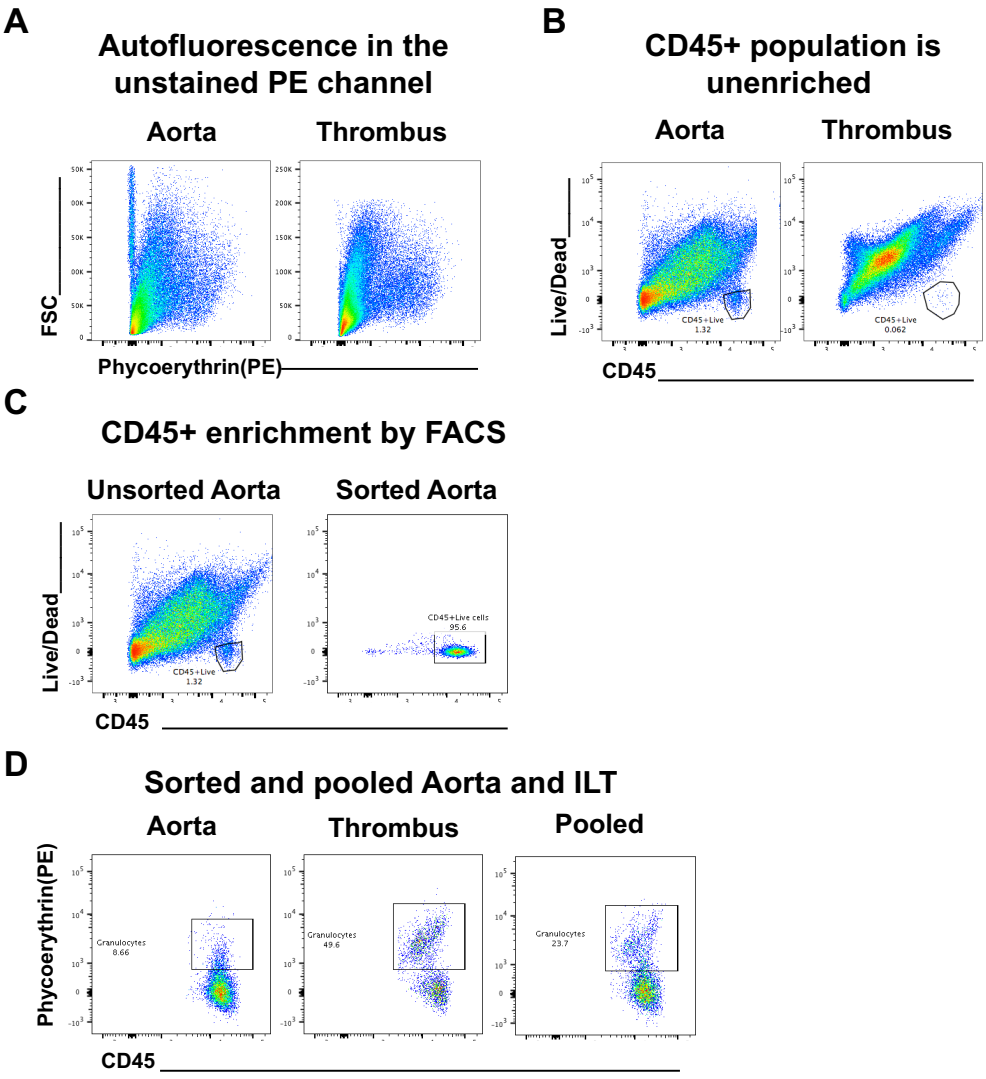


Figure 7.1: Flow cytometry analysis describing optimisation steps for the Biolegend® antibody array

In preparation for the Biolegend® antibody array, optimisation experiments were performed on aortic and ILT tissues. The Biolegend® antibody array uses 361 lyophilised antibodies conjugated to phycoerythrin (PE) to screen cells for surface marker expression in a 96-well plate configuration. Previously isolated (chapter 2.5.1) and cryopreserved cells were resuscitated and stained with CD45 (FITC) and CD66b (PE) for flow cytometry (chapter 2.6).

(A, B) Autofluorescence in the PE channel obscured visualisation of cells.
(B) In addition, the CD45 fraction was unenriched (1.32 and 0.062%). Cells were thus FACS sorted on a BD FACS ARIAII (chapter 2.6.2).
(C) FACS sorting enriched the CD45 fraction
(D) In order to maximise cell numbers prior to the array, ILT and aortic cells required pooling. This was assessed by adding 3 x10^4 FACS sorted aortic and ILT cells individually and combined and staining with PE conjugated antibodies. A comparison of individual ILT and aorta with the pooled sample and capturing only 10000 events. This demonstrated the cumulative benefit of pooling and the efficacy of only 10000 events.

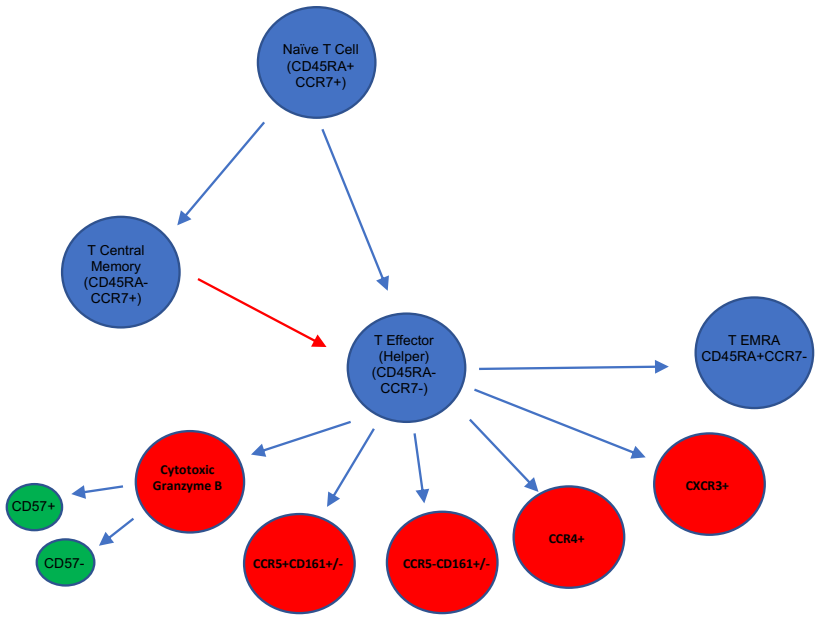
7.3 Defining T cell subsets

Single cell technologies have revealed the complex heterogeneity of the T cell compartment(151). Many phenotypic subsets are enumerated from multiple antibody combinations, and a consensus has still to be reached on some T cell subtypes. Cytokine output defines the T helper cell subtypes, and these cannot be inferred from surface marker phenotypes alone(241). For example, distinguishing effector cells from effector memory cells is not always clear without knowledge of cytokine or cytolytic outputs. In this study, subsets were clustered in an unbiased manner using software packages (Cytobank and PhenographR), and these clusters were subsequently characterised using the following commonly used T cell antibody combinations to define the major T cell subtypes(242).

- Naïve T cells: $CD45RA^{+}CCR7^{+}$
- Central memory: $CD45RA^{-}CCR7^{+}$
- Effector/Helper: $CD45RA^{-}CCR7^{-}$
- T regulatory (Treg) cells: $CD45RA^{-}CCR7^{-}FoxP3^{+}CD25^{+}CD127^{+}$
- T follicular helper (TFh) cells: $CD45RA^{-}CCR7^{-}CXCR5^{+}ICOS^{+}PD1^{+}$
- T Effector memory RA^{+} (EmRA): $CD45RA^{+}CCR7^{-}$

These are summarised in **Figure 7.2**

CD8 cell types



CD4 cell types

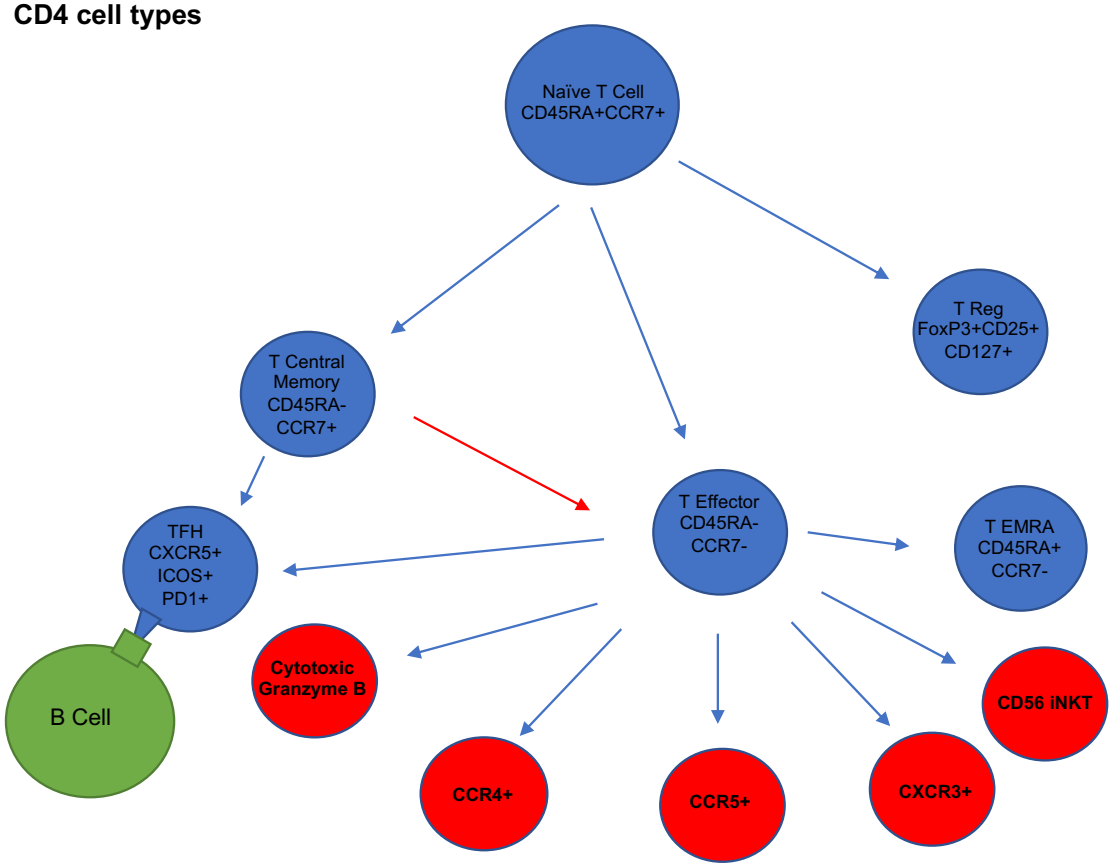


Figure 7.2: CD8 and CD4 T cell subtype definitions

7.4 Research publications arising during DPhil

Cassimjee I, Lee R, Patel J, Inflammatory Mediators in Abdominal Aortic Aneurysms: IntechOpen; 2017 (Book chapter)

Cassimjee I, Monareng T. Letter Re: 'Endovascular Therapy for Large Vessel Vasculopathy in HIV-infected Patients'. Eur J Vasc Endovasc Surg. 2016;52(5):705-6

Lee R, Bellamkonda K, Jones A, Killough N, Woodgate F, Cassimjee I, et al. Flow Mediated Dilatation and Progression of Abdominal Aortic Aneurysms. Eur J Vasc Endovasc Surg. 2017;53(6):820-9.

Lee R, Jones A, Woodgate F, Killough N, Bellamkonda K, Cassimjee I, et al. Data for the Oxford Abdominal Aortic Aneurysm Study international survey of vascular surgery professionals. Data Brief. 2017;14:298-301.

Lee R, Jones A, Cassimjee I, Handa A. International opinion on priorities in research for small abdominal aortic aneurysms and the potential path for research to impact clinical management. Int J Cardiol. 2017;245:253-5.

Lee R, Jones A, Cassimjee I, Handa A. Patients' opinions regarding research and management of abdominal aortic aneurysms. Int Angiol. 2017;36(6):526-30.

Lee R, Jones A, Woodgate F, Bellamkonda K, Cassimjee I, Fulford-Smith L, et al. The Experience of Patients During the Clinical Management Pathway of Abdominal Aortic Aneurysms at a NHS Trust. J Patient Exp. 2017;4(4):202-9.

Lee R, Jones A, Cassimjee I, Handa A. Engaging patients for their opinions regarding research of abdominal aortic aneurysms. Int J Cardiol. 2018;257:298.

Lee R, Jarchi D, Perera R, Jones A, Cassimjee I, Handa A, et al. Applied Machine Learning for the Prediction of Growth of Abdominal Aortic Aneurysm in Humans. EJVES Short Reports. 2018;39:24-8.

Lee R, Charles PD, Lapolla P, Cassimjee I, Huang H, Kessler B, et al. Integrated Physiological and Biochemical Assessments for the Prediction of Growth of Abdominal Aortic Aneurysms in Humans. Ann Surg. 2018.

Lee R, Stoddart M, Dyson I, Cassimjee I, Handa A, Cheng CP. Length Redundancy and Twist Improve the Biomechanical Properties of Polytetrafluoroethylene Bypass Grafts. Ann Vasc Surg. 2019.

Whaley ZL, Cassimjee I, Novak Z, Rowland D, Lapolla P, Chandrashekar A, et al. The Spatial Morphology of Intraluminal Thrombus Influences Type II Endoleak After Endovascular Repair of Abdominal Aortic Aneurysms. Ann Vasc Surg. 2019.

Kolkenbeck-Ruh A, Woodiwiss AJ, Monareng T, Sadiq E, Cassimjee I, Robinson C, et al. Complementary Impact of Carotid Intima-Media Thickness With Plaque in Associations With Noncardiac Arterial Vascular Events. Angiology. 2019:3319719

7.5 Abstract presentations at scientific meetings

I Cassimjee, R Lee, D Ahern, P Green, I Park, A Handa, C Monaco- On behalf of the Oxford Abdominal Aortic Aneurysm study investigators
Single cell characterisation of abdominal aortic aneurysms by mass cytometry (CyTOF) reveals a chronic inflammatory cell infiltrate predominated by T and B cells.
British Atherosclerosis Society meeting, September 2018, Cambridge, UK (Young investigator award)

I Cassimjee, R Lee, D Ahern, P Green, I Park, A Handa, C Monaco- On behalf of the Oxford Abdominal Aortic Aneurysm study investigators
Single cell characterisation of abdominal aortic aneurysms by mass cytometry (CyTOF) reveals a chronic inflammatory cell infiltrate predominated by T and B cells.
Vascular association of Southern Africa, October 2018, Cape Town, SA

I Cassimjee, R Lee, D Ahern, P Green, I Park, A Handa, C Monaco- On behalf of the Oxford Abdominal Aortic Aneurysm study investigators
Single cell characterisation of abdominal aortic aneurysms by mass cytometry (CyTOF) reveals a chronic inflammatory cell infiltrate predominated by T and B cells.
Vascular Society meeting of Ireland and Great Britain, November 2018, Glasgow. (Prize session)

7.6 Acknowledgments

I consider myself incredibly fortunate and privileged to have pursued a DPhil in my chosen speciality. I left my consultant vascular surgery position in Johannesburg becoming a full-time student again, in a foreign country and on a student stipend. To many starting all over again seemed foolish, but I lost nothing and gained everything. I am grateful to the incredible people I met along the way, and I am sure to miss some out in this acknowledgment. Please excuse me.

Firstly, I must acknowledge and sincerely thank my incredible wife, Sha'ista. I pried her away from her comfortable existence and relocated her to Wolfson college and the English weather where she worked out of our bedroom for three years. She has been a guiding light for most of my adult life and I hope I can repay the sacrifice someday. I would thank my kids (Suleiman and Talhah), but I think that they were actually the biggest beneficiaries of the Oxford experience.

Next I want to thank my primary supervisors Prof. Ashok Handa and Dr Regent Lee. They took a risk accepting me, and without them this would not have been possible. Ashok is a remarkable human being with a heart of gold and his generosity of spirit to both myself and my family cannot ever really be repaid. Regent is the archetypal clinician scientist, and one of the most driven people I have ever encountered. His scientific rigour and continuous probing are what I hope to carry with me into the future.

To my immunology supervisor, Prof. Claudia Monaco, I am eternally grateful. I started as an outsider in the Monaco group, but it became my home for almost two years. When I began this project, I could never have imagined it developing in this way. Thank you for introducing me to the world of immunology and encouraging me to take bold and decisive scientific steps when needed. Your qualities as a leader are inspirational.

I met many formidable women in Oxford. To Patricia Green, I am indebted. She walked me through my initial steps in the lab and passed on her skills assiduously. To my other Monaco lab mates, Dr Inhye Park, Dr Natacha Zanin, Dr Christina Kassiteridi, Dr Lea Dib, Alice Robinson and Dr Jennifer Cole who are incredible scientists and wonderful human beings, I thank you. Within the OxAAA group, my initial sparring partner and friend Amy Jones deserves a special mention. Others who took a special interest in my work were Dr Jyoti Patel and Prof Samira Lakhal-Littleton.

This work would not have been possible without the continual input of Dr David Ahern. He was instrumental in the build-up to the CyTOF experiments, the planning and execution of them, and the analysis. During the write-up phase, he continually critiqued and edited analysis, figures and the content with absolutely no compulsion to do so. For this, I extend sincere gratitude. I wish to acknowledge the extended Monaco lab, Warren Baker and Michael Goddard for their support and in particular to mention Jonathan Weber, who guided me through flow cytometry and cell sorting.

To my vascular surgical mentors in South Africa, Prof. Martin Veller and Prof. Abdool-Carrim, thank you for shaping my vascular surgical career and inspiring me

to achieve more, and to my dear friend Dr Taalib Monareng for sacrificing himself for my selfish pursuit. There were many dark days in the lab. Dr Vuyane Mhlomi was always a pillar that I turned to and I thank him for this and the close friendship we have subsequently enjoyed. Prof Nikita Sud and Prof Dev Ganjee were always there to provide a welcoming distraction and Dr Ashruf and Dr Aadila Peer provided a home away from home.

The OxAAA patients were sterling, and I was always amazed at how willing they were to participate in this research. This is particularly admirable as I recruited many of them just before their aneurysm repairs, during an extremely stressful time for them. I thank them. That also goes for the vascular surgery team at the John Radcliffe, especially the consultants and registrars.

This journey was possible through a generous scholarship from Netcare – Physicians Partnership Trust. It was initially called the Hamilton Naki and now aptly renamed the Bongani Mayosi scholarship. Prof Bongani Mayosi was the most instrumental figure behind this DPhil. A brilliant clinician, leader and scientist. He understood the need to train a Vascular surgeon in basic science and I looked forward to him shaping my future trajectory. Unfortunately, Prof Mayosi passed on during my time in Oxford. The world lost a giant, and I dedicate this thesis to his memory.

I also dedicate this thesis to my parents who have always encouraged me to act decisively and independently, guiding but never dictating. My father fell ill during my DPhil, and those were the most difficult days for me. In adversity we learn what we truly value.

This journey was not walked alone, it took an incredible team and a lot of luck.

*"Excellence is an art won by training and habituation: we do not act rightly because we have virtue or excellence, but rather we have these because we have acted rightly; these virtues are formed in man by his doing the actions**;***
we are what we repeatedly do. Excellence, then, is not an act but a habit."

Will Durant, The Story of Philosophy (1926)

References

1. Powell JT, Sweeting MJ, Thompson MM, Ashleigh R, Bell R, Gomes M, et al. Endovascular or open repair strategy for ruptured abdominal aortic aneurysm: 30 day outcomes from IMPROVE randomised trial. BMJ. 2014;348:f7661.
2. Kniemeyer HW, Kessler T, Reber PU, Ris HB, Hakki H, Widmer MK. Treatment of ruptured abdominal aortic aneurysm, a permanent challenge or a waste of resources? Prediction of outcome using a multi-organ-dysfunction score. Eur J Vasc Endovasc Surg. 2000;19(2):190-6.
3. Prevention CfDCa. Underlying Cause of Death 1999-2013 on CDC WONDER Online Database, released 2015. Data are from the Multiple Cause of Death Files, 1999-2013, as compiled from data provided by the 57 vital statistics jurisdictions through the Vital Statistics Cooperative Program: Centers for disease control and prevention; 2015 [Available from: http://wonder.cdc.gov/ucd-icd10.html.
4. Elkin D. Aneurysm of the Abdominal Aorta: Treatment by Ligation. Annals of Surgery. 1940;112(5):895-908.
5. Thompson JE. Early history of aortic surgery. J Vasc Surg. 1998;28(4):746-52.
6. Cohen JR, Graver LM. The ruptured abdominal aortic aneurysm of Albert Einstein. Surg Gynecol Obstet. 1990;170(5):455-8.
7. Endovascular aneurysm repair versus open repair in patients with abdominal aortic aneurysm (EVAR trial 1): randomised controlled trial. Lancet. 2005;365(9478):2179-86.
8. Patel R, Sweeting MJ, Powell JT, Greenhalgh RM. Endovascular versus open repair of abdominal aortic aneurysm in 15-years' follow-up of the UK endovascular aneurysm repair trial 1 (EVAR trial 1): a randomised controlled trial. Lancet. 2016;388(10058):2366-74.
9. Powell JT, Greenhalgh RM, Ruckley CV, Fowkes FG. The UK Small Aneurysm Trial. Ann N Y Acad Sci. 1996;800:249-51.
10. Lederle FA, Wilson SE, Johnson GR, Reinke DB, Littooy FN, Acher CW, et al. Immediate repair compared with surveillance of small abdominal aortic aneurysms. N Engl J Med. 2002;346(19):1437-44.
11. Ashton HA, Buxton MJ, Day NE, Kim LG, Marteau TM, Scott RA, et al. The Multicentre Aneurysm Screening Study (MASS) into the effect of abdominal aortic aneurysm screening on mortality in men: a randomised controlled trial. Lancet. 2002;360(9345):1531-9.
12. Lindholt JS, Juul S, Fasting H, Henneberg EW. Screening for abdominal aortic aneurysms: single centre randomised controlled trial. Bmj. 2005;330(7494):750.
13. Norman PE, Jamrozik K, Lawrence-Brown MM, Le MT, Spencer CA, Tuohy RJ, et al. Population based randomised controlled trial on impact of screening on mortality from abdominal aortic aneurysm. Bmj. 2004;329(7477):1259.
14. Earnshaw JJ, Lees T. Update on Screening for Abdominal Aortic Aneurysm. Eur J Vasc Endovasc Surg. 2017;54(1):1-2.
15. Hirose Y, Hamada S, Takamiya M, Imakita S, Naito H, Nishimura T. Aortic aneurysms: growth rates measured with CT. Radiology. 1992;185(1):249-52.
16. Lee R, Bellamkonda K, Jones A, Killough N, Woodgate F, Williams M, et al. Flow Mediated Dilatation and Progression of Abdominal Aortic Aneurysms. Eur J Vasc Endovasc Surg. 2017;53(6):820-9.

17. Thompson RW, Liao S, Curci JA. Vascular smooth muscle cell apoptosis in abdominal aortic aneurysms. Coron Artery Dis. 1997;8(10):623-31.
18. Campa JS, Greenhalgh RM, Powell JT. Elastin degradation in abdominal aortic aneurysms. Atherosclerosis. 1987;65(1-2):13-21.
19. Johnston KW RR, Tilson MD, Shah DM, Hollier L, Stanley JC. Suggested standards for reporting on arterial aneurysms. Subcommittee on Reporting Standards for Arterial Aneurysms, Ad Hoc Committee on Reporting .. NCBI. J Vasc Surg. 1991;13(3):452-8.
20. Wakefield TW, Strieter RM, Wilke CA, Kadell AM, Wrobleski SK, Burdick MD, et al. Venous thrombosis-associated inflammation and attenuation with neutralizing antibodies to cytokines and adhesion molecules. Arterioscler Thromb Vasc Biol. 1995;15(2):258-68.
21. Reiter M, Bucek RA, Koca N, Dirisamer A, Minar E. Deep vein thrombosis and systemic inflammatory response: a pilot trial. Wien Klin Wochenschr. 2003;115(3-4):111-4.
22. Newman AB, Arnold AM, Burke GL, O'Leary DH, Manolio TA. Cardiovascular disease and mortality in older adults with small abdominal aortic aneurysms detected by ultrasonography: the cardiovascular health study. Ann Intern Med. 2001;134(3):182-90.
23. Bahia SS, Holt PJ, Jackson D, Patterson BO, Hinchliffe RJ, Thompson MM, et al. Systematic Review and Meta-analysis of Long-term survival After Elective Infrarenal Abdominal Aortic Aneurysm Repair 1969-2011: 5 Year Survival Remains Poor Despite Advances in Medical Care and Treatment Strategies. Eur J Vasc Endovasc Surg. 2015;50(3):320-30.
24. Hari DM, Leung AM, Lee JH, Sim MS, Vuong B, Chiu CG, et al. AJCC-7TH Edition Staging Criteria for Colon Cancer: Do the Complex Modifications Improve Prognostic Assessment? J Am Coll Surg. 2013;217(2):181-90.
25. Thompson SG, Ashton HA, Gao L, Buxton MJ, Scott RA. Final follow-up of the Multicentre Aneurysm Screening Study (MASS) randomized trial of abdominal aortic aneurysm screening. Br J Surg. 2012;99(12):1649-56.
26. Powell JT, Brown LC, Forbes JF, Fowkes FG, Greenhalgh RM, Ruckley CV, et al. Final 12-year follow-up of surgery versus surveillance in the UK Small Aneurysm Trial. Br J Surg. 2007;94(6):702-8.
27. Bath MF, Gokani VJ, Sidloff DA, Jones LR, Choke E, Sayers RD, et al. Systematic review of cardiovascular disease and cardiovascular death in patients with a small abdominal aortic aneurysm. Br J Surg. 2015;102(8):866-72.
28. Bath MF, Saratzis A, Saedon M, Sidloff D, Sayers R, Bown MJ. Patients with Small Abdominal Aortic Aneurysm are at Significant Risk of Cardiovascular Events and this Risk is not Addressed Sufficiently. Eur J Vasc Endovasc Surg. 2017;53(2):255-60.
29. Parr A, McCann M, Bradshaw B, Shahzad A, Buttner P, Golledge J. Thrombus volume is associated with cardiovascular events and aneurysm growth in patients who have abdominal aortic aneurysms. J Vasc Surg. 2011;53(1):28-35.
30. Kazi M, Johan T, Religa P, Roy J, Eriksson P. Influence of intraluminal thrombus on structural and cellular composition of abdominal aortic aneurysm wall. Journal of Vascular Surgery. 2003;38(6):1283–92.
31. Tang W, Yao L, Roetker NS, Alonso A, Lutsey PL, Steenson CC, et al. Lifetime Risk and Risk Factors for Abdominal Aortic Aneurysm in a 24-Year Prospective Study: The ARIC Study (Atherosclerosis Risk in Communities). Arterioscler Thromb Vasc Biol. 2016;36(12):2468-77.

32. Chaikof EL, Dalman RL, Eskandari MK, Jackson BM, Lee WA, Mansour MA, et al. The Society for Vascular Surgery practice guidelines on the care of patients with an abdominal aortic aneurysm. J Vasc Surg. 2018;67(1):2-77.e2.
33. Kobeissi E, Hibino M, Pan H, Aune D. Blood pressure, hypertension and the risk of abdominal aortic aneurysms: a systematic review and meta-analysis of cohort studies. Eur J Epidemiol. 2019;34(6):547-55.
34. Aune D, Schlesinger S, Norat T, Riboli E. Diabetes mellitus and the risk of abdominal aortic aneurysm: A systematic review and meta-analysis of prospective studies. J Diabetes Complications. 2018;32(12):1169-74.
35. Dattani N, Sayers RD, Bown MJ. Diabetes mellitus and abdominal aortic aneurysms: A review of the mechanisms underlying the negative relationship. Diab Vasc Dis Res. 2018;15(5):367-74.
36. Yu X, Jiang D, Wang J, Wang R, Chen T, Wang K, et al. Metformin prescription and aortic aneurysm: systematic review and meta-analysis. Heart. 2019.
37. Fujimura N, Xiong J, Kettler EB, Xuan H, Glover KJ, Mell MW, et al. Metformin treatment status and abdominal aortic aneurysm disease progression. J Vasc Surg. 2016;64(1):46-54.e8.
38. Golledge J, Moxon J, Pinchbeck J, Anderson G, Rowbotham S, Jenkins J, et al. Association between metformin prescription and growth rates of abdominal aortic aneurysms. Br J Surg. 2017;104(11):1486-93.
39. Vasamsetti SB, Karnewar S, Kanugula AK, Thatipalli AR, Kumar JM, Kotamraju S. Metformin inhibits monocyte-to-macrophage differentiation via AMPK-mediated inhibition of STAT3 activation: potential role in atherosclerosis. Diabetes. 2015;64(6):2028-41.
40. Wanhainen A, Bergqvist D, Boman K, Nilsson TK, Rutegard J, Bjorck M. Risk factors associated with abdominal aortic aneurysm: a population-based study with historical and current data. J Vasc Surg. 2005;41(3):390-6.
41. Norman PE, Powell JT. Site specificity of aneurysmal disease. Circulation. 2010;121(4):560-8.
42. Okuyama K, Yaginuma G, Takahashi T, Sasaki H, Mori S. The development of vasa vasorum of the human aorta in various conditions. A morphometric study. Arch Pathol Lab Med. 1988;112(7):721-5.
43. Halloran BG, Davis VA, McManus BM, Lynch TG, Baxter BT. Localization of aortic disease is associated with intrinsic differences in aortic structure. J Surg Res. 1995;59(1):17-22.
44. Kelleher CM, McLean SE, Mecham RP. Vascular extracellular matrix and aortic development. Curr Top Dev Biol. 2004;62:153-88.
45. Taylor CA, Cheng CP, Espinosa LA, Tang BT, Parker D, Herfkens RJ. In vivo quantification of blood flow and wall shear stress in the human abdominal aorta during lower limb exercise. Ann Biomed Eng. 2002;30(3):402-8.
46. Gregory AK, Yin NX, Capella J, Xia S, Newman KM, Tilson MD. Features of autoimmunity in the abdominal aortic aneurysm. Arch Surg. 1996;131(1):85-8.
47. Kadoglou NP, Liapis CD. Matrix metalloproteinases: contribution to pathogenesis, diagnosis, surveillance and treatment of abdominal aortic aneurysms. Curr Med Res Opin. 2004;20(4):419-32.
48. Sakalihasan N, Delvenne P, Nusgens BV, Limet R, Lapiere CM. Activated forms of MMP2 and MMP9 in abdominal aortic aneurysms. J Vasc Surg. 1996;24(1):127-33.

49. Knox JB, Sukhova GK, Whittemore AD, Libby P. Evidence for altered balance between matrix metalloproteinases and their inhibitors in human aortic diseases. Circulation. 1997;95(1):205-12.
50. Courtois A, Nusgens BV, Hustinx R, Namur G, Gomez P, Somja J, et al. 18F-FDG uptake assessed by PET/CT in abdominal aortic aneurysms is associated with cellular and molecular alterations prefacing wall deterioration and rupture. J Nucl Med. 2013;54(10):1740-7.
51. Ghosh A, Pechota A, Coleman D, Upchurch GR, Jr., Eliason JL. Cigarette smoke-induced MMP2 and MMP9 secretion from aortic vascular smooth cells is mediated via the Jak/Stat pathway. Hum Pathol. 2015;46(2):284-94.
52. Wang S, Zhang C, Zhang M, Liang B, Zhu H, Lee J, et al. Activation of AMP-activated protein kinase alpha2 by nicotine instigates formation of abdominal aortic aneurysms in mice in vivo. Nat Med. 2012;18(6):902-10.
53. Meijer CA, Stijnen T, Wasser MN, Hamming JF, van Bockel JH, Lindeman JH. Doxycycline for stabilization of abdominal aortic aneurysms: a randomized trial. Ann Intern Med. 2013;159(12):815-23.
54. Johnsen SH, Forsdahl SH, Singh K, Jacobsen BK. Atherosclerosis in abdominal aortic aneurysms: a causal event or a process running in parallel? The Tromso study. Arterioscler Thromb Vasc Biol. 2010;30(6):1263-8.
55. Toghill BJ, Saratzis A, Bown MJ. Abdominal aortic aneurysm-an independent disease to atherosclerosis? Cardiovasc Pathol. 2017;27:71-5.
56. Jagadesham VP, Scott DJ, Carding SR. Abdominal aortic aneurysms: an autoimmune disease? Trends Mol Med. 2008;14(12):522-9.
57. Caligiuri G, Rossignol P, Julia P, Groyer E, Mouradian D, Urbain D, et al. Reduced immunoregulatory CD31+ T cells in patients with atherosclerotic abdominal aortic aneurysm. Arterioscler Thromb Vasc Biol. 2006;26(3):618-23.
58. Xia S, Ozsvath K, Hirose H, Tilson MD. Partial amino acid sequence of a novel 40-kDa human aortic protein, with vitronectin-like, fibrinogen-like, and calcium binding domains: aortic aneurysm-associated protein-40 (AAAP-40) [human MAGP-3, proposed]. Biochem Biophys Res Commun. 1996;219(1):36-9.
59. Chew DK, Knoetgen J, Xia S, Tilson MD. The role of a putative microfibrillar protein (80 kDa) in abdominal aortic aneurysm disease. J Surg Res. 2003;114(1):25-9.
60. Ozsvath KJ, Hirose H, Xia S, Tilson MD. Molecular mimicry in human aortic aneurysmal diseases. Ann N Y Acad Sci. 1996;800:288-93.
61. Bergoeing MP, Arif B, Hackmann AE, Ennis TL, Thompson RW, Curci JA. Cigarette smoking increases aortic dilatation without affecting matrix metalloproteinase-9 and -12 expression in a modified mouse model of aneurysm formation. J Vasc Surg. 2007;45(6):1217-27.
62. Jin J, Arif B, Garcia-Fernandez F, Ennis TL, Davis EC, Thompson RW, et al. Novel mechanism of aortic aneurysm development in mice associated with smoking and leukocytes. Arterioscler Thromb Vasc Biol. 2012;32(12):2901-9.
63. Koch AE, Haines GK, Rizzo RJ, Radosevich JA, Pope RM, Robinson PG, et al. Human abdominal aortic aneurysms. Immunophenotypic analysis suggesting an immune-mediated response. Am J Pathol. 1990;137(5):1199-213.
64. Platsoucas CD, Lu S, Nwaneshiudu I, Solomides C, Agelan A, Ntaoula N, et al. Abdominal aortic aneurysm is a specific antigen-driven T cell disease. Ann N Y Acad Sci. 2006;1085:224-35.
65. Rasmussen TE, Hallett JW, Jr., Metzger RL, Richardson DM, Harmsen WS, Goronzy JJ, et al. Genetic risk factors in inflammatory abdominal aortic aneurysms:

polymorphic residue 70 in the HLA-DR B1 gene as a key genetic element. J Vasc Surg. 1997;25(2):356-64.
66. Lu S, White JV, Lin WL, Zhang X, Solomides C, Evans K, et al. Aneurysmal lesions of patients with abdominal aortic aneurysm contain clonally expanded T cells. J Immunol. 2014;192(10):4897-912.
67. Dale MA, Xiong W, Carson JS, Suh MK, Karpisek AD, Meisinger TM, et al. Elastin-Derived Peptides Promote Abdominal Aortic Aneurysm Formation by Modulating M1/M2 Macrophage Polarization. J Immunol. 2016;196(11):4536-43.
68. Ocana E, Bohorquez JC, Perez-Requena J, Brieva JA, Rodriguez C. Characterisation of T and B lymphocytes infiltrating abdominal aortic aneurysms. Atherosclerosis. 2003;170(1):39-48.
69. Samadzadeh KM, Chun KC, Nguyen AT, Baker PM, Bains S, Lee ES. Monocyte activity is linked with abdominal aortic aneurysm diameter. J Surg Res. 2014;190(1):328-34.
70. Juvonen J, Surcel HM, Satta J, Teppo AM, Bloigu A, Syrjala H, et al. Elevated circulating levels of inflammatory cytokines in patients with abdominal aortic aneurysm. Arterioscler Thromb Vasc Biol. 1997;17(11):2843-7.
71. Galle C, Schandene L, Stordeur P, Peignois Y, Ferreira J, Wautrecht JC, et al. Predominance of type 1 CD4+ T cells in human abdominal aortic aneurysm. Clin Exp Immunol. 2005;142(3):519-27.
72. Liao M, Xu J, Clair AJ, Ehrman B, Graham LM, Eagleton MJ. Local and systemic alterations in signal transducers and activators of transcription (STAT) associated with human abdominal aortic aneurysms. J Surg Res. 2012;176(1):321-8.
73. Chan WL, Pejnovic N, Liew TV, Hamilton H. Predominance of Th2 response in human abdominal aortic aneurysm: mistaken identity for IL-4-producing NK and NKT cells? Cell Immunol. 2005;233(2):109-14.
74. Madhur MS, Funt SA, Li L, Vinh A, Chen W, Lob HE, et al. Role of interleukin 17 in inflammation, atherosclerosis, and vascular function in apolipoprotein e-deficient mice. Arterioscler Thromb Vasc Biol. 2011;31(7):1565-72.
75. Yin M, Zhang J, Wang Y, Wang S, Bockler D, Duan Z, et al. Deficient CD4+CD25+ T regulatory cell function in patients with abdominal aortic aneurysms. Arterioscler Thromb Vasc Biol. 2010;30(9):1825-31.
76. Dale MA, Ruhlman MK, Baxter BT. Inflammatory cell phenotypes in AAAs: their role and potential as targets for therapy. Arterioscler Thromb Vasc Biol. 2015;35(8):1746-55.
77. Ehrenstein MR, Evans JG, Singh A, Moore S, Warnes G, Isenberg DA, et al. Compromised function of regulatory T cells in rheumatoid arthritis and reversal by anti-TNFalpha therapy. J Exp Med. 2004;200(3):277-85.
78. Venigalla RK, Tretter T, Krienke S, Max R, Eckstein V, Blank N, et al. Reduced CD4+,CD25- T cell sensitivity to the suppressive function of CD4+,CD25high,CD127 -/low regulatory T cells in patients with active systemic lupus erythematosus. Arthritis Rheum. 2008;58(7):2120-30.
79. Uhlig HH, Coombes J, Mottet C, Izcue A, Thompson C, Fanger A, et al. Characterization of Foxp3+CD4+CD25+ and IL-10-secreting CD4+CD25+ T cells during cure of colitis. J Immunol. 2006;177(9):5852-60.
80. Sumpter TL, Wilkes DS. Role of autoimmunity in organ allograft rejection: a focus on immunity to type V collagen in the pathogenesis of lung transplant rejection. Am J Physiol Lung Cell Mol Physiol. 2004;286(6):L1129-39.

81. Zhou Y, Wu W, Lindholt JS, Sukhova GK, Libby P, Yu X, et al. Regulatory T cells in human and angiotensin II-induced mouse abdominal aortic aneurysms. Cardiovasc Res. 2015;107(1):98-107.
82. Zhu J, Paul WE. CD4 T cells: fates, functions, and faults. Blood. 2008;112(5):1557-69.
83. Whaley ZL, Cassimjee I, Novak Z, Rowland D, Lapolla P, Chandrashekar A, et al. The Spatial Morphology of Intraluminal Thrombus Influences Type II Endoleak After Endovascular Repair of Abdominal Aortic Aneurysms. Ann Vasc Surg. 2019.
84. Harter LP, Gross BH, Callen PW, Barth RA. Ultrasonic evaluation of abdominal aortic thrombus. J Ultrasound Med. 1982;1(8):315-8.
85. Roy J, Labruto F, Beckman MO, Danielson J, Johansson G, Swedenborg J. Bleeding into the intraluminal thrombus in abdominal aortic aneurysms is associated with rupture. J Vasc Surg. 2008;48(5):1108-13.
86. Stenbaek J, Kalin B, Swedenborg J. Growth of thrombus may be a better predictor of rupture than diameter in patients with abdominal aortic aneurysms. Eur J Vasc Endovasc Surg. 2000;20(5):466-9.
87. Touat Z, Ollivier V, Dai J, Huisse MG, Bezeaud A, Sebbag U, et al. Renewal of mural thrombus releases plasma markers and is involved in aortic abdominal aneurysm evolution. Am J Pathol. 2006;168(3):1022-30.
88. Folkesson M, Silveira A, Eriksson P, Swedenborg J. Protease activity in the multi-layered intra-luminal thrombus of abdominal aortic aneurysms. Atherosclerosis. 2011;218(2):294-9.
89. Folkesson M, Kazi M, Zhu C, Silveira A, Hemdahl AL, Hamsten A, et al. Presence of NGAL/MMP-9 complexes in human abdominal aortic aneurysms. Thromb Haemost. 2007;98(2):427-33.
90. Folkesson M, Li C, Frebelius S, Swedenborg J, Wagsater D, Williams KJ, et al. Proteolytically active ADAM10 and ADAM17 carried on membrane microvesicles in human abdominal aortic aneurysms. Thromb Haemost. 2015;114(6).
91. Vorp DA, Lee PC, Wang DH, Makaroun MS, Nemoto EM, Ogawa S, et al. Association of intraluminal thrombus in abdominal aortic aneurysm with local hypoxia and wall weakening. J Vasc Surg. 2001;34(2):291-9.
92. O'Leary SA, Kavanagh EG, Grace PA, McGloughlin TM, Doyle BJ. The biaxial mechanical behaviour of abdominal aortic aneurysm intraluminal thrombus: classification of morphology and the determination of layer and region specific properties. J Biomech. 2014;47(6):1430-7.
93. Adolph R, Vorp DA, Steed DL, Webster MW, Kameneva MV, Watkins SC. Cellular content and permeability of intraluminal thrombus in abdominal aortic aneurysm. J Vasc Surg. 1997;25(5):916-26.
94. Matusik P, Mazur P, Stepien E, Pfitzner R, Sadowski J, Undas A. Architecture of intraluminal thrombus removed from abdominal aortic aneurysm. J Thromb Thrombolysis. 2010;30(1):7-9.
95. Rao J, Brown BN, Weinbaum JS, Ofstun EL, Makaroun MS, Humphrey JD, et al. Distinct macrophage phenotype and collagen organization within the intraluminal thrombus of abdominal aortic aneurysm. J Vasc Surg. 2015;62(3):585-93.
96. Sagan A, Mrowiecki W, Mikolajczyk TP, Urbanski K, Siedlinski M, Nosalski R, et al. Local inflammation is associated with aortic thrombus formation in abdominal aortic aneurysms. Relationship to clinical risk factors. Thromb Haemost. 2012;108(5):812-23.

97. Houard X, Touat Z, Ollivier V, Louedec L, Philippe M, Sebbag U, et al. Mediators of neutrophil recruitment in human abdominal aortic aneurysms. Cardiovasc Res. 2009;82(3):532-41.
98. Houard X, Ollivier V, Louedec L, Michel JB, Back M. Differential inflammatory activity across human abdominal aortic aneurysms reveals neutrophil-derived leukotriene B4 as a major chemotactic factor released from the intraluminal thrombus. Faseb j. 2009;23(5):1376-83.
99. Wiernicki I, Parafiniuk M, Kolasa-Wolosiuk A, Gutowska I, Kazimierczak A, Clark J, et al. Relationship between aortic wall oxidative stress/proteolytic enzyme expression and intraluminal thrombus thickness indicates a novel pathomechanism in the progression of human abdominal aortic aneurysm. Faseb J. 2019;33(1):885-95.
100. Eliason JL, Hannawa KK, Ailawadi G, Sinha I, Ford JW, Deogracias MP, et al. Neutrophil depletion inhibits experimental abdominal aortic aneurysm formation. Circulation. 2005;112(2):232-40.
101. Kazi M, Johan T, Religa P, Roy J, Eriksson P. Influence of intraluminal thrombus on structural and cellular composition of abdominal aortic aneurysm wall ☆. Journal of Vascular Surgery. 2003;38(6):1283–92.
102. Back M. Inflammatory signaling through leukotriene receptors in atherosclerosis. Curr Atheroscler Rep. 2008;10(3):244-51.
103. Moxon JV, Padula MP, Clancy P, Emeto TI, Herbert BR, Norman PE, et al. Proteomic analysis of intra-arterial thrombus secretions reveals a negative association of clusterin and thrombospondin-1 with abdominal aortic aneurysm. Atherosclerosis. 2011;219(2):432-9.
104. Celermajer DS, Sorensen KE, Gooch VM, Spiegelhalter DJ, Miller OI, Sullivan ID, et al. Non-invasive detection of endothelial dysfunction in children and adults at risk of atherosclerosis. Lancet. 1992;340(8828):1111-5.
105. Sung SH, Wu TC, Chen JS, Chen YH, Huang PH, Lin SJ, et al. Reduced number and impaired function of circulating endothelial progenitor cells in patients with abdominal aortic aneurysm. Int J Cardiol. 2013;168(2):1070-7.
106. Medina F, de Haro J, Florez A, Acin F. Relationship between endothelial dependent vasodilation and size of abdominal aortic aneurysms. Ann Vasc Surg. 2010;24(6):752-7.
107. Knipp BS, Peterson DA, Rajagopalan S, Kehrer C, Ford JW, D'Alecy LG, et al. Impaired vasoreactivity despite an increase in plasma nitrite in patients with abdominal aortic aneurysms. J Vasc Surg. 2002;35(2):363-7.
108. Freiberg MS, Arnold AM, Newman AB, Edwards MS, Kraemer KL, Kuller LH. Abdominal aortic aneurysms, increasing infrarenal aortic diameter, and risk of total mortality and incident cardiovascular disease events: 10-year follow-up data from the Cardiovascular Health Study. Circulation. 2008;117(8):1010-7.
109. Sohrabi S, Wheatcroft S, Barth JH, Bailey MA, Johnson A, Bridge K, et al. Cardiovascular risk in patients with small and medium abdominal aortic aneurysms, and no history of cardiovascular disease. Br J Surg. 2014;101(10):1238-43.
110. Lee R, Jarchi D, Perera R, Jones A, Cassimjee I, Handa A, et al. Applied Machine Learning for the Prediction of Growth of Abdominal Aortic Aneurysm in Humans. EJVES Short Reports. 2018;39:24-8.
111. Lee R, Antonopoulos AS, Alexopoulou Z, Margaritis M, Kharbanda RK, Choudhury RP, et al. Artifactual elevation of plasma sCD40L by residual platelets in patients with coronary artery disease. Int J Cardiol. 2013;168(2):1648-50.

112. Autengruber A, Gereke M, Hansen G, Hennig C, Bruder D. Impact of enzymatic tissue disintegration on the level of surface molecule expression and immune cell function. Eur J Microbiol Immunol (Bp). 2012;2(2):112-20.
113. Abuzakouk M, Feighery C, O'Farrelly C. Collagenase and Dispase enzymes disrupt lymphocyte surface molecules. J Immunol Methods. 1996;194(2):211-6.
114. Monaco C, Andreakos E, Kiriakidis S, Mauri C, Bicknell C, Foxwell B, et al. Canonical pathway of nuclear factor κB activation selectively regulates proinflammatory and prothrombotic responses in human atherosclerosis. Proc Natl Acad Sci U S A. 2004;101(15):5634-9.
115. Huang H-L, Hsing H-W, Lai T-C, Chen Y-W, Lee T-R, Chan H-T, et al. Trypsin-induced proteome alteration during cell subculture in mammalian cells. Journal of Biomedical Science. 2010;17(1):36.
116. Matos TR, Liu H, Ritz J. Research Techniques Made Simple: Experimental Methodology for Single-Cell Mass Cytometry. J Invest Dermatol. 2017;137(4):e31-e8.
117. Newell EW, Cheng Y. Mass cytometry: blessed with the curse of dimensionality. Nat Immunol. 2016;17(8):890-5.
118. Kimball AK, Oko LM, Bullock BL, Nemenoff RA, van Dyk LF, Clambey ET. A Beginner's Guide to Analyzing and Visualizing Mass Cytometry Data. J Immunol. 2018;200(1):3-22.
119. Bendall SC, Simonds EF, Qiu P, Amir el AD, Krutzik PO, Finck R, et al. Single-cell mass cytometry of differential immune and drug responses across a human hematopoietic continuum. Science. 2011;332(6030):687-96.
120. Newell EW, Sigal N, Bendall SC, Nolan GP, Davis MM. Cytometry by time-of-flight shows combinatorial cytokine expression and virus-specific cell niches within a continuum of CD8+ T cell phenotypes. Immunity. 2012;36(1):142-52.
121. Amir el AD, Davis KL, Tadmor MD, Simonds EF, Levine JH, Bendall SC, et al. viSNE enables visualization of high dimensional single-cell data and reveals phenotypic heterogeneity of leukemia. Nat Biotechnol. 2013;31(6):545-52.
122. Chen H, Lau MC, Wong MT, Newell EW, Poidinger M, Chen J. Cytofkit: A Bioconductor Package for an Integrated Mass Cytometry Data Analysis Pipeline. PLoS Comput Biol. 2016;12(9):e1005112.
123. Carmina E, Chu MC, Moran C, Tortoriello D, Vardhana P, Tena G, et al. Subcutaneous and omental fat expression of adiponectin and leptin in women with polycystic ovary syndrome. Fertil Steril. 2008;89(3):642-8.
124. Maury E, Ehala-Aleksejev K, Guiot Y, Detry R, Vandenhooft A, Brichard SM. Adipokines oversecreted by omental adipose tissue in human obesity. https://doiorg/101152/ajpendo001272007. 2007.
125. Payne GA, Borbouse L, Kumar S, Neeb Z, Alloosh M, Sturek M, et al. Epicardial perivascular adipose-derived leptin exacerbates coronary endothelial dysfunction in metabolic syndrome via a protein kinase C-beta pathway. Arterioscler Thromb Vasc Biol. 2010;30(9):1711-7.
126. Badimon L, Badimon JJ. Mechanisms of arterial thrombosis in nonparallel streamlines: platelet thrombi grow on the apex of stenotic severely injured vessel wall. Experimental study in the pig model. The Journal of Clinical Investigation. 1989;84(4):1134-44.
127. Mustard JF, Canadian Heart Foundation Toronto OC, Murphy EA, Toronto OC, Rowsell HC, Guelph OC, et al. Factors influencing thrombus formation in vivo. The American Journal of Medicine. 1962;33(5):621-47.

128. Roumen-Klappe EM, Departments of General Internal Medicine Nijmegen TN, Heijer Md, Epidemiology and Biostatistics Nijmegen TN, Endocrinology Nijmegen TN, Uum SHMv, et al. Inflammatory response in the acute phase of deep vein thrombosis. Journal of Vascular Surgery. 2002;35(4):701-6.
129. Kakisis JD, Moulakakis KG, Antonopoulos CN, Mylonas SN, Giannakopoulos TG, Sfyroeras GS, et al. Volume of new-onset thrombus is associated with the development of postimplantation syndrome after endovascular aneurysm repair. J Vasc Surg. 2014;60(5):1140-5.
130. Desjardins P, Hansen JB, Allen M. Microvolume Protein Concentration Determination using the NanoDrop 2000c Spectrophotometer. J Vis Exp2009.
131. Smith PK, Krohn RI, Hermanson GT, Mallia AK, Gartner FH, Provenzano MD, et al. Measurement of protein using bicinchoninic acid. Anal Biochem. 1985;150(1):76-85.
132. Trent MS, Stead CM, Tran AX, Hankins JV. Diversity of endotoxin and its impact on pathogenesis. J Endotoxin Res. 2006;12(4):205-23.
133. Forester ND, Cruickshank SM, Scott DJA, Carding SR. Functional characterization of T cells in abdominal aortic aneurysms. Immunology. 2005;115(2):262-70.
134. Quintana RA, Taylor WR. Cellular Mechanisms of Aortic Aneurysm Formation. Circ Res. 2019;124(4):607-18.
135. Newman KM, Jean-Claude J, Li H, Scholes JV, Ogata Y, Nagase H, et al. Cellular localization of matrix metalloproteinases in the abdominal aortic aneurysm wall. J Vasc Surg. 1994;20(5):814-20.
136. Bobryshev YV, Lord RS, Parsson H. Immunophenotypic analysis of the aortic aneurysm wall suggests that vascular dendritic cells are involved in immune responses. Cardiovasc Surg. 1998;6(3):240-9.
137. Zhang L, Wang Y. B lymphocytes in abdominal aortic aneurysms. Atherosclerosis. 2015;242(1):311-7.
138. Lu S, White JV, Judy RI, Merritt LL, Lin WL, Zhang X, et al. Clonally expanded alpha-chain T-cell receptor (TCR) transcripts are present in aneurysmal lesions of patients with Abdominal Aortic Aneurysm (AAA). PLoS One. 142019.
139. Galle C, Schandene L, Dereume JP, Goldman M. CD8+ T-cell subpopulations in human abdominal aortic aneurysm lesion. Arterioscler Thromb Vasc Biol. 26. United States2006. p. e19; author reply e-20.
140. Bobryshev YV, Lord RS. Vascular-associated lymphoid tissue (VALT) involvement in aortic aneurysm. Atherosclerosis. 2001;154(1):15-21.
141. Raffort J, Lareyre F, Clement M, Hassen-Khodja R, Chinetti G, Mallat Z. Monocytes and macrophages in abdominal aortic aneurysm. Nat Rev Cardiol. 2017;14(8):457-71.
142. Boytard L, Spear R, Chinetti-Gbaguidi G, Acosta-Martin AE, Vanhoutte J, Lamblin N, et al. Role of proinflammatory CD68(+) mannose receptor(-) macrophages in peroxiredoxin-1 expression and in abdominal aortic aneurysms in humans. Arterioscler Thromb Vasc Biol. 2013;33(2):431-8.
143. Dutertre CA, Clement M, Morvan M, Schakel K, Castier Y, Alsac JM, et al. Deciphering the stromal and hematopoietic cell network of the adventitia from non-aneurysmal and aneurysmal human aorta. PLoS One. 2014;9(2):e89983.
144. Tieu BC, Lee C, Sun H, Lejeune W, Recinos A, 3rd, Ju X, et al. An adventitial IL-6/MCP1 amplification loop accelerates macrophage-mediated vascular inflammation leading to aortic dissection in mice. J Clin Invest. 2009;119(12):3637-51.

145. Ghigliotti G, Barisione C, Garibaldi S, Brunelli C, Palmieri D, Spinella G, et al. CD16(+) monocyte subsets are increased in large abdominal aortic aneurysms and are differentially related with circulating and cell-associated biochemical and inflammatory biomarkers. Dis Markers. 2013;34(2):131-42.
146. Rubio-Navarro A, Amaro Villalobos JM, Lindholt JS, Buendia I, Egido J, Blanco-Colio LM, et al. Hemoglobin induces monocyte recruitment and CD163-macrophage polarization in abdominal aortic aneurysm. Int J Cardiol. 2015;201:66-78.
147. Patel J, McNeill E, Douglas G, Hale AB, de Bono J, Lee R, et al. RGS1 regulates myeloid cell accumulation in atherosclerosis and aortic aneurysm rupture through altered chemokine signalling. Nat Commun. 2015;6:6614.
148. Curci JA, Liao S, Huffman MD, Shapiro SD, Thompson RW. Expression and localization of macrophage elastase (matrix metalloproteinase-12) in abdominal aortic aneurysms. J Clin Invest. 1998;102(11):1900-10.
149. White JV, Haas K, Phillips S, Comerota AJ. Adventitial elastolysis is a primary event in aneurysm formation. J Vasc Surg. 1993;17(2):371-80; discussion 80-1.
150. Bandura DR, Baranov VI, Ornatsky OI, Antonov A, Kinach R, Lou X, et al. Mass cytometry: technique for real time single cell multitarget immunoassay based on inductively coupled plasma time-of-flight mass spectrometry. Anal Chem. 2009;81(16):6813-22.
151. Bendall SC, Nolan GP, Roederer M, Chattopadhyay PK. A deep profiler's guide to cytometry. Trends Immunol. 2012;33(7):323-32.
152. Spitzer MH, Nolan GP. Mass Cytometry: Single Cells, Many Features. Cell. 2016;165(4):780-91.
153. Finck R, Simonds EF, Jager A, Krishnaswamy S, Sachs K, Fantl W, et al. Normalization of mass cytometry data with bead standards. Cytometry A. 2013;83(5):483-94.
154. Zunder ER, Finck R, Behbehani GK, Amir Ea D, Krishnaswamy S, Gonzalez VD, et al. Palladium-based Mass-Tag Cell Barcoding with a Doublet-Filtering Scheme and Single Cell Deconvolution Algorithm. Nat Protoc. 2015;10(2):316-33.
155. Lai L, Ong R, Li J, Albani S. A CD45-based barcoding approach to multiplex mass-cytometry (CyTOF). Cytometry A. 2015;87(4):369-74.
156. Takahashi S. Molecular functions of SIRPα and its role in cancer. Biomed Rep. 2018;9(1):3-7.
157. Dondossola E, Rangel R, Guzman-Rojas L, Barbu EM, Hosoya H, St. John LS, et al. CD13-positive bone marrow-derived myeloid cells promote angiogenesis, tumor growth, and metastasis. Proc Natl Acad Sci U S A. 2013;110(51):20717-22.
158. Alkhatib G. The biology of CCR5 and CXCR4. Curr Opin HIV AIDS. 2009;4(2):96-103.
159. Teo FH, de Oliveira RTD, Villarejos L, Mamoni RL, Altemani A, Menezes FH, et al. Characterization of CD4(+) T Cell Subsets in Patients with Abdominal Aortic Aneurysms. Mediators Inflamm. 2018;2018:6967310.
160. Winkels H, Ehinger E, Vassallo M, Buscher K, Dinh HQ, Kobiyama K, et al. Atlas of the Immune Cell Repertoire in Mouse Atherosclerosis Defined by Single-Cell RNA-Sequencing and Mass Cytometry. Circ Res. 2018;122(12):1675-88.
161. Chevrier S, Levine JH, Zanotelli VRT, Silina K, Schulz D, Bacac M, et al. An Immune Atlas of Clear Cell Renal Cell Carcinoma. Cell. 2017;169(4):736-49 e18.
162. Lindeman JH, Abdul-Hussien H, van Bockel JH, Wolterbeek R, Kleemann R. Clinical trial of doxycycline for matrix metalloproteinase-9 inhibition in patients with

an abdominal aneurysm: doxycycline selectively depletes aortic wall neutrophils and cytotoxic T cells. Circulation. 2009;119(16):2209-16.
163. Curci JA, Mao D, Bohner DG, Allen BT, Rubin BG, Reilly JM, et al. Preoperative treatment with doxycycline reduces aortic wall expression and activation of matrix metalloproteinases in patients with abdominal aortic aneurysms. J Vasc Surg. 2000;31(2):325-42.
164. Charles A Janeway J, Travers P, Walport M, Shlomchik MJ. The Humoral Immune Response: Garland Science; 2001 2001.
165. Walker DI, Bloor K, Williams G, Gillie I. Inflammatory aneurysms of the abdominal aorta. Br J Surg. 1972;59(8):609-14.
166. Kasashima S, Zen Y, Kawashima A, Endo M, Matsumoto Y, Kasashima F. A new clinicopathological entity of IgG4-related inflammatory abdominal aortic aneurysm. J Vasc Surg. 2009;49(5):1264-71; discussion 71.
167. Hamano H, Kawa S, Horiuchi A, Unno H, Furuya N, Akamatsu T, et al. High serum IgG4 concentrations in patients with sclerosing pancreatitis. N Engl J Med. 2001;344(10):732-8.
168. Weisel FJ, Zuccarino-Catania GV, Chikina M, Shlomchik MJ. A Temporal Switch in the Germinal Center Determines Differential Output of Memory B and Plasma Cells. Immunity. 2016;44(1):116-30.
169. Stebegg M, Kumar SD, Silva-Cayetano A, Fonseca VR, Linterman MA, Graca L. Regulation of the Germinal Center Response. Front Immunol. 2018;9:2469.
170. Yin C, Mohanta SK, Srikakulapu P, Weber C, Habenicht AJ. Artery Tertiary Lymphoid Organs: Powerhouses of Atherosclerosis Immunity. Front Immunol. 2016;7:387.
171. Yin C, Mohanta S, Maffia P, Habenicht AJR. Editorial: Tertiary Lymphoid Organs (TLOs): Powerhouses of Disease Immunity. Front Immunol. 2017;8.
172. Clement M, Guedj K, Andreata F, Morvan M, Bey L, Khallou-Laschet J, et al. Control of the T follicular helper-germinal center B-cell axis by CD8(+) regulatory T cells limits atherosclerosis and tertiary lymphoid organ development. Circulation. 2015;131(6):560-70.
173. Chaudhry MS, Karadimitris A. Role and regulation of CD1d in normal and pathological B cells. J Immunol. 2014;193(10):4761-8.
174. Santner-Nanan B, Seddiki N, Zhu E, Quent V, Kelleher A, Fazekas de St Groth B, et al. Accelerated age-dependent transition of human regulatory T cells to effector memory phenotype. Int Immunol. 2008;20(3):375-83.
175. Valmori D, Merlo A, Souleimanian NE, Hesdorffer CS, Ayyoub M. A peripheral circulating compartment of natural naive CD4 Tregs. J Clin Invest. 2005;115(7):1953-62.
176. Gregg R, Smith CM, Clark FJ, Dunnion D, Khan N, Chakraverty R, et al. The number of human peripheral blood CD4+ CD25high regulatory T cells increases with age. Clin Exp Immunol. 2005;140(3):540-6.
177. Yodoi K, Yamashita T, Sasaki N, Kasahara K, Emoto T, Matsumoto T, et al. Foxp3+ regulatory T cells play a protective role in angiotensin II-induced aortic aneurysm formation in mice. Hypertension. 2015;65(4):889-95.
178. Geginat J, Fondazione Istituto Nazionale di Genetica Molecolare “Romeo ed Enrica Invernizzi” INGM I, geginat@ingm.org, Paroni M, Fondazione Istituto Nazionale di Genetica Molecolare “Romeo ed Enrica Invernizzi” INGM I, Maglie S, et al. Plasticity of Human CD4 T Cell Subsets. Frontiers in Immunology. 2014;5.

179. Dawson J, Cockerill GW, Choke E, Belli AM, Loftus I, Thompson MM. Aortic aneurysms secrete interleukin-6 into the circulation. J Vasc Surg. 2007;45(2):350-6.
180. Vangelista L, Vento S. The Expanding Therapeutic Perspective of CCR5 Blockade. Front Immunol. 2017;8:1981.
181. Pervaiz A, Zepp M, Mahmood S, Ali DM, Berger MR, Adwan H. CCR5 blockage by maraviroc: a potential therapeutic option for metastatic breast cancer. Cell Oncol (Dordr). 2019;42(1):93-106.
182. Mencarelli A, Cipriani S, Francisci D, Santucci L, Baldelli F, Distrutti E, et al. Highly specific blockade of CCR5 inhibits leukocyte trafficking and reduces mucosal inflammation in murine colitis. Sci Rep. 62016.
183. Sandford B, Bown M, London N, Sayers R. The role of the CCR5 Delta32 polymorphism in abdominal aortic aneurysms. Int J Immunogenet. 2009;36(4):199-205.
184. Ghilardi G, Biondi ML, Battaglioli L, Zambon A, Guagnellini E, Scorza R. Genetic risk factor characterizes abdominal aortic aneurysm from arterial occlusive disease in human beings: CCR5 Delta 32 deletion. J Vasc Surg. 2004;40(5):995-1000.
185. Jiang Y, Li Y, Zhu B. T-cell exhaustion in the tumor microenvironment. Cell Death Dis. 2015;6:e1792.
186. Fontaine V, Touat Z, Mtairag el M, Vranckx R, Louedec L, Houard X, et al. Role of leukocyte elastase in preventing cellular re-colonization of the mural thrombus. Am J Pathol. 2004;164(6):2077-87.
187. Krausgruber T, Blazek K, Smallie T, Alzabin S, Lockstone H, Sahgal N, et al. IRF5 promotes inflammatory macrophage polarization and TH1-TH17 responses. Nat Immunol. 2011;12(3):231-8.
188. Sander J, Schmidt SV, Cirovic B, McGovern N, Papantonopoulou O, Hardt AL, et al. Cellular Differentiation of Human Monocytes Is Regulated by Time-Dependent Interleukin-4 Signaling and the Transcriptional Regulator NCOR2. Immunity. 2017;47(6):1051-66.e12.
189. Bots M, Medema JP. Granzymes at a glance. J Cell Sci. 2006;119(Pt 24):5011-4.
190. Choy JC, McDonald PC, Suarez AC, Hung VH, Wilson JE, McManus BM, et al. Granzyme B in atherosclerosis and transplant vascular disease: association with cell death and atherosclerotic disease severity. Mod Pathol. 2003;16(5):460-70.
191. Tak PP, Spaeny-Dekking L, Kraan MC, Breedveld FC, Froelich CJ, Hack CE. The levels of soluble granzyme A and B are elevated in plasma and synovial fluid of patients with rheumatoid arthritis (RA). Clin Exp Immunol. 1999;116(2):366-70.
192. Chamberlain CM, Ang LS, Boivin WA, Cooper DM, Williams SJ, Zhao H, et al. Perforin-independent extracellular granzyme B activity contributes to abdominal aortic aneurysm. Am J Pathol. 2010;176(2):1038-49.
193. Lenk GM, Tromp G, Weinsheimer S, Gatalica Z, Berguer R, Kuivaniemi H. Whole genome expression profiling reveals a significant role for immune function in human abdominal aortic aneurysms. BMC Genomics. 2007;8:237.
194. Chamberlain CM, Granville DJ. The role of Granzyme B in atheromatous diseases. Can J Physiol Pharmacol. 2007;85(1):89-95.
195. Robinson PN, Godfrey M. The molecular genetics of Marfan syndrome and related microfibrillopathies. J Med Genet. 2000;37(1):9-25.

196. Boivin WA, Cooper DM, Hiebert PR, Granville DJ. Intracellular versus extracellular granzyme B in immunity and disease: challenging the dogma. Lab Invest. 2009;89(11):1195-220.
197. White MJ, Nielsen CM, McGregor RHC, Riley EM, Goodier MR. Differential activation of CD57-defined natural killer cell subsets during recall responses to vaccine antigens. Immunology. 2014;142(1):140-50.
198. Hassin D, Garber OG, Meiraz A, Schiffenbauer YS, Berke G. Cytotoxic T lymphocyte perforin and Fas ligand working in concert even when Fas ligand lytic action is still not detectable. Immunology. 2011;133(2):190-6.
199. Mellor-Heineke S, Cincinnati Childrens Hospital Medical Center BMT, Cincinnati, 45229, OH, United States, Bini_mellor@yahoo.com, Villanueva J, Cincinnati Childrens Hospital Medical Center BMT, Cincinnati, 45229, OH, United States, joyce.villanueva@cchmc.org, et al. Elevated Granzyme B in Cytotoxic Lymphocytes is a Signature of Immune Activation in Hemophagocytic Lymphohistiocytosis. Frontiers in Immunology. 2013;4.
200. Spaeny-Dekking EH, Hanna WL, Wolbink AM, Wever PC, Kummer JA, Swaak AJ, et al. Extracellular granzymes A and B in humans: detection of native species during CTL responses in vitro and in vivo. J Immunol. 1998;160(7):3610-6.
201. Csiszar A, Wang M, Lakatta EG, Ungvari Z. Inflammation and endothelial dysfunction during aging: role of NF-κB. J Appl Physiol (1985). 2008;105(4):1333-41.
202. Donato AJ, Pierce GL, Lesniewski LA, Seals DR. Role of NFκB in age-related vascular endothelial dysfunction in humans. Aging (Albany NY). 2009;1(8):678-80.
203. Pierce GL, Lesniewski LA, Lawson BR, Beske SD, Seals DR. Nuclear factor-{kappa}B activation contributes to vascular endothelial dysfunction via oxidative stress in overweight/obese middle-aged and older humans. Circulation. 2009;119(9):1284-92.
204. de Winther MP, Kanters E, Kraal G, Hofker MH. Nuclear factor kappaB signaling in atherogenesis. Arterioscler Thromb Vasc Biol. 2005;25(5):904-14.
205. Rossol M, Heine H, Meusch U, Quandt D, Klein C, Sweet MJ, et al. LPS-induced cytokine production in human monocytes and macrophages. Crit Rev Immunol. 2011;31(5):379-446.
206. Sharif O, Bolshakov VN, Raines S, Newham P, Perkins ND. Transcriptional profiling of the LPS induced NF-κB response in macrophages. BMC Immunology. 2007;8(1):1.
207. Scheller J, Chalaris A, Garbers C, Rose-John S. ADAM17: a molecular switch to control inflammation and tissue regeneration. Trends Immunol. 2011;32(8):380-7.
208. Pannekoek H, Veerman H, Lambers H, Diergaarde P, Verweij CL, van Zonneveld AJ, et al. Endothelial plasminogen activator inhibitor (PAI): a new member of the Serpin gene family. Embo j. 1986;5(10):2539-44.
209. Abderrahmani R, Francois A, Buard V, Tarlet G, Blirando K, Hneino M, et al. PAI-1-dependent endothelial cell death determines severity of radiation-induced intestinal injury. PLoS One. 2012;7(4):e35740.
210. Urbich C, Walter DH, Zeiher AM, Dimmeler S. Laminar shear stress upregulates integrin expression: role in endothelial cell adhesion and apoptosis. Circ Res. 2000;87(8):683-9.
211. Siedlinski M, Nosalski R, Szczepaniak P, Ludwig-Galezowska AH, Mikolajczyk T, Filip M, et al. Vascular transcriptome profiling identifies Sphingosine

kinase 1 as a modulator of angiotensin II-induced vascular dysfunction. Sci Rep. 2017;7:44131.
212. Bohm F, Pernow J. The importance of endothelin-1 for vascular dysfunction in cardiovascular disease. Cardiovasc Res. 2007;76(1):8-18.
213. Dengler VL, Galbraith M, Espinosa JM. Transcriptional Regulation by Hypoxia Inducible Factors. Crit Rev Biochem Mol Biol. 2014;49(1):1-15.
214. Oladipupo SS, Smith C, Santeford A, Park C, Sene A, Wiley LA, et al. Endothelial cell FGF signaling is required for injury response but not for vascular homeostasis. Proc Natl Acad Sci U S A. 2014;111(37):13379-84.
215. Yang X, Liaw L, Prudovsky I, Brooks PC, Vary C, Oxburgh L, et al. Fibroblast Growth Factor Signaling in the Vasculature. Curr Atheroscler Rep. 2015;17(6):509.
216. Rohrs JA, Sulistio CD, Finley SD. Predictive model of thrombospondin-1 and vascular endothelial growth factor in breast tumor tissue. NPJ Syst Biol Appl. 2016;2.
217. Nor JE, Mitra RS, Sutorik MM, Mooney DJ, Castle VP, Polverini PJ. Thrombospondin-1 induces endothelial cell apoptosis and inhibits angiogenesis by activating the caspase death pathway. J Vasc Res. 2000;37(3):209-18.
218. Goumans M-J, Liu Z, Dijke Pt. TGF-β signaling in vascular biology and dysfunction. Cell Research. 2008;19(1):116.
219. Walshe TE, Saint-Geniez M, Maharaj AS, Sekiyama E, Maldonado AE, D'Amore PA. TGF-beta is required for vascular barrier function, endothelial survival and homeostasis of the adult microvasculature. PLoS One. 2009;4(4):e5149.
220. Oliver PM, John SW, Purdy KE, Kim R, Maeda N, Goy MF, et al. Natriuretic peptide receptor 1 expression influences blood pressures of mice in a dose-dependent manner. Proc Natl Acad Sci U S A. 1998;95(5):2547-51.
221. Chistiakov DA, Orekhov AN, Bobryshev YV. Endothelial Barrier and Its Abnormalities in Cardiovascular Disease. Front Physiol. 2015;6.
222. Yu JC, Pickard JD, Davenport AP. Endothelin ETA receptor expression in human cerebrovascular smooth muscle cells. Br J Pharmacol. 1995;116(5):2441-6.
223. Rodriguez-Tarduchy G, Collins M, López-Rivas A. Regulation of apoptosis in interleukin-3-dependent hemopoietic cells by interleukin-3 and calcium ionophores. EMBO J. 1990;9(9):2997-3002.
224. Wilson CL, Gough PJ, Chang CA, Chan CK, Frey JM, Liu Y, et al. Endothelial deletion of ADAM17 in mice results in defective remodeling of the semilunar valves and cardiac dysfunction in adults. Mech Dev. 2013;130(4-5):272-89.
225. Brodsky SV, Malinowski K, Golightly M, Jesty J, Goligorsky MS. Plasminogen activator inhibitor-1 promotes formation of endothelial microparticles with procoagulant potential. Circulation. 2002;106(18):2372-8.
226. Takeshita K, Hayashi M, Iino S, Kondo T, Inden Y, Iwase M, et al. Increased expression of plasminogen activator inhibitor-1 in cardiomyocytes contributes to cardiac fibrosis after myocardial infarction. Am J Pathol. 2004;164(2):449-56.
227. Eitzman DT, McCoy RD, Zheng X, Fay WP, Shen T, Ginsburg D, et al. Bleomycin-induced pulmonary fibrosis in transgenic mice that either lack or overexpress the murine plasminogen activator inhibitor-1 gene. J Clin Invest. 1996;97(1):232-7.
228. Eitzman DT, Westrick RJ, Xu Z, Tyson J, Ginsburg D. Plasminogen activator inhibitor-1 deficiency protects against atherosclerosis progression in the mouse carotid artery. Blood. 2000;96(13):4212-5.
229. Li MW, Mian MO, Barhoumi T, Rehman A, Mann K, Paradis P, et al. Endothelin-1 overexpression exacerbates atherosclerosis and induces aortic

aneurysms in apolipoprotein E knockout mice. Arterioscler Thromb Vasc Biol. 2013;33(10):2306-15.
230. Treska V, Wenham PW, Valenta J, Topolcan O, Pecen L. Plasma endothelin levels in patients with abdominal aortic aneurysms. Eur J Vasc Endovasc Surg. 1999;17(5):424-8.
231. Wei H, Bedja D, Koitabashi N, Xing D, Chen J, Fox-Talbot K, et al. Endothelial expression of hypoxia-inducible factor 1 protects the murine heart and aorta from pressure overload by suppression of TGF-beta signaling. Proc Natl Acad Sci U S A. 2012;109(14):E841-50.
232. Akhtar S, Hartmann P, Karshovska E, Rinderknecht FA, Subramanian P, Gremse F, et al. Endothelial Hypoxia-Inducible Factor-1alpha Promotes Atherosclerosis and Monocyte Recruitment by Upregulating MicroRNA-19a. Hypertension. 2015;66(6):1220-6.
233. Wang W, Xu B, Xuan H, Ge Y, Wang Y, Wang L, et al. Hypoxia-inducible factor 1 in clinical and experimental aortic aneurysm disease. J Vasc Surg. 2018;68(5):1538-50.e2.
234. Tsai SH, Huang PH, Hsu YJ, Peng YJ, Lee CH, Wang JC, et al. Inhibition of hypoxia inducible factor-1alpha attenuates abdominal aortic aneurysm progression through the down-regulation of matrix metalloproteinases. Sci Rep. 2016;6:28612.
235. McLaughlin JN, Mazzoni MR, Cleator JH, Earls L, Perdigoto AL, Brooks JD, et al. Thrombin modulates the expression of a set of genes including thrombospondin-1 in human microvascular endothelial cells. J Biol Chem. 2005;280(23):22172-80.
236. Liu Z, Morgan S, Ren J, Wang Q, Annis DS, Mosher DF, et al. Thrombospondin-1 (TSP1) contributes to the development of vascular inflammation by regulating monocytic cell motility in mouse models of abdominal aortic aneurysm. Circ Res. 2015;117(2):129-41.
237. Baylis RA, Gomez D, Mallat Z, Pasterkamp G, Owens GK. The CANTOS Trial. One Important Step for Clinical Cardiology but a Giant Leap for Vascular Biology. 2017;37(11):e174-e7.
238. Ridker PM, Everett BM, Thuren T, MacFadyen JG, Chang WH, Ballantyne C, et al. Antiinflammatory Therapy with Canakinumab for Atherosclerotic Disease. NEJM. 2017.
239. Da Ros F, Carnevale R, Cifelli G, Bizzotto D, Casaburo M, Perrotta M, et al. Targeting Interleukin-1beta Protects from Aortic Aneurysms Induced by Disrupted Transforming Growth Factor beta Signaling. Immunity. 2017;47(5):959-73.e9.
240. Young JL, Sukhova GK, Foster D, Kisiel W, Libby P, Schonbeck U. The serpin proteinase inhibitor 9 is an endogenous inhibitor of interleukin 1beta-converting enzyme (caspase-1) activity in human vascular smooth muscle cells. J Exp Med. 2000;191(9):1535-44.
241. Appay V, van Lier RA, Sallusto F, Roederer M. Phenotype and function of human T lymphocyte subsets: consensus and issues. Cytometry A. 2008;73(11):975-83.
242. Mahnke YD, Brodie TM, Sallusto F, Roederer M, Lugli E. The who's who of T-cell differentiation: human memory T-cell subsets. Eur J Immunol. 2013;43(11):2797-809.